NUMERICAL STUDY ON A SPAR TYPE FLOATING OFFSHORE WIND TURBINE USING COUPLE-FAST CODE

A Dissertation

by

CHENG PENG

Submitted to the Office of Graduate and Professional Studies of
Texas A&M University
in partial fulfillment of the requirements for the degree of

DOCTOR OF PHILOSOPHY

Chair of Committee,	Jun Zhang
Committee Members,	Moo-Hyun Kim
	Hamn-Ching Chen
	David Brooks
Head of Department,	Robin Autenrieth

May 2015

Major Subject: Ocean Engineering

ABSTRACT

Floating offshore wind turbine (FOWT) attracts more and more attention for harnessing wind power over the surface of relatively deep ocean water, where steady and strong wind occurs. Although it has been shown that the knowledge gained from the development of floating platforms for oil and gas production is helpful for the development of FOWTs, it alone is insufficient for understanding dynamic interactions between the supporting platform and the wind turbine. Therefore, it is desirable to conduct numerical simulations of a FOWT under the impact of different combinations of winds, waves and currents.

In this study, a numerical code named as COUPLE-FAST has been developed to investigate the motions of a selected FOWT and the tensions in its mooring lines. The selected FOWT mainly consists of a 5MW NREL wind turbine and OC3-Hywind Spar support platform. COUPLE-FAST is made based two existing codes COUPLE and FAST. The former is an in-house code developed and being continuously expanded for the simulation of an offshore floating platform positioned by a mooring-line/tendon system. FAST is an open-source code capable of predicting both the extreme and fatigue loads of two- and three- bladed horizontal-axis wind turbines [1]. In COUPLE-FAST, COUPLE module is used to calculate the external loads on the support floating platform, mooring line forces and its motions, and FAST module to calculate the aerodynamic loads and flexible responses of the wind turbine. The displacements, velocities and

accelerations predicted in COUPLE are transferred to FAST. The forces at the tower bases calculated by FAST are transferred to COUPLE.

Total 25 cases with different combination of winds, waves and currents are simulated for calculating the motions of the FOWT and tensions in its mooring lines. Among many interesting observations made based on these simulations, it is confirmed that when the mean wind speed is above the rated wind speed the blade pitch control system may induce resonant interaction (also known as ‘negative damping’) between the surge of the FOWT and dynamic wind loads induced by the adjustment of blade pitch angle. However, the resonant effects on surge of the FOWT in the case of turbulent winds are not as significant as in the case of steady winds of the corresponding wind speed.

ACKNOWLEDGEMENTS

I would like to thank my committee chair, Dr. Zhang, and my committee members, Dr. Kim, Dr. Chen and Dr. Brooks, for their guidance and support throughout the course of this research.

I want to thank my classmate Dongxing Jia for his help in my research, especially for his guidance on the use of UHWM code.

I also want to thank my friends, colleagues, the department faculties and staffs for making my time at Texas A&M University a great experience.

Finally, I want to give special thanks to my wife for her patience, supports and love. Thanks also go to my mother, father, and mother-in-law for their support on taking care of my families during this research. Thanks go to my son for the happiness brought by his birth and growing up.

NOMENCLATURE

BEM	Blade Element Momentum
COG	Center of Gravity
CPU	Central Processing Unit
CS	Coordinate System
DLL	Dynamic Link Library
DOE	Department of Energy
DOF	Degree of Freedom
FAST	Fatigue, Aerodynamics, Structures, and Turbulence
FOWT	Floating Offshore Wind Turbine
EU	European Union
EWEA	European Wind Energy Association
FEM	Finite Element Method
FFT	Fast Fourier Transform
GDW	Generalized Dynamic Wake
HF	High Frequency
IFFT	Inverse Fast Fourier Transform
JONSWAP	Joint North Sea Wave Project
LF	Low Frequency
ML	Mooring Line
NREL	National Renewable Energy Laboratory

PSD	Power Spectrum Density
STD	Standard Deviation
SWL	Still Water Level
TLP	Tension Leg Platform
UHWM	Uni-direction Hybrid Wave Model
WF	Wave Frequency

TABLE OF CONTENTS

Page

LIST OF FIGURES

Page

LIST OF TABLES

Page

1. INTRODUCTION

1.1 Background and Significance

Wind is a source of renewable energy. In May 2008, the U.S. Department of Energy (DOE) released a report detailing a deployment scenario by which the United States could achieve 20% of its electric energy supply from wind energy by 2030. Under this scenario, offshore wind will be an essential contributor, providing 54 GW of installed electric capacity to the grid [2]. In Europe, wind energy met 3.7 % of EU (European Union) electricity demand in 2008. The European Commission's goal of increasing that share to 12 % by 2020 is regarded as achievable by European Wind Energy Association (EWEA) [3].

The resource of offshore wind energy encourages the activities in the offshore wind energy development. Many coastal areas in the United States have large electricity demand but limited access to a high-quality land-based wind resource. In addition, these areas are typically limited in their access to interstate grid transmission. Offshore wind resource has the potential to be a significant domestic renewable energy source for coastal electricity needs. Since they do not use land and are usually far away from the shoreline, and thus having fewer objections raised from the mentality of "not in my back yard" (Nimby). Because the locations of offshore wind turbines are likely far away from the shore line, winds there are general stronger and steadier than those over land and even near shorelines. Based on the investigation by DOE and National Renewable

Energy Laboratory (NREL), the total US offshore wind power potential within 50 nm (nautical miles) off shore is 4,150 GW, and almost 60% of it is in the area with relatively deep water depth (>60m) [4]. The resource from Florida to Maine out to 200 m water depth can achieve the one-third of US or all of Florida to Maine electric needs [5].

The offshore wind energy is no longer the "potential energy". Right now, Europe and China lead the offshore wind energy development. In Europe, at the end of 2013, 2,080 offshore turbines have been installed and grid connected, making a cumulative total of 6,562 MW, which are in 69 wind farms of eleven European countries. There are also two full-scale grid-connected floating turbines, and two down-scaled prototypes [6]. In US, a New England company, Deepwater Wind LLC, has successfully bid $3.8 million for the rights to develop offshore wind farms in nearly 165,000 acres of specially designated federal waters off the coasts of Massachusetts and Rhode Island with 200 turbines capable of producing enough energy to power roughly 350,000 homes. Construction could begin as early as 2017 [7].

Until now, overwhelming majority offshore wind turbines have a fixed foundation and hence are located in relatively shallow water and close to the shoreline. However, floating offshore wind turbines (FOWT) deployed in relatively deep water begin to attract more attention.

The world's first operational deep-water floating large-capacity wind turbine, Hywind, was deployed in the North Sea off Norway in summer 2009. It is equipped with a 2.3 MW turbine and mounted on a Spar hull of 117-metre long [8].

WindFloat is a semi-submersible type of FOWT, designed and patented by Principle Power. The complete system was assembled and commissioned onshore in 2011. The assembled WindFloat was then wet-towed about 400 kilometers to its final deployed location 5 km offshore of Agucaduora, Portugal. WindFloat is equipped with a 2.0 MW turbine and its installation was completed on October 2011 [9].

In many ways, a FOWT is similar to a floating oil & gas platform. Both float on the sea surface and positioned by a mooring-line or tendon system. However, the former has its own unique characteristics. First, the wind pressure center applied at the wind turbine is far above the sea surface, producing a large pitch/roll moment on the support platform. Secondly, the tower of a wind turbine is less rigid than its support platform, which may result in additional difficulties in the simulation of the interactions between them. Last but not the least, the interaction between a moored support platform and a rotating wind turbine under the impact of wind, wave and current is much more complicated than its cousin used in the offshore oil/gas development and not well understood. Therefore, it is worth conducting the study of aero-hydro-servo-elastic fully coupled analysis of a FOWT.

1.2 Review of Previous Work

Floating platforms have been developed and deployed by the offshore industry to produce oil and gas in deep water for more than two decades. Profound knowledge gained by the offshore industry has been applied to the development of floating wind turbines. Different types of floating platforms, such as tension leg platform (TLP), Spar,

Semi-submersible and barge, have been considered as the candidates for hosting wind turbines [10].

Many studies had been conducted on dynamic interactions between a wind turbines and its support floating structure. Jonkman developed the HydroDyn module for FAST (Fatigue, Aerodynamics, Structures, and Turbulence) to simulate the aero-hydro-servo-elastic coupled response of FOWT [11], Shim [12], and Bae, et al. [13], integrated FAST-Charm3D to make uncoupled and coupled analysis on the TLP and Spar type floating wind turbines. Jonkman and Matha [10] used FAST to investigate the dynamics of three types of platforms mentioned above. Masciola, et al. [14] developed a FAST-OrcaFlex coupling code for the study of interactions between a wind turbine and its supporting Spar under the impact of periodic waves. Madjid, et al. [15] used HAWC2 and DeepC to study the dynamic response from wind and wave for a Spar FOWT. Peng, et al. [16] and Yan, et al. [17] develop a COUPLE-FAST coupling code and use limited coupled and fully coupled methods to study the dynamic responses of a Spar FOWT. Bae, et al. [18] studied on the second order wave loads for mono-column-TLP type FOWT with integrated FAST-Charm3D. Peng, et al. [19] explored the environment conditions effects on the FOWT.

Larsen, et al.[20] reveal the “negative damping” effect, which is a special characteristic of the FOWT. However, until now there is no numerical simulation to demonstrate how the “negative damping” effects on the motions of a FOWT and the tensions in mooring lines.

The model tests were conducted by many researchers. Tests of 1/50 scale models for three generic floating wind turbine system were conducted in MARIN [21-27]. Many other experiments about FOWT were done all around the world [28-37].

2 DEVELOPMENT OF COUPLED SIMULATION CAPACITY FOR FOWT

A numerical code called COUPLE-FAST has been developed by this research for investigating the dynamics of a FOWT. The overview of the FOWT model in COUPLE-FAST is described in 2.1. In 2.2~2.5, several important numerical models are briefly described, such as the platform model, the aerodynamic model, the wind turbine model and the control system model. What described then are the coordinate systems in COUPLE-FAST and followed by the discussion about the coupling between COUPLE and FAST. The aerodynamic model, wind turbine model and control system model are adapted from FAST. They are only briefly introduced in this chapter for completeness. The details about the three FAST models are given in [38, 39].

2.1 Overview of FOWT Model of COUPLE-FAST

2.1.1 FOWT Model in COUPLE

One of the two major modules of COUPLE-FAST is COUPLE, which is initially developed for the computation of the interaction between a floating structure and its mooring line/riser/tendon system in time domain. It was developed and is continuously expanded and improved by Professor J. Zhang at Texas A&M University and his former and current graduate students [40-42].

In this research the FOWT and its mooring system are modeled by COUPLE module. The FOWT is modeled in COUPLE as a rigid body. The flexibility of tower and blades is neglected. The reference point is the center of gravity (COG) of the whole

FOWT system. The kinematics and kinetics of supporting platform at the reference point are simulated by COUPLE. The hydrodynamic forces, hydrostatic restoring forces, current forces, mooring forces and wind forces on the support platform are computed in the COUPLE module as well.

2.1.2 FOWT Model in FAST

The other major module of COUPLE-FAST is FAST, which is an open source code developed by NREL[1]. FAST is a comprehensive aero-elastic simulator capable of predicting both the extreme and fatigue loads of two- and three-bladed horizontal-axis wind turbines. In FAST the base of wind turbine can be a fixed foundation or a support floating platform. The aerodynamic forces on the wind turbines are calculated by FAST through the aerodynamic subroutine package, AeroDyn . The hydrodynamic forces, hydrostatic restoring forces and mooring forces can be generated by hydrodynamic package, HydroDyn, or input by user [11].

In this research the FOWT is modeled in FAST module as well, except the mooring system. Whether consider the tower or blades flexibility can be controlled by a user. The reference point for the FOWT kinematics and kinetics is at the COG of FOWT as in COUPLE. The aerodynamic forces are calculated with AeroDyn package[43]. Hydrodynamic forces are from COUPLE module and the HydroDyn package is not used in this research.

2.2 Support Platform Kinematics and Kinetics Modeling

In COUPLE-FAST, the kinematics and kinetics of the whole FOWT are calculated in the COUPLE module. The 6-DOF (Degree of Freedom) platform motion equation has the formation as **(2-1)**:

$$\left[\mathbf{M}_S + \mathbf{M}_a\right]\ddot{\mathbf{x}}(t) + \mathbf{B}\dot{\mathbf{x}}(t) + \mathbf{K}\mathbf{x}(t) = \mathbf{F} \qquad \textbf{(2-1)}$$

where, $\mathbf{M}_S$ is the mass matrix of the structure, $\mathbf{M}_a$ is the added mass matrix, $\mathbf{B}$ is the damping matrix, $\mathbf{K}$ is the stiffness matrix, $\mathbf{F}$ is the external force vector and $\mathbf{x}$ is the platform motion vector.

2.2.1 Wave Force in COUPLE-FAST

The external forces on the FOWT are divided into different sub-forces, such as: wave force, hydrostatic restoring force, buoyancy force, gravity force, mooring/riser/tendon system restoring force, current force, aerodynamic force, etc. Among all external forces, wave force is one of the most complicated in computation. It can be further divided into viscous part and potential part. In COUPLE-FAST, the viscous wave loads on structure are calculated based on the Morison Equation. The potential wave loads on a moored structure can be calculated based on either a diffraction/radiation wave theory, e.g. WAMIT, or the Morison Equation based on a slender body assumption.

In using a diffraction/radiation wave theory, the potential wave forces are solved numerically using a Boundary Element Method in the frequency domain. Forces obtained using this method include wave exciting force, radiation damping force and

added mass force. Wave drift damping force can be obtained using a heuristic formula without directly solving a second-order low-forward speed diffraction/radiation problem. All forces applied on the hull are calculated in frequency domain then transformed to time domain using the IFFT (Inverse Fast Fourier Transform) or convolution techniques [44].

When the ratio of wavelength to the diameter of a cylinder $\lambda/D>5$, Morison equation is a good approximation to simplify the computation of potential forces.

The hull of the FOWT studied in this research is more or less a small diameter cylinder in comparison with respect to typical wavelength. Morison equation is valid to compute wave and current loads on the hull. The derivations of motion equations incorporating with the use of Morison equation mainly follow Chen [44].

2.2.2 Wave Kinematics in COUPLE-FAST

Accurate wave kinematics is crucial to render accurate wave loads in the use of Morison equation. One of the unique characteristics of COUPLE-FAST is that the wave kinematics used in Morison Equation are computed by a nonlinear UHWM (Uni-direction Hybrid Wave Model) to reach fast convergence of a truncated wave solution for a wave field of a broad-banded wave spectrum [45].

UHWM considers nonlinear effects of wave-wave interactions on the resultant wave elevations, kinematics and pressure. In the model, only strong interactions (which are noticeable after the duration of about one dominant wave period) are considered while weak interactions are ignored [45]. Because of the purpose of predicting wave

properties in a short distance, like a few wave lengths of the dominant wave component, weak interactions are insignificant and can be neglected.

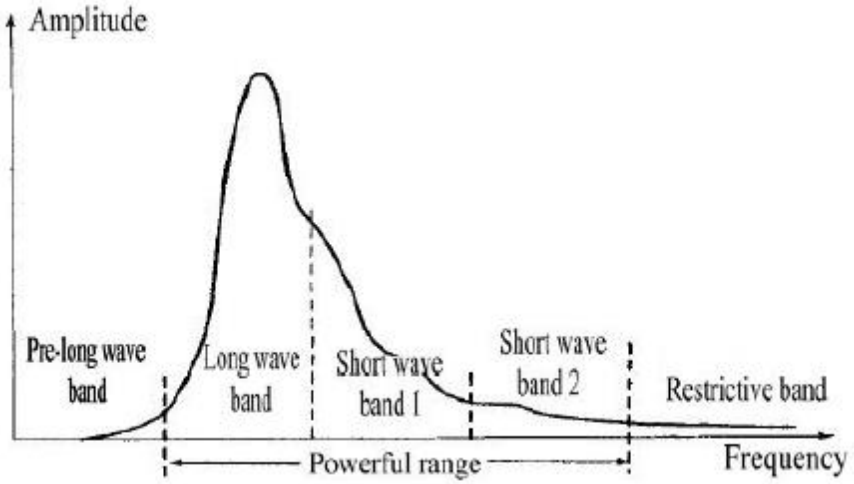

Figure 2-1 Sketch of JONSWAP Spectrum Band Division [41]

The JONSWAP (Joint North Sea Wave Project) spectrum is applied to simulate wave elevations in the UHWM and usually divided into three regions: a very low frequency region (pre-long wave band), a 'powerful' region and a very high frequency region (restrictive band), as shown in the Figure 2-1. Since the amplitude of the wave components located in the very low or high frequency regions are relatively small, and interactions involving wave components in either region are not significant which can be ignored for simplifying the computation. The 'powerful' region is further divided into three bands: the long-wave band, the short-wave band 1 and 2, as shown in Figure 2-1 [41].

The capital letter ‘H’ in the UHWM, stands for ‘hybrid’ which refers to selectively using the conventional perturbation and phase-modulation approach to address nonlinear interactions at the second order between two free-wave components based on their frequency ratios. The conventional perturbation approach is used for modeling interactions between two wave components with close frequencies (that means they are in the same frequency band) as depicted in Figure 2-1. The phase modulation approach is used for the interactions between two wave components of quite different frequencies, and in general they are located in different bands. It is known that the solution of interactions between two wave components with quite different frequencies using the conventional approach, when truncated at second order, may not converge because of the use of a linear phase function to describe the strongly modulated short-wave phase [46]. The subtraction of the nonlinear wave effects from the measured wave properties is conducted in the order from low to high frequency. Finally, the free-wave components are obtained by iteratively decoupling the free-wave components and their nonlinear interactions.

In using UHWM, when the simulation duration increases, the CPU time rises significantly. This is because the basic frequency in FFT (Fast Fourier Transform) decreases with increased duration ($\mathrm{df} = 1/\mathrm{T}$, where df is the basic frequency and T is the duration), which results in more free-wave components given a fixed cut-off frequency ($\mathrm{N} = \mathrm{f}_{cut}/\mathrm{df}$, where f_{cut} is the fixed cut-off frequency and N is the number of free-wave components) and in turn increases the calculation efforts for the linear wave computation and especially non-linear wave-wave interaction. To reduce the CPU time,

which is roughly proportion to N^3 [41], an attempt is made to divide continuous time series into several segments and inversely to decompose each of them into related wave amplitude spectra and initial phases. Therefore, reducing duration of each segment reduces the number of free wave components and hence the CPU time. Since the discontinuity due to Gibbs phenomenon occurs at the connection of two neighboring time-series segments, to avoid the discontinuity at the connection, an overlap time duration between two neighboring segments is required. It allows the simulation to stop at the middle of overlap duration which is before the end of the previous segment and start at the middle of overlap region which is after the beginning of the next segment. Therefore, the discontinuity at the connection is avoided [41]. Figure 2-2 shows the connection between the two neighboring segments.

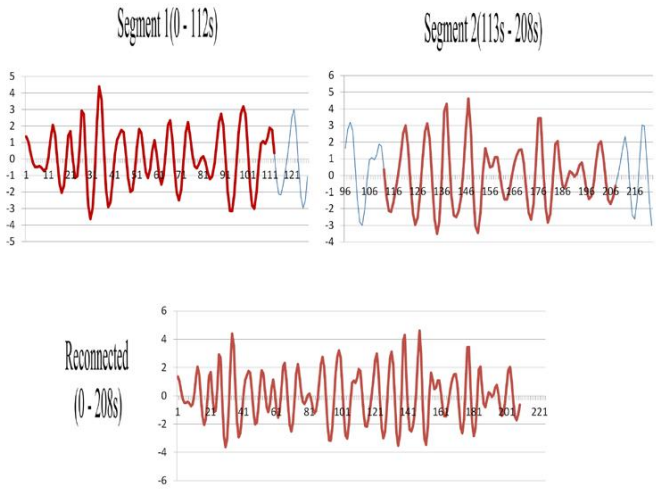

Figure 2-2 The Sketch of How to Connect the Two Neighboring Segments [41]

2.2.3 The Mooring System Model in COUPLE-FAST

The restoring force of the mooring system is another critical force applied on the FOWT. In COUPLE, two different types of the flexible rods (such as mooring lines and risers) are considered. One is the beam element for small extensible slender rods with bending stiffness and the other is the bar element for extensible mooring lines without bending stiffness. The Galerkin's method is used to discretize the dynamic equations in space, resulting in a set of nonlinear 2nd-order ordinary differential equations in the time domain. Finally a Newmark-β method is employed for the integration of the discretized equations in time-domain. The models are based on a FEM (Finite Element Method) and they can account for cable dynamics effects in the simulation. The model of a mooring system is also able to consider the concentrated mass and forces, connection between elements, bottom support and friction [44].

2.2.4 The Kinetics Model in COUPLE-FAST

As discussed above, The 6-DOF (Degree of Freedom) FOWT motion equation at the reference point is given in **(2-1)**.

Motion equations of a rigid body are coupled to dynamic equations of slender rods through hinged boundary conditions. Static coupling problem is solved by the Newton’s method. Dynamic coupling problem is solved by a Newmark-β integration scheme with an iterative procedure.

2.2.5 Numerical Implementation of Kinetics of FOWT

2.2.5.1 Static Coupling Problem

The static problem of kinetics of FOWT is solved in COUPLE module. At the initial position of the hull, the static equilibrium of the mooring/riser/tendon system is solved given the fairlead position, pretension or anchor position. Then mooring stiffness, $\frac{\partial \mathbf{F}_M}{\partial \mathbf{x}}$, is calculated at this initial position. It will be used for solving dynamic coupling problem.

2.2.6 Dynamic Coupling Problem in COUPLE Module

In general, 6-DOF nonlinear equations can be written in the form shown in **(2-2)**:

$$\tilde{\mathbf{A}}\ddot{\mathbf{x}}(t)+\tilde{\mathbf{B}}\dot{\mathbf{x}}(t)+\mathbf{C}\mathbf{x}(t)=\tilde{\mathbf{F}}_{other}(t)+\mathbf{F}_M(t) \quad \textbf{(2-2)}$$

where, $\mathbf{F}_M(t)$ represents mooring system forces and $\tilde{\mathbf{F}}_{other}(t)$ includes all other forces. Consequently, the motion equation at the time step (K) can be re-write in the form shown in **(2-3)**.

$$\tilde{\mathbf{A}}^{(K)}\ddot{\mathbf{x}}^{(K)}+\tilde{\mathbf{B}}^{(K)}\dot{\mathbf{x}}^{(K)}+\mathbf{C}^{(K)}\mathbf{x}^{(K)}=\tilde{\mathbf{F}}^{(K)}+\mathbf{F}_M{}^{(K)} \quad \textbf{(2-3)}$$

In a coupled dynamic analysis, the motion equations for the hull and dynamic equations for mooring lines/tendons/risers are solved almost simultaneously using the Newmark-β method.

2.3 Aero-Dynamic Model in COUPLE-FAST

In COUPLE-FAST, the aero-dynamic model is calculated by AeroDyn package in the FAST module. The AeroDyn package is briefly introduced below, for completeness, following [39].

AeroDyn calculates the aerodynamic lift, drag, and pitching moment of airfoil sections along a wind turbine blade. It is accomplished by first breaking each blade into a number of segments along the span of a blade. It then uses this information to calculate the various forces on each segment, which are used by the aeroelastic simulation program, such as FAST, to calculate the distributed forces on the turbine blades. The aerodynamic forces affect the turbine deflections and vice versa, making the interaction fully aeroelastic. AeroDyn models use relations based on two-dimensional localized flow, and the characteristics of the airfoils along the blade are represented typically by lift, drag, and pitching moment coefficients. The wind input allows a wide variety of atmospheric conditions: three-dimensional and time-varying atmospheric turbulence as well as discrete gusts or uniform and steady wind speeds.

Several different aerodynamic models are included in AeroDyn for a user to select. AeroDyn contains two wake models: the blade element momentum (BEM) theory and the generalized dynamic wake (GDW) theory. Both are used to calculate the axial induced velocities from the wake in the rotor plane.

BEM theory is implemented by dividing the blades of a wind turbine into many elements spanwise. As these elements rotate in the rotor plane, they trace out annular regions, across which the momentum balance takes place. BEM theory does have its

limitations. One primary assumption made in the theory is that the calculations are static; it is assumed that the airflow field around the airfoil is always in equilibrium and that the passing flow accelerates instantaneously to adjust to the changes in the vorticity in the wake. The BEM theory may not valid when the blades experience large deflections out of the rotor plane. Another limitation of BEM theory is based on the assumption that the forces acting on the blade element are essentially two-dimensional, meaning that spanwise flow is neglected.

The GDW method is based on a potential flow solution for Laplace's equation. The main advantages of the GDW over BEM include inherent modeling of the dynamic wake effect, tip losses, and skewed wake aerodynamics. Additional advantage of this method is that the induced velocities in the rotor plane are determined from a set of first-order differential equations, which can be solved using a non-iterative technique. One of the limitations of GDW model is that the generalized dynamic wake is developed for lightly loaded rotors and assumes that the induced velocities are small relative to the mean flow. AeroDyn currently switches to the BEM method when the mean wind speed is below 8 m/s. Another disadvantage of the GDW model is that it does not account for wake rotation. To correct for this, AeroDyn uses the BEM equation to calculate the tangential induction factor. Finally, the GDW method assumes that the rotor plane is a flat disk. Therefore, the effect of large aeroelastic deflections or significant coning of the rotor blades on the wake aerodynamics cannot be accurately calculated.

The aerodynamics calculations in AeroDyn are based on the pseudo two-dimensional properties of the local airfoil aerodynamics. The user has two options for

calculating the airfoil aerodynamics: static airfoil tables or a dynamic stall model. If the static airfoil tables are used, the aerodynamic performance of each airfoil is simply a table lookup of the data provided in the airfoil input file. If the user selects the dynamic stall option, the static airfoil coefficients are modified as a function of angle of attack and rate of change of angle of attack. [39]

In this research, the BEM theory and static airfoil are chosen for aerodynamic computation.

2.4 Wind Turbine Model in COUPLE-FAST

The FAST code is a nonlinear time-domain simulator that employs a combined modal- and multi-body dynamics formulation. FAST can model most common wind turbine configurations and control scenarios, including three-bladed turbines with a rigid hub, two-bladed turbines with a rigid or teetering hub, turbines with gearboxes or direct drives, turbines with induction generators or variable-speed controllers, turbines with active blade-pitch regulation or passive stall regulation, turbines with active or passive nacelle-yaw control, and turbines with passive rotor or tail furling. [11]

In FAST, flexibility in the blades and tower is characterized using a linear modal representation that assumes small deflections within each member. The flexibility characteristics of these members are determined by specifying distributed stiffness and mass properties along the span of the members, and by prescribing their mode shapes as equivalent polynomials. FAST allows for two flapwise and one edgewise bending-mode DOFs per blade and two fore-aft and two side-to-side bending-mode DOFs in the tower.

Along with one variable generator speed DOF, torsional flexibility in the drivetrain is modeled using a single-DOF equivalent linear-spring and -damper model in the low-speed shaft. The nacelle (or at least the load-bearing base plate of the nacelle) and hub are modeled in FAST as rigid bodies with appropriate lumped mass and inertia terms. All DOFs can be enabled or locked through switches, permitting one to easily increase or decrease the fidelity of the model. Time marching of the nonlinear equations of motion is performed using a constant-time-step Adams-Bashforth-Adams-Moulton predictor-corrector integration scheme. [11]

2.5 Control System Effects

The wind turbine control system is designed to maintain wind turbine dynamic stability and enhance performance under variable wind conditions [47]. Because it may cause the change in wind forces on the FOWT, the control system selected for the simulations in this research is discussed in 2.5.1, which is based on the control system designed for NREL 5MW wind turbine [38, 48]. The interaction between the blade control system and the FOWT motions is discussed in 2.5.2.

2.5.1 Control System of NREL 5MW Wind Turbine

In this research, a conventional variable-speed, variable blade-pitch-to-feather control system is used for the NREL 5-MW wind turbine installed on the OC3-Hywind Spar. The conventional approach relies on the two basic control systems: a generator-torque controller and a full-span rotor-collective blade-pitch controller.

The generator torque is computed as a tabulated function of the filtered generator speed. It is divided into different ranges based on its response with different generator speed as shown in Figure 2-3. Region 1 is a control region below the cut-in wind speed (3m/s), where the generator torque is zero and no power is extracted from the wind. Region 2 is a control region for optimizing power capture. In Region 3, wind speed is above the rated wind speed (11.4m/s) and the generator torque is held constant and the overloading of power may happen in this region [38, 48].

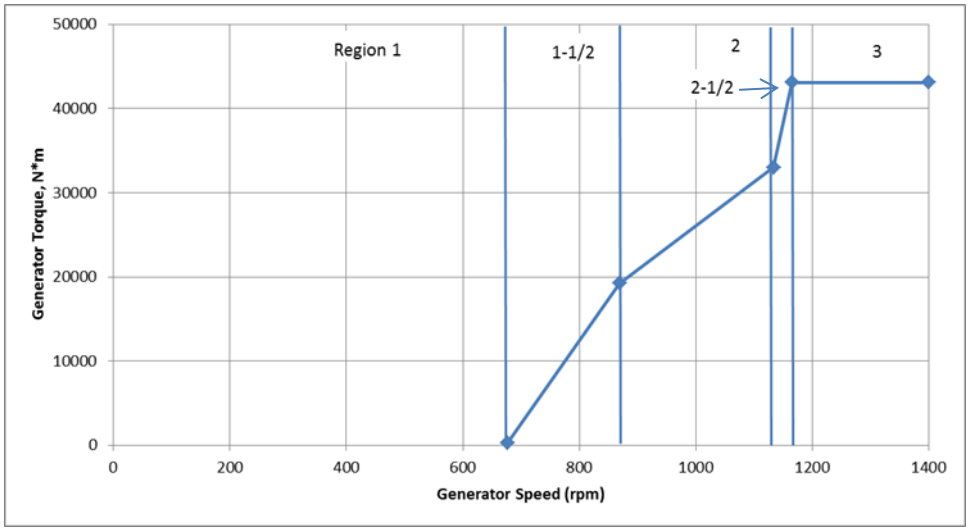

Figure 2-3 Generator Torque vs Generator Speed [38,48]

When the relative wind speed is lower than the rated wind speed (in Region 1, 1-1/2, 2, 2-1/2), the blade pitch angle remains the same. When the relative wind speed is above the rated wind speed (in Region 3), the blade pitch control system adjusts the blade pitch angle.

In the PI-based control system used by NREL 5-MW offshore wind turbine, the speed of blade pitch angle change is related to the speed of blade rotation, as shown in **(2-4)**:

$$\Delta\theta = K_P N\Delta\Omega + K_I \int_0^t N\Delta\Omega dt \quad \textbf{(2-4)}$$

where, K_P, K_I are the blade-pitch controller proportional and integral gains, respectively. They are preset functions of low-speed shaft (blade) rotational speed. N is the high-speed to low-speed gearbox ratio. Ω is the low-speed shaft rotational speed (blade rotational speed). $\Delta\theta$ is the speed of blade pitch angle change [38]. The natural frequency of the low-speed shaft rotation (blade rotation) is 0.20 rad/s [48].

The control system in this research is incorporated into dynamic link library (DLL), which is included in the FAST software module.

2.5.2 The Effects of Control System on FOWT Motions

Due to the surge and pitch motion of FOWT, the relative wind speed at the hub of a wind turbine (about 90m above still water level (SWL) in this research) may increase or decrease periodically, which may trigger the periodic change in blade pitch angle when the mean wind speed is above the rated wind speed. The interaction between the blade pitch angle change and the FOWT motion is qualitatively explored here.

When the relative wind speed at the hub is above the rated wind speed, the blade pitch control system may adjust the blade pitch angle based on the relative wind speed, which results in changes in the horizontal wind forces (to be further addressed in 3.3). Therefore, the FOWT translational and rotational responses are affected by the control system. On the other hand, the FOWT surge and pitch velocities change the relative

wind speed at the hub. As a result, they may enhance the interaction, or result in resonance. [20]

The speed of blade rotation is affected by the wind torques applied on the blades and it affects the speed of blade pitch angle change (as shown in **(2-4)**), which in turn can affect the wind forces. As discussed above, the blade pitch angle has interaction with the FOWT surge and pitch motion. As a result, the blade rotation, blade pitch angle, FOWT surge and pitch may interact among them.

2.6 Coordinate Systems in COUPLE-FAST

There are several coordinate systems used to describe the motions of the FOWT in the code of COUPLE-FAST, such as Space-fixed Coordinate System (CS), Body-fixed CS and Global Reference CS. They are defined below.

The Space-fixed CS is used in both of COUPLE module and FAST module (which is called Inertial Frame CS in FAST). This CS is fixed in space and denoted by $\widehat{O}\widehat{X}\widehat{Y}\widehat{Z}$ in this research. The origin (reference point) $\widehat{O}$ is located at COG of the FOWT. The positive $\widehat{X}$-axis is in the downwind direction. (FAST defines $\widehat{X}$-axis pointing in the wind direction). The $\widehat{X}\widehat{O}\widehat{Y}$ plane parallels to the still water level (SWL) and the $\widehat{Z}$-axis is positive upwards.

The Body-fixed CS is only used in COUPLE module. This CS is fixed on the floating structure, i.e. the Spar in our study. When the FOWT is at its initial position, the Body-fixed CS coincides with the Space-fixed CS. The moments applied on FOWT in COUPLE module are calculated in the Body-fixed CS. This CS is denoted as OXYZ

The motions between Body-fixed CS and the Space-fixed CS are related by a transform matrix T as shown in **(2-5)** and **(2-6)**.

$$\{\hat{\mathbf{X}}\} = \{\hat{\boldsymbol{\varepsilon}}\} + [\mathbf{T}]\{\mathbf{X}\} \quad \textbf{(2-5)}$$

where,

$$[\mathbf{T}] = \begin{bmatrix} \cos\alpha_3\cos\alpha_2 & -\sin\alpha_3\cos\alpha_2 & \sin\alpha_2 \\ \sin\alpha_3\cos\alpha_1 + \cos\alpha_3\sin\alpha_2\sin\alpha_1 & \cos\alpha_3\cos\alpha_1 - \sin\alpha_3\sin\alpha_2\sin\alpha_1 & -\cos\alpha_2\sin\alpha_1 \\ \sin\alpha_3\sin\alpha_1 - \cos\alpha_3\sin\alpha_2\cos\alpha_1 & \cos\alpha_3\sin\alpha_1 + \sin\alpha_3\sin\alpha_2\cos\alpha_1 & \cos\alpha_2\cos\alpha_1 \end{bmatrix} \textbf{(2-6)}$$

where, α_1, α_2, α_3 are roll, pitch and yaw angle in Space-fixed CS, respectively. $\{\hat{\mathbf{X}}\}$ is the translation motions in Space-fixed CS. {**X**} is the coordinates of the points in Body-fixed CS. $\{\hat{\boldsymbol{\epsilon}}\}$ is the translation motion of the origin of Body-fixed CS in Space-fixed CS.

Due to the definition ($\hat{X}$-axis and the wind direction) made in FAST, the Space-fixed CS used in COUPLE-FAST depends on the wind direction. However, many other parameters are independent of wind direction, such as the mooring lines layout, the hull orientation, wave/current direction, etc. Therefore another CS is introduced in COUPLE-FAST. This CS is also fixed in space. Its axes are obtained from rotating the $\hat{X}$ and $\hat{Y}$ axes of Space-fixed CS around the $\hat{Z}$ axis of Space-fixed CS by an angle. We name this CS as Global Reference CS and denoted it by $\dot{O}\dot{X}\dot{Y}\dot{Z}$. The origin $\dot{O}$ of the Global Reference CS coincides with the origin $\hat{O}$ of the Space-fixed CS. That means the angle between $\dot{X}$-axis of Global Reference CS and the True North is fixed and independent of the wind direction, while $\hat{X}$ in the space-fixed CS always points in the wind direction.

In preparing the input data, including the environment data (wind, wave, current, etc.), FOWT model and the mooring lines layout, damping/stiffness matrix, etc., they are initially all expressed in the Global Reference CS. After the data is input into COUPLE-

FAST program, all of the data expressed in the Global Reference CS are converted these in the Space-fixed CS through rotating the data by an angle $\dot{\theta}_{wi}$ around the $\dot{Z}$ axis.

The transformation matrix expression used to convert vectors between Global Reference CS and Space-fixed CS is shown in **(2-7)** and **(2-8)**.

$$\{\hat{\mathbf{X}}\} = [\mathbf{R}]\{\dot{\mathbf{X}}\} \tag{2-7}$$

where,

$$[\mathbf{R}] = \begin{bmatrix} \cos\dot{\theta}_{wi} & -\sin\dot{\theta}_{wi} & 0 \\ \sin\dot{\theta}_{wi} & \cos\dot{\theta}_{wi} & 0 \\ 0 & 0 & 1 \end{bmatrix} \tag{2-8}$$

and $\dot{\theta}_{wi}$ is the direction of wind in Global Reference CS.

The conversion of a matrix from Global Reference CS to the Space-fixed CS is given by **(2-9)**.

$$[\hat{\mathbf{X}}] = [\mathbf{R}][\dot{\mathbf{X}}][\mathbf{R}]^{-1} \tag{2-9}$$

If there is no pitch of the FOWT, the three coordinates are sketched in Figure 2-4. If the FOWT pitches at a small angle, the coordinates are shown in Figure 2-5. Here, 0XYZ is the Body-fixed CS; $\hat{0}\hat{X}\hat{Y}\hat{Z}$ is the Space-fixed CS; $\dot{0}\dot{X}\dot{Y}\dot{Z}$ is the Global Reference CS.

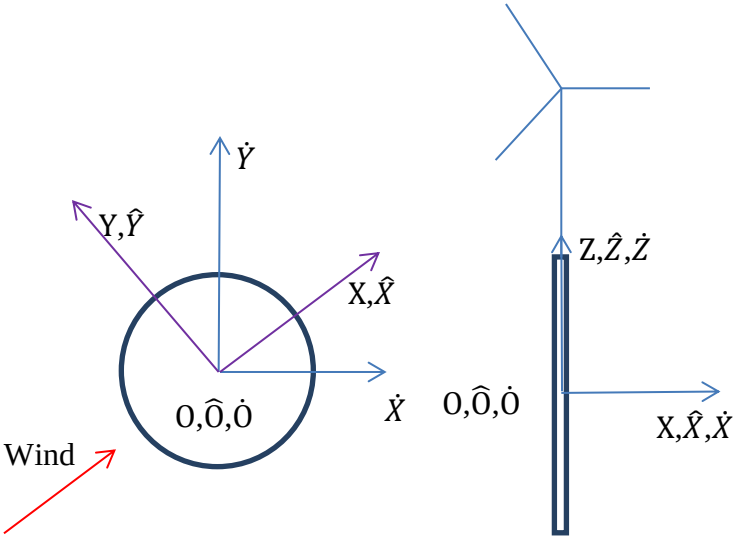

Figure 2-4 View of CS, without Rotation

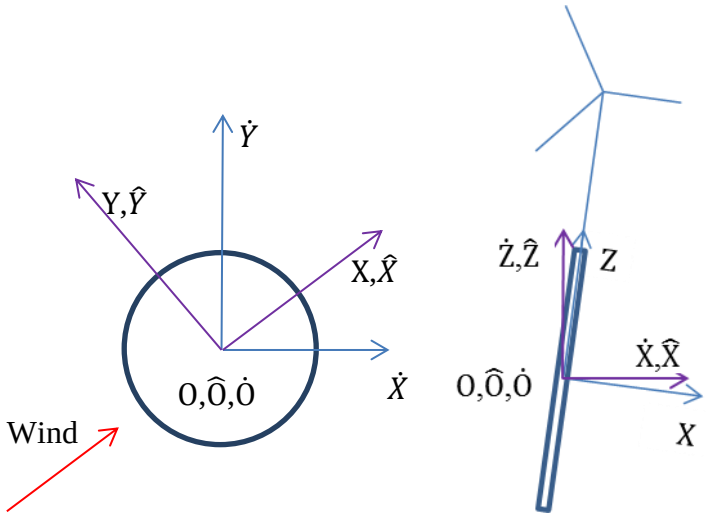

Figure 2-5 View of CS, with Rotation

2.7 Coupling of the Two Codes: FAST and COUPLE

In modeling the FOWT using FAST and COUPLE codes, it is noted that there are differences between the two codes. These differences should be taken care of before they can be linked. In FAST, the platform is considered as a rigid body, while the tower of the wind turbine may allow the fore-aft and side-side flexibilities. On the contrast, COUPLE considers the whole FOWT as a rigid body. That means although the motions at the reference point (the COG of the whole FOWT) are the same, the two modules will predict different motions of the tower, which may result in different inertial forces. In FAST, the tower base forces include the effect from the flexible inertial forces of tower/rotor/blade and the aerodynamic forces on blades. While in COUPLE, the tower/rotor/blade inertial forces are predicted as if they are a rigid body based on the predicted accelerations. Therefore, correction of the tower bases forces applied on the platform must be made when transferring the tower base forces calculated by FAST into COUPLE to account for the different predicted accelerations or inertial forces.

As mentioned earlier, the numerical integration used for the dynamic simulation in COUPLE module is Newmark-β method, while, the 4th order Runge-Kutta method and Adams-Bashforth-Moulton predictor-corrector method are used in FAST.

The responses of the support floating platform have much lower natural frequencies than those of the tower. Also, the mooring and wave forces change slowly in time in comparison with respect to the turbulence wind forces applied on the wind turbine. Hence, it is possible to update the responses of the support floating platform and

the forces on it only once in COUPLE while there are the several steps in FAST. In this way the CPU time can be reduced significantly.

To minimize the revision made on the existing codes, the following efforts are made to match the two codes correctly.

1. Initially, the 4th order Runger-Kutta method is used in FAST
    a. FAST predicts the initial positions of the reference point (COG of the FOWT) of all 6 DOF in the absence of wind, wave and current.
    b. Transferring the initial positions of the reference point to COUPLE.
    c. Conducting static analysis in COUPLE and calculating the mooring forces, hydrostatic forces, etc. applied on the platform.
    d. Transferring those forces into FAST.
2. If step≤3, the 4th order Runger-Kutta method is used in FAST. If step>3, the Adams-Bashforth-Moulton predict-correct method is used instead.
    a. FAST calculates the aerodynamics and tower/rotor/blade responses. It also predicts the displacements, velocities and accelerations for all 6 DOF of the reference point. At the same time, it computes the reaction forces applied at the tower base.
    b. In general, for every five steps ($\Delta t_f = 0.01s$) run in FAST, correspondingly, there is one step run in COUPLE ($\Delta t_c = 0.05s$). When running each step in COUPLE, the following computation is made.

i. COUPLE calculates the inertial forces of the tower/rotor/blade, where it is based on the assumption of the rigid body accelerations predicted in COUPLE.

ii. The inertial forces from COUPLE are subtracted from the inertial forces obtained at the tower base forces predicted by FAST. The difference represents the force difference between that predicted in FAST which considers the flexibility of the tower and blades and that predicted in COUPLE which considers the whole FOWT as a rigid body.

iii. Then it transfers the corrected force at the tower base into COUPLE.

iv. It conducts dynamic simulations in COUPLE and calculates the FOWT displacements, velocities, accelerations. In doing so, the related forces, such as wave force, mooring force, hydrostatic restoring force, current force, applied on FOWT are calculated in COUPLE.

v. Finally it transfers the FOWT displacements, velocities, accelerations and the applied forces in COUPLE back into FAST.

c. For every five steps running in FAST, there is one step run in COUPLE. When there is no update step run in COUPLE,

i. The external forces calculated in COUPLE remain the same. That is, they are also kept same in these time steps run in FAST.

d. FAST corrects the FOWT motion responses and comes to the next time step.

The flow chart of the numerical scheme is depicted in Figure 2-6.

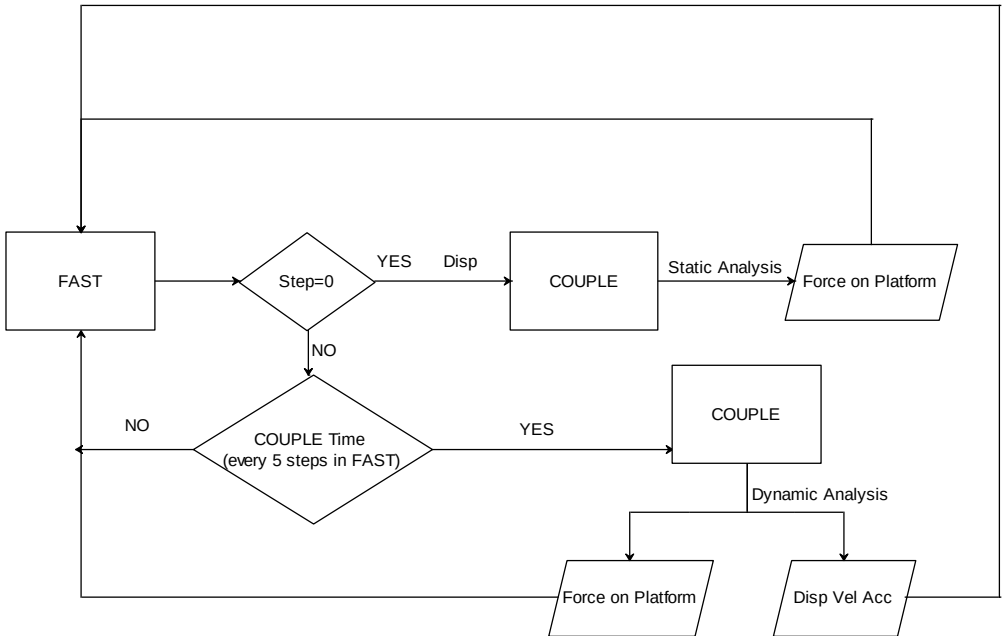

Figure 2-6 Progress Flow Chart of COUPLE-FAST

2.7.1 Communication between COUPLE Module and FAST Module

To investigate the fully coupled response of the FOWT, a numerical code called COUPLE-FAST is developed by combining two existing codes: COUPLE and FAST to take advantage of the merits of the two codes. Generally speaking, the COUPLE is used to calculate the external loads on the support floating platform and the motion responses of it; while the FAST is used to calculate the aerodynamic loads and responses of the wind turbine.

To execute the fully coupled analysis with the COUPLE-FAST program, data needs to be transferred between the two modules. The simplified flow chart describing data transfer is plotted in Figure 2-7.

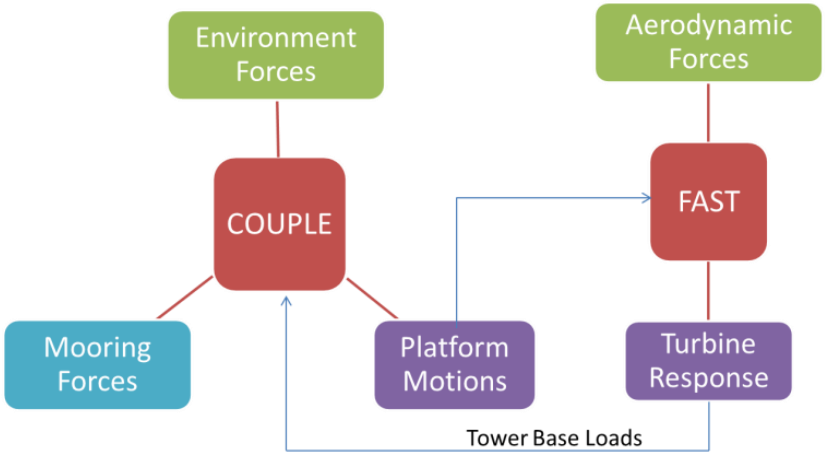

Figure 2-7 Data Transfer Flow Chart of COUPLE-FAST

At each time step, given the displacements, velocities and accelerations at the reference point of the floating platform which is predicted and provided by COUPLE, the aerodynamic forces and the tower/blade/generator responses are calculated using FAST. Then the aerodynamic forces are calculated by FAST, and the reaction loads at the tower base (after making correction on the inertial forces) are transferred into COUPLE. In COUPLE, the wave, wind, current and mooring line forces on the supporting platform are calculated. The motion responses of FOWT at the reference point are predicted together with the corrected reaction loads at the tower base applied by the wind turbine. In this way, the COUPLE takes the consideration of aerodynamics

and the wind turbine flexibility. Finally, at the next step, the platform's displacements, velocities and accelerations at the reference point, as well as the loads calculated on the platform using COUPLE module, are transferred back into FAST. Through this method, the wind turbine and the support floating platform responses are coupled together.

It should be noted that FAST has the user input module to input forces into user defined routine and solve the platform motions/velocities/accelerations in FAST. The reasons for "transfer motions into FAST and transfer forces into COUPLE" in our study are given below:

1. The mass of wind turbine is much smaller than that of the floating platform. Consequently, the total motion determined by the platform in COUPLE is more accurate.
2. The COUPLE has internal iterations to minimize the error, and hence it may provide better results.
3. The mooring line loads are nonlinear to the platform motion. The FEM is used in COUPLE and it is much more accurate than the quasi-static mooring line model, used in HydroDyn module of FAST.

3 BASICS OF THE FOWT AND CONVERGENCE OF THE SIMULATION

3.1 FOWT Particulars

The FOWT considered in our simulation consists of the NREL offshore 5-MW baseline wind turbine and OC3-Hywind Spar support floating platform. The NREL offshore 5-MW turbine is a conventional three-bladed, upwind variable-speed, and variable blade-pitch-to-feather-controlled turbine. Its characteristics are summarized in Table 3-1 [38]. The OC3-Hywind Spar support floating platform is a classic Spar platform and its dimensions are described in Table 3-2 [48].

Table 3-1 Turbine Properties

Rating	5 MW
Rotor orientation, configuration	Upwind, 3 blades
Rotor / hub diameter	126 m / 3 m
Hub height above SWL	90 m
Cut-in / rated wind speed	3 m/s / 11.4 m/s
Cut-in / rated rotor speed	6.9 rpm / 12.1 rpm
Rotor / nacelle / tower mass	110,000 kg / 240,000 kg / 249,718 kg

Table 3-2 Platform Properties

Depth to platform base below SWL (draft)	120 m
Elevation to platform top (tower base) above SWL	10 m
Depth to top / bottom of taper below SWL	4 m / 12 m
Platform diameter above / below taper	6.5 m / 9.4 m
Platform mass, including ballast	7,466,330 kg
COG below SWL (Spar only / Spar and the wind turbine)	89.9 m / 78.0 m

Table 3-2 Continued

Platform roll & pitch inertia about platform COG	4,229,230,000 kg•m^2
Platform yaw inertia about platform centerline	164,230,000 kg•m^2

To simplify the simulation of the mooring system specified in the OC3-Hywind Spar, some simplifications are made. First, a hinge connection at the fairlead of each mooring line is used to replace the delta connections. Second, a homogenous line with the equivalent wet weight and stiffness is used instead of a mooring line consisting of the multiple segments of different wet weights. The properties of the mooring system are given in Table 3-3 [48].

Table 3-3 Mooring Line Properties

Number of mooring lines	3
Angle between adjacent lines	120 º
Depth to anchors below SWL (water depth)	320 m
Depth to fairleads below SWL	70.0 m
Radius to anchors from platform centerline	853.87 m
Radius to fairleads from platform centerline	5.2 m
Line mass density	77.71 kg/m
Line extensional stiffness	3.842e8 N

The layout of the mooring lines and the wind direction are depicted in Figure 3-1. More detailed information about the NREL 5 MW wind turbine and OC3-Hywind Spar can be found in related references [48]. The ȮẊẎŻ CS shown in Figure 3-1 is the Global Reference CS, which is independent of the wind.

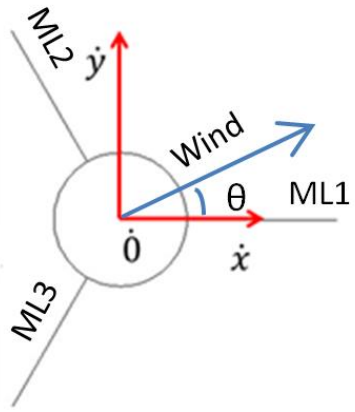

Figure 3-1 Mooring Lines Layout and the Wind Direction

Since the hull of OC3-Hywind Spar is virtually a vertical cylinder with relatively small diameter ($\leq$ 9.4m), the Morison Equation is valid for the computation of the potential wave forces, in addition to the drag and lifting forces. The in-line added-mass and drag coefficients of the Spar used in the Morison Equation are listed in Table 3-4. Also listed in the table are the vertical direction drag and added mass coefficients applied near the bottom of the Spar and the added-mass and drag coefficients for mooring lines.

Table 3-4 Hydrodynamic Coefficients

Added-mass / drag coefficient of Spar	0.97 / 0.6
Vertical added-mass / drag coefficient of Spar at the bottom	0.0 / 3.0
Lifting coefficient of Spar	0.45
Additional damping in surge and sway	10^5 N/(rad/s)
Additional damping in heave	$1.3\text{x}10^5$ N/(rad/s)
Additional damping in yaw	$1.3\text{x}10^7$ Nm/(rad/s)
Additional stiffness in yaw	$9.8\text{x}10^7$ Nm/rad

Table 3-4 Continued

Normal added-mass / drag coefficient of mooring lines	2.00 / 2.45

3.2 Convergence Tests for Time Step

It's known that the size of time step used in the simulation may determine whether or not the simulation converges. To make sure that the size of time steps used in the simulation is appropriate, two different time steps, 0.05s and 0.01s, are used in COUPLE module for the 11.4 m/s turbulent wind only cases. The time step in FAST module is kept 0.01s for both cases. The simulated results are compared in Figure 3-2. The blue solid lines represent the results in the case of 0.01s time step (in Couple); while the red dash lines represent the results in the case of 0.05s time step (in Couple).

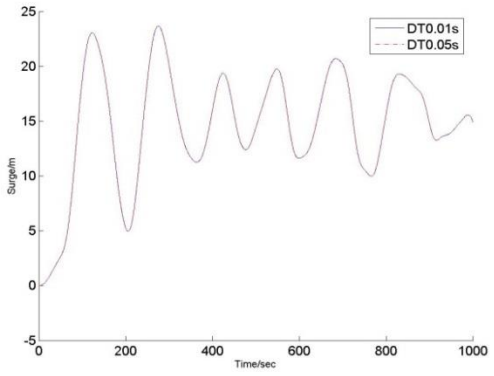

a) Surge Comparison

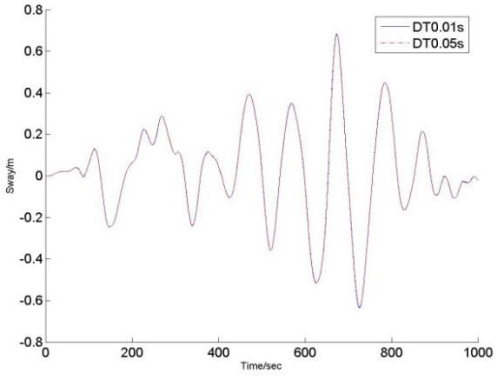

b) Sway Comparison

Figure 3-2 Motion Comparison between Different Time Steps

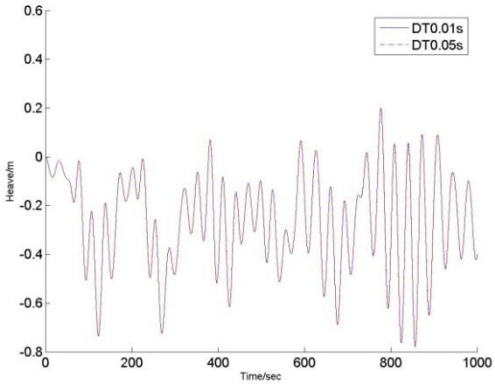

c) Heave Comparison

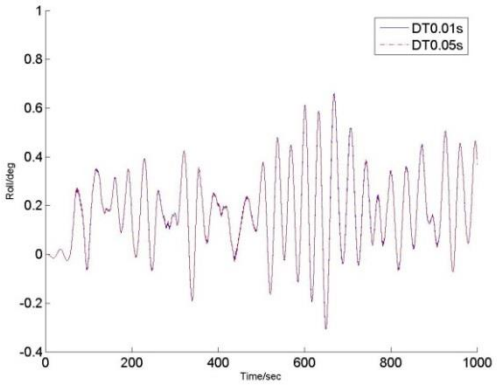

d) Roll Comparison

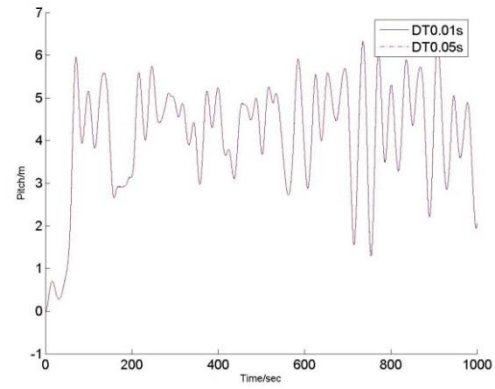

e) Pitch Comparison

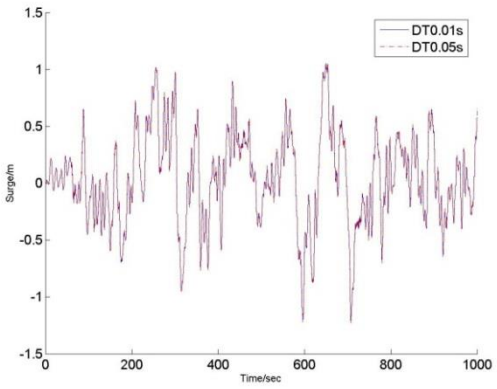

f) Yaw Comparison

Figure 3-2 Continued

The comparisons show that the differences in all 6 DOF motions simulated respectively using two different time steps are negligible. Therefore, the 0.05s time step (in Couple) is used in the remaining simulation.

3.3 Relationship between Wind Speed, Blade Pitch Angle and Wind Force

When the relative wind speed at the hub is higher than the rated wind speed (11.4m/s), the control system of the NREL 5MW wind turbine increases the blade pitch

angle with the increase in relative wind speed, as described in Section 2.5. Therefore, the attack angle of wind at each blade is changed, which affects the drag force (in the axial direction of hub) and lift force (the driven torque to drive for the wind turbine shaft (blades) rotation). The transverse force on tower base is related to the blade rotation, which is affected by the relative wind speed as well. The relationships between the relative wind speed, the wind drag force, the blade pitch angle, the transverse force on tower base are depicted in Figure 3-3. The data is obtained from 500s simulation for a NREL 5MW wind turbine with a fixed foundation with uniform and steady winds. As shown in Figure 3-3 a) and c), with increase in wind speed the mean wind drag force and mean tower base transverse force increase when the wind speed is below the rated wind speed (11.4m/s) and decrease when the wind speed is above the rated wind speed. At the same time, as shown in Figure 3-3 b), with increase in wind speed the blade pitch angle keeps at zero when the wind speed is below the rated wind speed and increases when the wind speed is above the rated wind speed. The dynamic tower base transverse force has a major trend that it approximately increases with increase in relative wind speed, as shown in Figure 3-3 d).

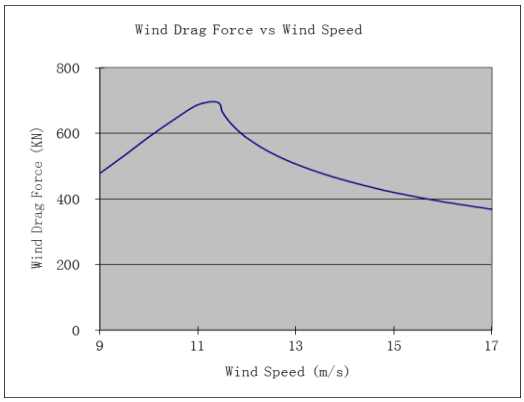

a) Relative Wind Speed vs Mean Wind Drag Force

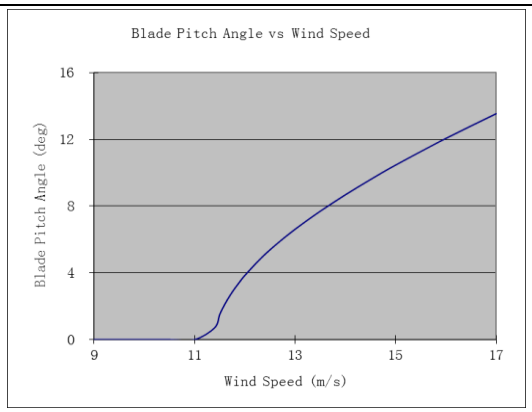

b) Relative Wind Speed vs Mean Blade Pitch Angle

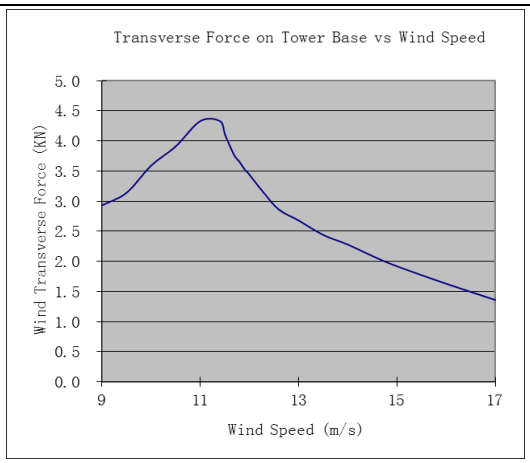

c) Relative Wind Speed vs Mean Transverse Force on Tower Base

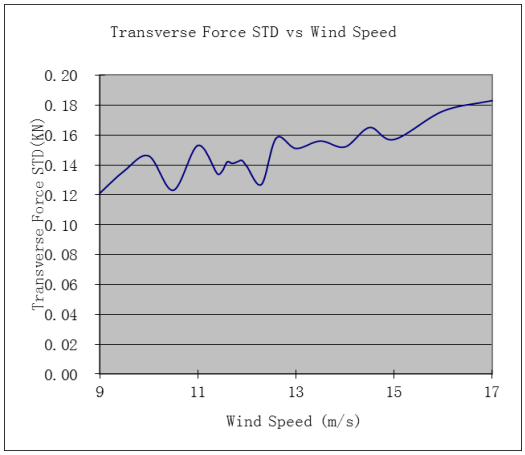

d) Relative Wind Speed vs Tower Base Dynamic Transverse Force STD

Figure 3-3 Wind Speed Effect on Wind Force and Blade Pitch Angle

3.4 Free Decay and Natural Periods of FOWT

The natural periods of the FOWT are determined based on the related free-decay simulations. In the first 100s simulation, the related force is gradually applied on the FOWT. Then the related forces applied on the FOWT disappear and it freely vibrates. The natural periods are obtained by averaging the first five cycles in the free-decay

vibrations and they are listed in Table 3-5. The results are close to the previous studies [13].

Table 3-5 Natural Periods of OC3-Hywind FOWT

DOF	Surge	Sway	Heave	Roll	Pitch	Yaw
Our Simulation	127.8s (0.05rad/s)	129.4s (0.05rad/s)	30.8s (0.21rad/s)	31.0s (0.20rad/s)	31.0s (0.20rad/s)	8.2s (0.77rad/s)
From [13]	0.05rad/s	0.05rad/s	0.20rad/s	0.22rad/s	0.22rad/s	0.71rad/s

3.5 Mooring Restoring Force Curves

The mooring restoring force vs the offsets curves are obtained by sequentially moving FOWT in a given direction and calculating the mooring forces at different positions. The mooring restoring curves for offsets in multiple directions (with respect to Global Reference CS) are shown in Figure 3-4. The cyan line is for 0 deg offset, the blue line 30 deg offset; the pink line 60 deg offset. The mooring stiffness is the slope of the restoring force curve. It is known from Figure 3-4 that 1) the mooring stiffness increases with increase in offset. 2) The 60 deg positive offset generates the largest stiffness. In this condition one of the mooring lines, ML3, is tightened and the other two lines are slack. 3) The 0 deg positive offset generates the smallest stiffness. In this condition one of the mooring lines, ML1, is slack and the other two lines are tightened.

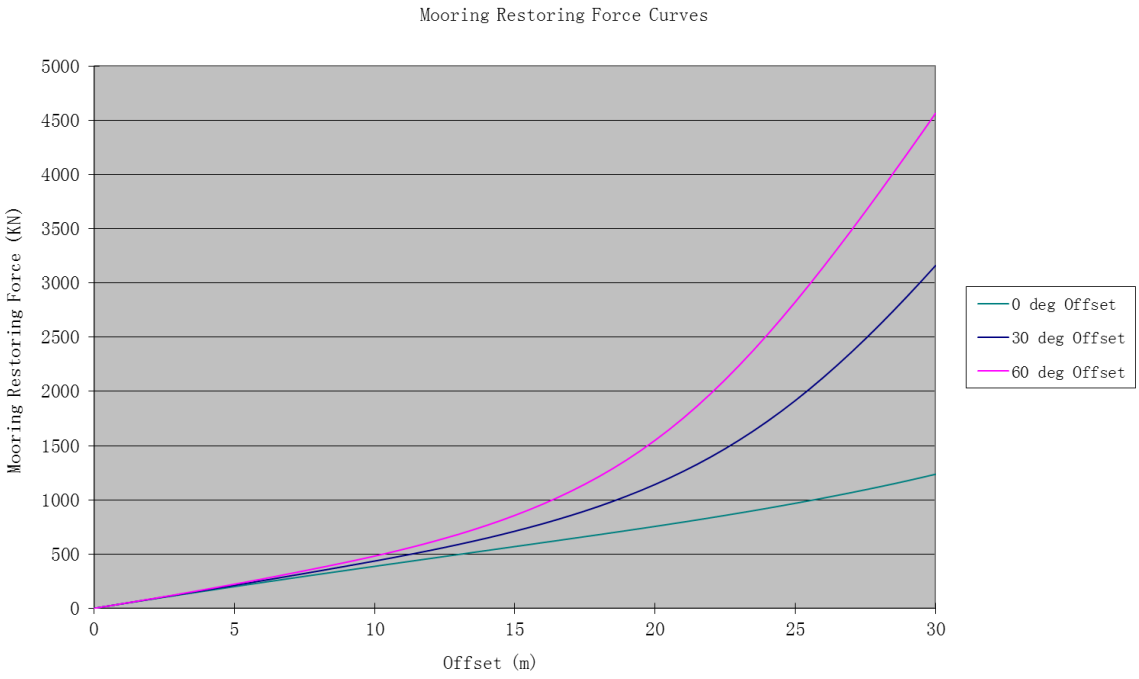

Figure 3-4 Mooring Restoring Force Curves for Offsets in Multiple Directions

3.6 Matrix of Simulated Cases

In this research, different cases are investigated for understanding the responses of the FOWT. These cases are categorized into four groups:

1. Uniform and steady wind only (case 1~3)
2. Turbulent wind only (case 4~13)
3. Turbulent wind and wave (case 14~21)
4. Turbulent wind, wave and current (case 22~25).

The details of those cases are listed in Table 3-6. For all cases, in the first 100s of the simulation, the environment forces are tampered with a ramp function, as shown in (3-1) to avoid the large sudden change in forces at the beginning.

$$\mathbf{F}_{ramp} = \mathbf{F} * \frac{1}{2}\left[1 - cos\left(\frac{t}{T_{ramp}}\pi\right)\right] \quad \textbf{(3-1)}$$

where, $\mathbf{F}$ is the external forces applied on the platform; $\mathbf{F}_{ramp}$ is the actural external forces applied on platform; t is the time; T_{ramp} is the total ramping time, which is 100s used in this research.

The JONSWAP wave spectrum with a shape factor as 3.3 is used to simulate irregular waves. For uniform and steady wind only cases, data between 300s and 1800s is used for post process. For other cases, data between 300s and 3300s is used.

Table 3-6 Case Matrix

Case Category	Case No.	Environment Heading			Wind Type	Wind Speed	JONSWAP Wave	
		Wind	Wave	Current			Hs	Tp
		(deg)				(m/s)	(m)	(s)
Uniform and Steady Wind Only	1	0	N/A	N/A	Uniform	11.4	N/A	N/A
	2	0	N/A	N/A	Uniform	11.6	N/A	N/A
	3	0	N/A	N/A	Uniform	12	N/A	N/A
Turbulent Wind Only	4	0	N/A	N/A	Turb	8	N/A	N/A
	5	0	N/A	N/A	Turb	11.4	N/A	N/A
	6	0	N/A	N/A	Turb	11.6	N/A	N/A
	7	0	N/A	N/A	Turb	17	N/A	N/A
	8	30	N/A	N/A	Turb	11.4	N/A	N/A
	9	60	N/A	N/A	Turb	11.4	N/A	N/A
	10	90	N/A	N/A	Turb	11.4	N/A	N/A
	11	120	N/A	N/A	Turb	11.4	N/A	N/A
	12	150	N/A	N/A	Turb	11.4	N/A	N/A
	13	180	N/A	N/A	Turb	11.4	N/A	N/A
Turbulent Wind and Wave	14	0	0	N/A	Turb	8	2	7.5
	15	0	0	N/A	Turb	11.4	6	10

Table 3-6 Continued

Case Category	Case No.	Environment Heading			Wind Type	Wind Speed	JONSWAP Wave	
		Wind	Wave	Current			Hs	Tp
		(deg)				(m/s)	(m)	(s)
Turbulent Wind and Wave	16	0	0	N/A	Turb	17	10.5	14.3
	17	0	0	N/A	Turb	11.4	10.5	14.3
	18	0	0	N/A	Turb	0	10.5	14.3
	19	0	30	N/A	Turb	11.4	6	10
	20	0	60	N/A	Turb	11.4	6	10
	21	0	90	N/A	Turb	11.4	6	10
Turbulent Wind, Wave and Current	22	0	0	0	Turb	11.4	6	10
	23	30	30	30	Turb	11.4	6	10
	24	60	60	60	Turb	11.4	6	10
	25	90	90	90	Turb	11.4	6	10

4 INVESTIGATION ON FOWT RESPONSES

4.1 The Responses of the FOWT under the Impact of Wind

The FOWT responses are highly related to the wind. Because the FOWT has a tall tower, the center of wind pressure is far above the SWL, which results in a large wind induced moment making the FOWT tilt (pitch) in the direction of the wind. Furthermore, the horizontal force induced by wind increases the FOWT offset in the wind direction and affects the mooring line tension. The control system adjusts the blade pitch angle and then affects the wind forces when the relative wind speed is higher than rated wind speed. The responses of the FOWT due to wind in the absence of wave and current will be investigated first.

4.1.1 The Responses of the FOWT under the Impact of Uniform and Steady Wind Only Conditions

As shown in Table 3-6, Case 1~3 consider uniform and steady wind only cases. In these cases, it is assumed that the FOWT encounters uniform and steady wind blowing in 0 deg direction during all three cases. However, the FOWT may oscillate under the combined effects of restoring forces and wind forces, and hence the relative wind velocity may not be steady.

There are three different wind speeds considered in Case 1~3, they are 11.4m/s (rated wind speed), 11.6m/s (a little higher than rated wind speed) and 12m/s (higher than rated wind speed), respectively. The comparisons of the surge, pitch and blade pitch

angle responses with different wind speeds are shown in Figure 4-1 ~ Figure 4-3, respectively. Since the wind is in 0 deg direction, the sway, heave, roll and yaw responses are insignificant and omitted for brevity.

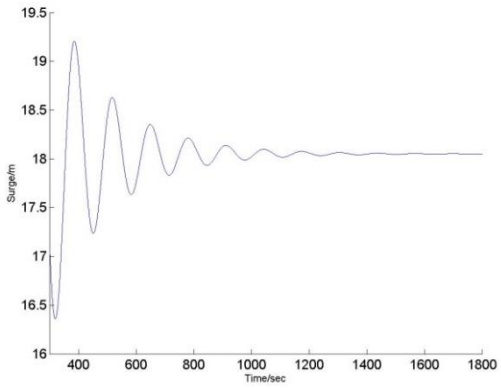

a) Surge Due to 11.4m/s Wind

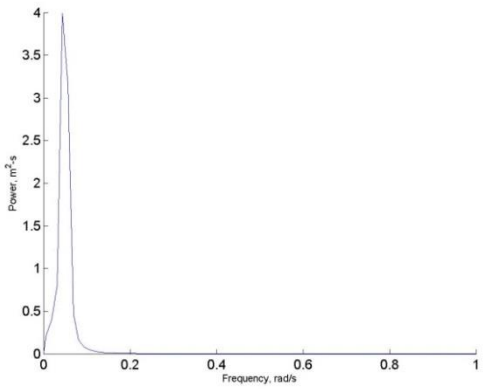

b) Surge Power Spectrum Density (PSD) Due to 11.4m/s Wind

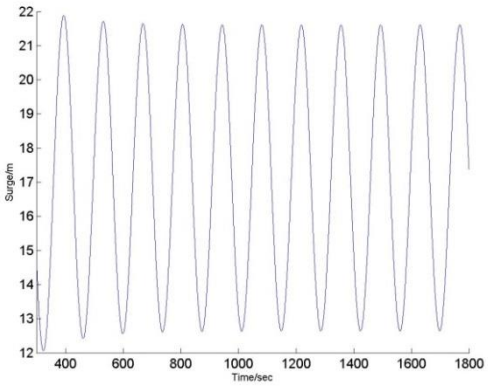

c) Surge Due to 11.6m/s Wind

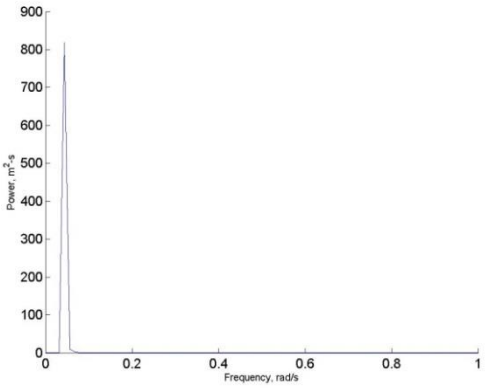

d) Surge PSD Due to 11.6m/s Wind

Figure 4-1 Surge Responses Comparison for Different Uniform and Steady Wind Speeds

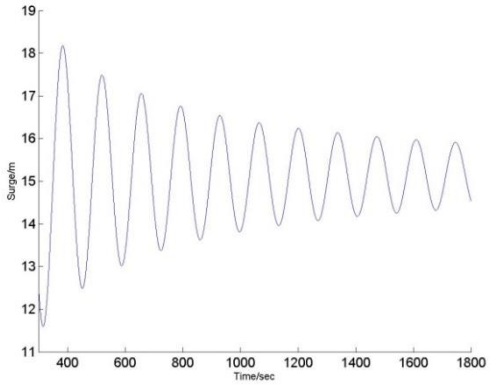

e) Surge Due to 12m/s Wind

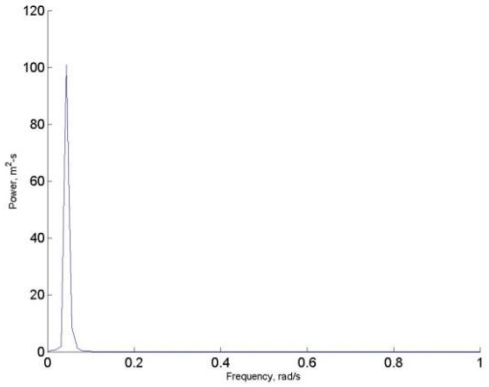

f) Surge PSD Due to 12m/s Wind

Figure 4-1 Continued

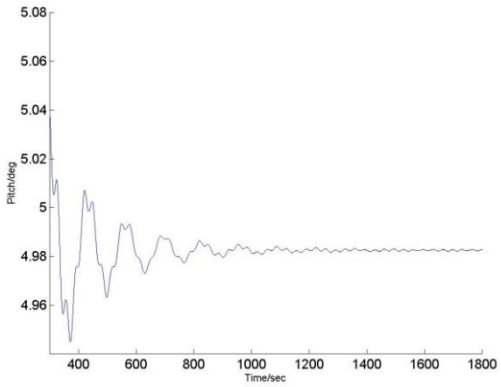

a) Pitch Due to 11.4m/s Wind

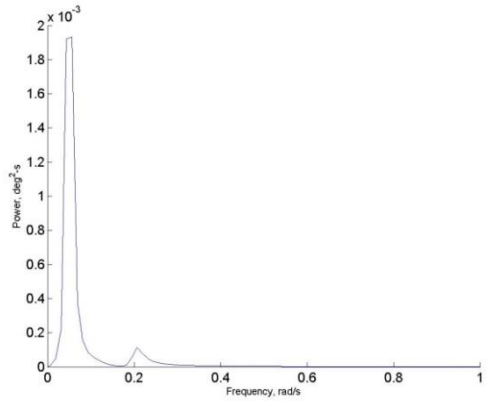

b) Pitch PSD Due to 11.4m/s Wind

Figure 4-2 Pitch Responses Comparison for Different Uniform and Steady Wind Speeds

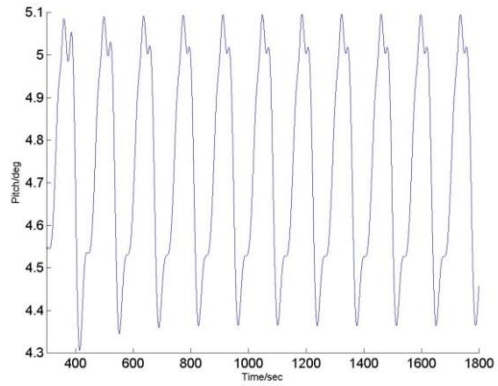

c) Pitch Due to 11.6m/s Wind

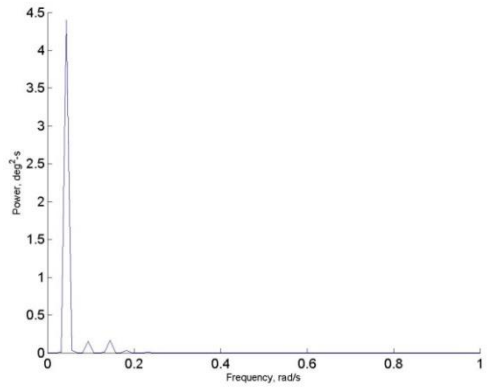

d) Pitch PSD Due to 11.6m/s Wind

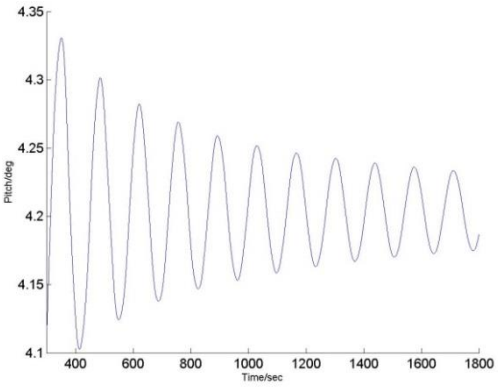

e) Pitch Due to 12m/s Wind

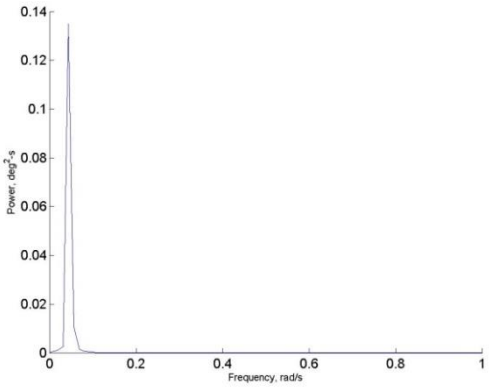

f) Pitch PSD Due to 12m/s Wind

Figure 4-2 Continued

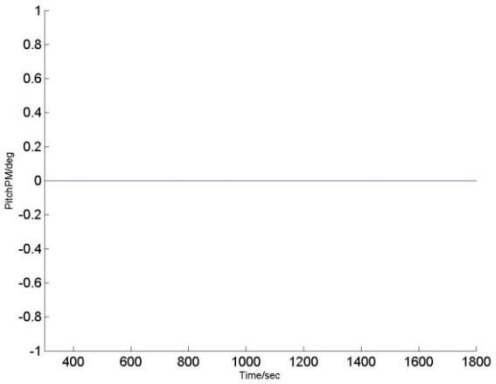

a) Blade Pitch Angle Due to 11.4m/s Wind

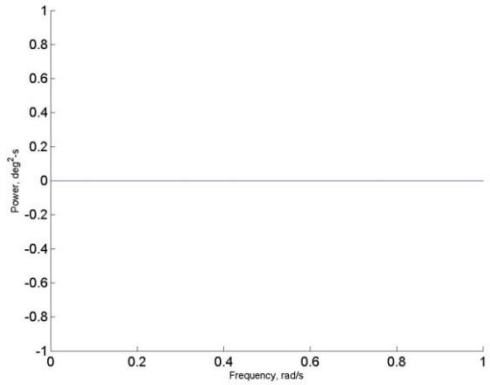

b) Blade Pitch Angle PSD Due to 11.4m/s Wind

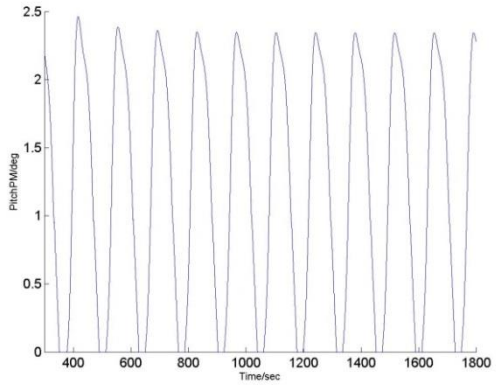

c) Blade Pitch Angle Due to 11.6m/s Wind

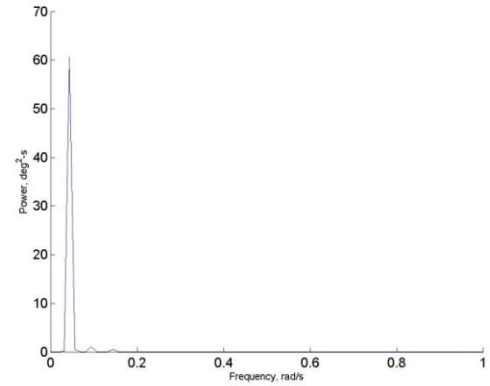

d) Blade Pitch Angle PSD Due to 11.6m/s Wind

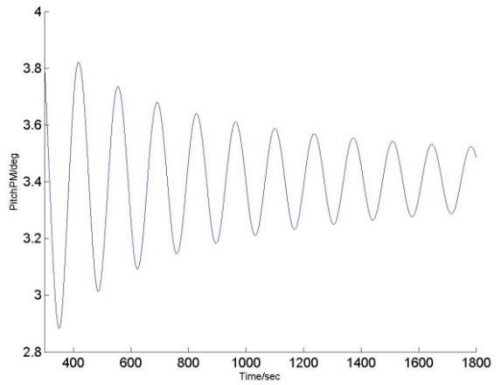

e) Blade Pitch Angle Due to 12m/s Wind

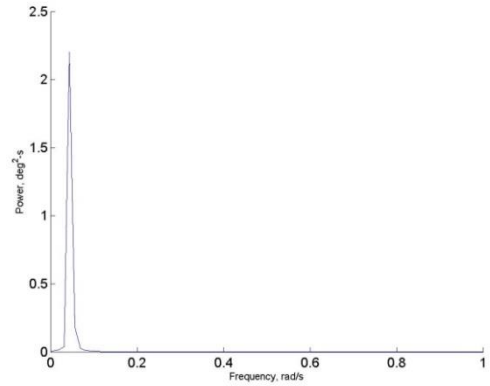

f) Blade Pitch Angle PSD Due to 12m/s Wind

Figure 4-3 Blade Pitch Angle Responses Comparison for Different Uniform and Steady Wind Speeds

Figure 4-3 reveals several interesting trends. The wind at rated wind speed (11.4m/s) generates the largest mean surge and pitch of the FOWT, while the wind at 12m/s generates the smallest. This is because the wind at 11.4m/s results in the largest wind drag force, as shown in Figure 3-3, which in turn induces the largest mean surge and mean pitch responses.

It is shown in Figure 4-1 that the peaks of surge PSD for all three cases are near the surge natural frequency (0.05rad/s) of the FOWT, which is expected. The FOWT surge oscillation induced by 11.4m/s wind gradually reduces to a constant value (no vibration). This is mainly due to hydrodynamic damping. Interestingly, the surge oscillation induced by 11.6m/s wind is the largest, while the surge oscillation due to 12m/s wind is smaller than that of 11.6m/s wind but much larger than that of 11.4m/s wind. And the surge oscillation due to 12m/s wind keeps constant after 3000s.

As shown in Figure 4-2, comparing the pitch PSD, there is a peak around the surge natural frequency for the cases of 11.6m/s and 12m/s winds. However, there are also small peaks around the harmonic frequencies of surge natural frequency in pitch PSD response of 11.6m/s wind, as shown in Figure 4-2 d).

Shown in Figure 4-3 a), there is no blade pitch angle in the case of 11.4m/s wind. As shown in Figure 4-3 b), the blade pitch angle periodically changes from 0 to 2.5 deg in the case of 11.6m/s wind. In the case of 12m/s wind, the blade pitch angle changes with much smaller range and decreasing amplitudes, between 3 to 4 deg, as shown in Figure 4-3 c).

The surge oscillations, in the cases of winds at 11.6m/s and 12m/s, result from the “resonance effect” from the wind force, which is due to the dynamic wind force during the surge oscillation. This phenomenon is also known as “negative damping” by some researchers[20]. As mentioned in 3.3, the wind force depends on the relative wind speed. Although the wind speed at the hub of FOWT (with respect to the earth) keeps steady in each case, the relative wind speed periodically changes (relative wind speed=wind speed-FOWT velocity at hub). As a result, the FOWT surge oscillation causes the change in the wind force, which is the dynamic wind force. Due to the control system of the FOWT, when the relative wind speed at the hub is below the rated wind speed, the wind drag force F increases with the increase in relative wind speed v, as shown in Figure 3-3 a). When the relative wind speed is above the rated wind speed, the wind drag force F decreases with the increase in relative wind speed, also shown in Figure 3-3 a). Also, the wind drag force F drops faster when the relative wind speed is just above the rated wind speed and it drops much slower when the relative wind speed is much higher. Based on this reason, it is found that

1. In the uniform and steady wind cases, the pitch velocity is small and the FOWT velocity at hub is mainly contributed from the FOWT surge velocity. As a result, the discussion below only considers the FOWT surge velocity.
2. If the wind speed (with respect to the earth) is below the rated wind speed, when the FOWT moves in the same direction as the wind, the relative wind speed decreases, and the wind force is smaller. When the

FOWT moves in the opposite direction of the wind, the relative wind speed increases and the wind force increases. Therefore, the dynamic wind force (i.e. the change in wind force) is against the FOWT surge velocity and the FOWT dynamic surge response would be smaller and smaller. In other words, the wind damps the dynamic surge in addition to the hydrodynamic damping on the support platform.

3. If the wind speed is above the rated wind speed, the control system adjusts the blade pitch angle based on the relative wind speed at hub. When the FOWT moves in the same direction as the wind, the relative wind speed decreases, but the wind force increases because of the decrease in the blade pitch angle. When the FOWT moves in the opposite direction as the wind, the relative wind speed increases, but the wind force decreases due to the increase in the blade pitch angle. Consequently, the dynamic wind force is in the same direction as the FOWT surge velocity. The dynamic wind force has the "resonance" effect on the surge motion and it amplifies the surge motion until it is balanced by the hydrodynamic damping on the support platform.
4. As shown in Figure 3-3 a), when the wind speed is above the rated wind speed, the wind force changes slower with higher mean wind speed (the slope of the curve is smaller). That means, even with the same surge velocity range, the dynamic wind force is smaller with larger mean wind speed. As a result, the surge oscillation is smaller with higher wind speed.

5. If the wind speed is just a little bit above the rated wind speed, the relative wind speed can be partially above the rated wind speed and partially below it, which results in the dynamic wind force partially in the same direction as that of the FOWT surge velocity and partially against it.
6. Therefore, the largest "resonance" effect happens when: (1) The wind speed with respect to the earth is above the rated wind speed 11.4m/s; (2) the relative wind speed during the whole oscillation is above the rated wind speed and the lowest relative wind speed is at the rated wind speed. This is why the 11.6m/s wind generates larger surge response than the 12m/s wind.

The comparisons also show that the pitch motion has the similar trend as the surge. In the case of 11.4m/s wind, the pitch oscillation decays quickly; in the case of 11.6m/s wind, the pitch is amplified by the "resonant" wind forces mentioned above; and in the case of 12m/s wind, the pitch response decays but with larger amplitude than that in the case of 11.4m/s wind. In all three cases, there is a large pitch response peak around the surge natural frequency. This is because in the case of uniform and steady wind, the oscillatory (or "resonant") wind forces are from the change in relative wind speed resulted from the surge oscillation. In the case of 11.6m/s wind, the peaks in the pitch PSD occur at the harmonic frequencies of surge natural frequency. In the case of 12m/s wind, the pitch response peak is only around the surge natural frequency. This is because the surge oscillation is smaller at the case of 12m/s wind.

4.1.2 The Responses of FOWT under Turbulent Wind

In reality, wind speed is unsteady. To explore the effect of turbulent winds on the FOWT responses, four turbulent winds with different mean speeds are considered in this research, as shown in Table 3-6, Case 4~7. The reference wind speeds, which are the mean wind speeds measured at the 90m above the SWL (the elevation of hub), are 8m/s, 11.4m/s, 11.6m/s and 17m/s, respectively. To explore the effects from different wind directions, 7 different wind directions are investigated with the mean wind speed at 11.4m/s wind, as Case 5 and Case 8~13. For the winds of 8m/s, 11.6m/s and 17m/s mean speed, only 0 deg wind direction is considered.

The wind speeds as a function of time and the related PSD are depicted in Figure 4-4 for the cases of winds of mean speed 8m/s, 11.4m/s, 11.6m/s and 17m/s. The FOWT motion and tension in the mooring lines for the cases of 8m/s, 11.4m/s, 11.6m/s and 17m/s winds with 0 deg direction (case 4~7) are presented in Figure 4-5 ~ Figure 4-11. The sway and yaw responses are not significant and they are omitted for brevity.

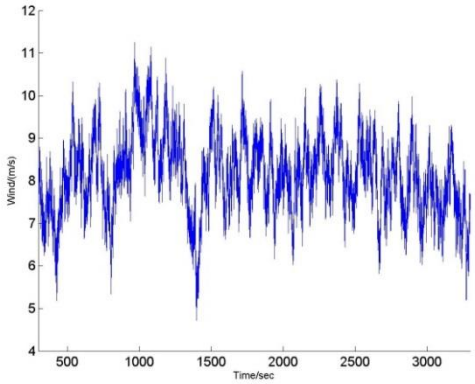

a) Wind Speed Due to 8m/s Turbulent Wind

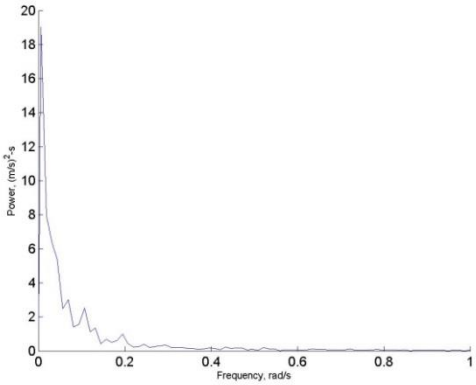

b) Wind Speed PSD Due to 8m/s Turbulent Wind

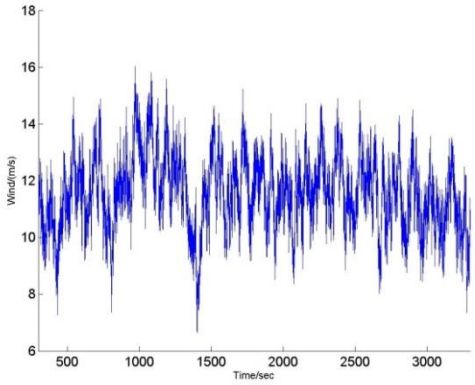

c) Wind Speed Due to 11.4m/s Turbulent Wind

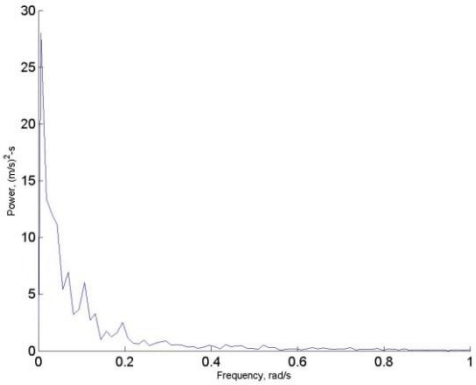

d) Wind Speed PSD Due to 11.4m/s Turbulent Wind

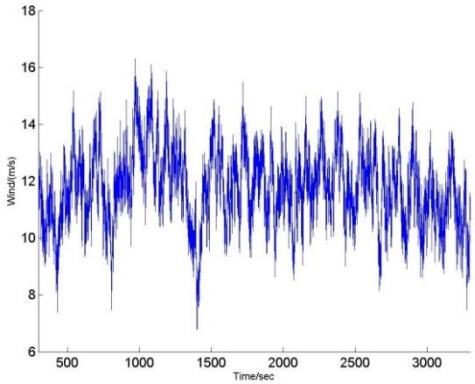

e) Wind Speed Due to 11.6m/s Turbulent Wind

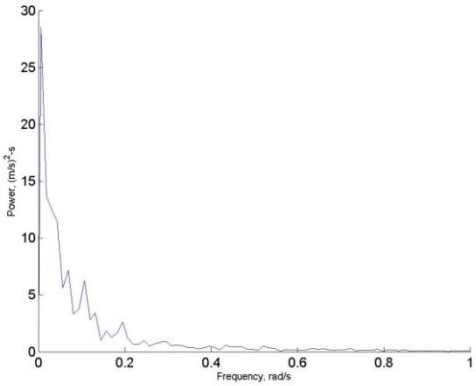

f) Wind Speed PSD Due to 11.6m/s Turbulent Wind

Figure 4-4 Wind Speed Comparisons for Different Turbulent Wind Speeds

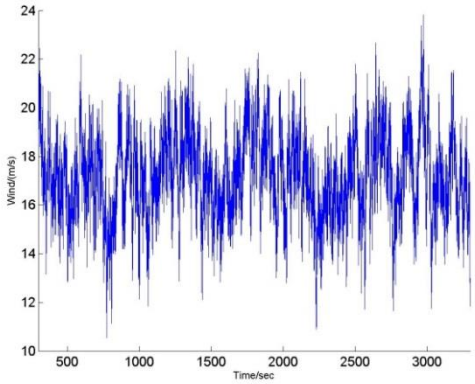

g) Wind Speed Due to 17m/s Turbulent Wind

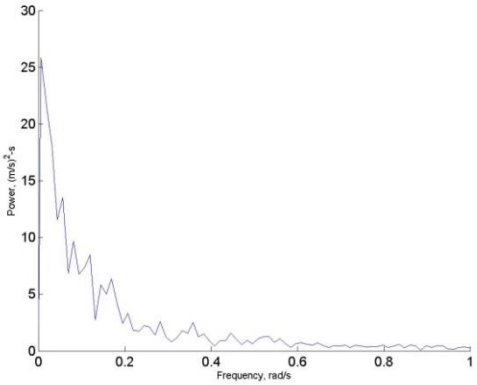

h) Wind Speed PSD Due to 17m/s Turbulent Wind

Figure 4-4 Continued

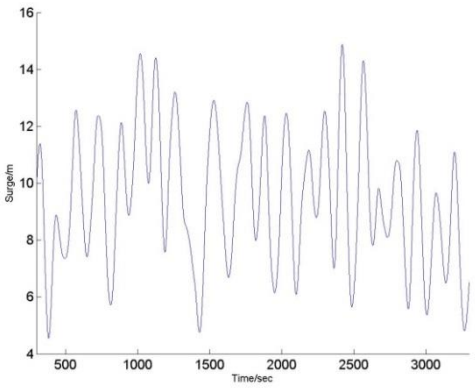

a) Surge Due to 8m/s Wind

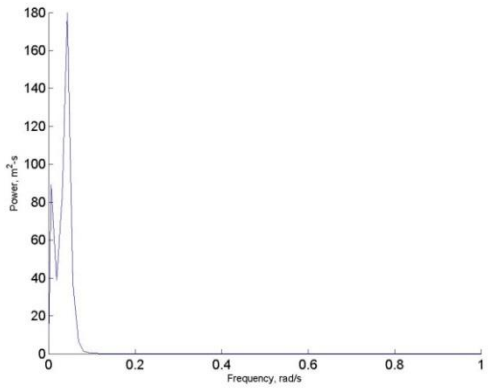

b) Surge PSD Due to 8m/s Wind

Figure 4-5 Surge Response Comparison for Different Turbulent Wind Speeds

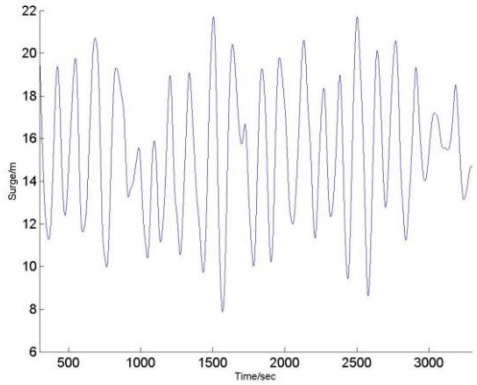

c) Surge Due to 11.4m/s Wind

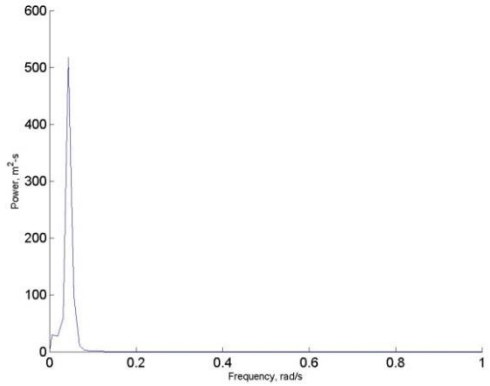

d) Surge PSD Due to 11.4m/s Wind

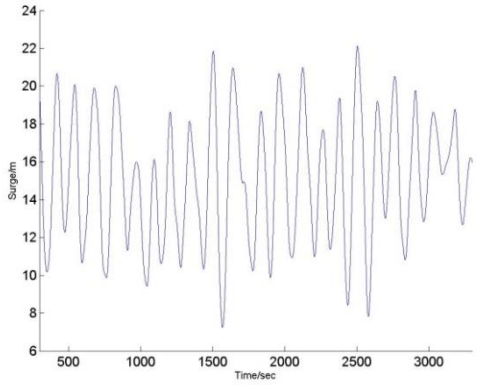

e) Surge with 11.6m/s Wind

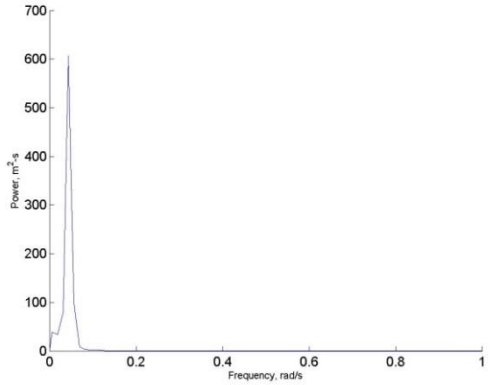

f) Surge PSD with 11.6m/s Wind

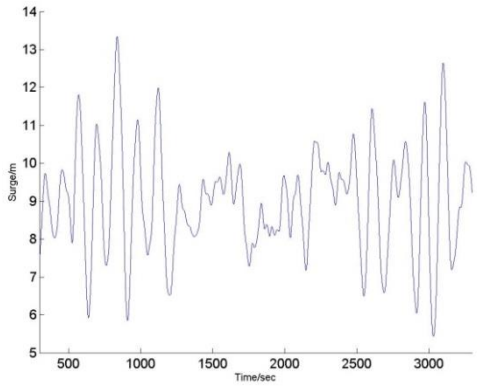

g) Surge with 17m/s Wind

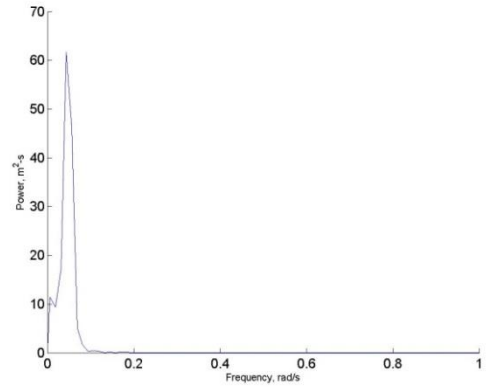

h) Surge PSD with 17m/s Wind

Figure 4-5 Continued

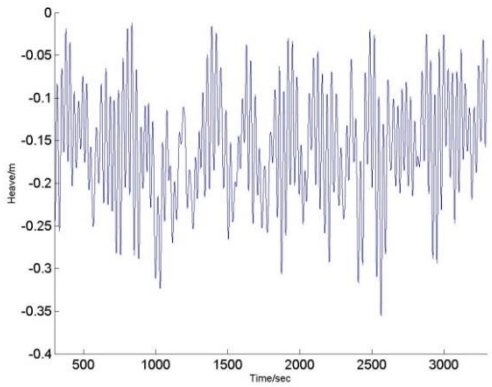

a) Heave Due to 8m/s Wind

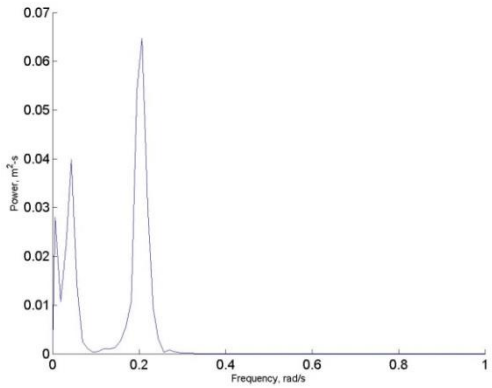

b) Heave PSD Due to 8m/s Wind

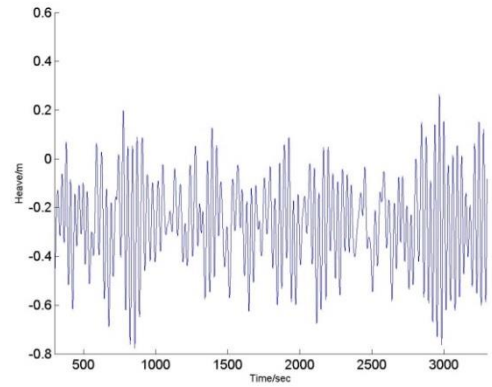

c) Heave Due to 11.4m/s Wind

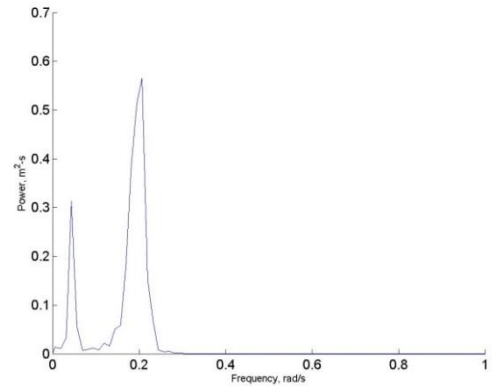

d) Heave PSD Due to 11.4m/s Wind

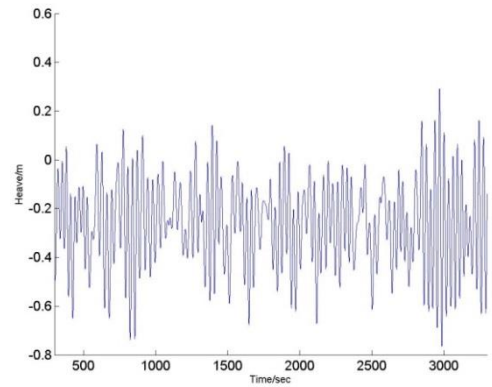

e) Heave with 11.6m/s Wind

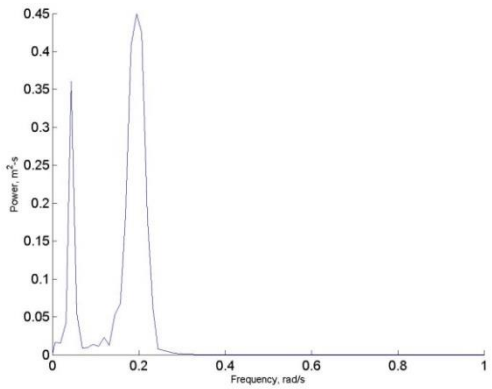

f) Heave PSD with 11.6m/s Wind

Figure 4-6 Heave Response Comparison for Different Turbulent Wind Speeds

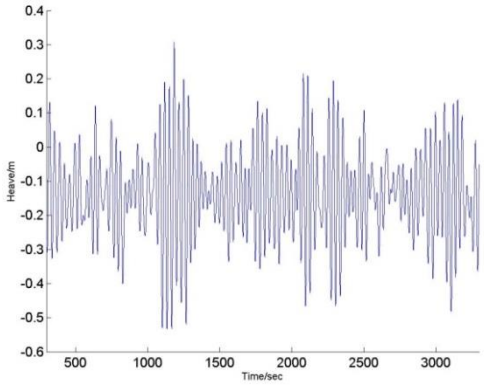

g) Heave Due to 17m/s Wind

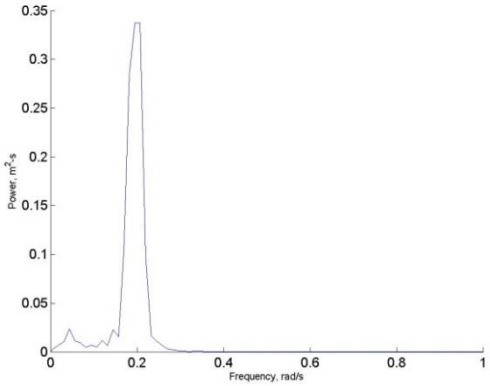

h) Heave PSD Due to 17m/s Wind

Figure 4-6 Continued

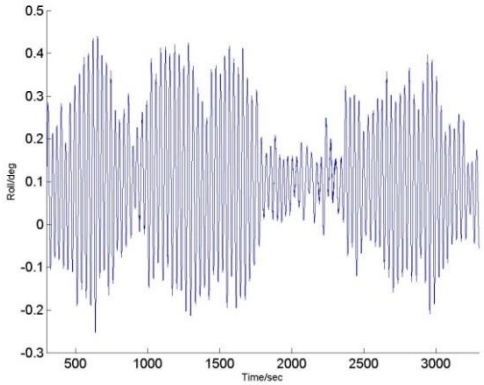

a) Roll Due to 8m/s Wind

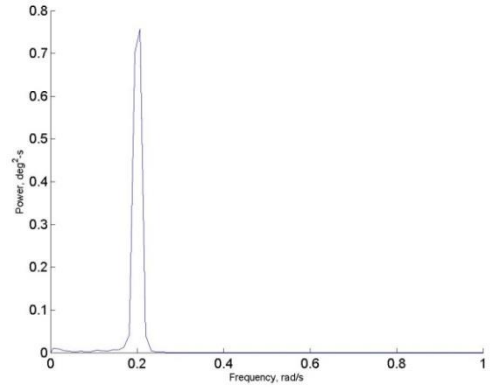

b) Roll PSD Due to 8 m/s Wind

Figure 4-7 Roll Response Comparison for Different Turbulent Wind Speeds

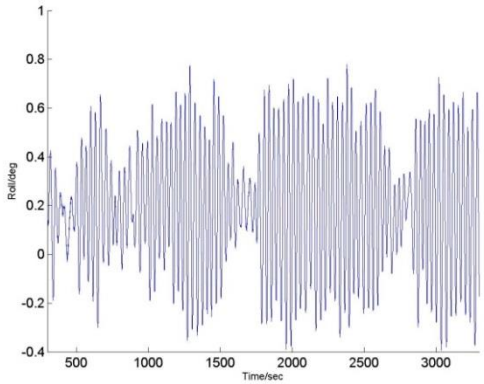

c) Roll Due to 11.4 m/s Wind

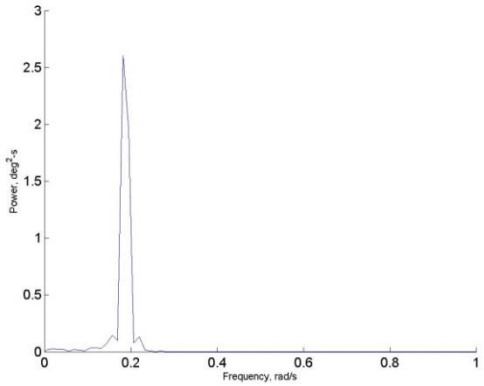

d) Roll PSD Due to 11.4 m/s Wind

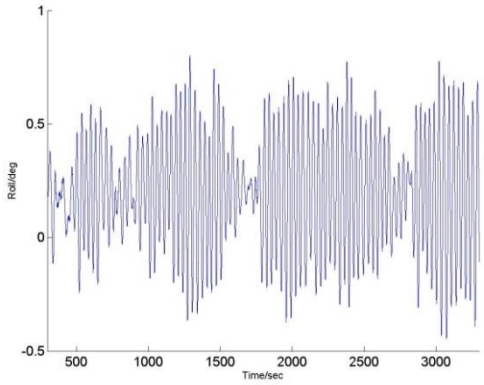

e) Roll with 11.6 m/s Wind

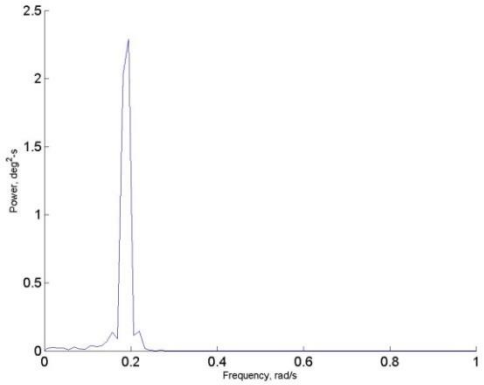

f) Roll PSD with 11.6 m/s Wind

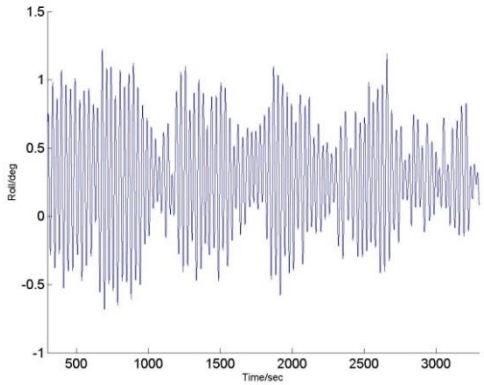

g) Roll Due to 17 m/s Wind

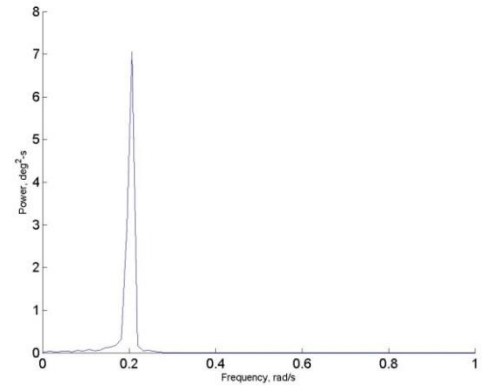

h) Roll PSD Due to 17 m/s Wind

Figure 4-7 Continued

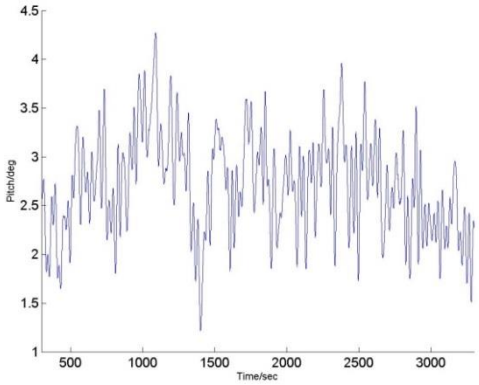

a) Pitch Due to 8 m/s Wind

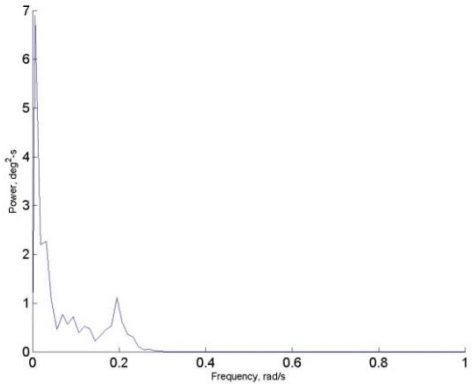

b) Pitch PSD Due to 8 m/s Wind

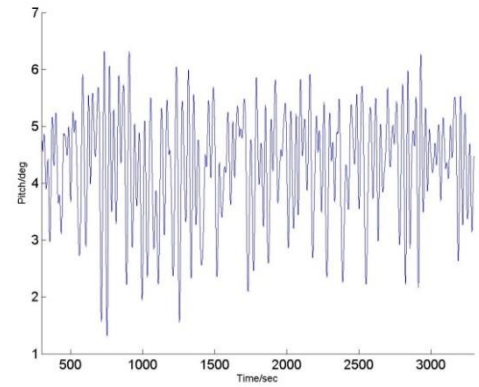

c) Pitch Due to 11.4 m/s Wind

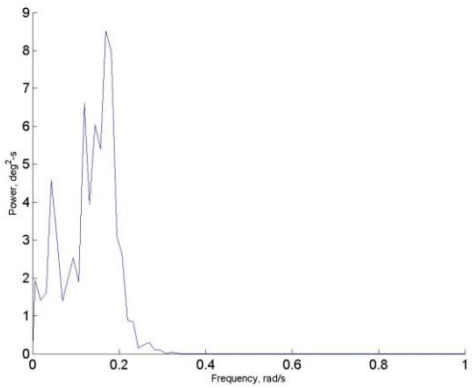

d) Pitch PSD Due to 11.4 m/s Wind

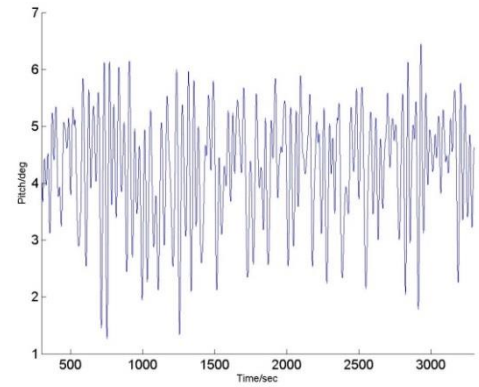

e) Pitch with 11.6 m/s Wind

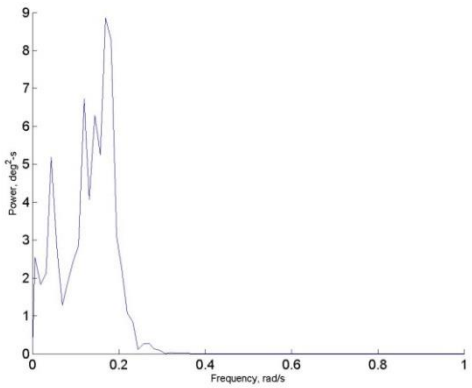

f) Pitch PSD with 11.6 m/s Wind

Figure 4-8 Pitch Response Comparison for Different Turbulent Wind Speeds

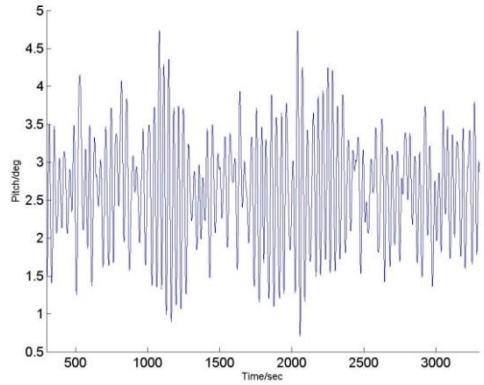

g) Pitch Due to 17 m/s Wind

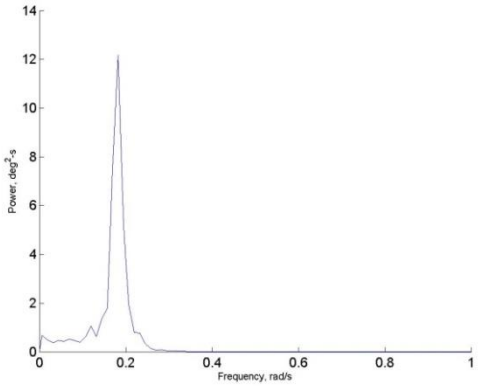

h) Pitch PSD Due to 17 m/s Wind

Figure 4-8 Continued

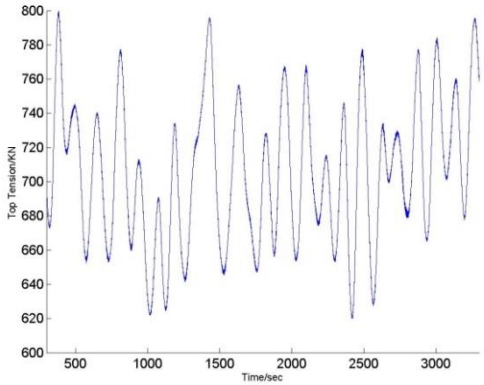

a) Top Tension of ML1 Due to 8 m/s Wind

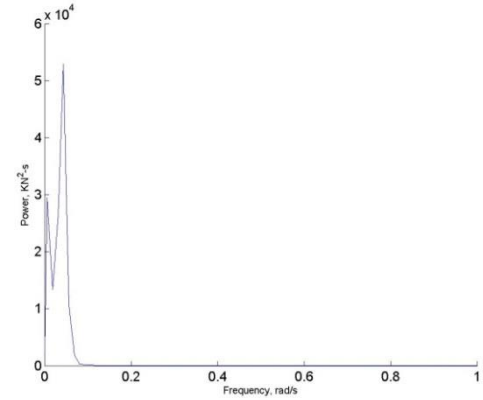

b) Top Tension PSD of ML1 Due to 8 m/s Wind

Figure 4-9 ML1 Top Tension Response Comparison for Different Turbulent Wind Speeds

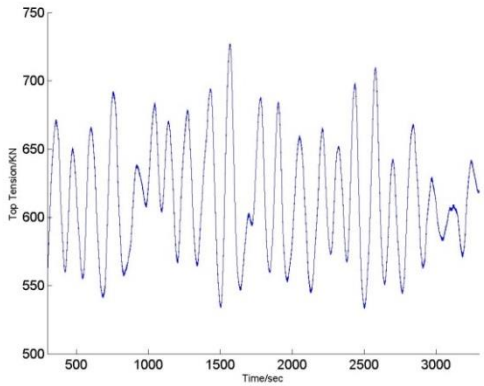

c) Top Tension of ML1 Due to 11.4 m/s Wind

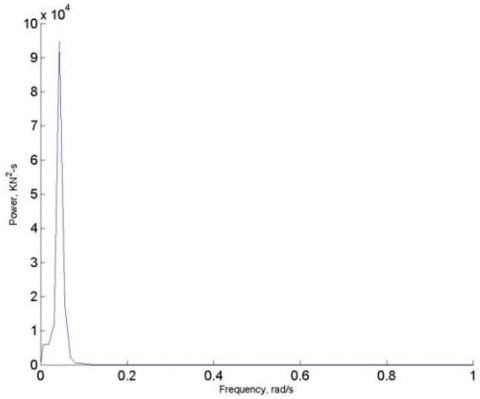

d) Top Tension PSD of ML1 Due to 11.4 m/s Wind

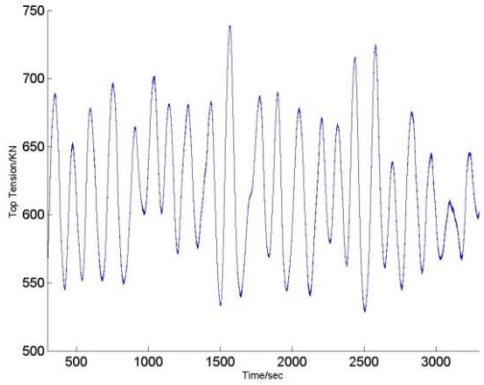

e) Top Tension of ML1 Due to 11.6 m/s Wind

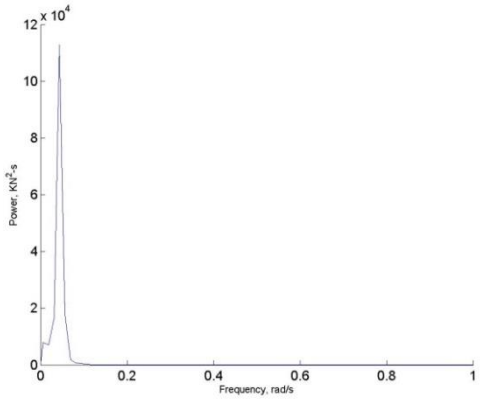

f) Top Tension PSD of ML1 Due to 11.6 m/s Wind

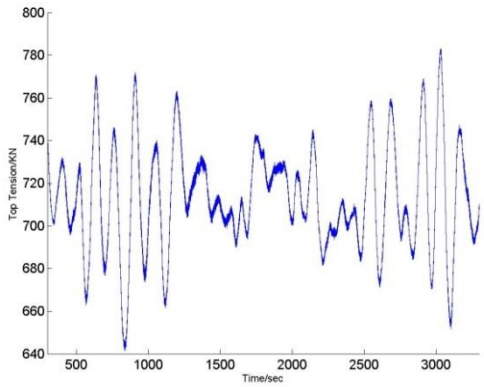

g) Top Tension of ML1 Due to 17m/s Wind

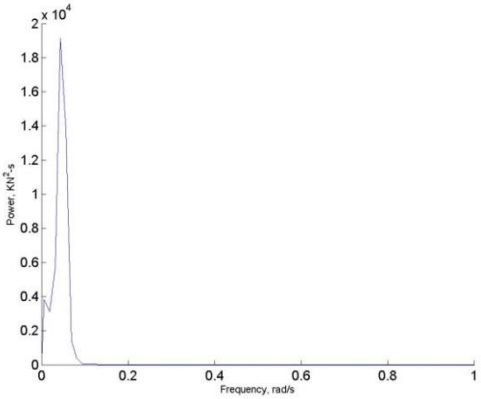

h) Top Tension PSD of ML1 Due to 17 m/s Wind

Figure 4-9 Continued

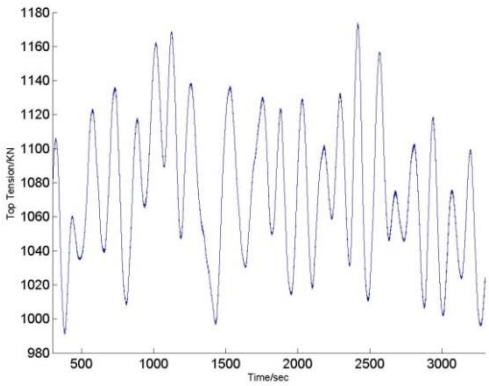

a) Top Tension of ML2 Due to 8 m/s Wind

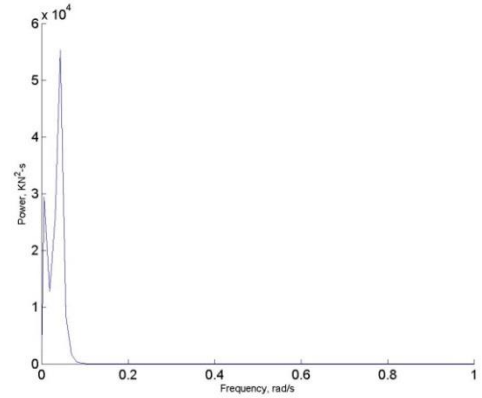

b) Top Tension PSD of ML2 Due to 8 m/s Wind

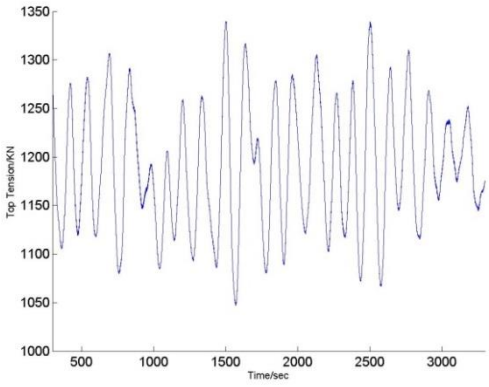

c) Top Tension of ML2 Due to 11.4m/s Wind

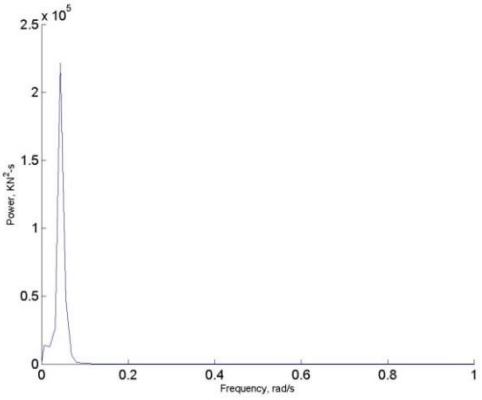

d) Top Tension PSD of ML2 Due to 11.4m/s Wind

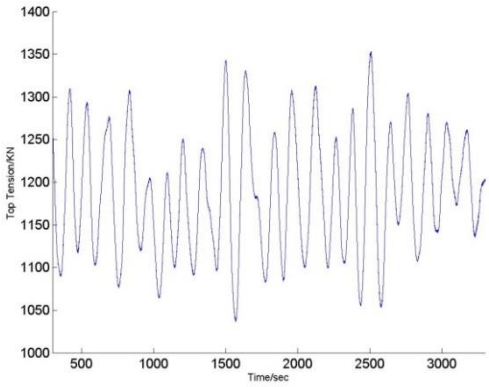

e) Top Tension of ML2 Due to 11.6m/s Wind

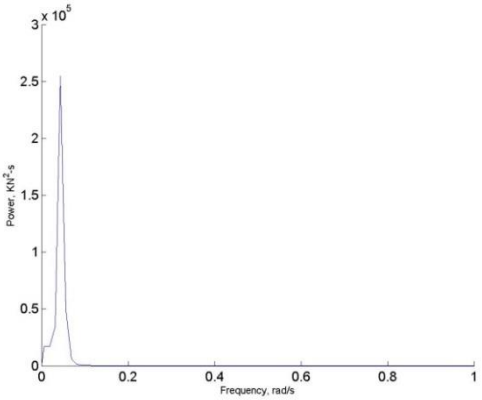

f) Top Tension PSD of ML2 Due to 11.6m/s Wind

Figure 4-10 ML2 Top Tension Response Comparison for Different Turbulent Wind Speeds

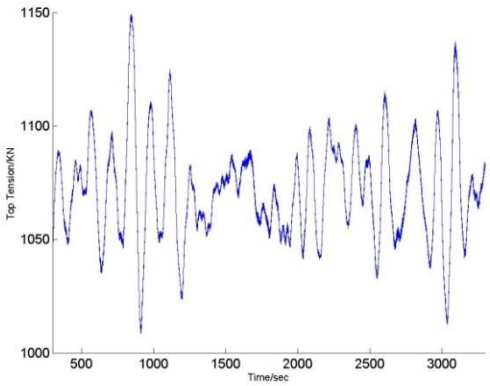

g) Top Tension of ML2 Due to 17 m/s Wind

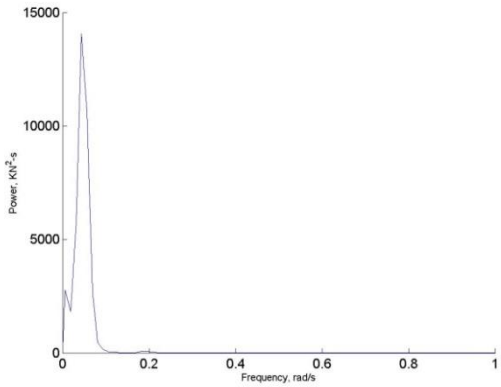

h) Top Tension PSD of ML2 Due to 17 m/s Wind

Figure 4-10 Continued

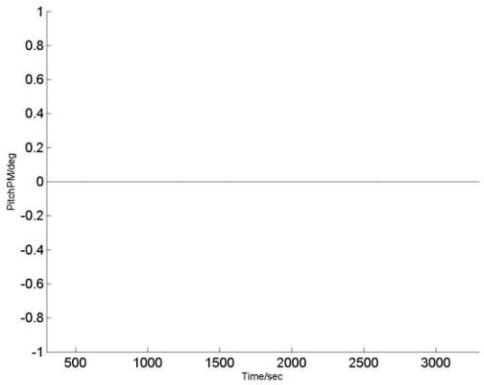

a) Blade Pitch Angle Due to 8 m/s Wind

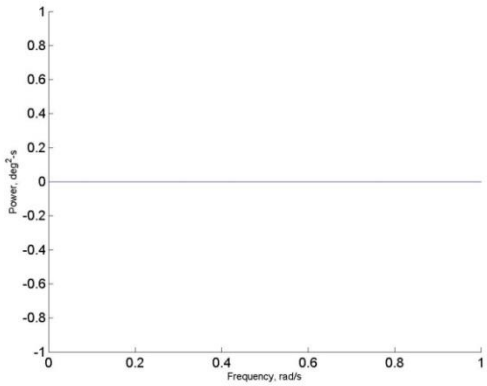

b) Blade Pitch Angle PSD Due to 8 m/s Wind

Figure 4-11 Blade Pitch Angle Response Comparison for Different Turbulent Wind Speeds

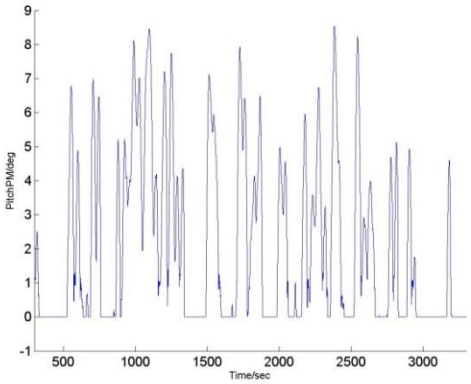

c) Blade Pitch Angle Due to 11.4 m/s Wind

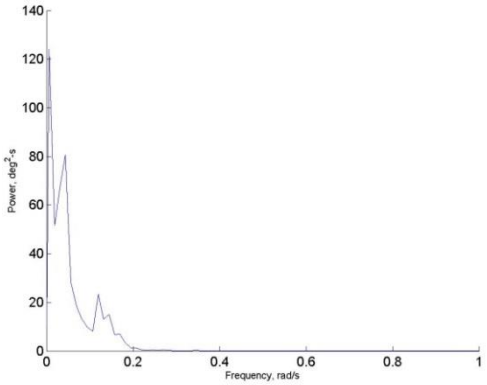

d) Blade Pitch Angle PSD Due to 11.4 m/s Wind

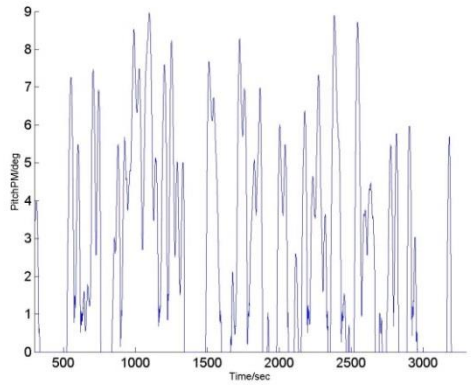

e) Blade Pitch Angle Due to 11.6 m/s Wind

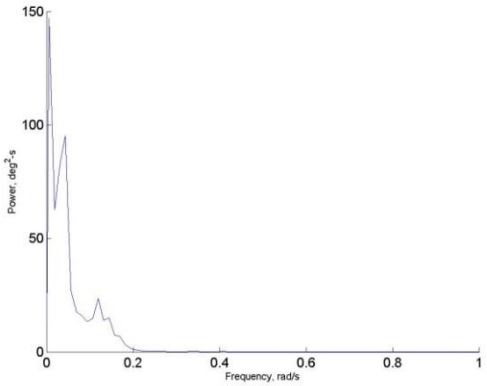

f) Blade Pitch Angle PSD Due to 11.6 m/s Wind

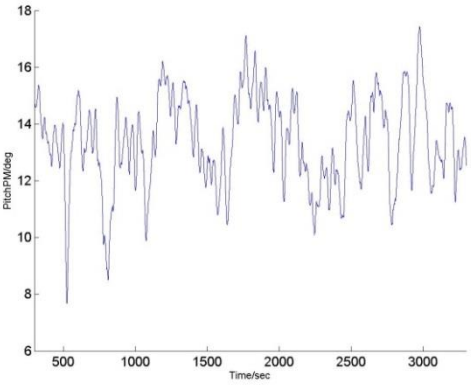

g) Blade Pitch Angle Due to 17 m/s Wind

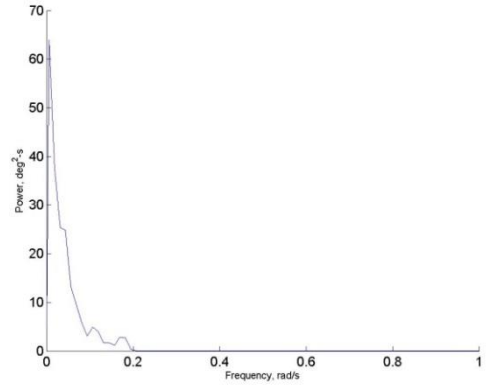

h) Blade Pitch Angle PSD Due to 17 m/s Wind

Figure 4-11 Continued

Table 4-1 Statistics Results for 0 deg Turbulent Wind Only Cases (Case 4-7)

		Surge	Sway	Heave	Roll	Pitch	Yaw	ML1 Tension	ML2 Tension
		(m)	(m)	(m)	(deg)	(deg)	(deg)	(KN)	(KN)
Mean	8m/s	9.5	0.0	-0.2	0.1	2.7	0.0	706	1074
	11.4m/s	15.3	0.0	-0.3	0.2	4.3	0.0	613	1190
	11.6m/s	15.1	0.0	-0.3	0.2	4.3	0.0	616	1186
	17m/s	9.0	-0.2	-0.1	0.3	2.6	-0.1	713	1072
Mean Compare with 11.4m/s	8m/s	-38%	-128%	-40%	-47%	-37%	-55%	15%	-10%
	11.4m/s	0%	0%	0%	0%	0%	0%	0%	0%
	11.6m/s	-1%	-28%	-2%	3%	-1%	-8%	1%	0%
	17m/s	-41%	-1244%	-48%	48%	-39%	-353%	16%	-10%
Standard Deviation (STD)	8m/s	2.3	0.1	0.1	0.1	0.5	0.2	41	41
	11.4m/s	3.1	0.2	0.2	0.3	0.9	0.4	42	65
	11.6m/s	3.3	0.2	0.2	0.3	0.9	0.4	46	69
	17m/s	1.4	0.3	0.1	0.4	0.7	0.5	25	22
STD Compare with 11.4m/s	8m/s	-24%	-52%	-65%	-45%	-45%	-41%	-1%	-36%
	11.4m/s	0%	0%	0%	0%	0%	0%	0%	0%
	11.6m/s	8%	2%	-1%	-2%	2%	1%	9%	7%
	17m/s	-55%	42%	-27%	47%	-24%	36%	-41%	-66%

The comparisons of the statistics of motions and top tensions in mooring lines under the impact of turbulence winds of different wind speeds and 0 deg wind direction (Case 4~7) are listed in Table 4-1. When the wind direction is 0 deg, the mooring system is symmetric with respect to the wind direction. The surge and pitch motions are dominated by the wind force. The mean wind force causes significant mean surge and mean pitch motions as expected. The mean wind force increases with the increase in the wind speed until it reaches the rated wind speed (11.4m/s). After that, the increase in the wind speed results in the increase in the blade pitch angle, which in turn decreases the mean wind forces. Therefore, the mean surge and pitch are the largest when the wind speed is at the rated wind speed (11.4m/s). Due to the “resonance” effect discussed in

4.1.1, the dynamic surge response is the largest in the case of 11.6m/s wind, which is almost 8% higher than it in the case of 11.4m/s wind, as shown in Table 4-1. In comparison with the corresponding cases of steady and uniform wind only, the "resonance" effect under turbulent wind is not as obviously as under the steady wind. The reason for this is that the turbulence (or gustiness) in the wind involves the components of frequencies nearby the surge natural frequency of the FOWT, which may directly excite the surge motion of the FOWT neat its natural frequency. In addition, turbulence winds also excite the dynamic pitch at the other frequencies as shown in Figure 4-8. As a result, the "resonance" effect is only one of the contributions to the dynamic surge of the FOWT. The increase in the wind speed results in the increase in the dynamic transverse force at the tower base, as explained in Figure 3-3 d). Consequently, the largest dynamic sway and roll responses happen in the case of 17m/s wind speed. The interaction among pitch and heave may increase the dynamic heave responses at the rated wind speed. Since the wind directions in these cases are constant at 0 deg, the mooring lines top tension mainly depends on the mooring lines layout (shown in Figure 3-1). When the wind direction is 0 deg, the ML1 is slack and the mean top tension in it is the smallest in the case of 11.4 m/s wind. On the contrast, the ML2 and ML3, which are tight, have the largest mean top tensions in the case of 11.4m/s wind. The dynamic top tensions are the largest in the case of 11.6m/s wind due to the largest surge oscillation caused by "resonance" effects.

All dynamic responses concentrate at their related natural frequency of the FOWT. The peaks in the wind spectrum may also result in the related peaks in the

response spectra. If any of the peaks in the wind spectrum is close to one of the natural frequencies, it would generate significant response at the frequency of wind peaks.

Besides the peaks from the wind in the low frequency range, interesting trends in the motion and mooring lines top tension of the FOWTare observed and discussed below.

1. The surge and sway responses mainly concentrate at their natural frequencies, both around 0.05rad/s.
2. The time series of the roll response have “beat” or “group” pattern shown in Figure 4-7, which result from the two dominant roll oscillations with close frequencies. There are two major peaks in roll PSD. One is around the roll natural frequency (around 0.203rad/s). The other is related to the blade rotation response. As discussed in 2.5, the blade rotation natural frequency is around 0.20 rad/s. It is close to the roll natural frequency. The two roll oscillations with close frequencies result in “beat” or “group” shapes.
3. In the cases of turbulent winds with mean speed as 8m/s, 11.4m/s and 11.6m/s, the wind loads result in significant pitch responses in very low frequency range. While in the case of 17m/s wind, the large blade pitch angle reduces the wind loads significantly and the pitch response focuses to only one peak near its natural frequency. It is noted that when the blade pitch angle is equal to 0 deg, the pitch natural frequency is around 0.20 rad/s, which is the same as the desired from the free-decay simulations, as listed in Table 3-5. However, when the blade pitch angle is not equal to 0

deg, the pitch natural frequency "shift" to around 0.18 rad/s. The reason for the frequency "shift" is not understood yet.

4. The mooring lines top tension is dominated by the surge in all cases. Based on the mooring lines layout with respect to the wind direction (ML1 is slack and ML2 is tight), ML2 has larger mean and dynamic top tension than those in ML1. Because of the symmetric mooring system, ML3 has similar response as ML2 and the ML3 results are omitted here.

Considering that the wind may come in the directions other than 0 deg, different wind directions are considered in the simulations but kept the same wind speed at 11.4m/s (Case 5 and 8~13). The statistics of motions and top tension in mooring lines are shown in Figure 4-12. The blue column represents the mean values and the pink column represents the STD, which results from the dynamic responses of the FOWT. The wind direction is with respect to the Global Reference CS and the motion responses are expressed in the Space-fixed CS, meaning the "surge" of the FOWT is always in the same direction as the wind. Therefore, the surge direction is different when the wind direction changes based on the view of the Global Reference CS (earth fixed CS). The time series and PSD for the motion and tension responses are provided in APPENDIX 2.

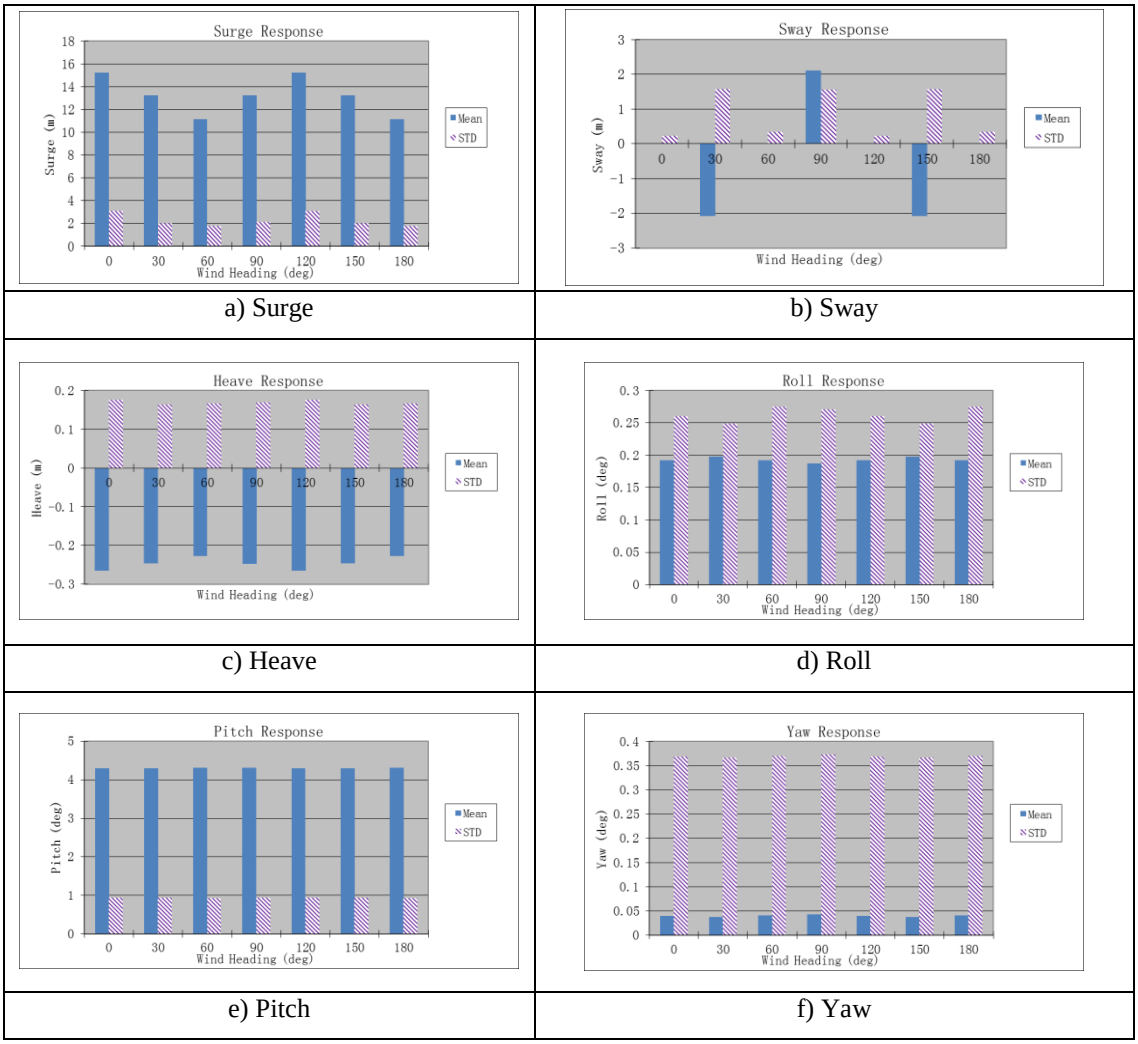

a) Surge | b) Sway

c) Heave | d) Roll

e) Pitch | f) Yaw

Figure 4-12 The FOWT Motion Responses Comparison with Different Wind Directions

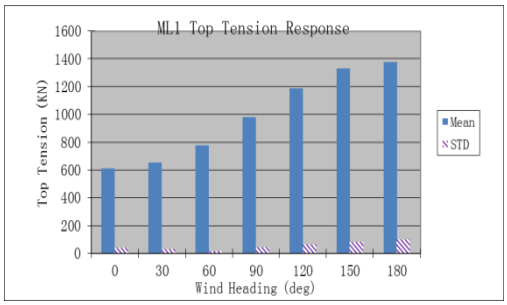

g) Top Tension of ML1

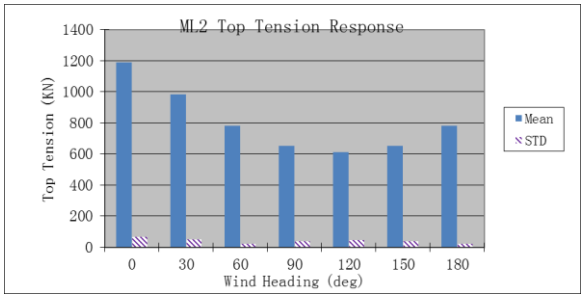

h) Top Tension of ML2

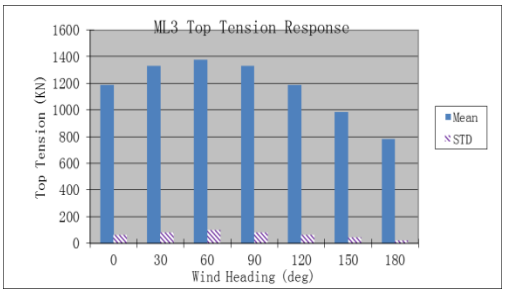

i) Top Tension of ML3

Figure 4-12 Continued

Figure 4-12 shows that the 6 DOF motions repeat the same statistics when the wind direction rotates every 120^{o}, which is expected because of the three mooring lines are evenly distributed, each separated by 120^{o}. The surge and sway motions are related to the different mooring restoring stiffness which depends on the direction of wind and is shown in Figure 3-4. When the wind direction is 0 deg, the direction of wind is in line with ML1. It slacks ML1 and tightens the other two mooring lines. The mooring stiffness in this direction is the smallest, and hence both of the mean and dynamic surges are the largest. When the wind direction is 60 deg, the wind is in the opposite direction of ML3. It tightens ML3 and slacks the other two. The mooring stiffness in this direction is the largest. Consequently, the mean and dynamic surge motions with 60 deg wind

direction are the smallest. When the wind direction is in 0 or 60 deg, the mooring system is symmetric with respect to the wind direction and hence the mean of sway motion is trivial. The dynamic sway response is induced by the blade rotation and mooring restoring forces. When the wind direction is 30 or 90 deg, the mooring system is asymmetric to the wind direction; therefore the FOWT has large mean and dynamic sway responses. On the other hand, the heave, roll and pitch responses are not sensitive to the wind directions. This is because that the restoring forces for the heave, roll and pitch are mainly from the hydrostatic stiffness. Since the FOWT supporting platform used in this research is Spar type, which is essentially a cylinder and provides the same hydrostatic stiffness in all directions, the responses in heave, roll and pitch do not change much with respect to the wind direction. For the 0 deg wind direction, the wind slacks ML1. Therefore, the mean tension in ML1 for this wind direction is the smallest. Conversely, for 180 deg wind direction, the wind tightens the ML1. As the result, the ML1 has the largest mean and dynamic top tension in the case of the 180 deg wind direction. The smallest dynamic top tension for ML1 happens with 60 deg wind direction. This is because that with this wind direction the ML1 is slack and the FOWT dynamic surge motion is the smallest.

4.2 The Responses of FOWT under the Impact of Wind and Wave

The FOWT is often under the impact of waves in addition to winds. Since the hull of the FOWT is more or less a vertical cylinder with relatively small diameter

($\leq$ 9.4 m), the Morison Equation is valid for the computation of the potential wave forces, in addition to the drag and lifting forces.

In simulating irregular waves, a JONSWAP wave spectrum of given significant wave height and peak period is used. Three typical wave cases are chosen in the simulations, corresponding to the operational, extreme and survival conditions, respectively. Turbulent winds are also included in the simulations but the current is neglected and will be considered in later cases. Two special cases are of particularly interest. The first considers both rated wind speed and survival wave condition, the second considers survival wave only. Although the wave only condition seldom happens in reality, it is desirable for understanding the FOWT responses under the wave impact only. Both collinear wind and wave and non-collinear wind and wave conditions are investigated in this section.

The responses of the FOWT in Case 15, (extreme condition, 11.4m/s mean wind speed, 6m significant wave height and 10s wave peak period), are shown in Figure 4-13.

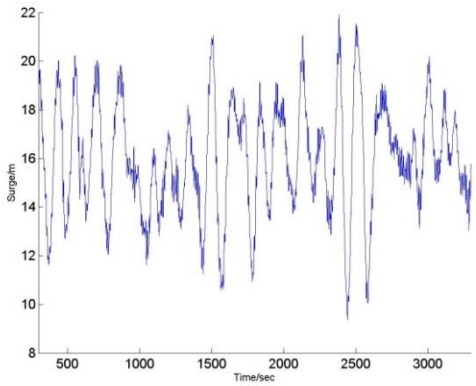

a) Surge

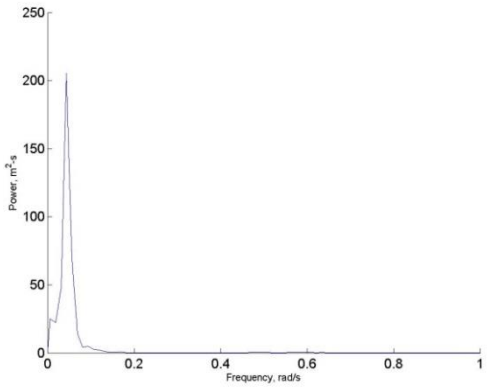

b) Surge PSD

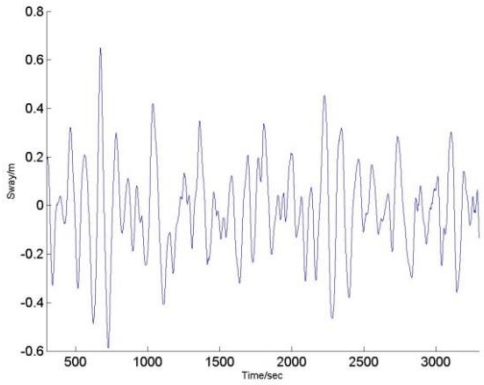

c) Sway

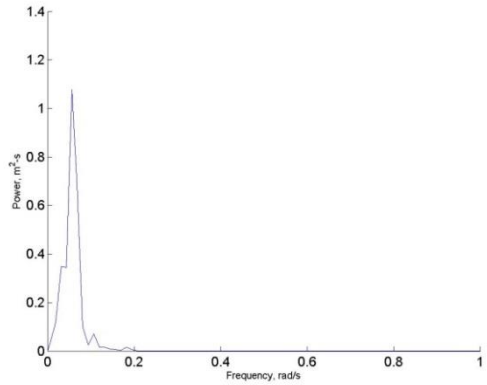

d) Sway PSD

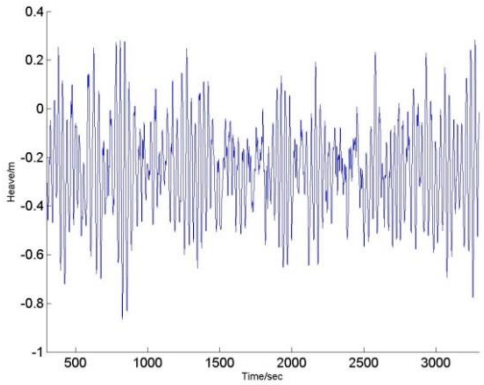

e) Heave

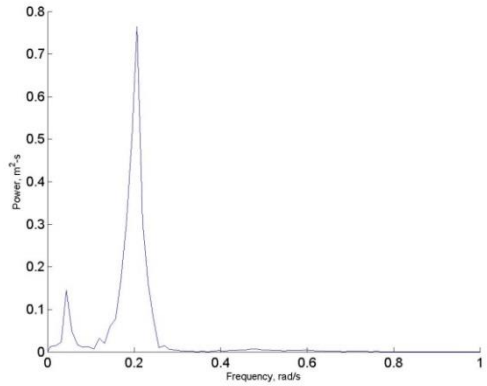

f) Heave PSD

Figure 4-13 The FOWT Results for Case 15

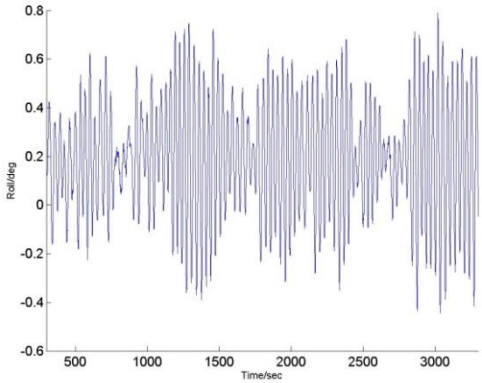

g) Roll

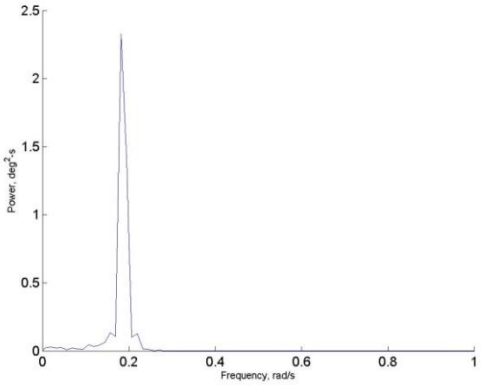

h) Roll PSD

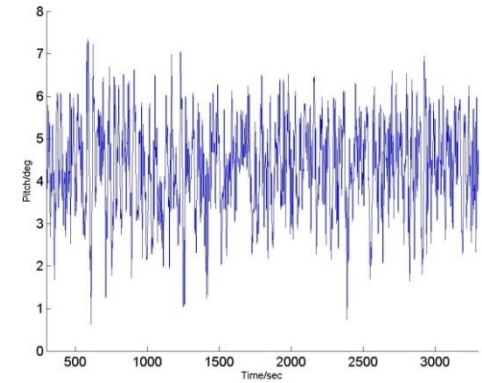

i) Pitch

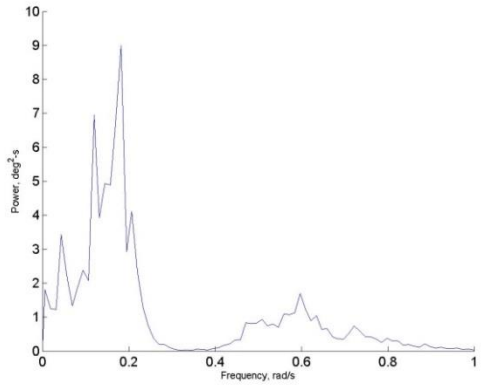

j) Pitch PSD

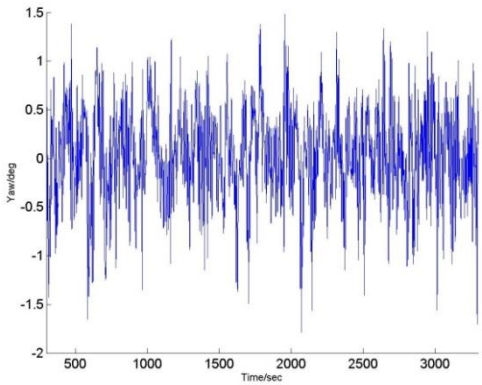

k) Yaw

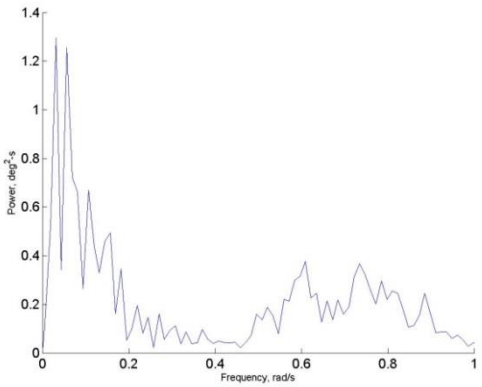

l) Yaw PSD

Figure 4-13 Continued

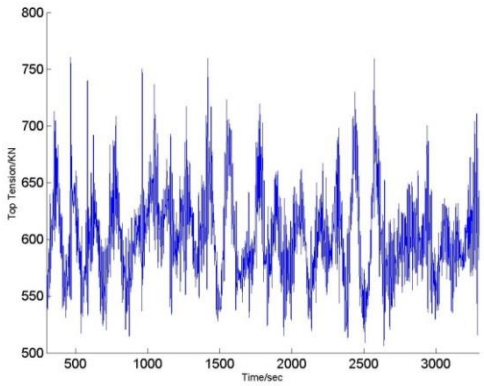

m) Top Tension of ML1

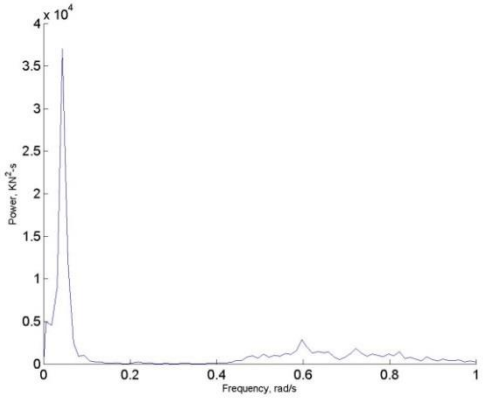

n) Top Tension PSD of ML1

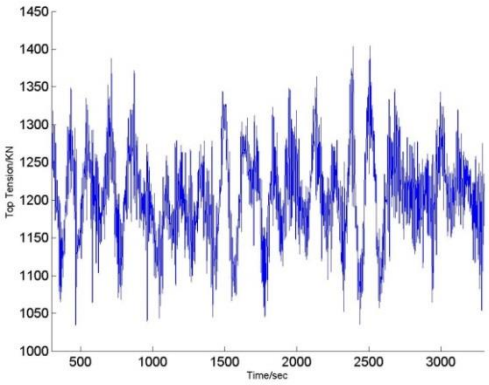

o) Top Tension of ML2

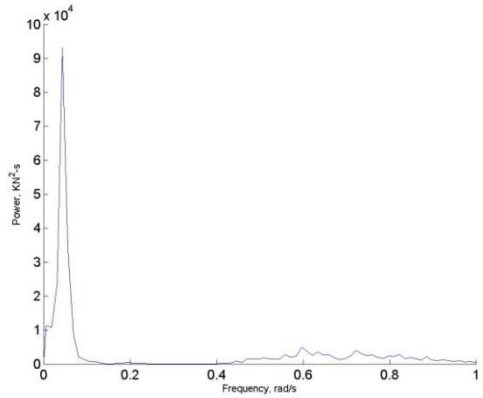

p) Top Tension PSD of ML2

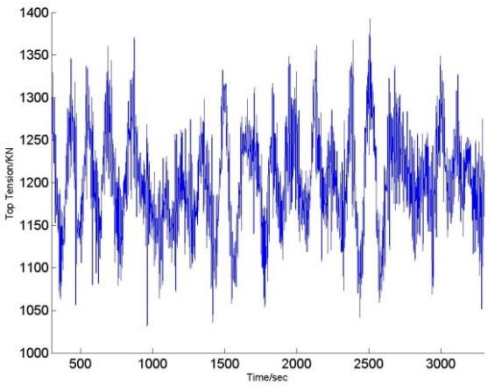

q) Top Tension of ML3

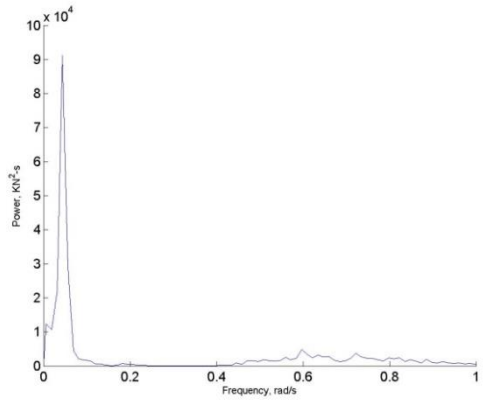

r) Top Tension PSD of ML3

Figure 4-13 Continued

The mean surge motion results mainly from the mean wind force and to less extent from mean wave force. As a result, the mean surge (16.0m in Case 15, shown in Figure 4-14 a)) in the case of combined wind and wave impact is greater than that in the corresponding wind only case (15.3m in Case 5, listed in Table 4-1). Since the mean top tension of mooring lines depends on the mean offset and the mooring lines layout with respect to the wind direction, compared with the results in the wind only case, the mean top tension of slacked ML1 is less and the mean top tensions of the other two tighten lines are larger in the wind and wave condition based on the comparison between Table 4-1 and Figure 4-14 m) (602.5KN in ML1 and 1205.0KN in ML2 in Case 15; 613.8KN in ML1 and 1189.8KN in ML2 in Case 5).

The dynamic responses are divided into three parts: low frequency (LF) responses, which are mainly induced by the wind and slow-drifting wave force; wave frequency (WF) responses, which are caused by the wave forces; and high frequency (HF) responses. The purpose of using different frequency ranges is to qualitatively distinguish the effects from wind and wave.

The frequency ranges are divided based on the response spectra to make sure that the peaks from wind are mainly in LF range and peaks from wave are mainly in WF range. In the simulations, the WF range is between 5s (1.26 rad/s) and 25s (0.25 rad/s). While the LF range is above 25s and the HF range is below 5s.

The heave, pitch, yaw and top tension show large responses in WF range. Since the sway and roll are perpendicular to the wave direction they are not affected much by

wave in WF range. The HF responses are small for the Spar type of platforms and they are omitted in the discussion.

The statistics for the simulations with different environment conditions and 0 deg environment directions (Case 14~18) are depicted in Figure 4-14. The blue column represents mean responses and STD of total dynamic responses. The pink column represents STD of LF dynamic responses. The red column represents STD of WF dynamic responses. In Figure 4-14 m), the blue, pink and red columns represent mean top tension responses of ML1, ML2 and ML3, respectively.

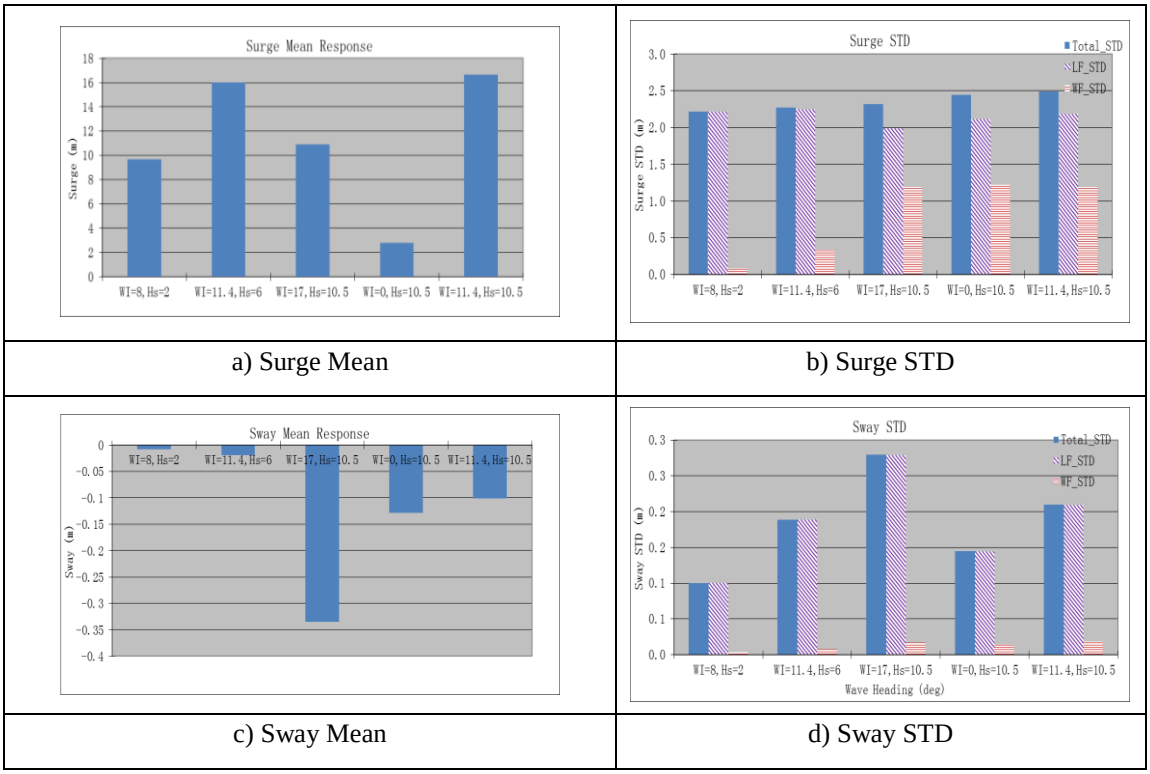

a) Surge Mean | b) Surge STD

c) Sway Mean | d) Sway STD

Figure 4-14 The FOWT Results Comparison for Case 14~18

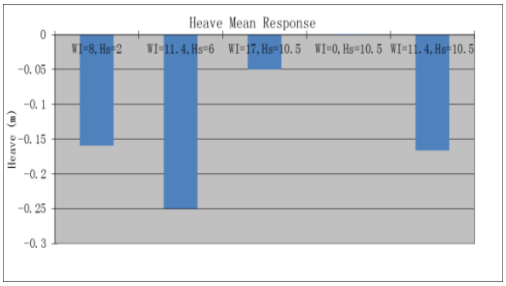

e) Heave Mean

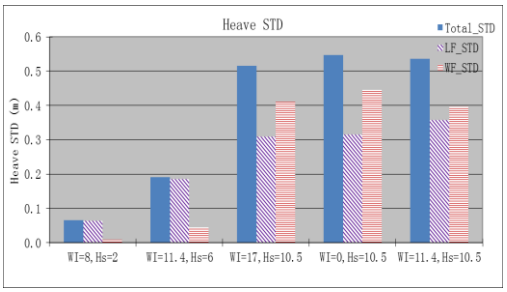

f) Heave STD

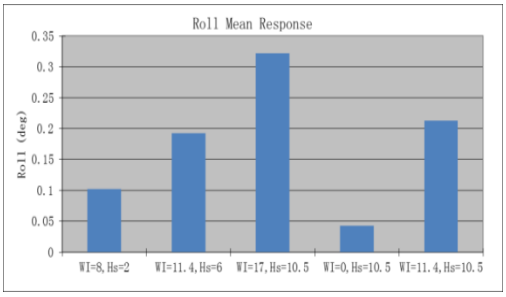

g) Roll Mean

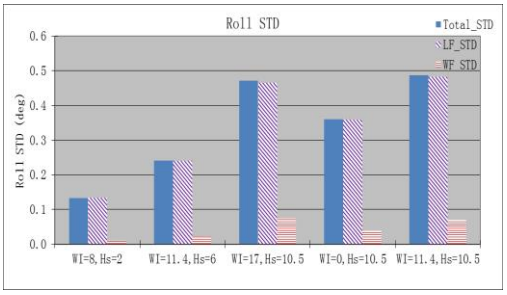

h) Roll STD

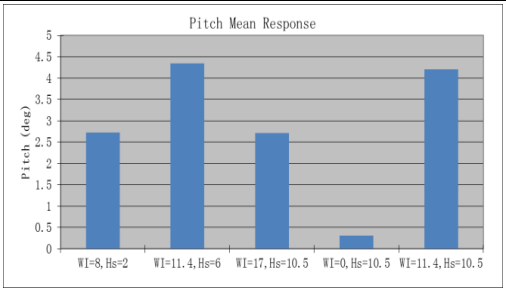

i) Pitch Mean

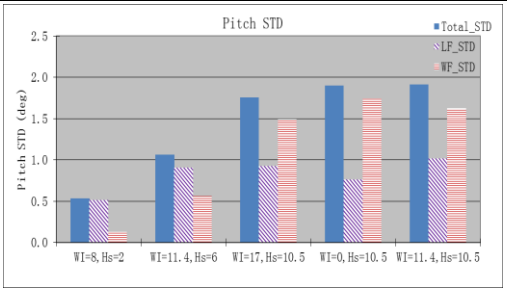

j) Pitch STD

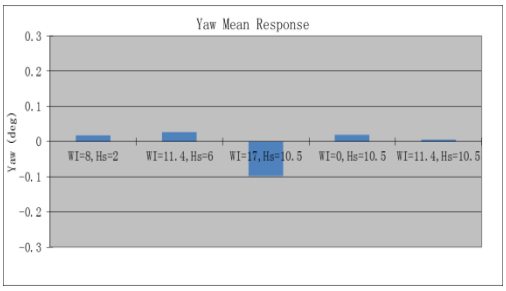

k) Yaw Mean

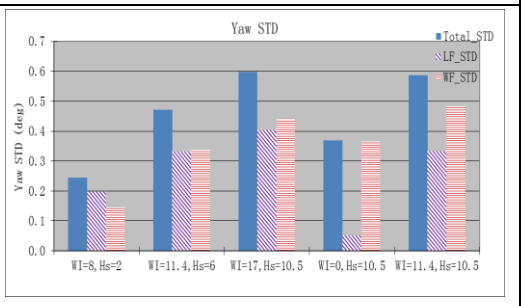

l) Yaw STD

Figure 4-14 Continued

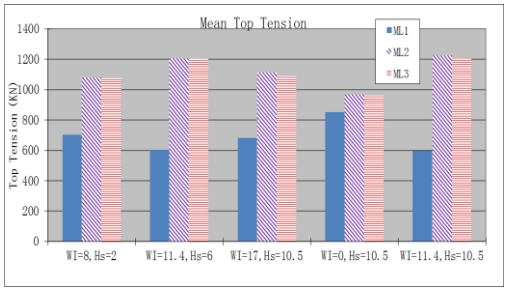

m) Top Tension Mean

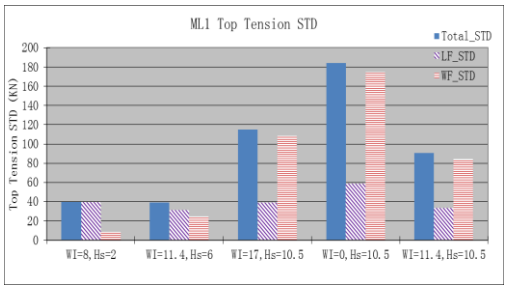

n) Top Tension STD of ML1

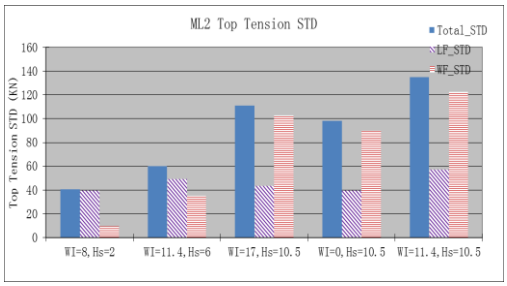

o) Top Tension STD of ML2

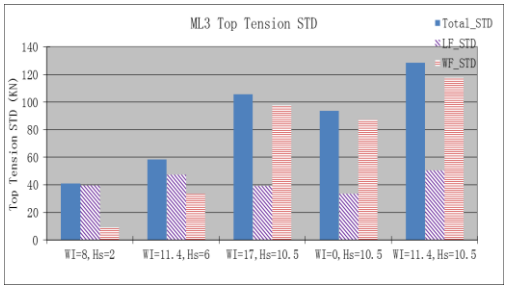

p) Top Tension STD of ML3

Figure 4-14 Continued

Noting that both wind and wave directions are in 0 deg, the mean surge is dominated by mean wind forces but also contributed from the mean wave forces. At the rated wind speed, the wind force dominants the mean surge response. The same trend is observed in mean pitch and mean top tensions in ML2 and ML3. The mean top tension of ML1 is the smallest with the rated wind speed. The sway, heave, roll and yaw mean responses are relatively small, which is expected.

The comparisons show that at the same wind speed higher significant wave height generates larger WF responses, which is also expected. Meanwhile, the LF dynamic responses are also increase with increased wave height, which result from the effects from second-order difference frequency wave forces.

At the same wind speed, higher significant wave height results in larger mean wave force, which causes larger mean surge and larger mooring stiffness in surge motion. Therefore, the LF surge response is slightly reduced in the case of larger wave conditions.

The sway and roll responses are mainly caused by the force induced by the blade rotation, which depends on the relative wind speed. Wave loads mainly induce the surge and pitch motions of the FOWT, which in turn increase the oscillating relative wind speed at the hub. Therefore, the sway and roll LF dynamic responses increase with the increase in the wave height as well. This phenomenon is clearly demonstrated in the wave only case. For the wave only case, the large pitch motion resulting from wave loads can introduce significant horizontal velocity at the hub. The relative velocity may make the blades rotate even in the absence of winds. As a result, the sway and roll low frequency dynamic responses are noticeable even in the wave only cases.

The statistics comparisons for Case 15 and Case 19-21 are shown in Figure 4-15. The four cases have the same mean wind speed at 11.4m/s and in 0 deg direction. They also have the same significant wave height of 6m and the same peak period at 10s, but the wave directions are different. In Figure 4-15, the blue column represents mean responses and total STD, the pink column STD of LF dynamic responses, the red column STD of WF dynamic responses. Also, in Figure 4-15 m), the blue, pink and red columns represent mean top tension responses of ML1, ML2 and ML3, respectively.

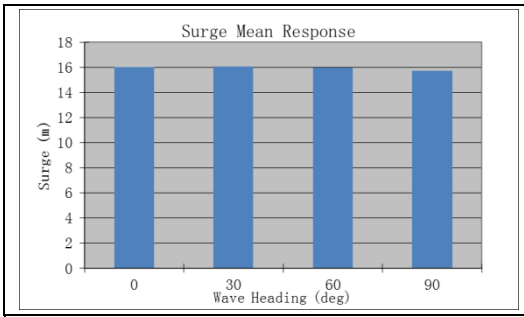

a) Surge Mean

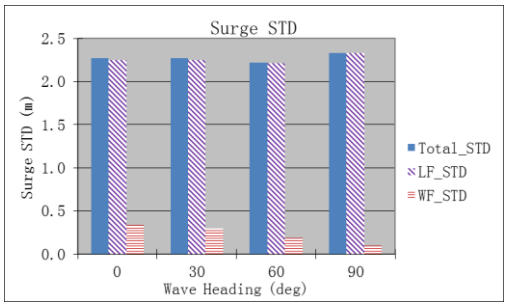

b) Surge STD

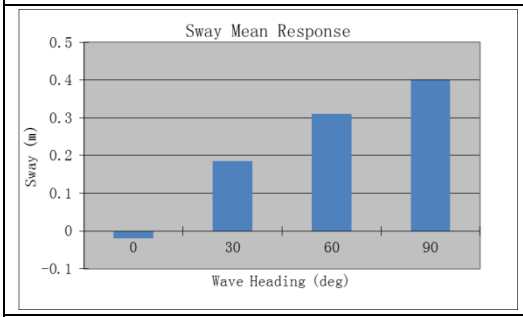

c) Sway Mean

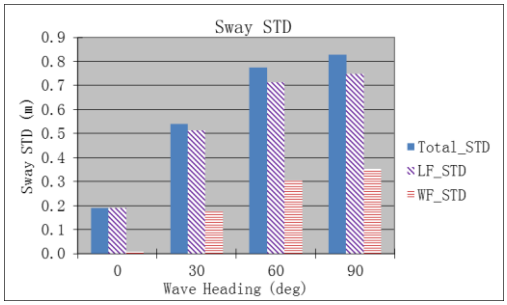

d) Sway STD

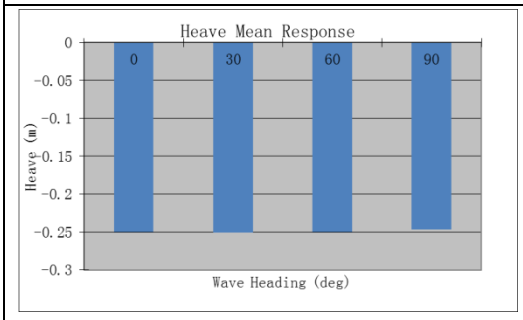

e) Heave Mean

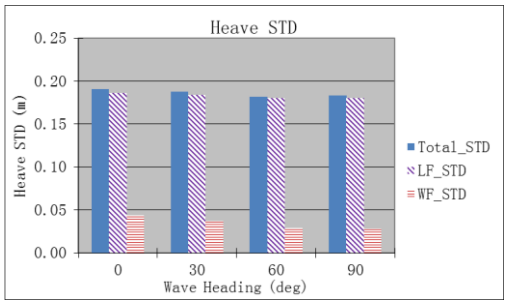

f) Heave STD

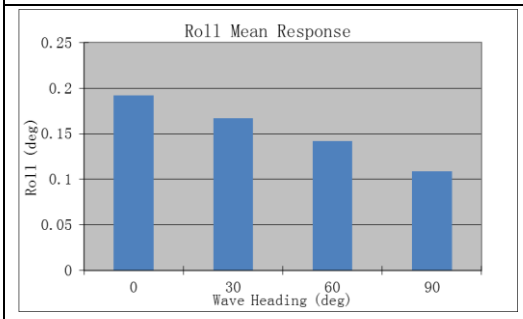

g) Roll Mean

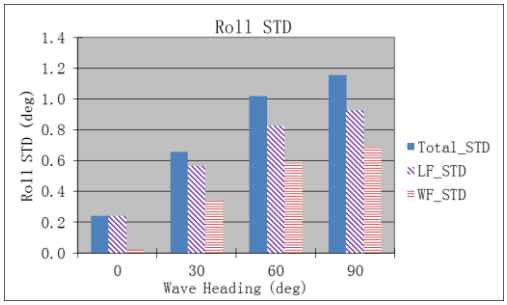

h) Roll STD

Figure 4-15 The FOWT Results Comparison for Case 15 and Case 19~21

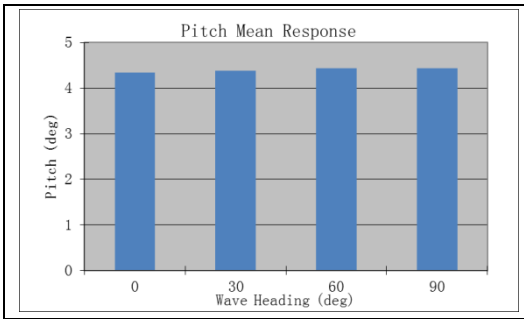

i) Pitch Mean

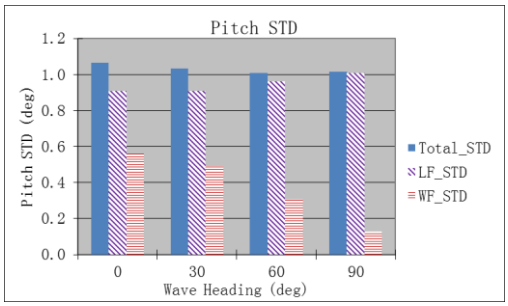

j) Pitch STD

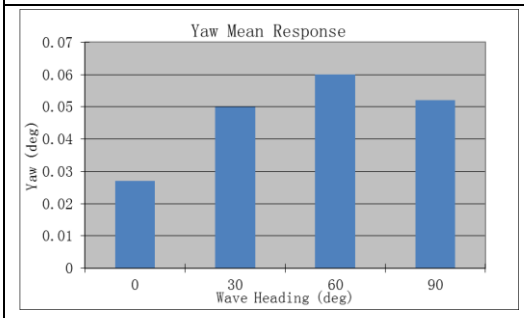

k) Yaw Mean

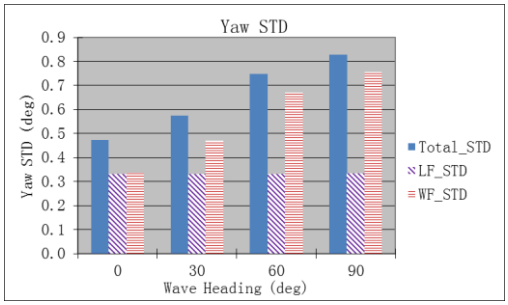

l) Yaw STD

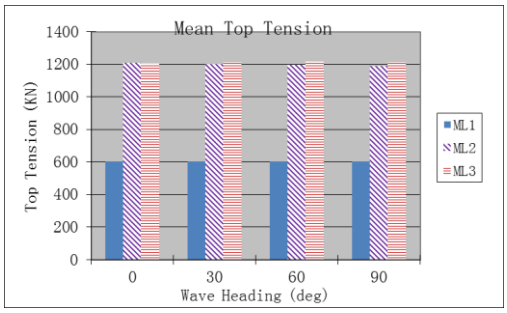

m) Top Tension Mean

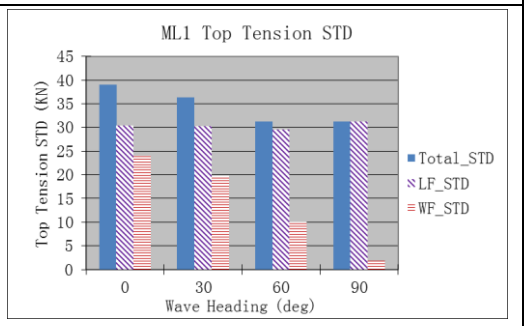

n) Top Tension STD of ML1

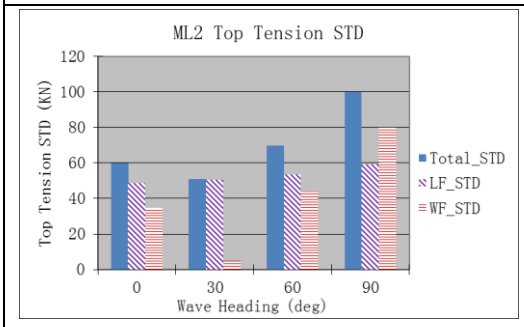

o) Top Tension STD of ML2

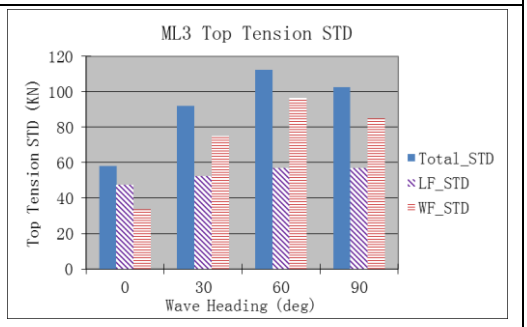

p) Top Tension STD of ML3

Figure 4-15 Continued

In these four cases, the wind direction is always 0 deg but the wave direction starts at 0 deg in Case 15 and gradually increases to 90 deg in Case 21.

It should be noted that the surge direction in Figure 4-15 is defined as the same direction of the wind. Hence it is always in the 0 deg direction. Except for Case 15, in the other three cases, wave and wind are in different directions, and the angle between them increases to 90 deg in Case 21. The trends observed in Figure 4-15 are summarized and discussed below.

1. The mean surge decreases with the increase in the angle between the wind and wave directions as shown in Figure 4-15 a). It is because the component of the wave mean force in the surge direction decreases when the wave direction increases from 0 deg to 90 deg. Because the mooring line stiffness in the surge direction decreases when the mean surge decreases, it is observed that the LF surge responses increase with the increase in the wave direction as shown in Figure 4-15 b). The WF surge responses are mainly from the wave loads. As a result, the WF surge responses decrease with increase in the wave direction, as shown in Figure 4-15 b).
2. The sway is mainly contributed by wave loads since the wind loads are virtually in the surge direction. The mean sway is the largest in Case 21 (90 deg wave) as shown in Figure 4-15 c). In addition, the dynamic sway responses (both LF and WF) are also the greatest in Case 21 as shown in Figure 4-15 d).

3. Both the LF and WF responses of the roll increases with the increase in the wave direction as shown in Figure 4-15 h), which is due to the wave loads and the asymmetric motion relative to the mooring layout.
4. The mean pitch virtually remains the same as shown in Figure 4-15 i). The pitch LF dynamic response increases with the increase in the wave direction as shown in Figure 4-15 j), which is due to the asymmetric motion relative to the mooring layout. Since the WF pitch is mainly from the wave loads, the pitch WF responses decrease with the increase in the wave direction.
5. The LF yaw responses are mainly from the wind and they virtually remain the same as shown in Figure 4-15 l). The WF yaw responses increase with increase in wave direction, which is from the asymmetric environment condition with respect to the mooring lines layout.
6. The mooring line top tensions mainly depend on the FOWT offset. Since the mean and LF offsets are dominated by winds, the mean and LF tensions do not change substantially when the wave direction changes. The WF dynamic top tensions depend on the angles between the mooring lines and the wave. When the wave is in-line with one of the mooring line, the WF dynamic top tension of this line is the largest (as ML3 with 60 deg wave). When the wave is perpendicular to one of the mooring line, the WF dynamic top tension is the smallest (as ML1 with 90 deg wave, or ML2 with 30 deg wave).

4.3 The Effect of Current on the FOWT

The Spar in our simulation has a deep draft and is susceptible to ocean currents. An assumed current profile described in Table 4-2 together with 11.4m/s wind speed, 6m significant wave height and 10s wave peak period are considered as the Met-Ocean condition in the simulation.

Table 4-2 Current Profile

Depth (m)	Current Velocity (m/s)
0	2
50	1
100	0.5
200	0.25

In Cases (22~25), the wind, wave and current are assumed to be collinear. However, their directions change from 0 deg to 90 deg with respect to the Global Reference CS from Case 22 to 25. The results are given in the Space-fixed CS in Figure 4-16, meaning that the "surge" is in the wind direction (also the wave and current directions). The blue column represents mean responses and STD of total dynamic responses. The pink column represents STD of LF dynamic responses, and the red column STD of WF dynamic responses.

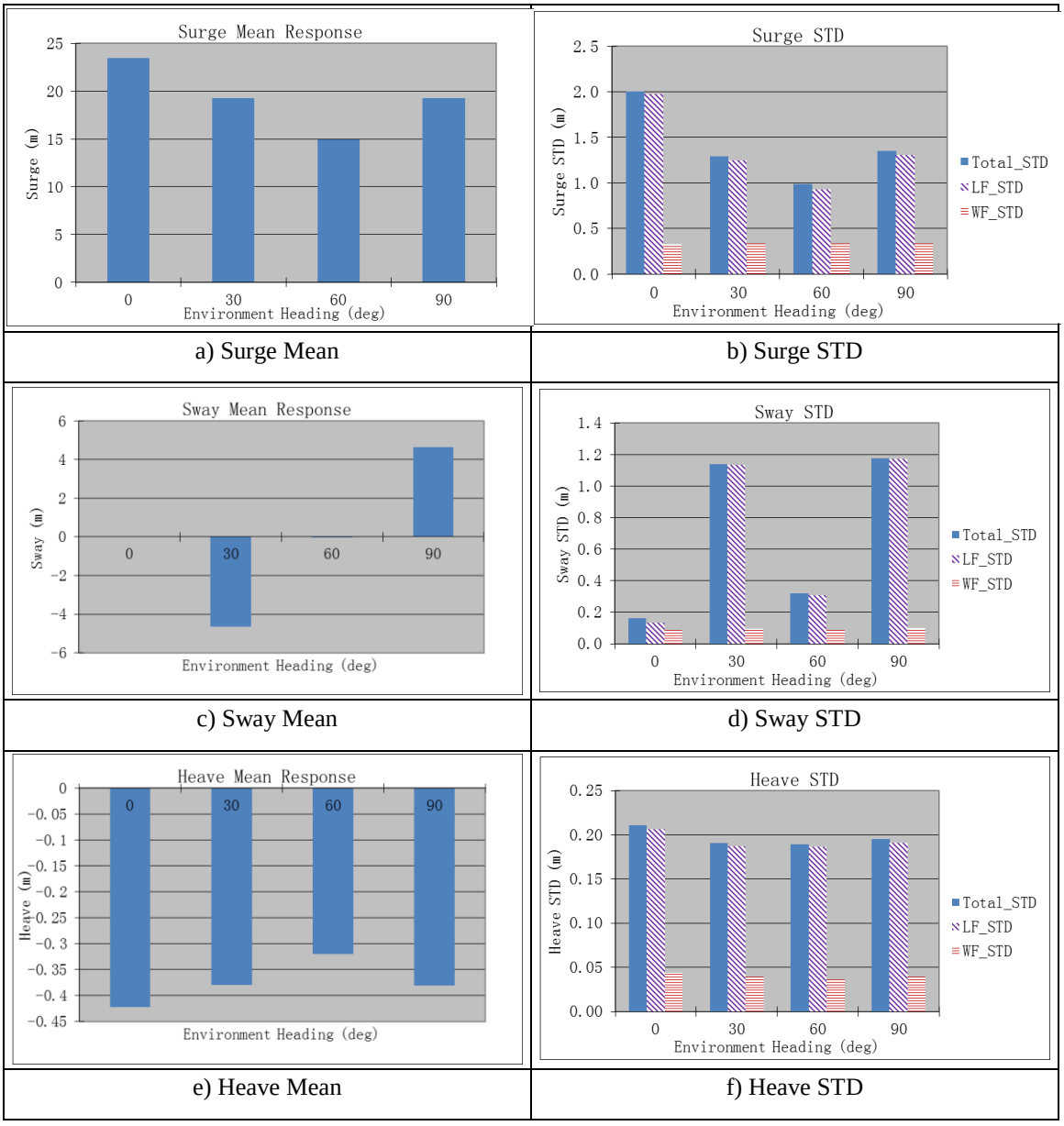

a) Surge Mean | b) Surge STD

c) Sway Mean | d) Sway STD

e) Heave Mean | f) Heave STD

Figure 4-16 The FOWT Results Comparison for Case 21~24

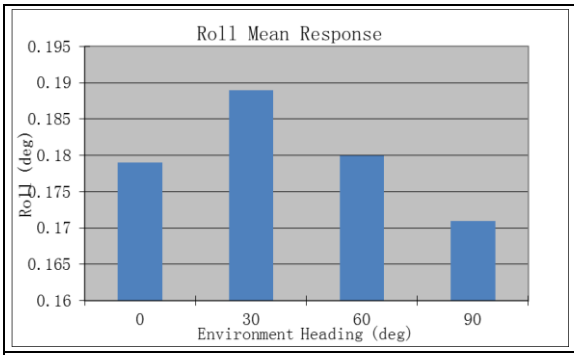

g) Roll Mean

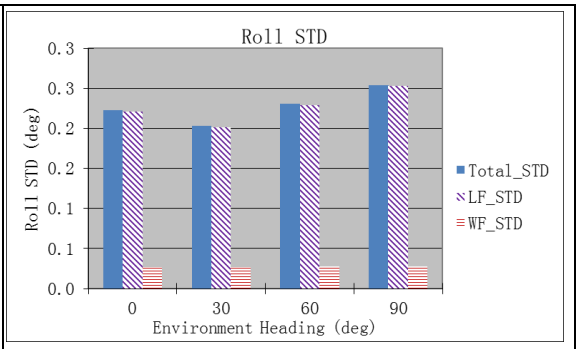

h) Roll STD

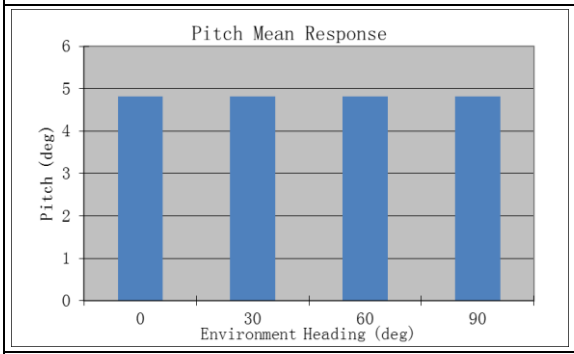

i) Pitch Mean

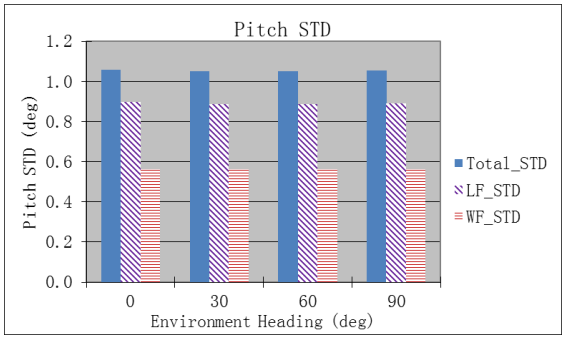

j) Pitch STD

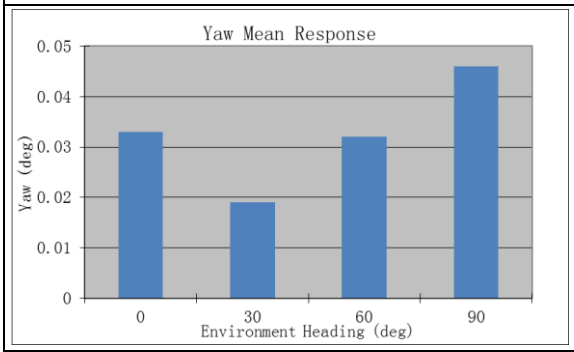

k) Yaw Mean

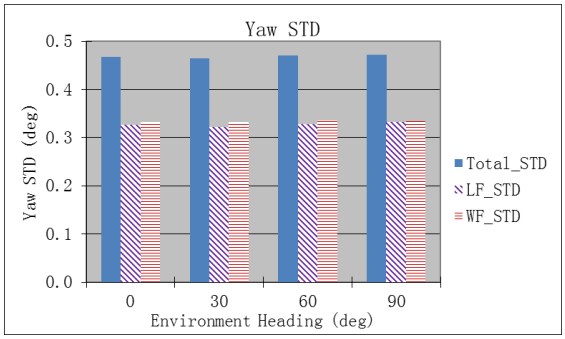

l) Yaw STD

Figure 4-16 Continued

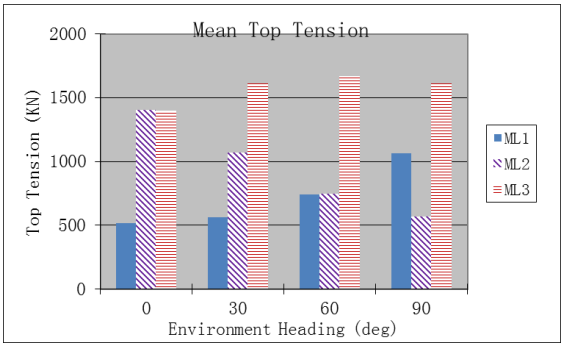

m) Top Tension Mean

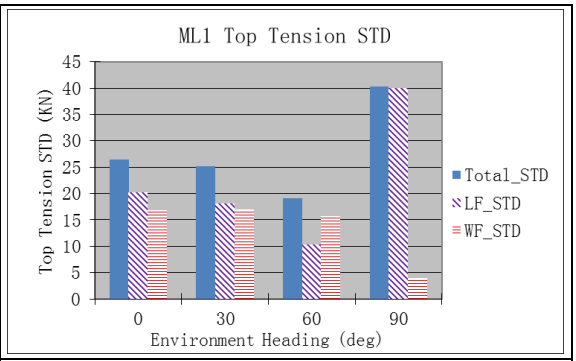

n) Top Tension STD of ML1

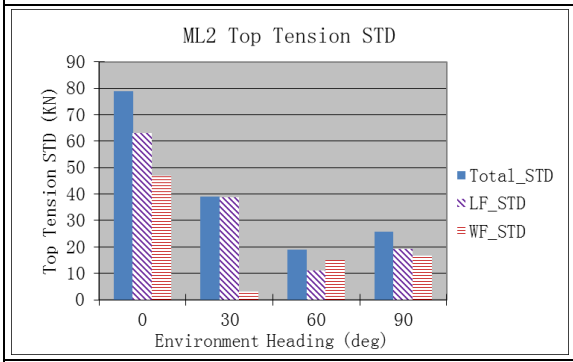

o) Top Tension STD of ML2

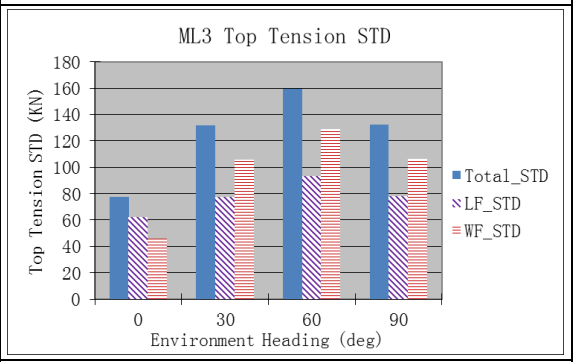

p) Top Tension STD of ML3

Figure 4-16 Continued

As shown in Figure 4-16, comparing with the "wind and wave" cases (case 15 and 19-21, shown in Figure 4-15), the current increases the mean surge response significantly, but it reduces the LF surge dynamic response. This is due to the increase in the mooring stiffness with the increase in the mean offset. For the pitch, the current loads increase the mean pitch. This is because the Spar platform has a deep draft and the center of current force is above the reference point (COG of FOWT). The dynamic pitch response is mainly from the wind and wave; therefore it is not changed significantly in the presence of the current. The mean tension in mooring lines is related to the mean offset and the directions of wind, wave and current with respect to the mooring system

layout. Since the current can increase offset, it increases the mooring stiffness as well. As a result, slack line top tension is reduced by current and the tighten line top tension is increases.

5 SUMMARY

Based on the two existing codes, COUPLE and FAST, a numerical code, known as, COUPLE-FAST, has been developed for simulating the dynamics of a FOWT in this study. To demonstrate the capabilities of COUPLE-FAST, a FOWT, known as OC3-Hywind, is selected as the theme FOWT for this study. OC3-Hywind has a NREL 5MW wind turbine installed on the top of a Spar-type floating platform. Total 25 cases for different combinations of winds, waves and currents are simulated, in which the motions of the FOWT and tension in the mooring lines are predicted. The simulated results reveal interesting trends of the FOWT motions and tensions in the mooring lines in relation to different met-ocean conditions. Although the simulations are made based on OC3-Hywind, COUPLE-FAST developed in this study can be applied to the simulations of other types of FOWTs, such as TLPs and semi-submersibles. The observations made based on the numerical simulation may have important implications for the future design of FOWTs. They are summarized below.

1) The mean wind loads applied on the wind turbine increase with the increase in the mean wind speed until it reaches the rated wind speed. Because the blade control system adjusts the blade pitch angle when the wind speed exceeds the rated wind speed, the mean wind loads decrease with the increase in the mean wind speed. Consequently, the winds at the rated wind speed result in the largest mean wind loads and hence largest mean surge and pitch

of the FOWT. Correspondingly, the mean top tension in the mooring line located at the upwind-side is the largest.

2) Even when the winds are uniform and steady, the wind speed with respect to the wind turbine may not remain steady because of the surge and pitch oscillations of the supporting platform. Our numerical simulation demonstrates that when the speed of the steady wind is above the rated wind speed, the wind speed with respect to the wind turbine may be fluctuated due mainly to the surge of the supporting platform. The fluctuating relative wind speed may trigger off the increase and decrease in the blade pitch angle by the blade control system. Therefore, a steady wind may still result in dynamic wind loads on the wind turbine. The dynamic wind loads and the surge of the platform can enhance each other and lead to the resonant interaction between them, also known as 'negative damping' [20]. Owing to the hydrodynamic damping to the supporting platform, the resonant surge eventually reaches a steady state. Because of the fact that the change rate of wind loads decreases fastest when the relative wind speed is slightly higher than the rated wind speed, the most significant resonant interaction or negative damping occurs at the steady wind of 11.6m/s, which is about 0.2m/s higher than the rated wind speed.
3) Our simulation shows that the turbulent winds of the mean speed 11.6m/s also result in the largest dynamic surge, which is consistent with the observation made in the case of 11.6m/s steady wind. However, the

‘resonance’ phenomenon is not as significant as seen in the cases of corresponding steady winds. This is because the wind speed of turbulent winds is fluctuating even in the absence of the surge or pitch, which induces dynamic wind loads of frequencies near the surge natural frequency of the FOWT. It is found the dynamic surge and pitch of the FOWT under the impact of 11.6m/s turbulent winds are marginally higher than those under 11.4m/s turbulent winds. This finding indicates it may not necessary to make additional efforts to improve the blade control system for reducing or eliminate ‘negative damping’.

4) The time series of the rolling of the FOWT demonstrate a ‘beat’ pattern, indicating that the rolling may consist of two dominant oscillations of close frequencies. It is found that one of the two dominant oscillations is at the rolling natural frequency of the FOWT and the other at the blade rotation natural frequency.
5) The mean top tension in a mooring line mainly depends on the offset and the orientation of the mooring line with respect to the major offsets.
6) Steeper waves result in larger oscillations (such as surge and pitch) of the FOWT. In turn, they enhance the turbulence in winds with respect to the wind turbine. The fluctuations in the wind speed may vary the rotational speed of the blades and result in larger LF response in the sway and roll of the FOWT.

7) Current loads on the hull of the FOWT in general increase the offset significantly when the current are collinear with winds and waves, which in turn increase the tensions in the mooring lines located at the upwind-side.

REFERENCES

[1] J. M. Jonkman and M. L. Buhl, "FAST User's Guide," National Renewable Energy Laboratory, Golden, CO, 2005.

[2] S. Lindenberg, B. Smith, K. O'Dell, E. DeMeo, B. Ram, B. Alderfer, *et al.*, "20% Wind Energy by 2030. Increasing Wind Energy's Contribution to U.S. Electricity Supply. Executive Summary," U.S. Department of Energy, Oak Ridge, TN, 2008.

[3] "Europe's Onshore and Offshore Wind Energy Potential," European Environment Agency, Copenhagen, Denmark, 2009.

[4] J. Beaudry-Losique, T. Boling, J. Brown-Saracino, P. Gilman, M. Hahn, C. Hart, *et al.*, "A National Offshore Wind Strategy: Creating an Offshore Wind Energy Industry in the United States.," U.S. Department of Energy, Washington, DC, 2011.

[5] M. J. Dvorak, B. A. Corcoran, J. E. T. Hoeve, N. G. Mclntyre, and M. Z. Jacobson, "US East Coast Offshore Wind Energy Resources and Their Relationship to Peak-time Electricity Demand," *Wind Energy*, vol. 16, pp. 977-997, 2013.

[6] G. Corbetta, I. Pineda, J. Moccia, and J. Guillet, "The European Offshore Wind Industry Key Trends and Statistics 2013," European Wind Energy Association, Brussels, Belgium, 2014.

[7] M. Drajem and A. Herndon, "Deepwater Wins First Auction for U.S. Offshore Wind Lease", 2013, Available: http://www.bloomberg.com/news/2013-07-31/deepwater-wind-wins-auction-for-first-offshore-wind-lease.html

[8] H. Stiesdal, "Hywind: The World's First Floating MW-scale Wind Turbine," *Wind Directions,* vol. 31, pp. 52-53, 2009.

[9] Z. Shahan, "1st-of-its-kind Floating Wind Turbine Technology to be Deployed by Vestas & WindPlus", 2011, Available: http://cleantechnica.com/2011/02/23/1st-of-its-kind-floating-wind-turbine-technology-to-be-deployed-by-vestas-windplus-video/

[10] J. Jonkman and D. Matha, "A Quantitative Comparison of the Responses of Three Floating Platforms," National Renewable Energy Laboratory, Golden, CO, 2010.

[11] J. M. Jonkman, "Dynamics Modeling and Loads_ Analysis of an Offshore Floating Wind Turbine," National Renewable Energy Laboratory, Golden, CO, 2007.

[12] S. Shim and M. H. Kim, "Rotor-floater-mooring Coupled Dynamic Analysis of Mini TLP-type Offshore Floating Windturbines," presented at the Proceedings of the Eighteenth (2008) International Offshore and Polar Engineering Conference, Vancouver, Canada, pp. 455-460, 2008.

[13] Y. H. Bae, M. H. Kim, S. W. Im, and I. H. Chang, "Aero-Elastic-Control-Floater-Mooring Coupled Dynamic Analysis of Floating Offshore Wind Turbines," presented at the Proceedings of the Twenty-first (2011) International

Offshore and Polar Engineering Conference, Maui, Hawaii, USA, pp. 429-435, 2011.

[14] M. Masciola, A. Robertson, J. Jonkman, and F. Driscoll, "Investigation of a FAST-OrcaFlex Coupling Module for Integrating Turbine and Mooring Dynamics of Offshore Floating Wind Turbines," National Renewable Energy Laboratory, Golden, CO, 2011.

[15] M. Karimirad and T. Moan, "Wave- and Wind-Induced Dynamic Response of a Spar-Type Offshore Wind Turbine," *Journal of Waterway, Port, Coastal, and Ocean Engineering,* vol. 138, pp. 9-20, 2012.

[16] C. Peng, F. S. Yan, and J. Zhang, "Coupled Dynamic Analysis of a Floating Offshore Wind Turbine," presented at the Proceedings of the 17th Offshore Symposium, Texas Section of the Society of Naval Architects and Marine Engineers Houston, Texas, pp. C31-C40, 2012.

[17] F. S. Yan, C. Peng, J. Zhang, and D. Zhang, "Dynamic Response of an Offshore Wind Turbine System Using Coupled and Limited Coupled Methods," presented at the Proceedings of the ASME 2012 31st International Conference on Ocean, Offshore and Arctic Engineering, OMAE2012, Rio de Janeiro, Brazil, pp. 605-616, 2012.

[18] Y. H. Bae and M. H. Kim, "Rotor-floater-tether Coupled Dynamics Including Second-order Sum–frequency Wave Loads for a Mono-column-TLP-type FOWT (Floating Offshore Wind Turbine)," *Ocean Engineering,* vol. 61, pp. 109-122, 2013.

[19] C. Peng, F. S. Yan, and J. Zhang, "Coupled Dynamic Response of a Spar Type Floating Offshore Wind Turbine," presented at the Proceedings of the ASME 2014 33rd International Conference on Ocean, Offshore and Arctic Engineering, OMAE2014, San Francisco, CA, pp. V09AT09A035, 2014.

[20] T. J. Larsen and T. D. Hanson, "A Method to Avoid Negative Damped Low Frequent Tower Vibrations for a Floating, Pitch Controlled Wind Turbine," *Journal of Physics: Conference Series*, vol. 75, pp. 1-11, 2007.

[21] A. N. Robertson, J. M. Jonkman, A. J. Goupee, A. J. Coulling, I. Prowell, J. Browning, *et al.*, "Summary of Conclusions and Recommendations Drawn from the DeepCwind Scaled Floating Offshore Wind System Test Campaign," presented at the Proceedings of the ASME 2013 32nd International Conference on Ocean, Offshore and Arctic Engineering, Nantes, France, pp. V008T09A053, 2013.

[22] B. Koo, A. J. Goupee, K. Lambrakos, and H. Lim, "Model Test Correlation Study for a Floating Wind Trubine on a Tension Leg Platform," presented at the Proceedings of the ASME 2013 32nd International Conference on Ocean, Offshore and Arctic Engineering, Nantes, France, pp. V008T09A101, 2013.

[23] A. J. Coulling, A. J. Goupee, A. N. Robertson, and J. M. Jonkman, "Importance of Second-order Difference-frequency Wave-diffraction Forces in the Validation of a FAST Semi FWT," presented at the Proceedings of the ASME 2013 32nd International Conference on Ocean, Offshore and Arctic Engineering (OMAE 2013), Nantes, France, pp. V008T09A019, 2013.

[24] A. J. Goupee, B. Koo, R. W. Kimball, K. F. Lambrakos, and H. J. Dagher, "Experimental Comparison of Three Floating Wind Turbine Concepts," presented at the Proceedings of the ASME 2012 31st International Conference on Ocean, Offshore and Arctic Engineering, Rio de Janeiro, Brazil, pp. 467-476, 2012.

[25] M. J. Fowler, R. W. Kimball, D. A. T. III, and A. J. Goupee, "Design and Testing of Scale Model Wind Turbines for Use in Wind Wave Basin Model Tests of Floating Offshore Wind Turbines," presented at the Proceedings of the ASME 2013 32nd International Conference on Ocean, Offshore and Arctic Engineering Nantes, France, pp. V008T09A004, 2013.

[26] J. R. Browning, J. Jonkman, and A. Robertson, "Calibration and Validation of a Spar-type Floating Offshore Wind Turbine Model Using the FAST Dynamic Simulation Tool," National Renewable Energy Laboratory, Golden, CO, 2012.

[27] G. M. Stewart, M. A. Lackner, A. Robertson, J. Jonkman, and A. J. Goupee, "Calibration and Validation of a FAST Floating Wind Turbine Model of the DeepCwind Scaled Tension-leg Platform," presented at the Proceedings of the Twenty-second (2012) International Offshore and Polar Engineering Conference, Rhodes, Greece, pp. 380-387, 2012.

[28] H. Shin and P. T. Dam, "Model Test of a Floating Offshore Wind Turbine Moored by a Spring-tensioned-leg," presented at the Proceedings of the Twenty-second (2012) International Offshore and Polar Engineering Conference, Rhodes, Greece, pp. 287-291, 2012.

[29] M. Nur-E-Mostafa, M. Murai, R. Nishimura, O. Fujita, and Y. Nihei, "Experimental Validation for Motion of Spar-type Floating Wind Turbine at Inclination with Effect of Gyro Moment of the Rotating Blade of Windmill," presented at the Proceedings of the Twenty-second (2012) International Offshore and Polar Engineering Conference, Rhodes, Greece, pp. 292-299, 2012.

[30] N. Ren, Y. Li, and J. Ou, "The Wind-wave Tunnel Test of a New Offshore Floating Wind Turbine with Combined Tension Leg-mooring Line System," presented at the Proceedings of the Twenty-second (2012) International Offshore and Polar Engineering Conference, Rhodes, Greece, pp. 255-261, 2012.

[31] K. Kokubun, S. Ishida, T. Nimura, T. Chujo, S. Yoshida, and T. Utsunomiya, "Model Experiment of a Spar Type Offshore Wind Turbine in Storm Condition," presented at the Proceedings of the ASME 2012 31st International Conference on Ocean, Offshore and Arctic Engineering (OMAE 2012), Rio de Janeiro, Brazil, pp. 569-575, 2012.

[32] H. Shin, B. Kim, P. T. Dam, and K. Jung, "Motion of OC4 5MW Semi-Submersible Offshore Wind Turbine in Irregular Waves," presented at the Proceedings of the ASME 2013 32nd International Conference on Ocean, Offshore and Arctic Engineering, Nantes, France, pp. V008T09A028, 2013.

[33] M. L. Boulluec, J. Ohana, A. Martin, and A. Houmard, "Tank Testing of a New Concept of Floating Offshore Wind Turbine," presented at the Proceedings of the ASME 2013 32nd International Conference on Ocean, Offshore and Arctic Engineering, Nantes, France, pp. V008T09A100, 2013.

[34] L. Sethuraman and V. Venugopal, "Hydrodynamic Response of a Stepped-spar Floating Wind Turbine: Numerical Modelling and Tank Testing," *Renewable Energy*, vol. 52, pp. 160-174, 2013.

[35] S. Ishida, K. Kokubun, T. Nimura, T. Utsunomiya, I. Sato, and S. Yoshida, "At-sea Experiment of a Hybrid Spar Type Offshore Wind Turbine," presented at the Proceedings of the ASME 2013 32nd International Conference on Ocean, Offshore and Arctic Engineering, Nantes, France, pp. V008T09A035, 2013.

[36] T. Utsunomiya, I. Sato, S. Yoshida, H. Ookubo, and S. Ishida, "Dynamic Response Analysis of a Floating Offshore Wind Turbine During Severe Typhoon Event," presented at the Proceedings of the ASME 2013 32nd International Conference on Ocean, Offshore and Arctic Engineering, Nantes, France, pp. V008T09A032, 2013.

[37] T. Chujo, Y. Minami, T. Nimura, and S. Ishida, "Experimental Study for SPAR Type Floating Offshore Wind Turbine With Blade Pitch-Angle Control," presented at the Proceedings of the ASME 2013 32nd International Conference on Ocean, Offshore and Arctic Engineering, Nantes, France, pp. V008T09A034, 2013.

[38] J. Jonkman, S. Butterfield, W. Musial, and G. Scott, "Definition of a 5-MW Reference Wind Turbine for Offshore System Development," National Renewable Energy Laboratory, Golden, CO2009.

[39] P. J. Moriarty and A. C. Hansen, "AeroDyn Theory Manual," National Renewable Energy Laboratory, Golden, CO2005.

[40] X. Chen, Y. Ding, J. Zhang, P. Liagre, J. Niedzwecki, and P. Teigen, "Coupled Dynamic Analysis of a Mini TLP: Comparison with Measurements," *Ocean Engineering,* vol. 33, pp. 93-117, 2006.

[41] D. Jia, "An Efficient Numerical Scheme for Simulating Unidirectional Irregular Waves Based on a Hybrid Wave Model," M.S. Thesis, Texas A&M University, 2012.

[42] C. Li, "Coupled Analysis of the Motion and Mooring Loads of a Spar 'Constitution'," M.S. Thesis, Texas A&M University, 2012.

[43] D. J. Laino and A. C. Hansen, "User's Guide to the Wind Turbine Aerodynamics Computer Software AeroDyn," Windward Engineering LC., Salt Lake City, UT, 2002.

[44] X. Chen, "Studies on Dynamic Interaction between Deep-water Floating Structures and Their Mooring Tendon Systems," PhD. dissertation, Texas A&M University, 2002.

[45] J. Zhang, L. Chen, M. Ye, and R. E. Randall, "Hybrid Wave Model for Unidirectional Irregular Waves Part1: Theory and Numerical Shceme," *Applied Ocean Research,* vol. 18, pp. 77-92, 1996.

[46] J. Zhang, K. Hong, and D. K. P. Yue, "Effects of Wavelength Ratio on Wave Modelling," *J. Fluid Mech.,* vol. 248, pp. 107-127, 1993.

[47] A. R. Jha, *Wind Turbine Technology*: Boca Raton, FL : CRC Press, 2011.

[48] J. Jonkman, "Definition of the Floating System for Phase IV of OC3," National Renewable Energy Laboratory, Golden, CO, 2010.

APPENDIX 1. FOWT PITCH NATURAL FREQUENCY WITH AND WITHOUT TOWER FLEXIBILITY

The FOWT can be separated into two parts: the wind turbine part and the supporting platform part. In the COUPLE-FAST, the supporting platform is a rigid body; the tower of wind turbine is a flexible body. The flexibility of tower may have effects to the combined platform pitch natural frequency. Different tower flexibilities are tested. The combined 1st order and 2nd order natural frequencies of tower and FOWT are obtained by solving Eigen analysis with FEM method. The results in the Eigen analysis are shown in Table A 1-1.

Table A 1-1 Results of Eigen Analysis

Flexibility(EI) Factor	Tower Bending Natural Frequency (rad/s)		FOWT Pitch Natural Frequency (rad/s)	
	1st	2nd	Rigid Tower	Flexible Tower
0.01	0.25	2.57	0.20	0.17
0.05	0.56	5.74	0.20	0.19
0.25	1.28	13.18	0.20	0.20
0.50	1.77	15.83	0.20	0.20
1.00	2.55	26.32	0.20	0.20
2.00	3.61	37.19	0.20	0.20
4.00	5.11	52.51	0.20	0.20

From the results, it is shown that when the tower 1st bending natural frequency is far away from the FOWT (rigid tower) pitch natural frequency, the FOWT (flexible tower) pitch natural frequency doesn't change much with the change in tower flexibility. If the tower 1st natural frequency is close to the FOWT (rigid tower) pitch natural frequency, the FOWT (flexible tower) pitch natural frequency would be reduced by the tower flexibility. With the properties used in this research, the tower flexibility doesn't affect the FOWT (flexible tower) pitch natural frequency.

APPENDIX 2. SIMULATION RESULTS FOR CASE 4 – CASE 25

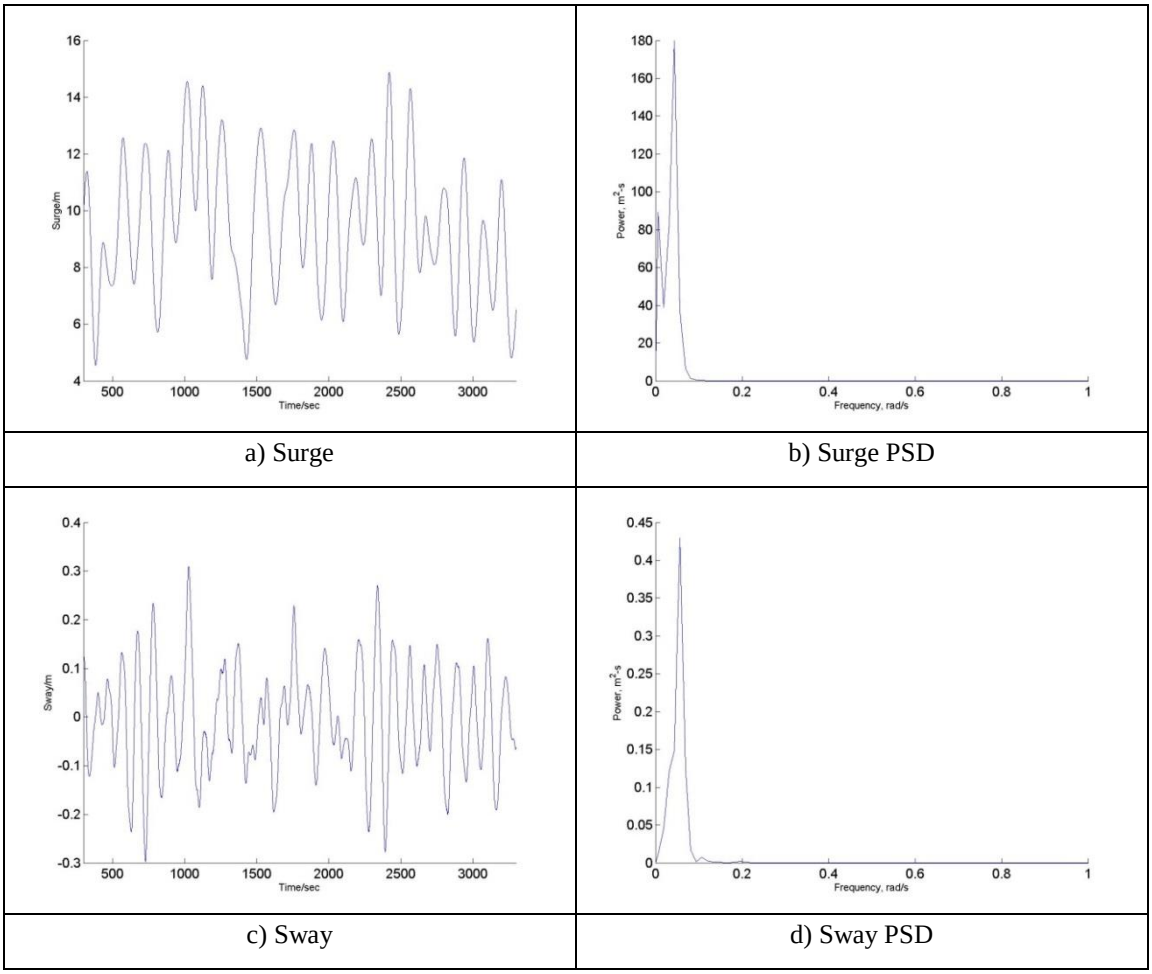

a) Surge | b) Surge PSD

c) Sway | d) Sway PSD

Figure A 2-1 The FOWT Results for Case 4

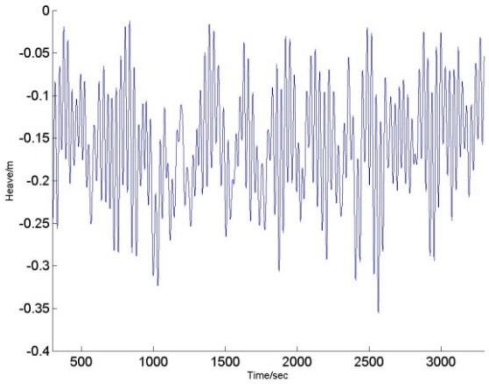

e) Heave

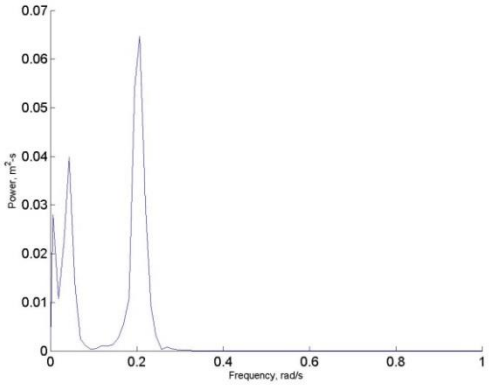

f) Heave PSD

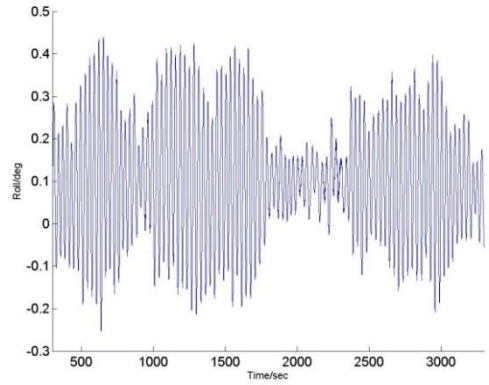

g) Roll

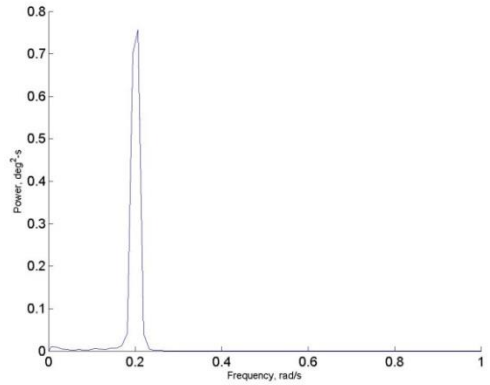

h) Roll PSD

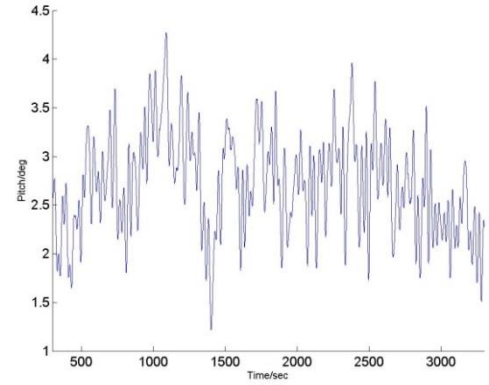

i) Pitch

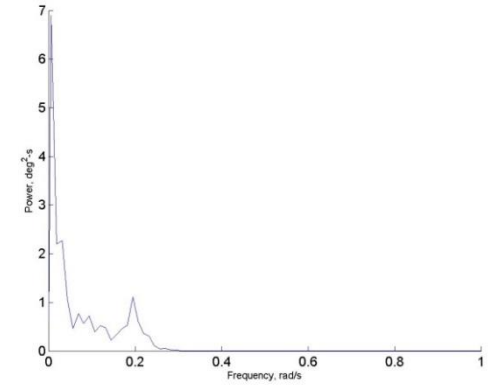

j) Pitch PSD

Figure A 2-1 Continued

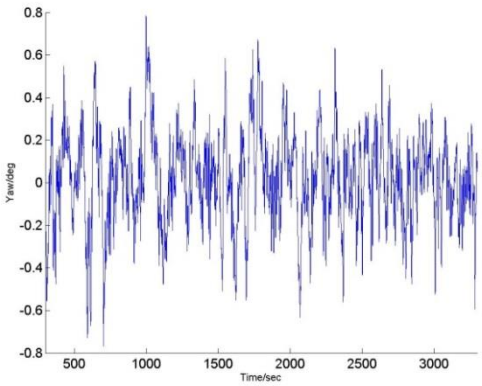

k) Yaw

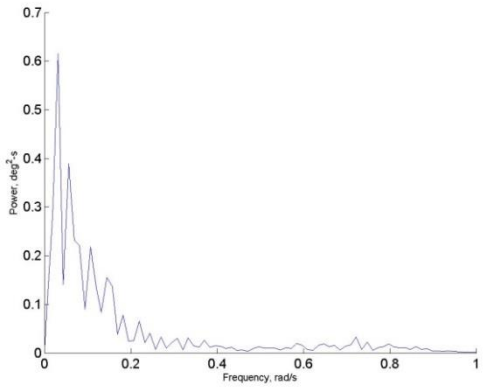

l) Yaw PSD

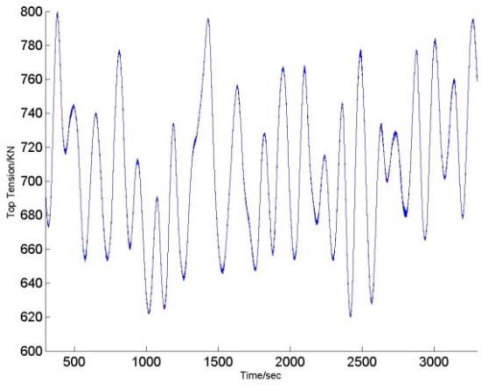

m) Top Tension of ML1

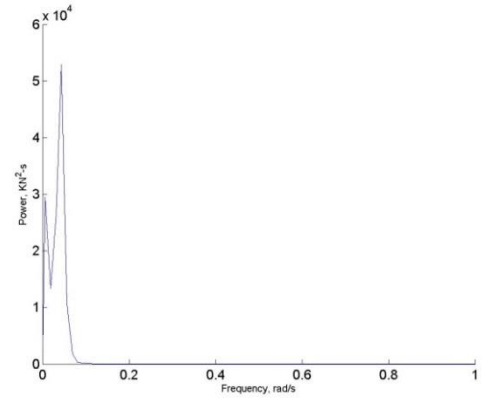

n) Top Tension PSD of ML1

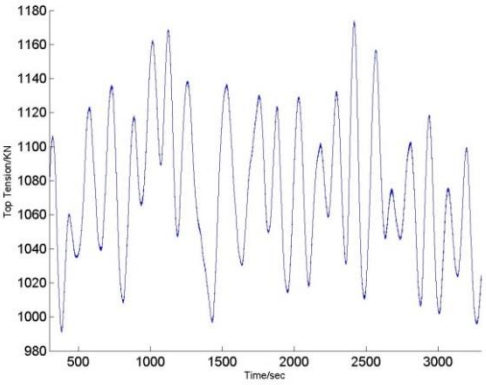

o) Top Tension of ML2

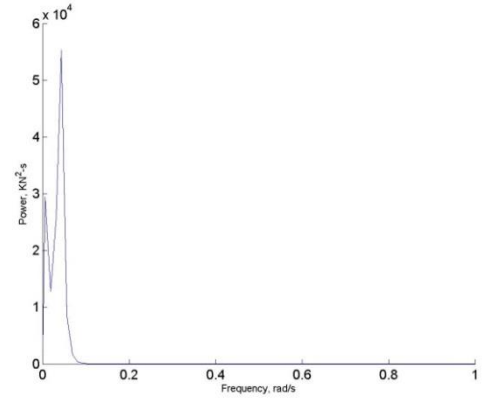

p) Top Tension PSD of ML2

Figure A 2-1 Continued

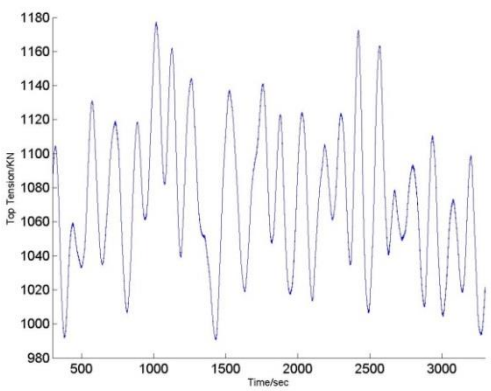

q) Top Tension of ML3

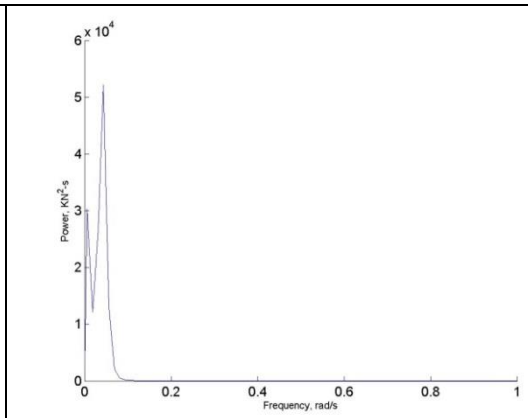

r) Top Tension PSD of ML3

Figure A 2-1 Continued

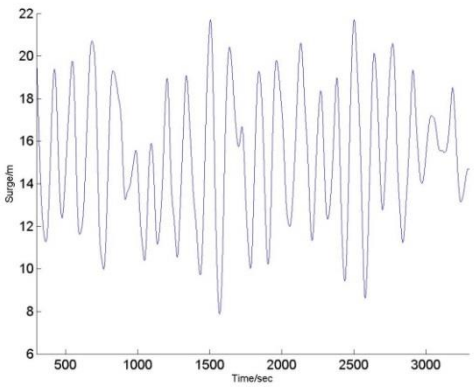

a) Surge

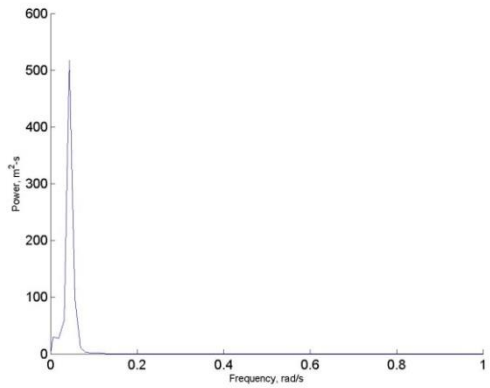

b) Surge PSD

Figure A 2-2 The FOWT Results for Case 5

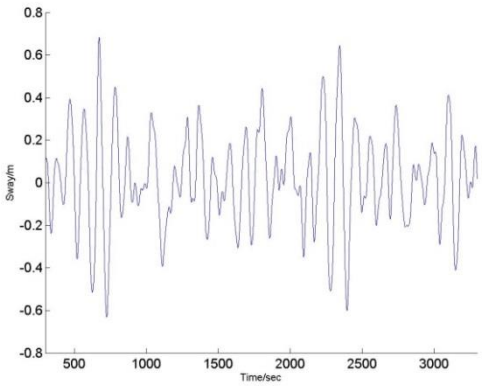

c) Sway

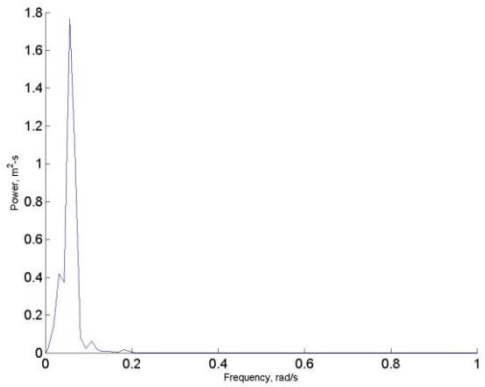

d) Sway PSD

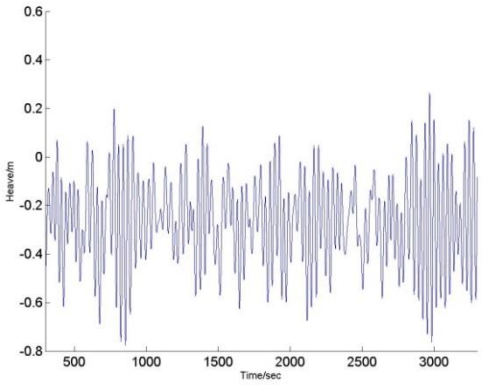

e) Heave

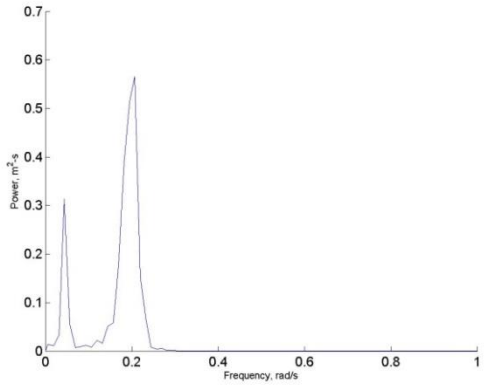

f) Heave PSD

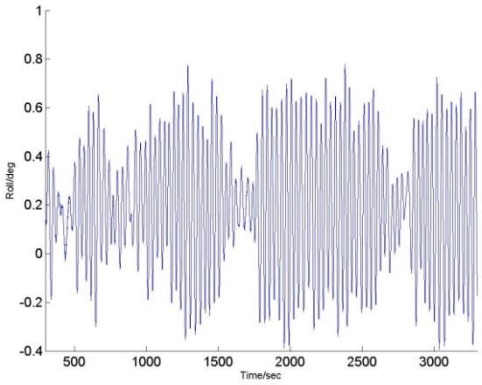

g) Roll

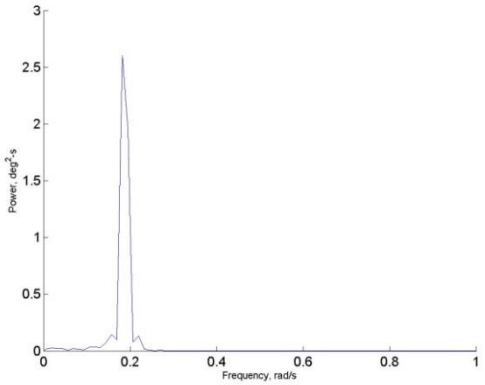

h) Roll PSD

Figure A 2-2 Continued

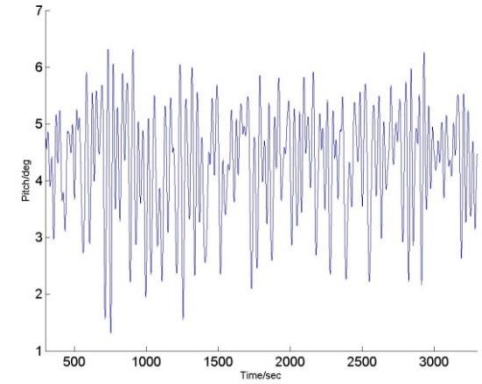

i) Pitch

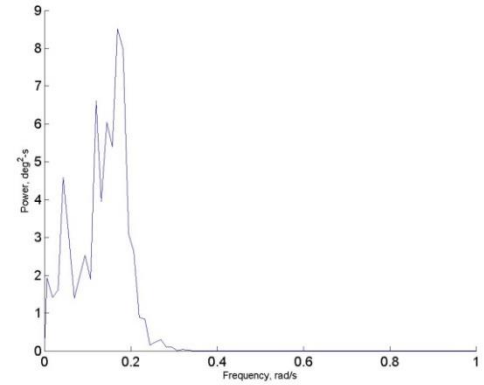

j) Pitch PSD

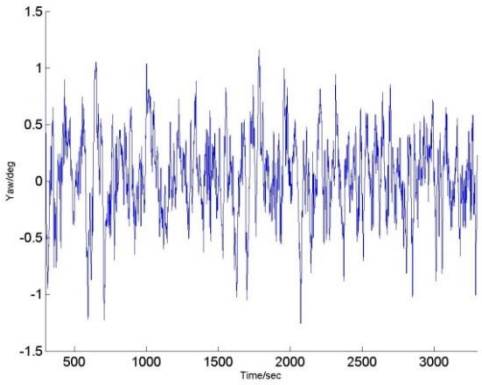

k) Yaw

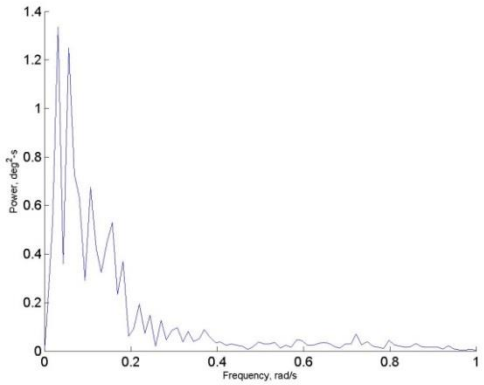

l) Yaw PSD

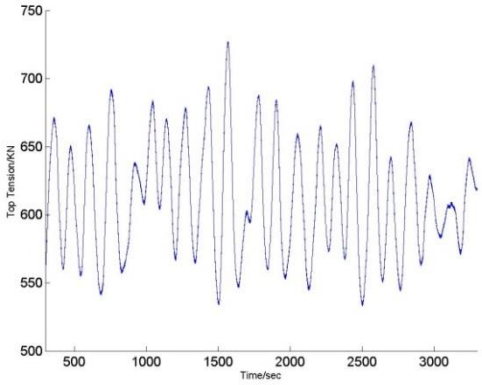

m) Top Tension of ML1

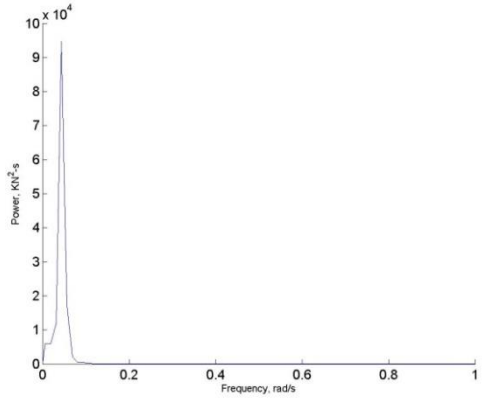

n) Top Tension PSD of ML1

Figure A 2-2 Continued

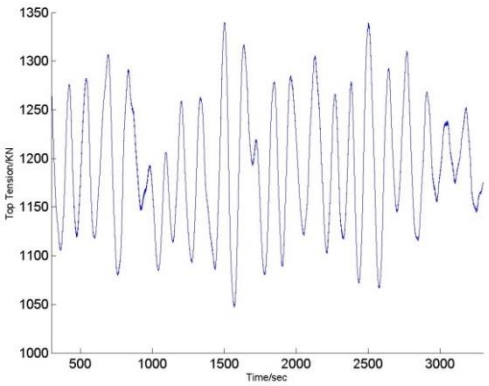

o) Top Tension of ML2

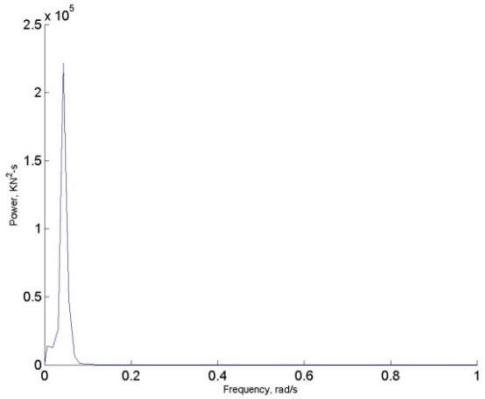

p) Top Tension PSD of ML2

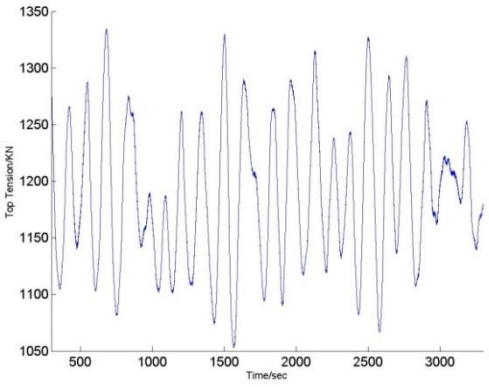

q) Top Tension of ML3

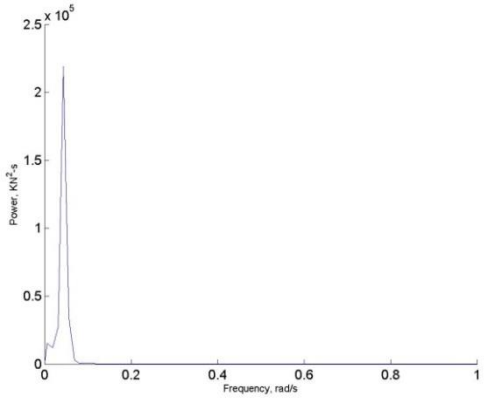

r) Top Tension PSD of ML3

Figure A 2-2 Continued

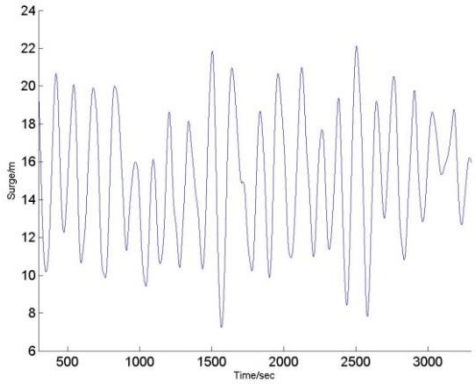

a) Surge

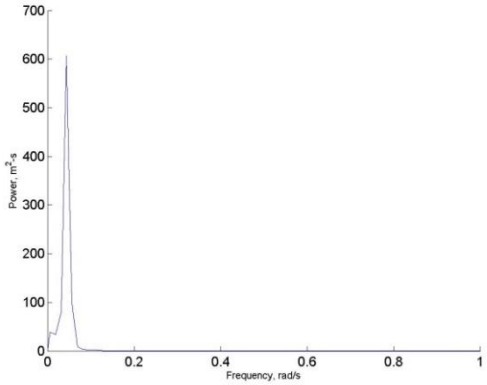

b) Surge PSD

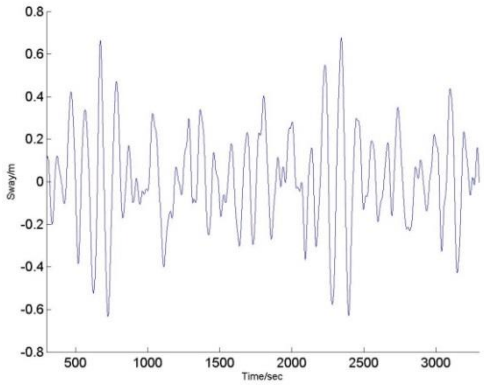

c) Sway

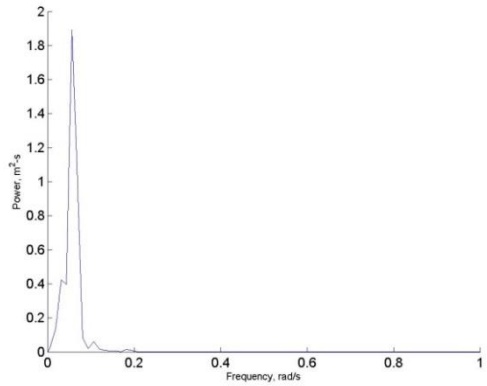

d) Sway PSD

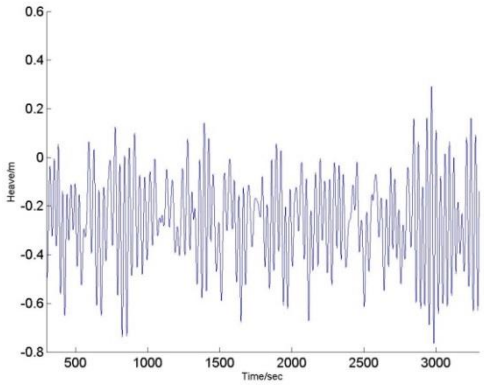

e) Heave

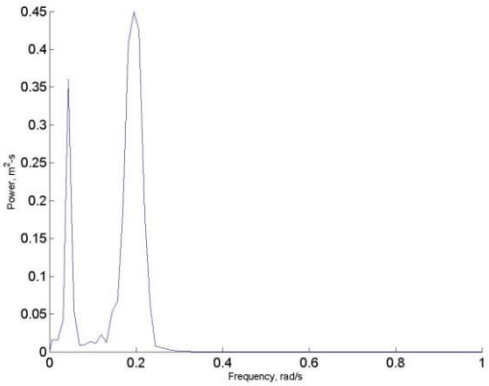

f) Heave PSD

Figure A 2-3 The FOWT Results for Case 6

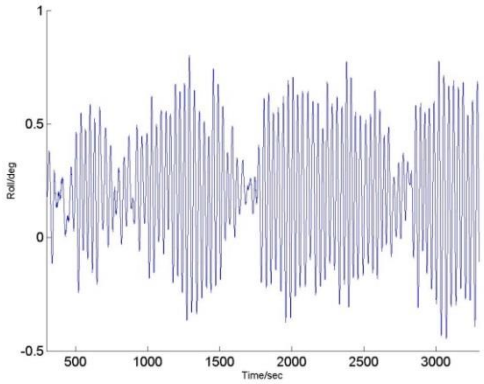

g) Roll

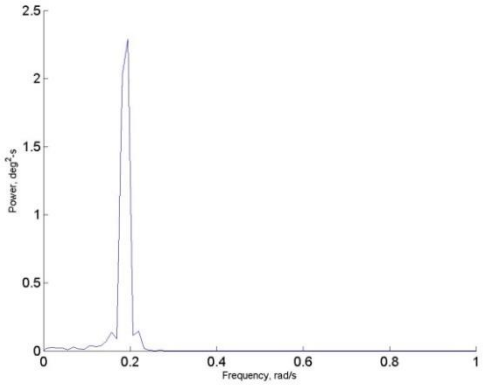

h) Roll PSD

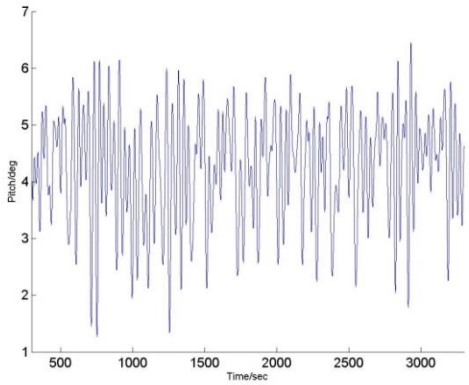

i) Pitch

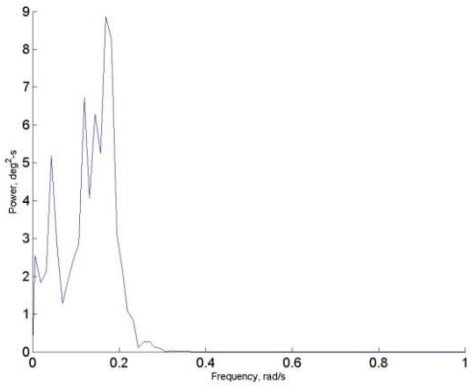

j) Pitch PSD

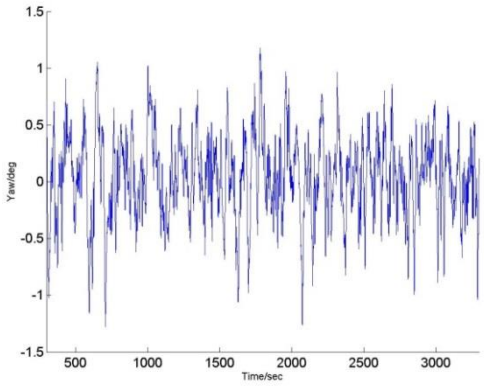

k) Yaw

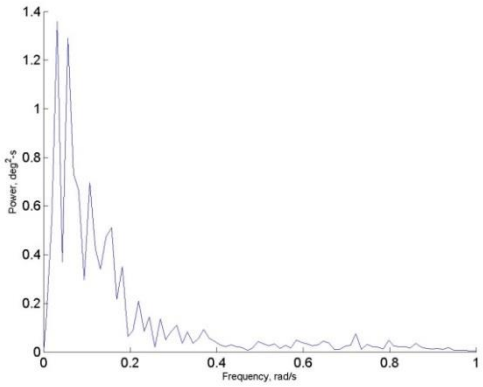

l) Yaw PSD

Figure A 2-3 Continued

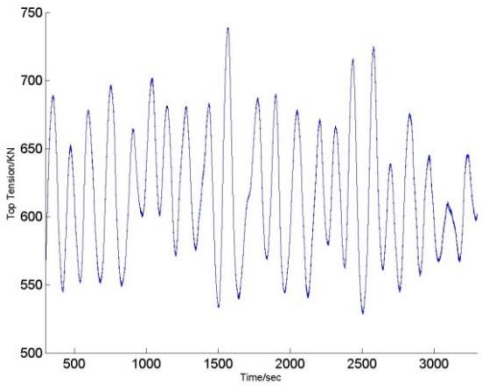

m) Top Tension of ML1

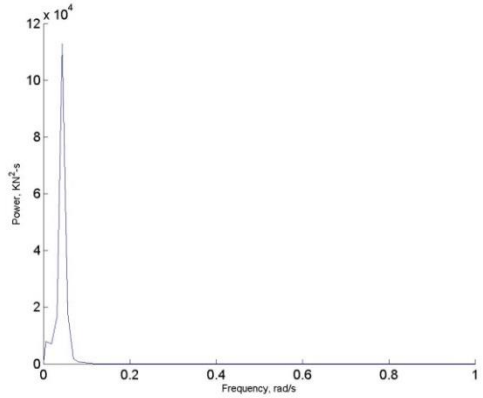

n) Top Tension PSD of ML1

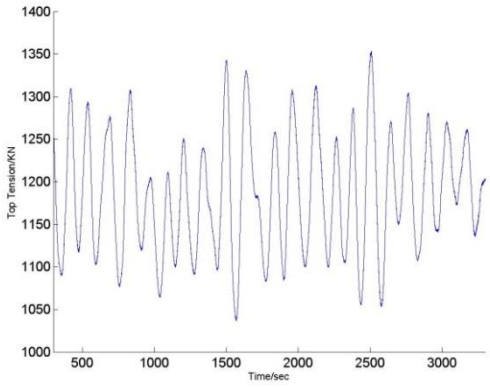

o) Top Tension of ML2

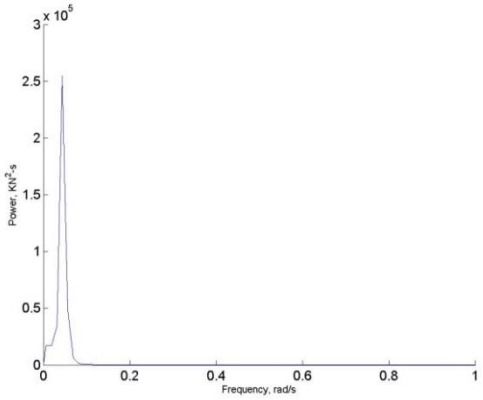

p) Top Tension PSD of ML2

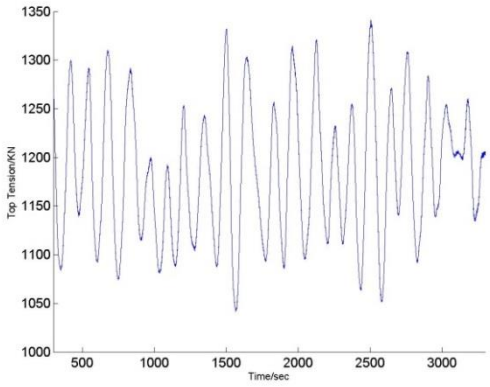

q) Top Tension of ML3

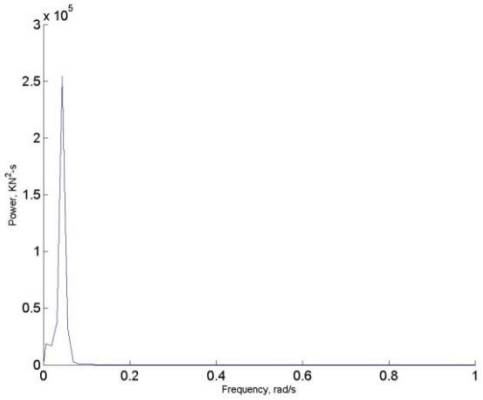

r) Top Tension PSD of ML3

Figure A 2-3 Continued

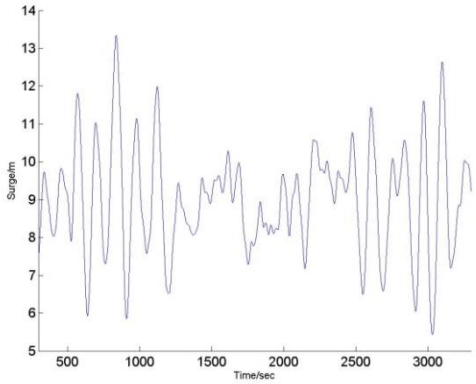

a) Surge

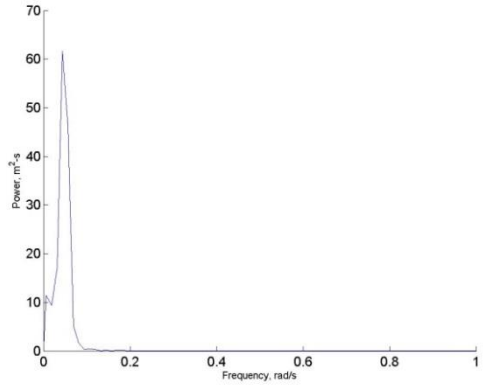

b) Surge PSD

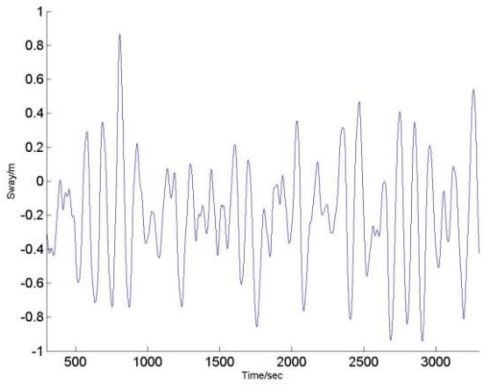

c) Sway

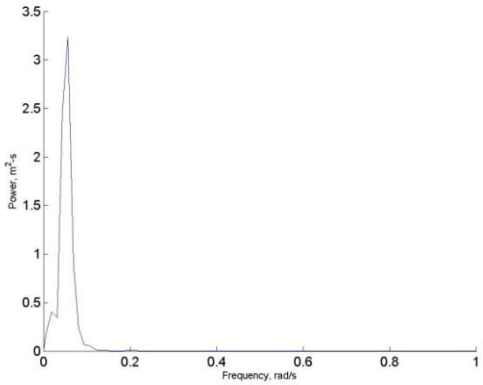

d) Sway PSD

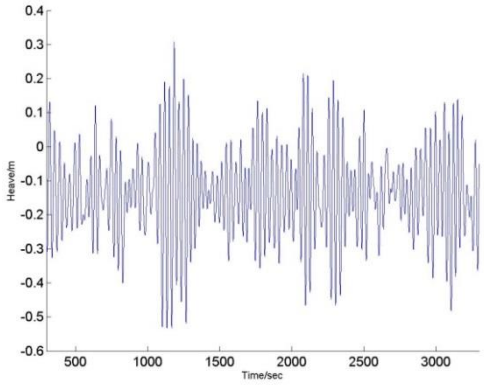

e) Heave

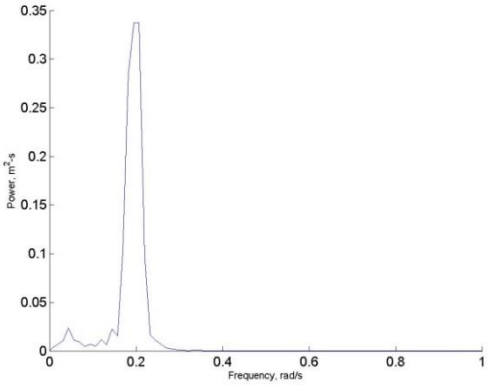

f) Heave PSD

Figure A 2-4 The FOWT Results for Case 7

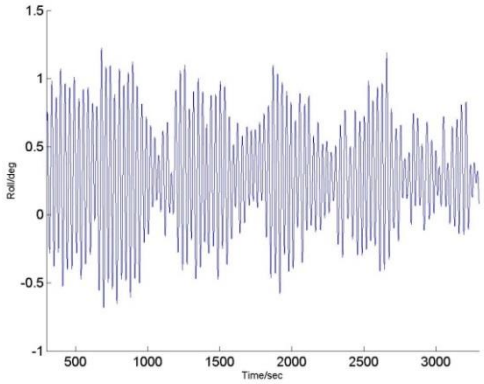

g) Roll

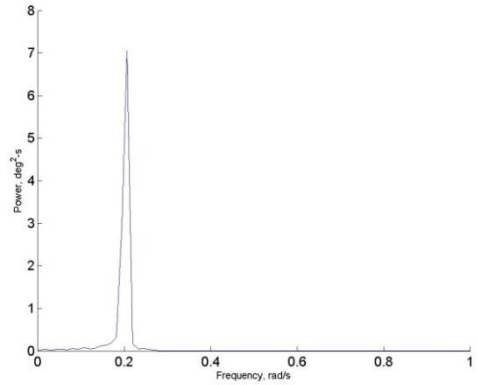

h) Roll PSD

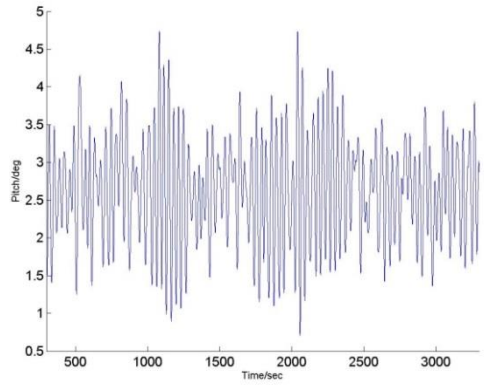

i) Pitch

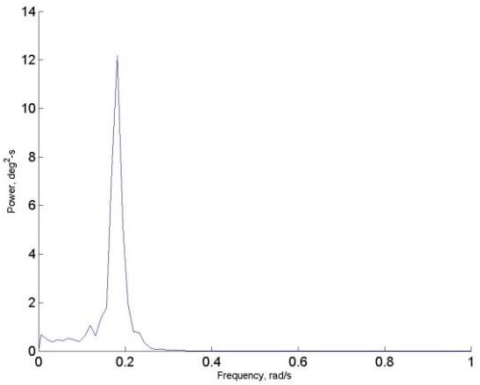

j) Pitch PSD

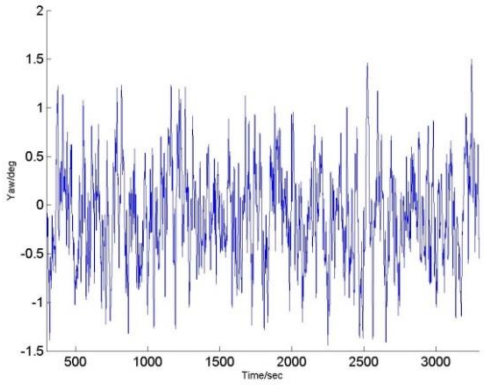

k) Yaw

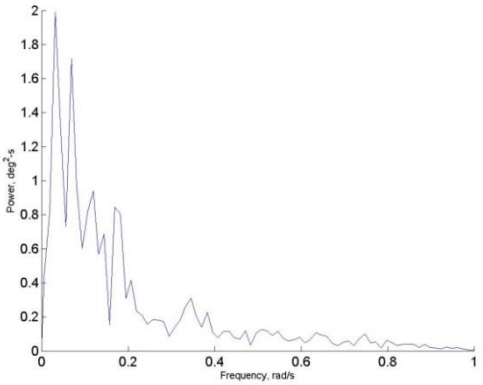

l) Yaw PSD

Figure A 2-4 Continued

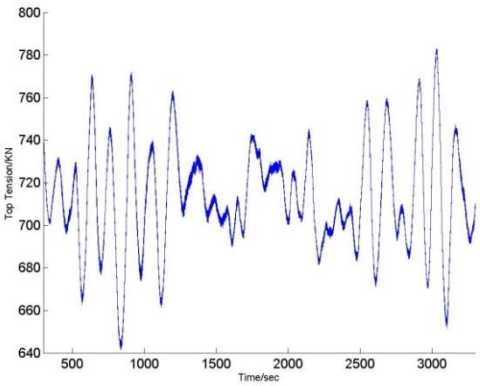

m) Top Tension of ML1

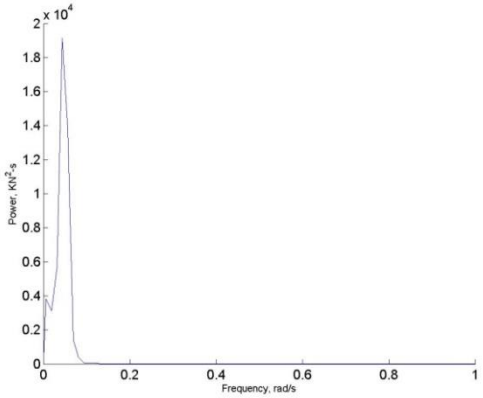

n) Top Tension PSD of ML1

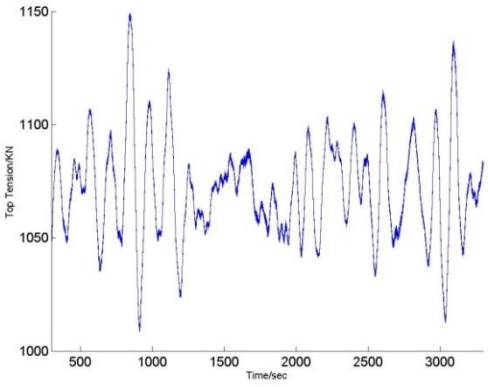

o) Top Tension of ML2

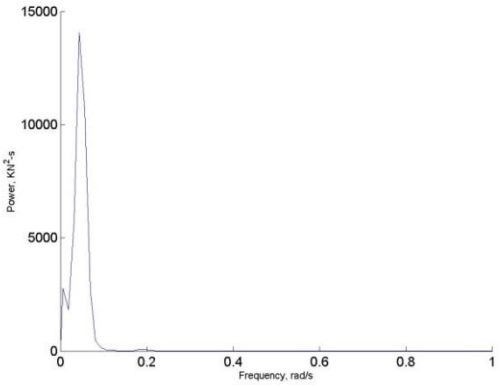

p) Top Tension PSD of ML2

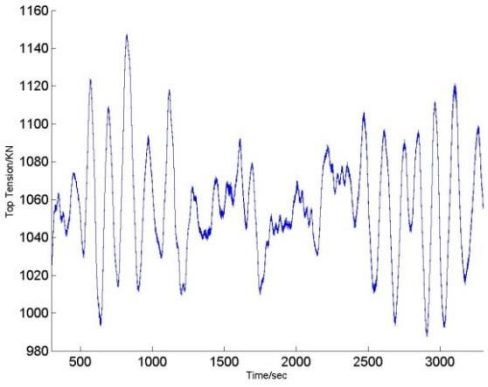

q) Top Tension of ML3

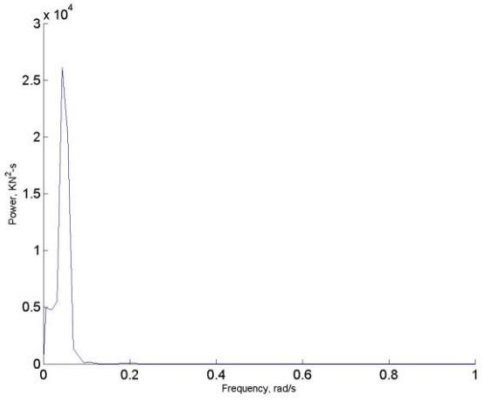

r) Top Tension PSD of ML3

Figure A 2-4 Continued

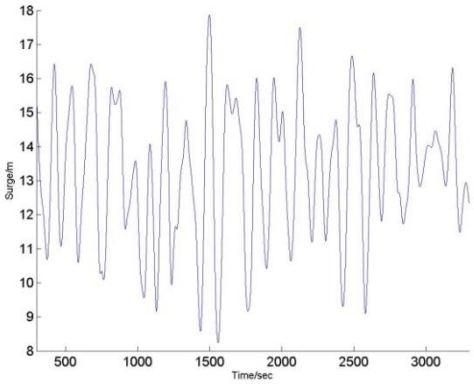

a) Surge

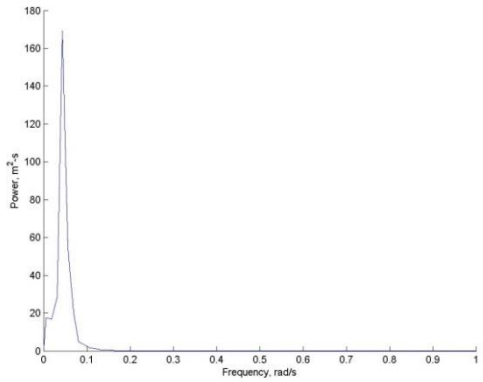

b) Surge PSD

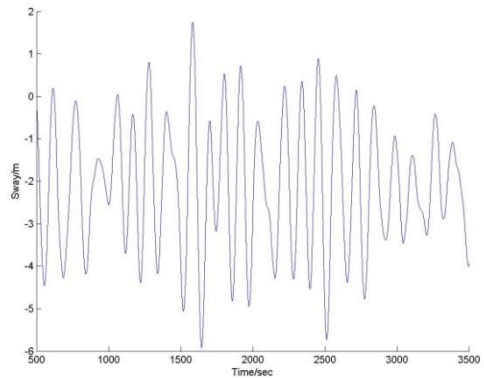

c) Sway

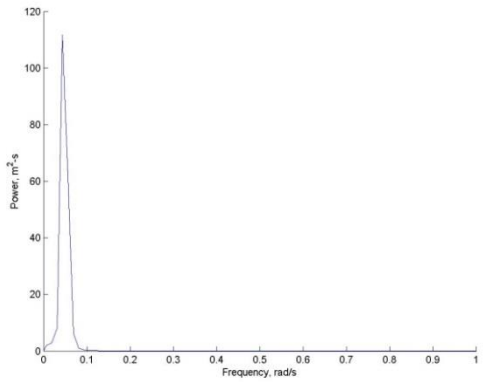

d) Sway PSD

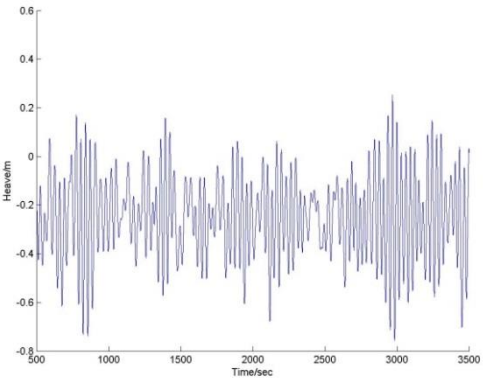

e) Heave

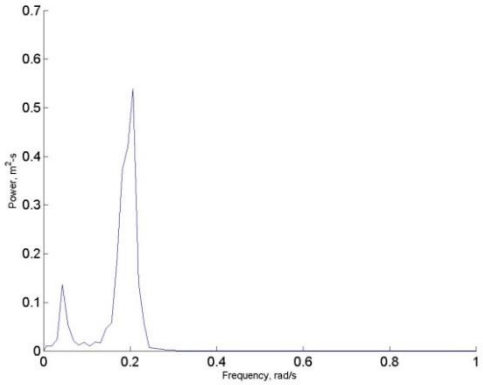

f) Heave PSD

Figure A 2-5 The FOWT Results for Case 8

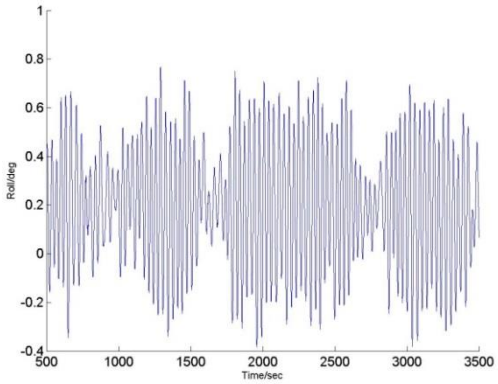

g) Roll

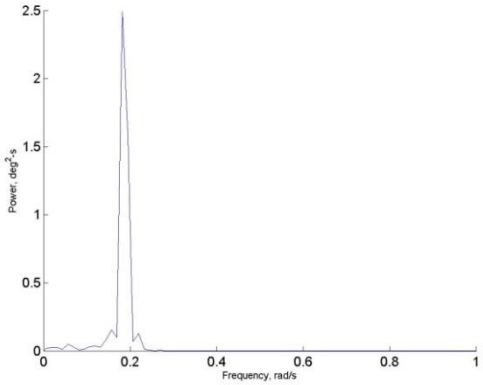

h) Roll PSD

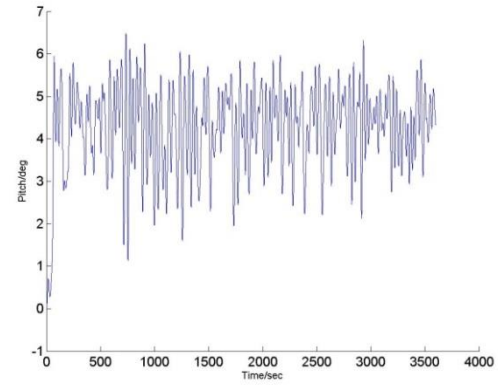

i) Pitch

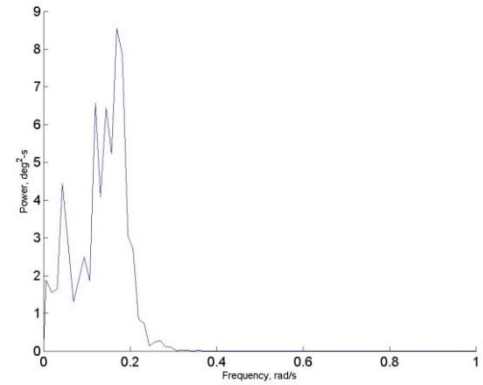

j) Pitch PSD

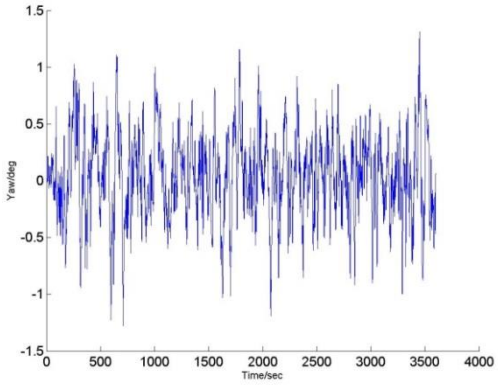

k) Yaw

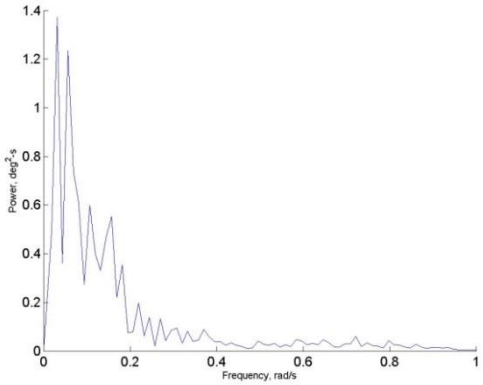

l) Yaw PSD

Figure A 2-5 Continued

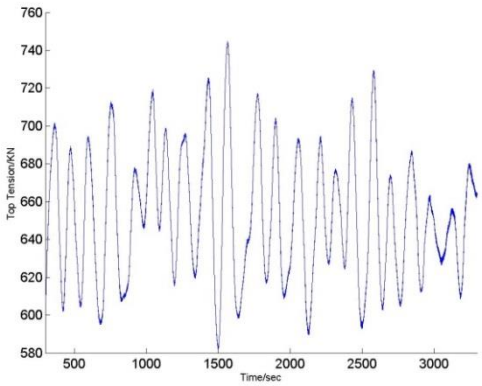

m) Top Tension of ML1

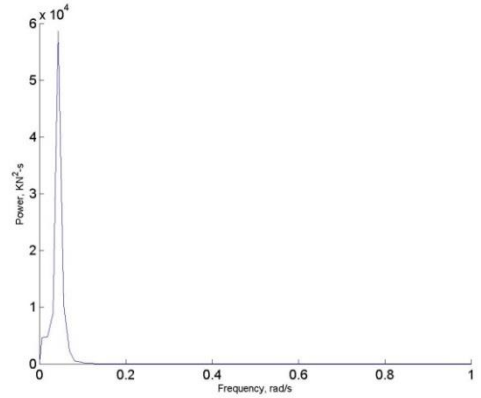

n) Top Tension PSD of ML1

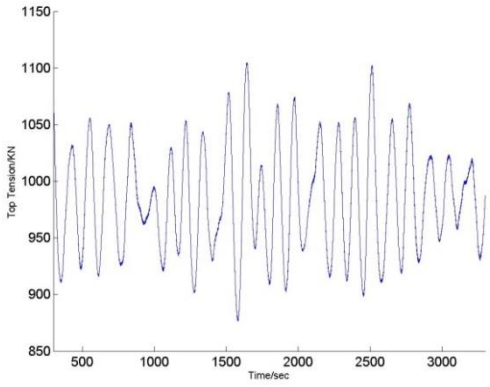

o) Top Tension of ML2

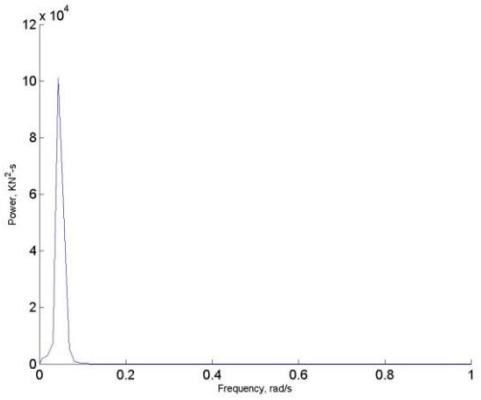

p) Top Tension PSD of ML2

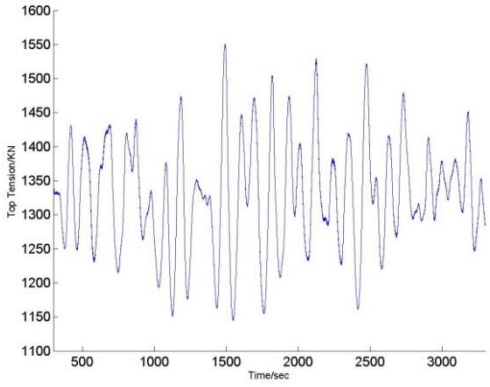

q) Top Tension of ML3

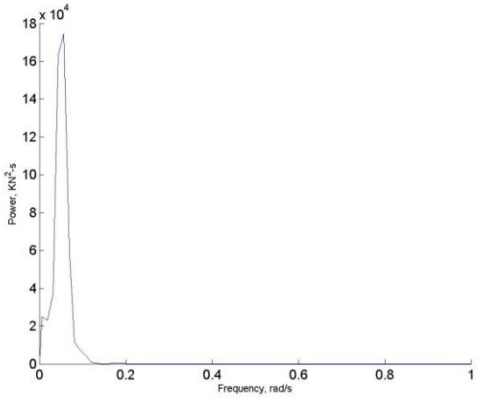

r) Top Tension PSD of ML3

Figure A 2-5 Continued

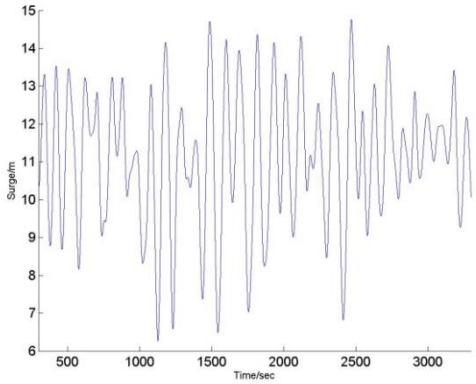

a) Surge

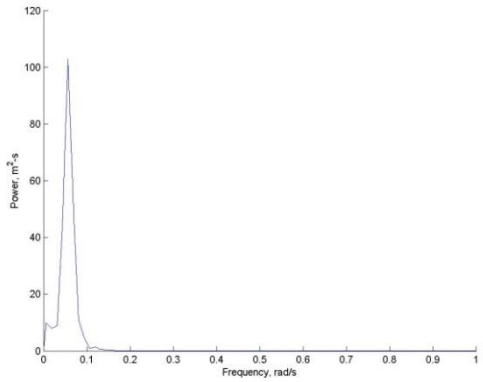

b) Surge PSD

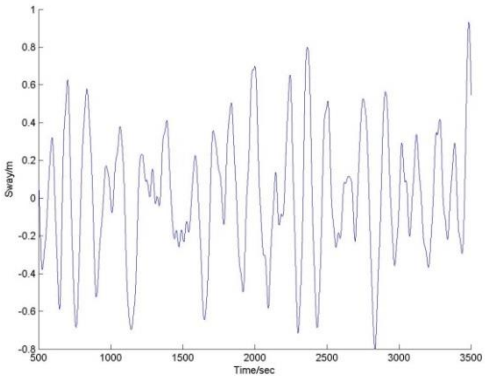

c) Sway

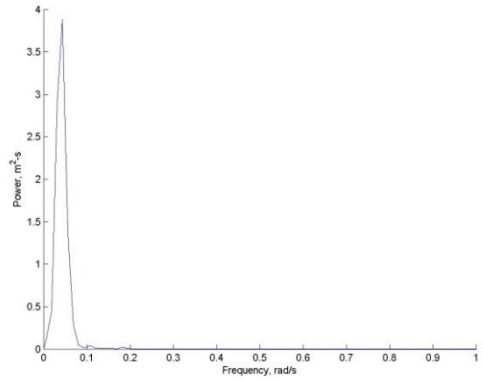

d) Sway PSD

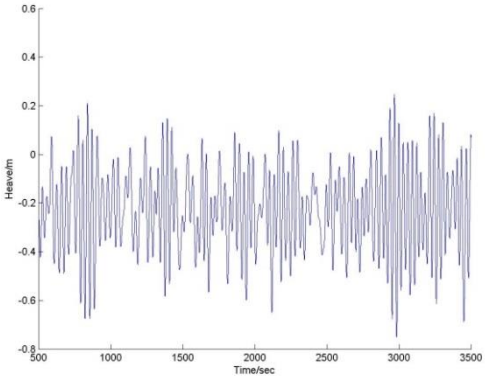

e) Heave

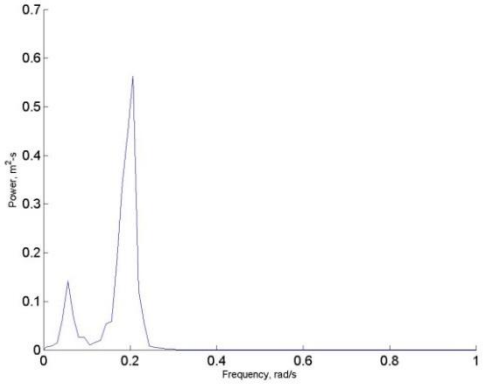

f) Heave PSD

Figure A 2-6 The FOWT Results for Case 9

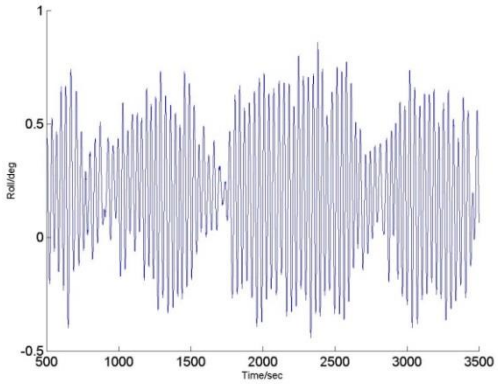

g) Roll

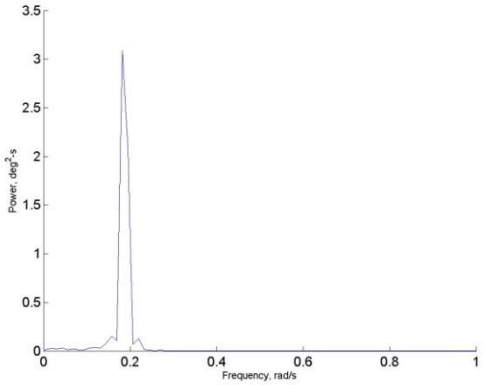

h) Roll PSD

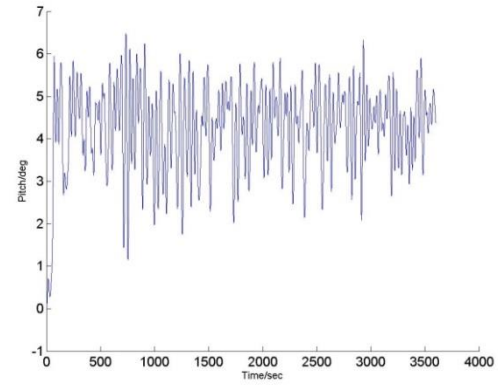

i) Pitch

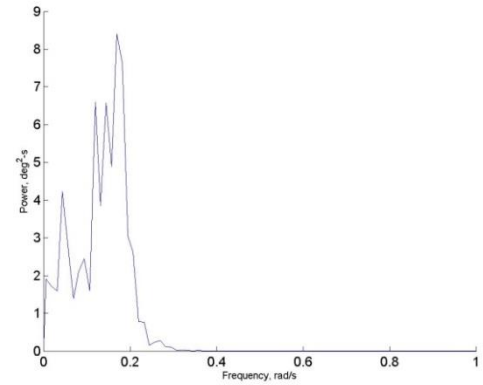

j) Pitch PSD

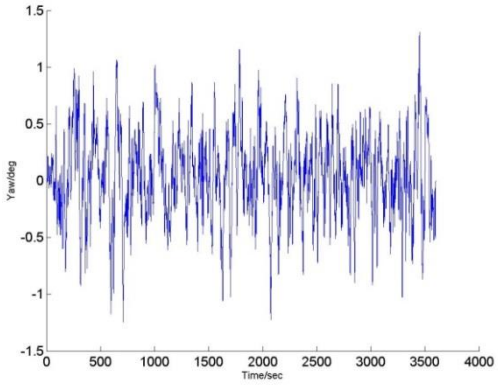

k) Yaw

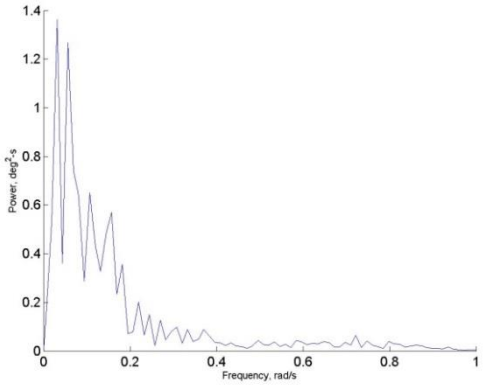

l) Yaw PSD

Figure A 2-6 Continued

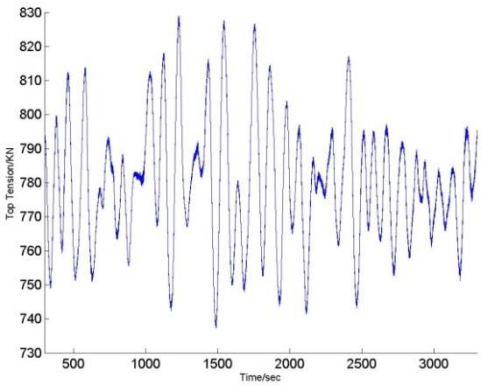

m) Top Tension of ML1

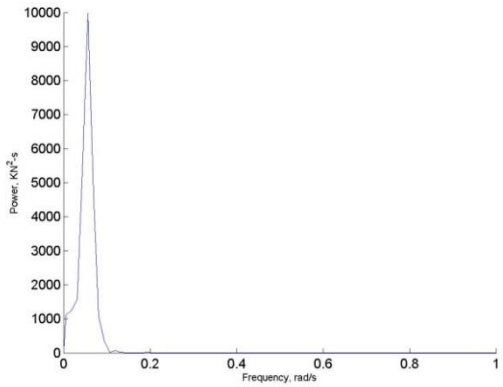

n) Top Tension PSD of ML1

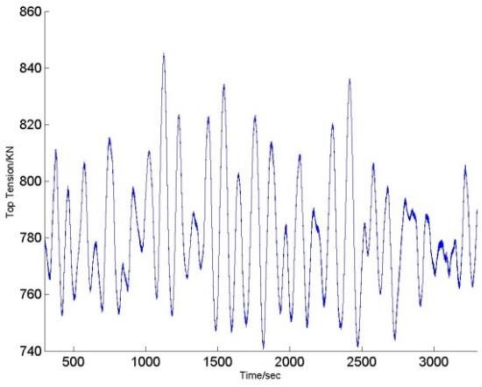

o) Top Tension of ML2

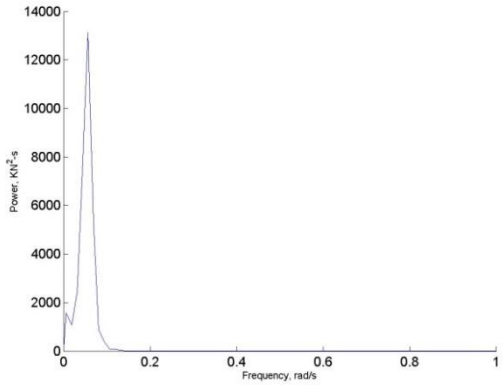

p) Top Tension PSD of ML2

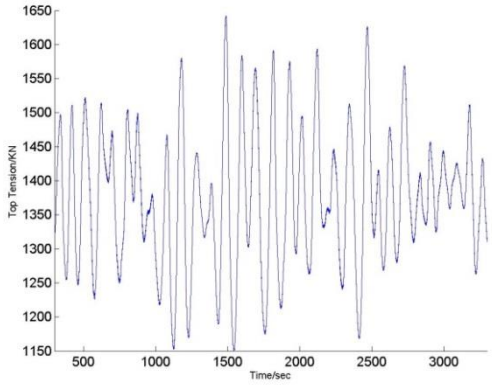

q) Top Tension of ML3

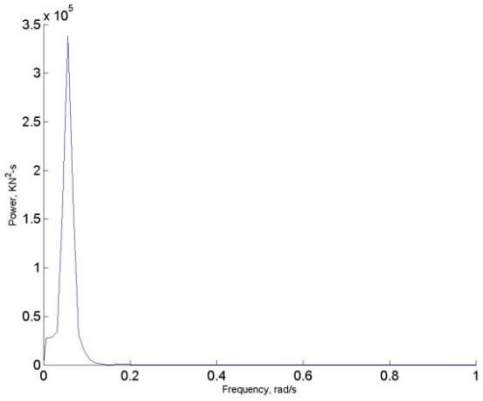

r) Top Tension PSD of ML3

Figure A 2-6 Continued

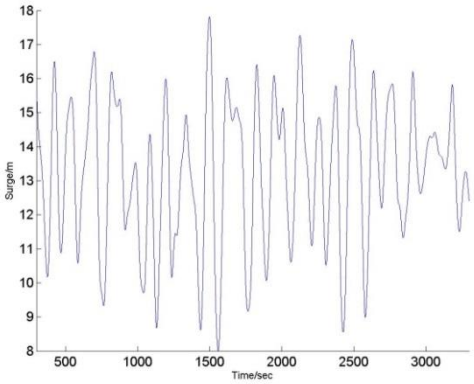

a) Surge

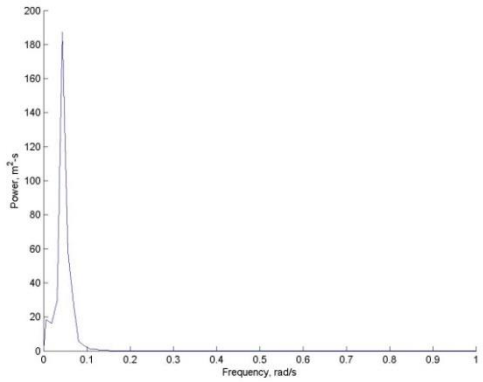

b) Surge PSD

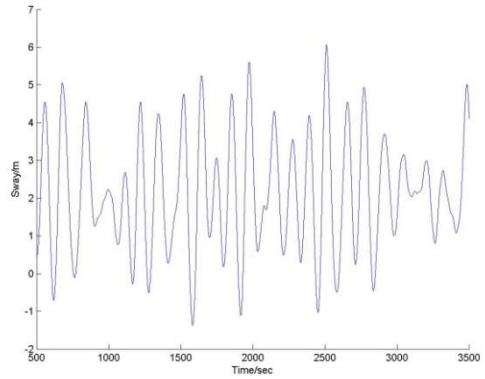

c) Sway

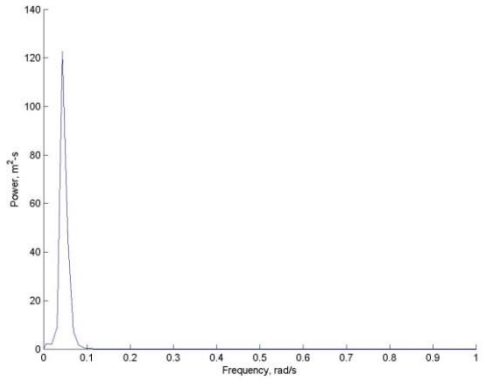

d) Sway PSD

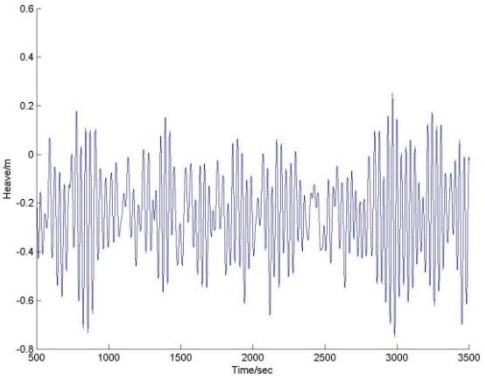

e) Heave

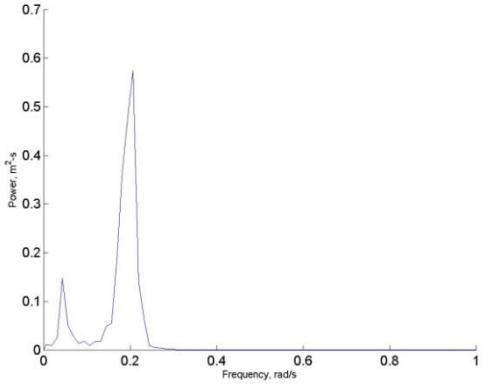

f) Heave PSD

Figure A 2-7 The FOWT Results for Case 10

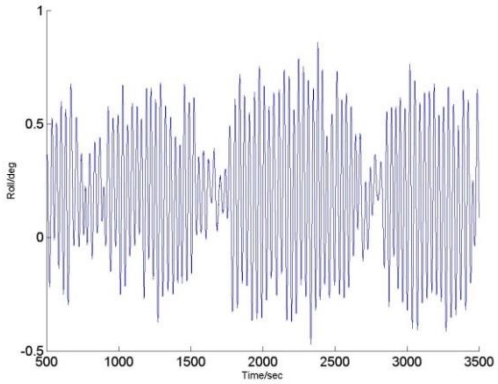

g) Roll

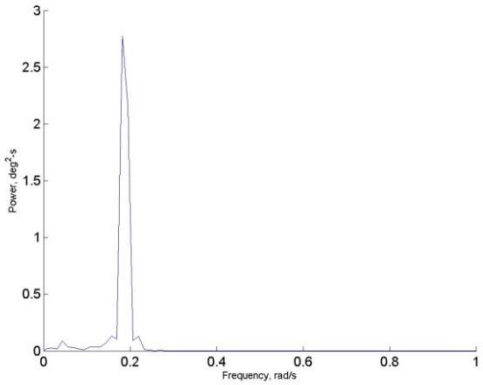

h) Roll PSD

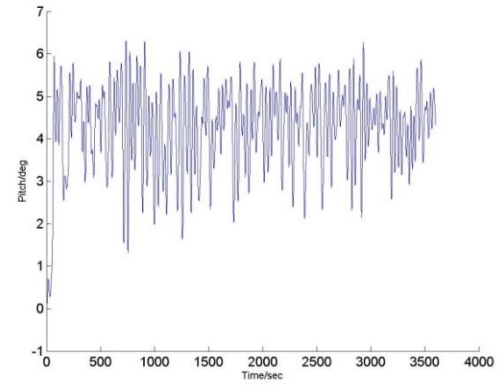

i) Pitch

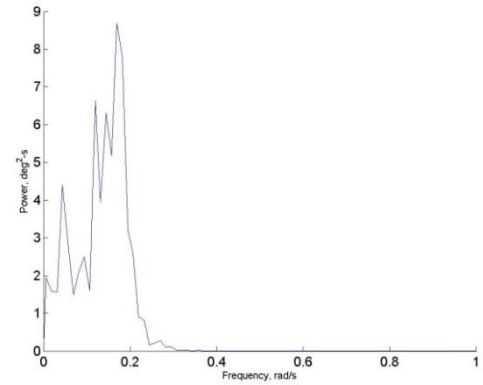

j) Pitch PSD

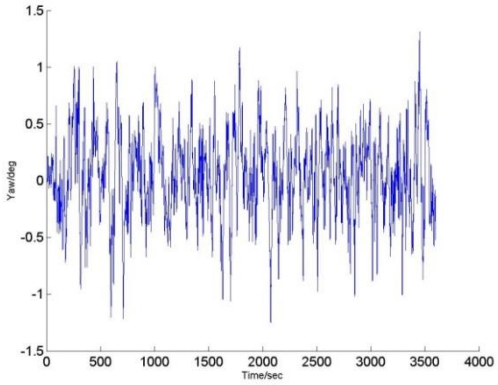

k) Yaw

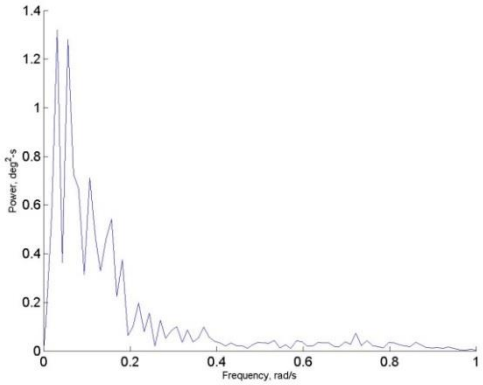

l) Yaw PSD

Figure A 2-7 Continued

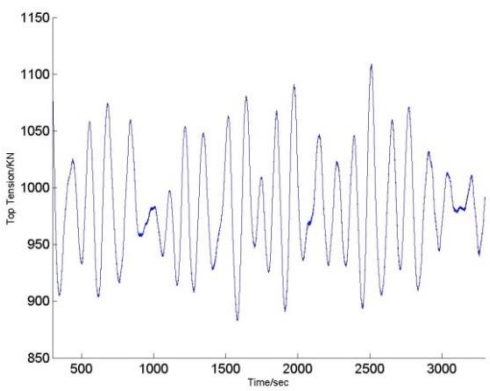

m) Top Tension of ML1

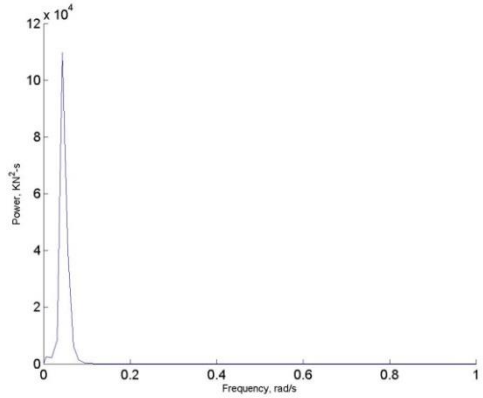

n) Top Tension PSD of ML1

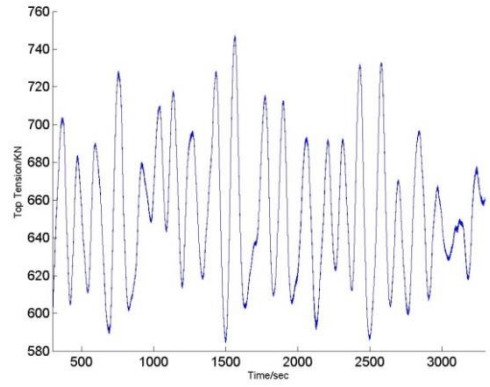

o) Top Tension of ML2

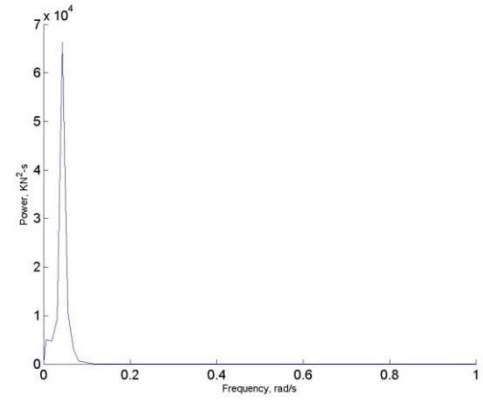

p) Top Tension PSD of ML2

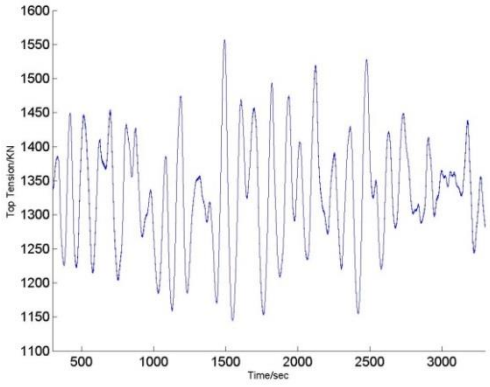

q) Top Tension of ML3

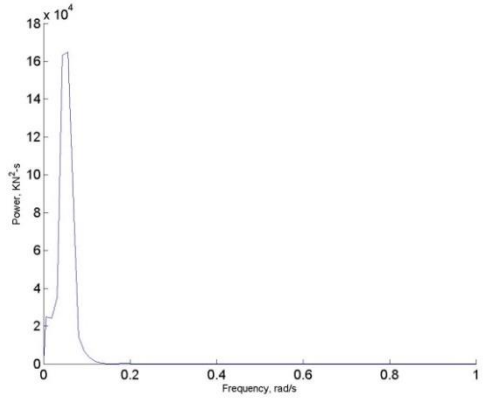

r) Top Tension PSD of ML3

Figure A 2-7 Continued

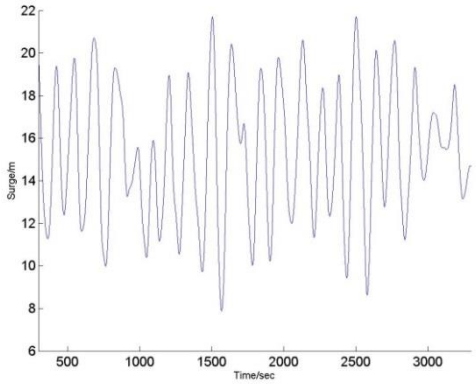

a) Surge

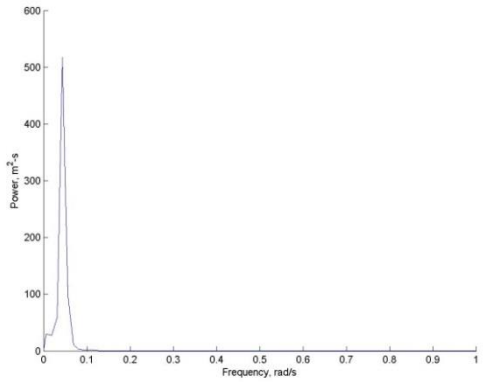

b) Surge PSD

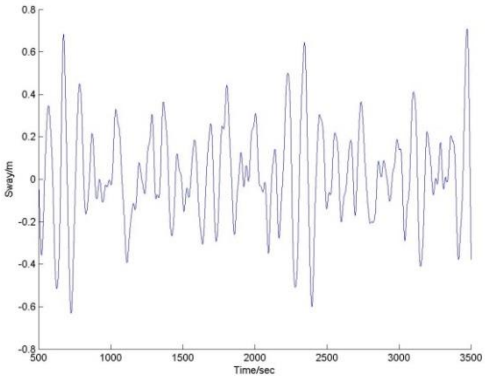

c) Sway

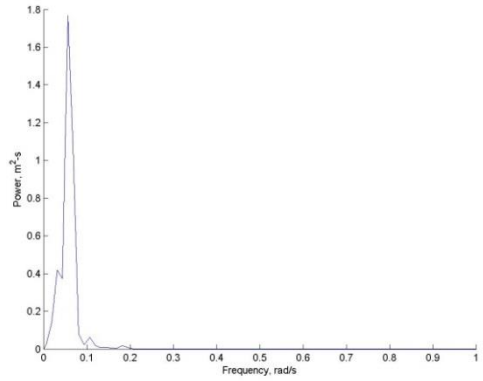

d) Sway PSD

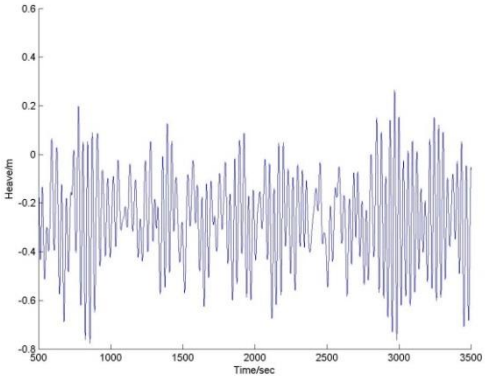

e) Heave

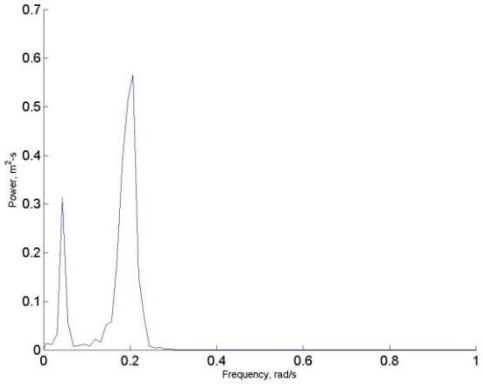

f) Heave PSD

Figure A 2-8 The FOWT Results for Case 11

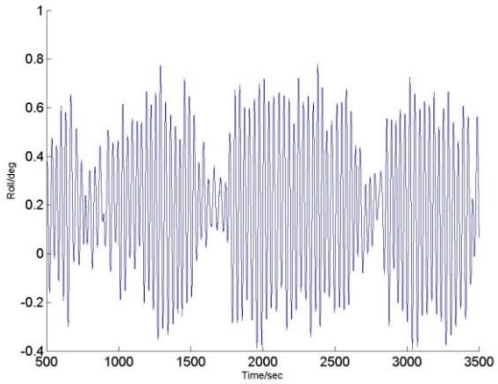

g) Roll

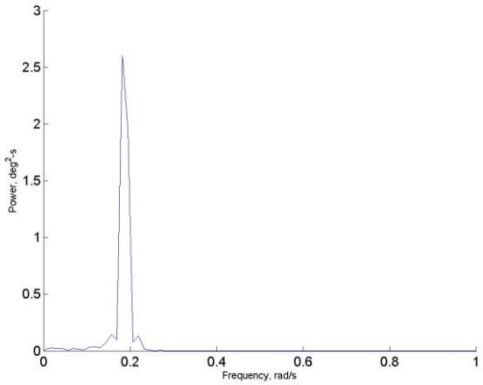

h) Roll PSD

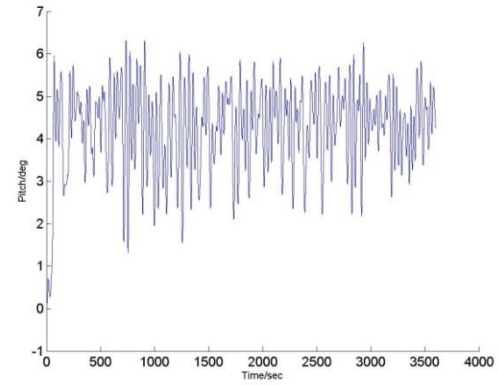

i) Pitch

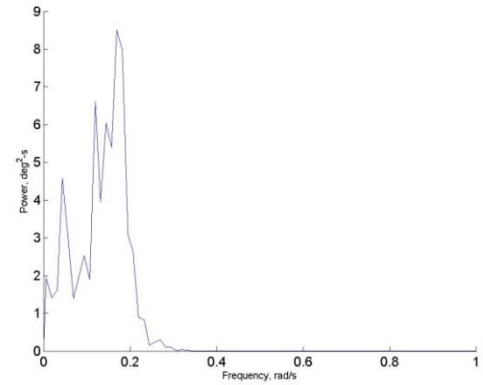

j) Pitch PSD

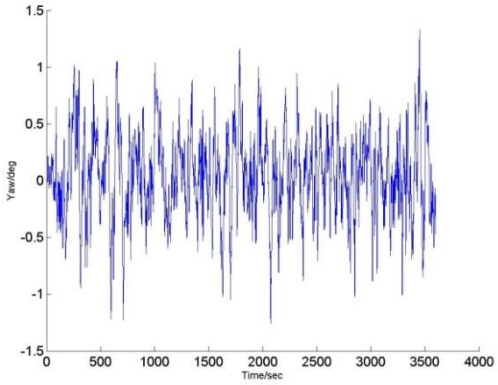

k) Yaw

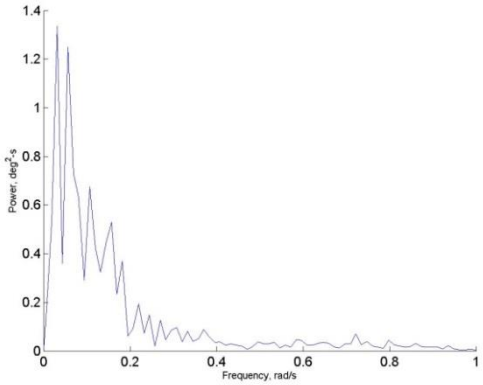

l) Yaw PSD

Figure A 2-8 Continued

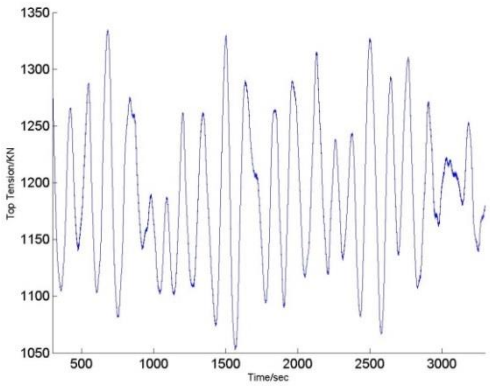

m) Top Tension of ML1

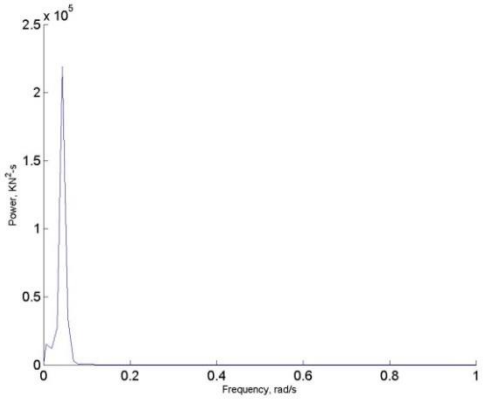

n) Top Tension PSD of ML1

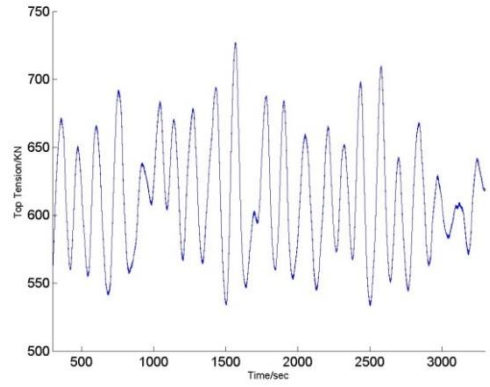

o) Top Tension of ML2

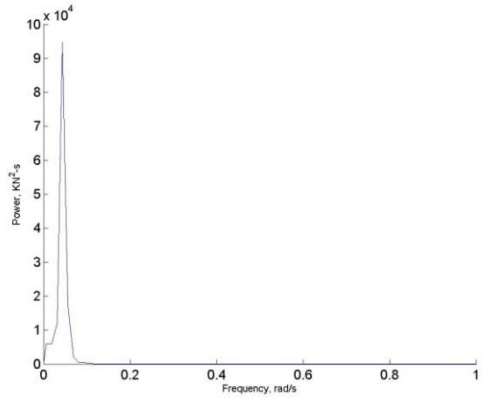

p) Top Tension PSD of ML2

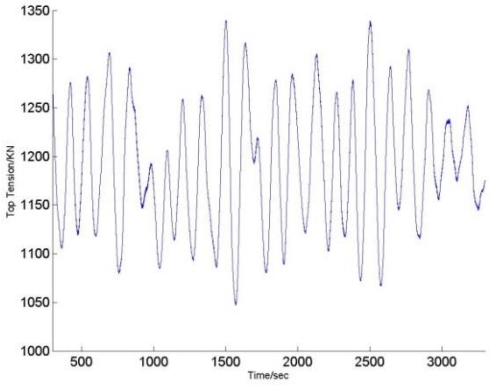

q) Top Tension of ML3

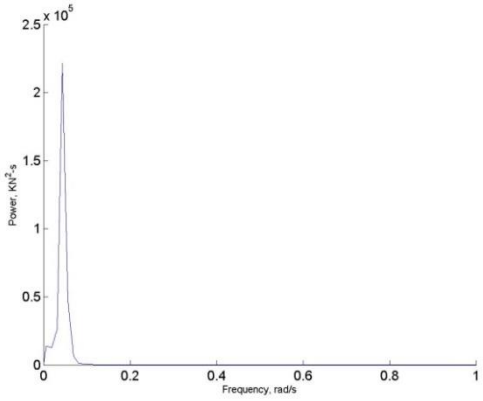

r) Top Tension PSD of ML3

Figure A 2-8 Continued

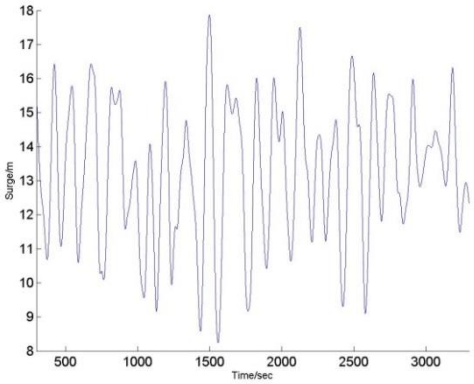

a) Surge

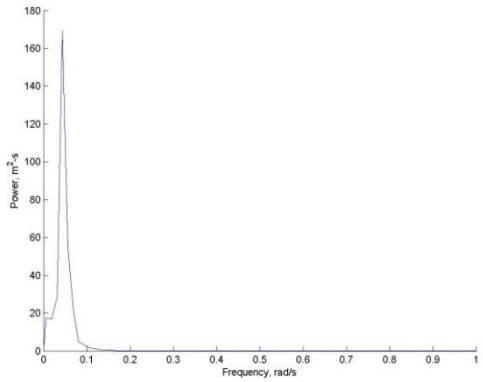

b) Surge PSD

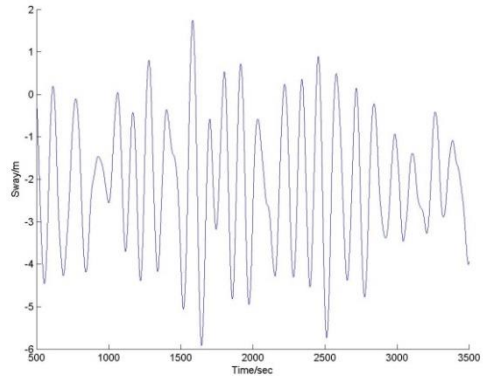

c) Sway

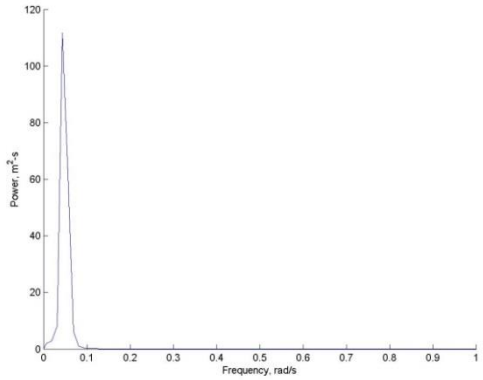

d) Sway PSD

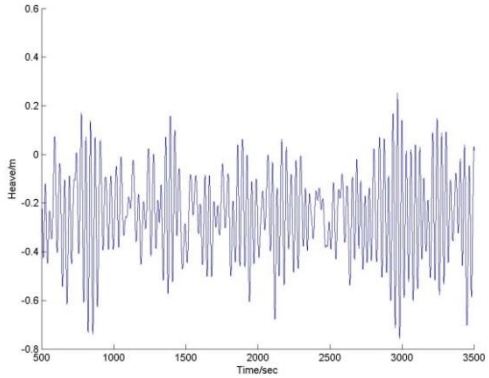

e) Heave

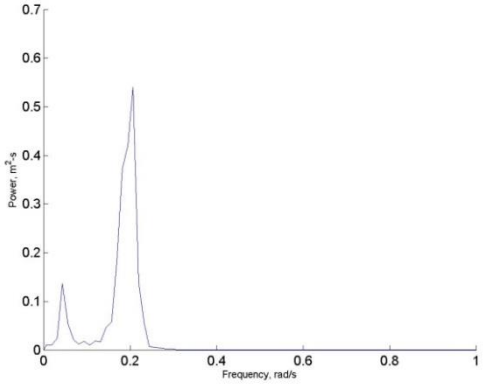

f) Heave PSD

Figure A 2-9 The FOWT Results for Case 12

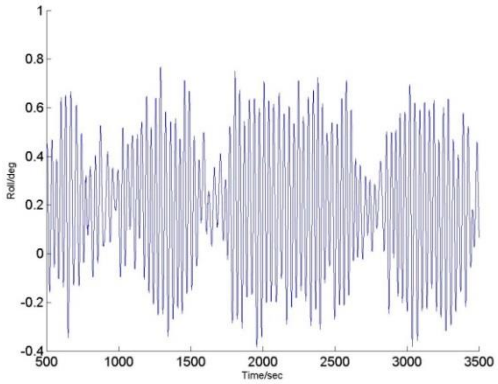

g) Roll

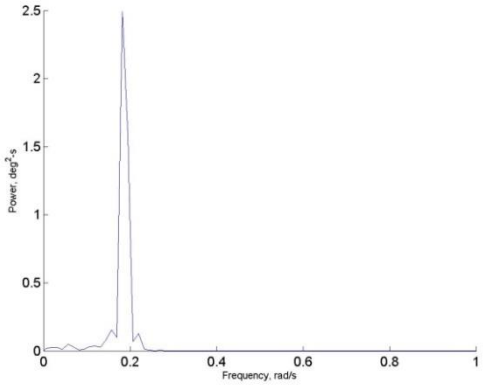

h) Roll PSD

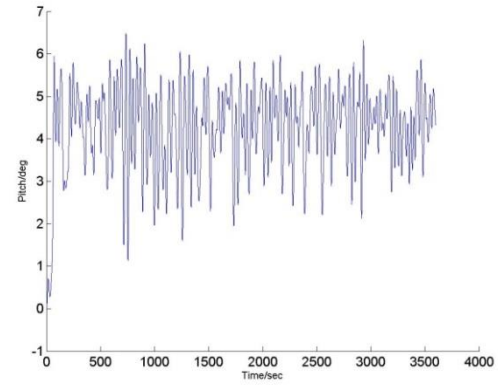

i) Pitch

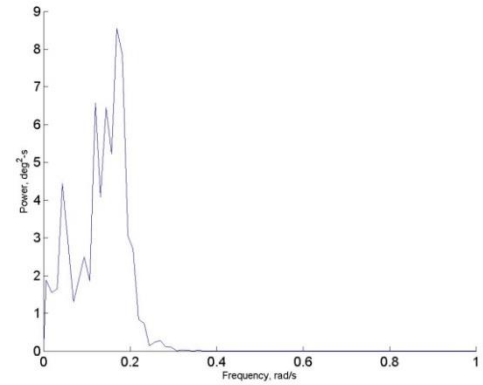

j) Pitch PSD

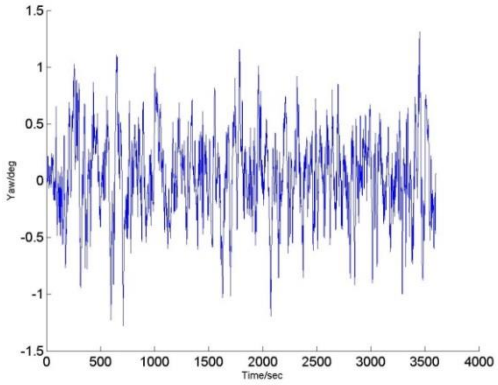

k) Yaw

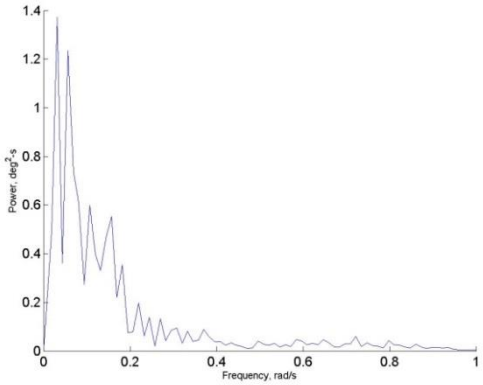

l) Yaw PSD

Figure A 2-9 Continued

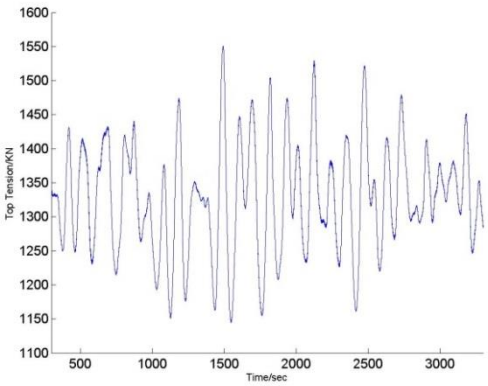

m) Top Tension of ML1

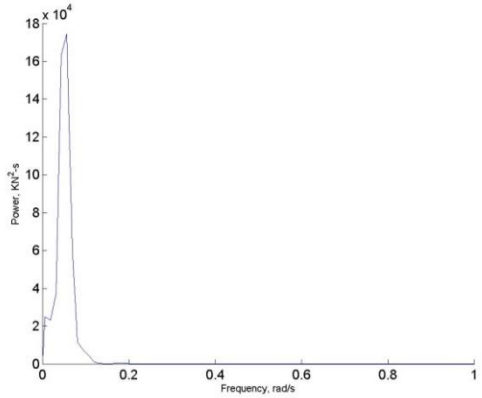

n) Top Tension PSD of ML1

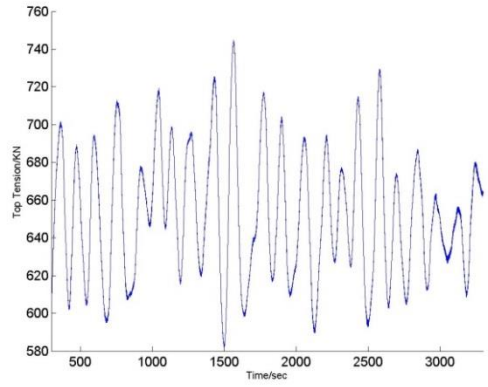

o) Top Tension of ML2

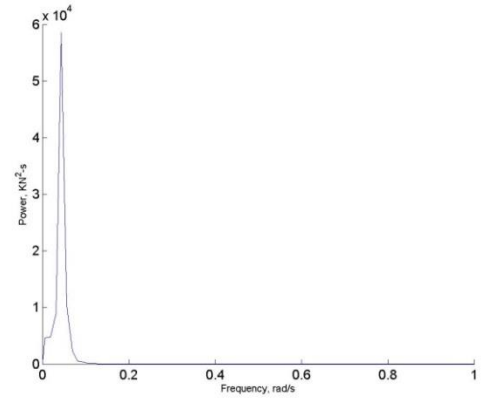

p) Top Tension PSD of ML2

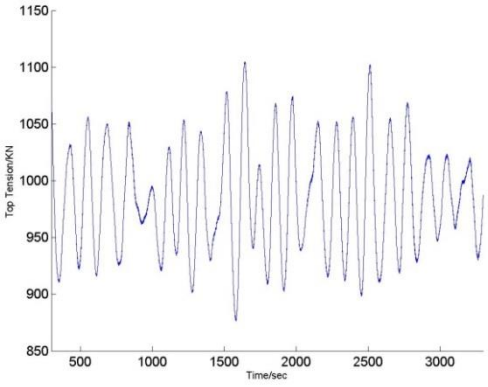

q) Top Tension of ML3

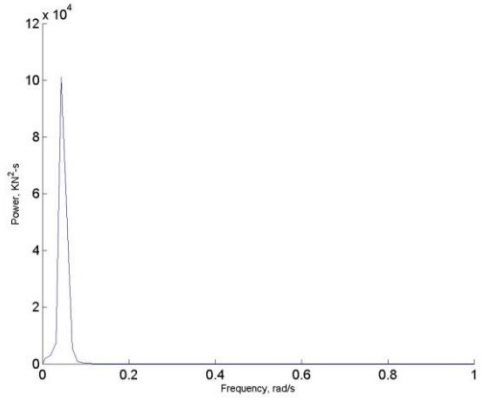

r) Top Tension PSD of ML3

Figure A 2-9 Continued

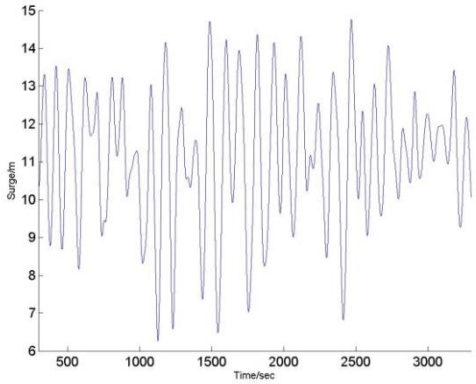

a) Surge

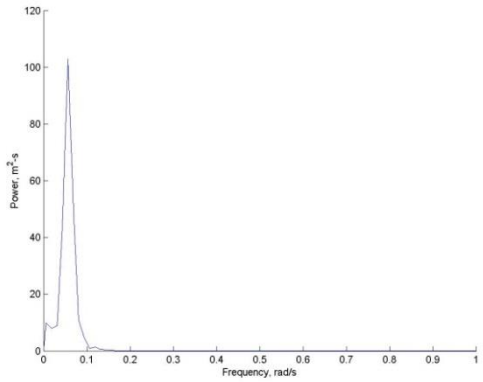

b) Surge PSD

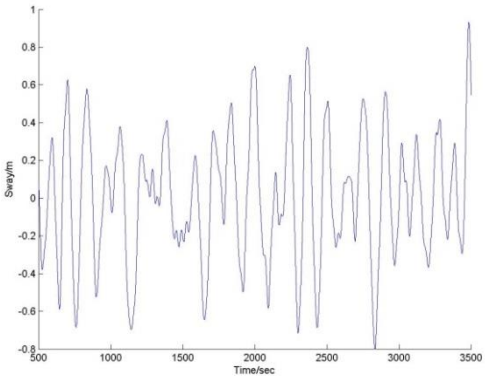

c) Sway

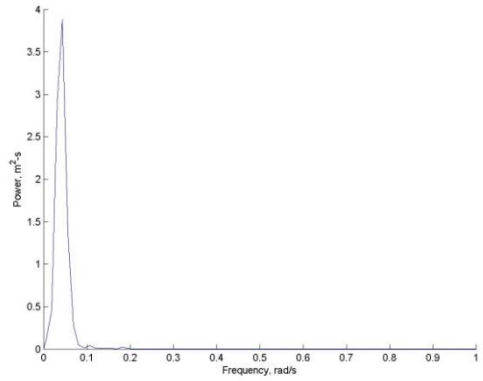

d) Sway PSD

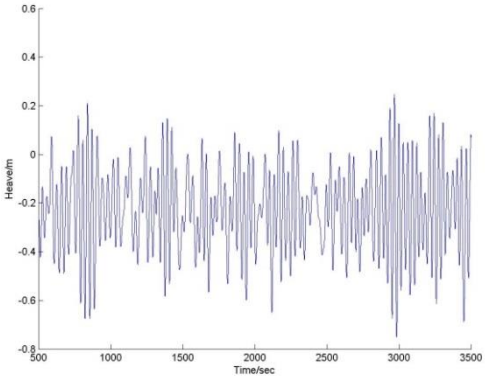

e) Heave

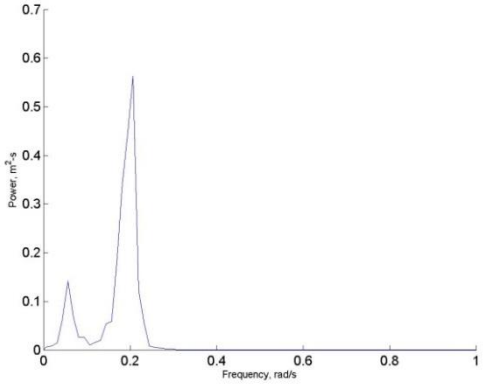

f) Heave PSD

Figure A 2-10 The FOWT Results for Case 13

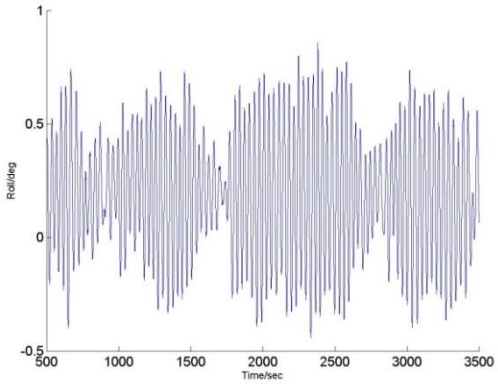

g) Roll

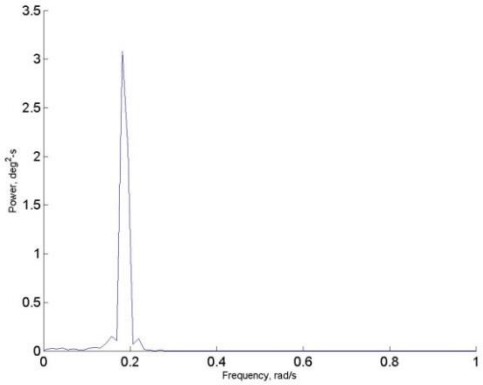

h) Roll PSD

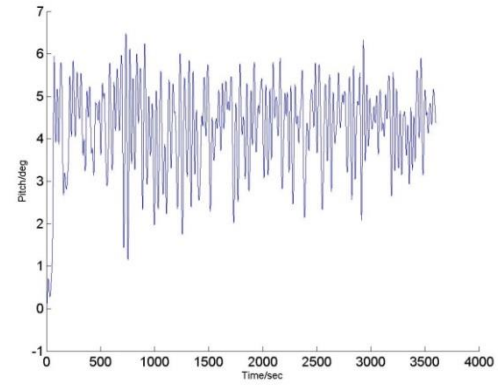

i) Pitch

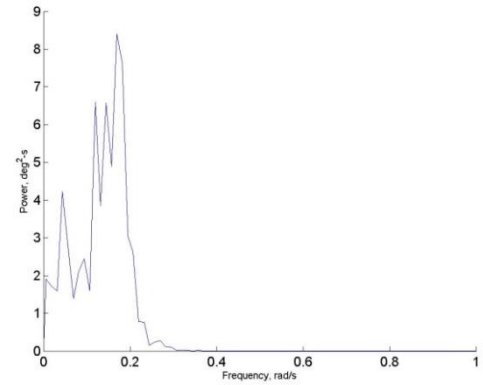

j) Pitch PSD

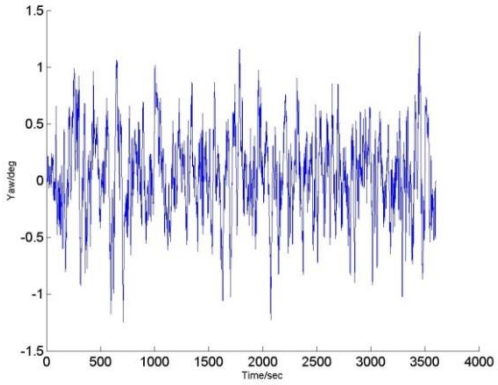

k) Yaw

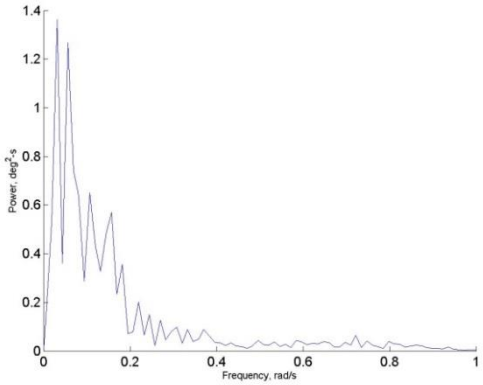

l) Yaw PSD

Figure A 2-10 Continued

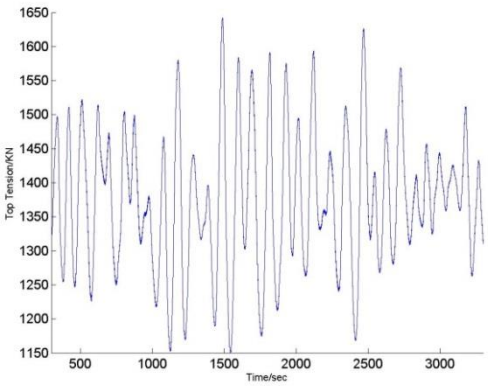

m) Top Tension of ML1

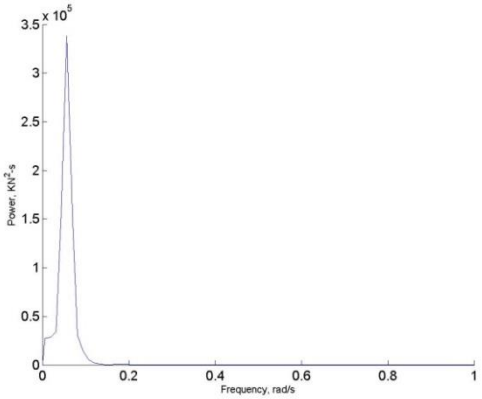

n) Top Tension PSD of ML1

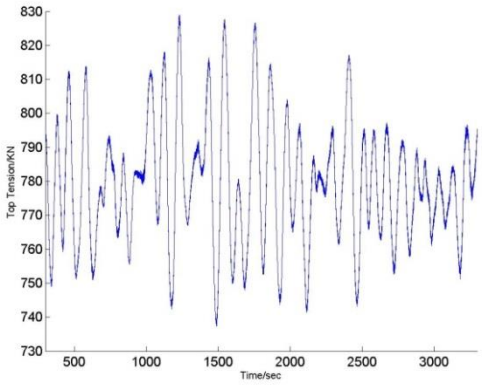

o) Top Tension of ML2

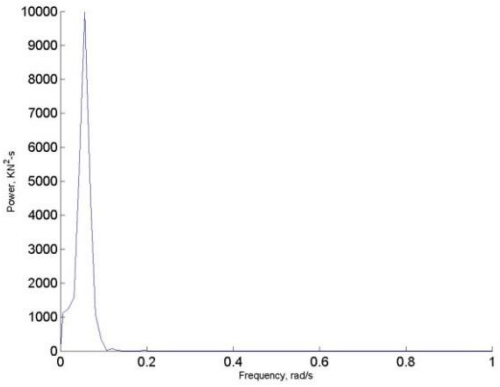

p) Top Tension PSD of ML2

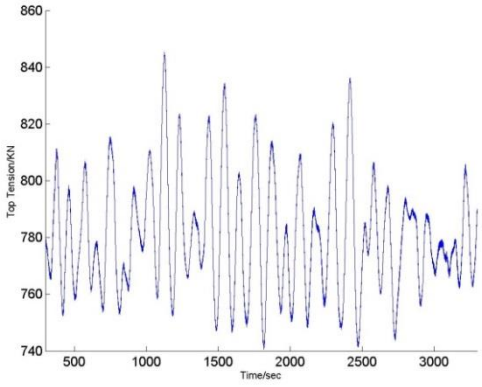

q) Top Tension of ML3

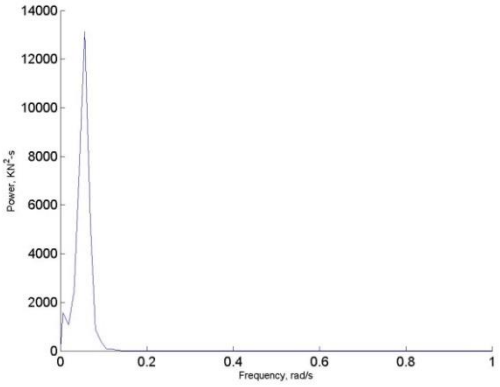

r) Top Tension PSD of ML3

Figure A 2-10 Continued

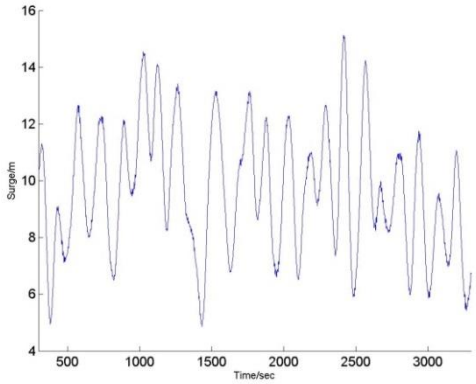

a) Surge

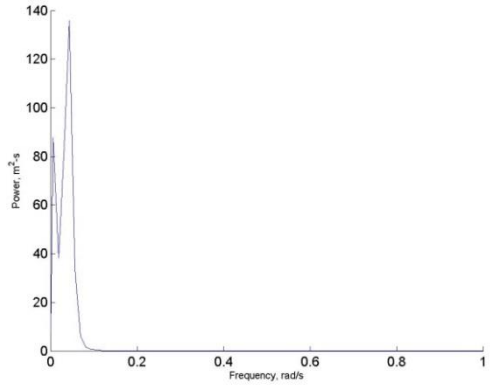

b) Surge PSD

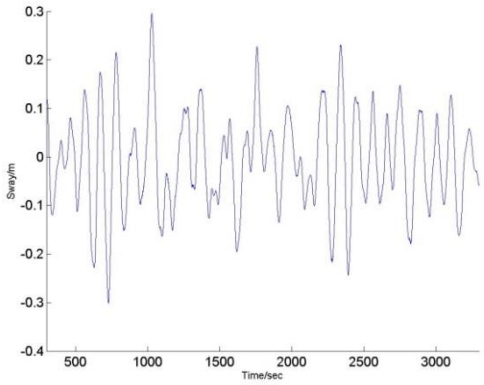

c) Sway

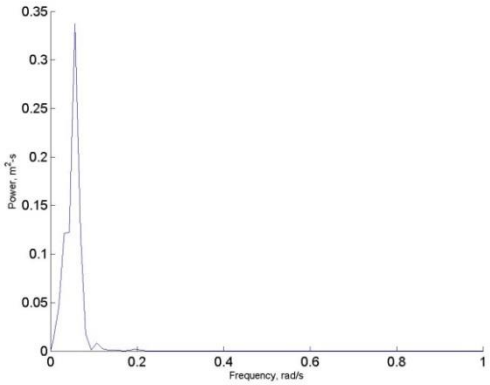

d) Sway PSD

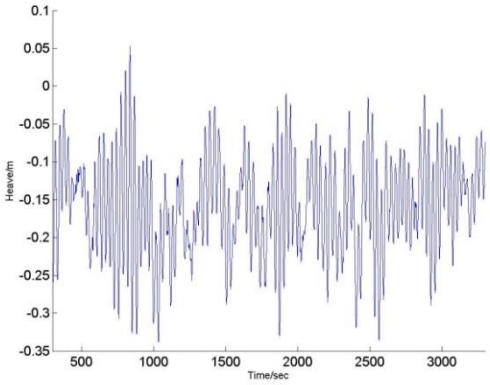

e) Heave

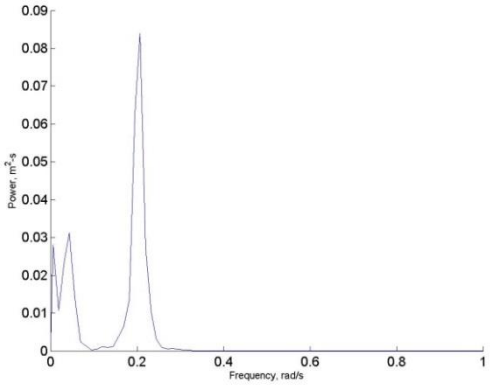

f) Heave PSD

Figure A 2-11 The FOWT Results for Case 14

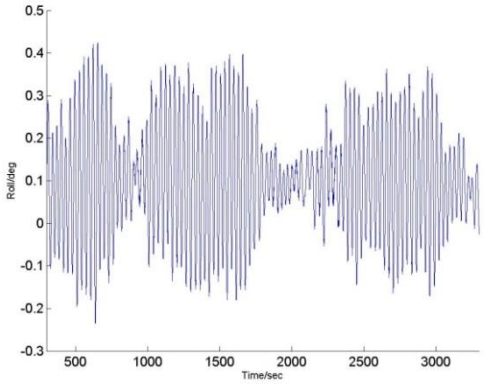

g) Roll

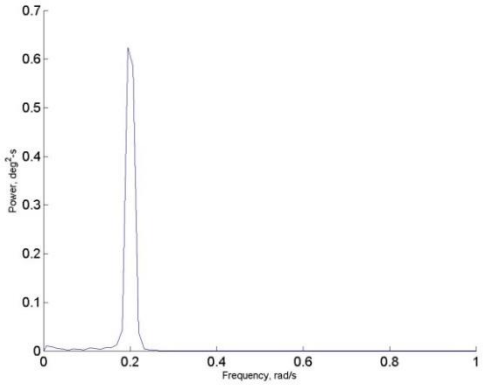

h) Roll PSD

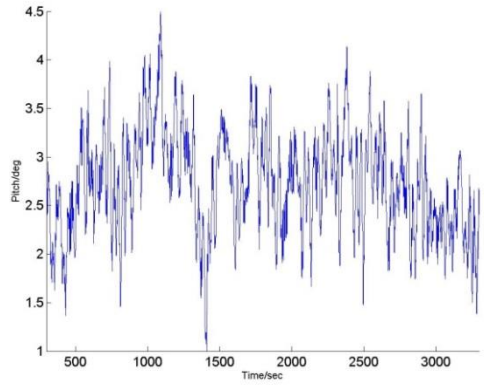

i) Pitch

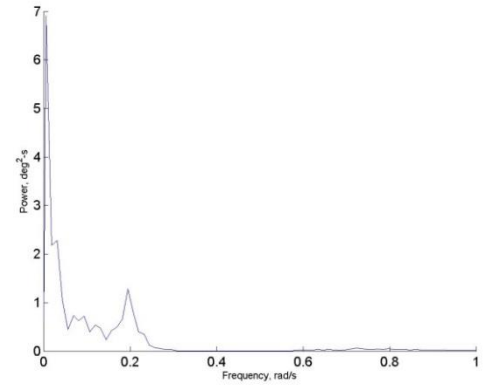

j) Pitch PSD

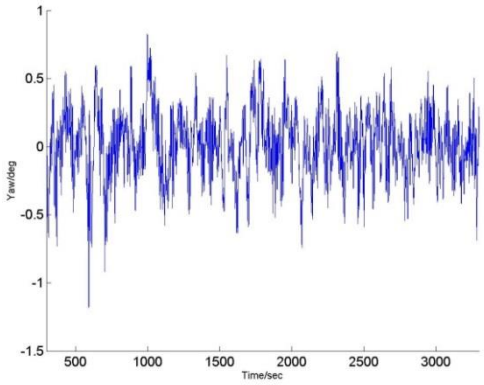

k) Yaw

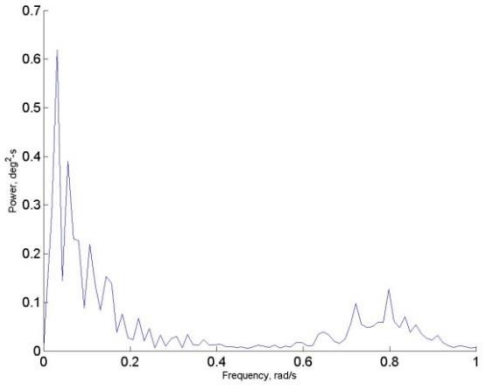

l) Yaw PSD

Figure A 2-11 Continued

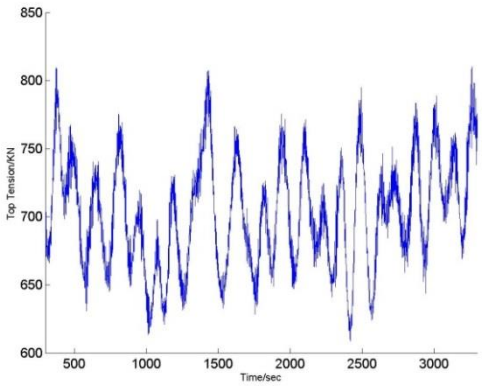

m) Top Tension of ML1

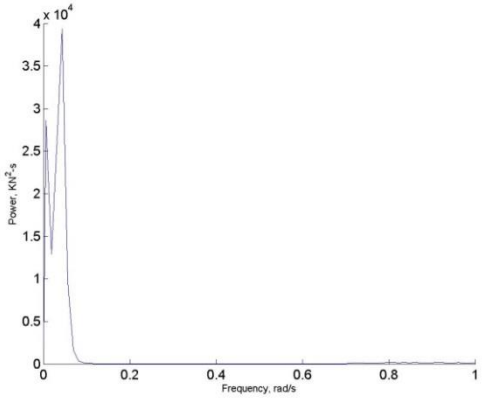

n) Top Tension PSD of ML1

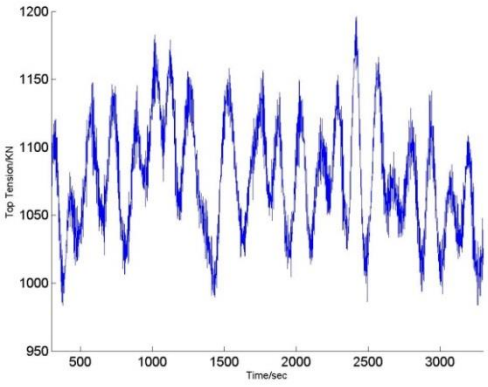

o) Top Tension of ML2

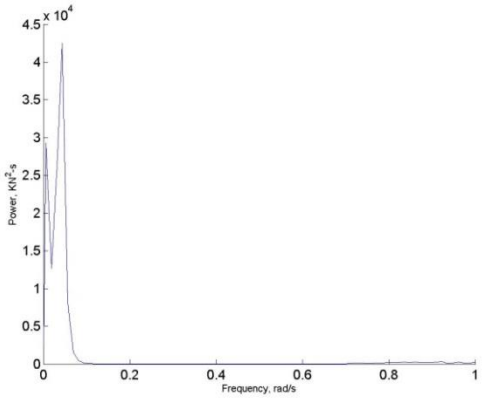

p) Top Tension PSD of ML2

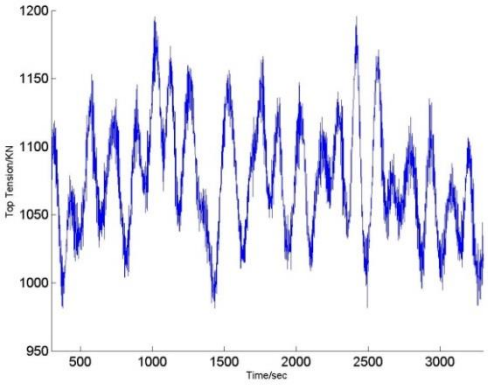

q) Top Tension of ML3

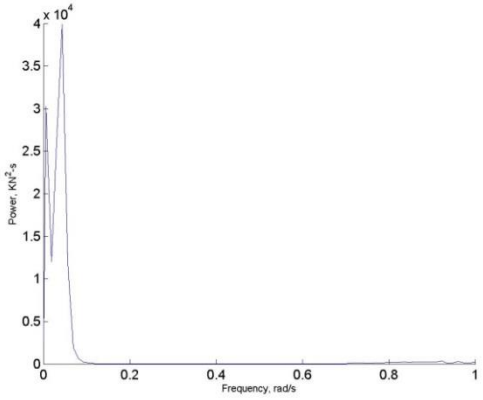

r) Top Tension PSD of ML3

Figure A 2-11 Continued

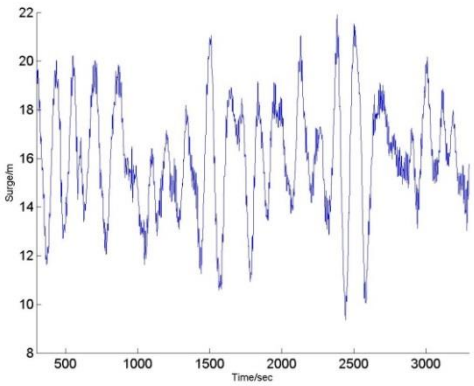

a) Surge

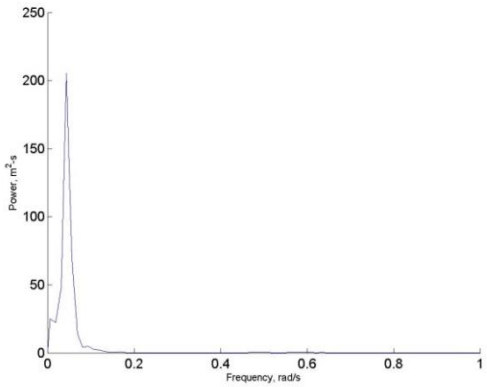

b) Surge PSD

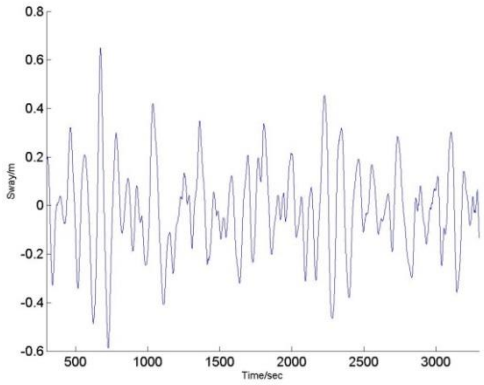

c) Sway

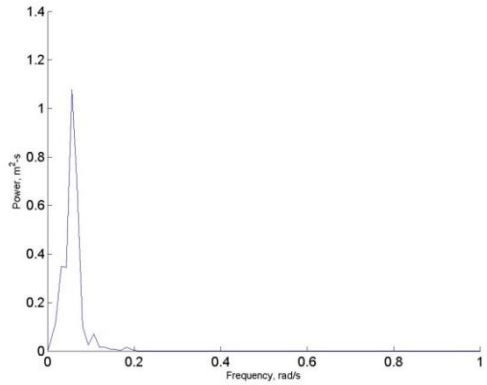

d) Sway PSD

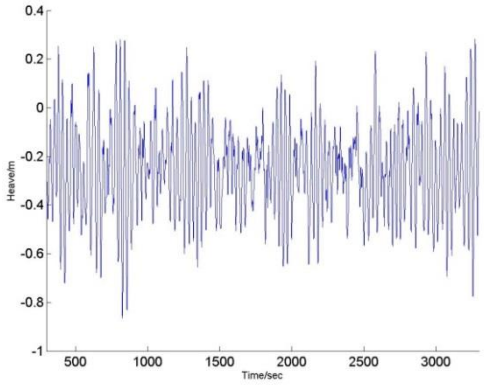

e) Heave

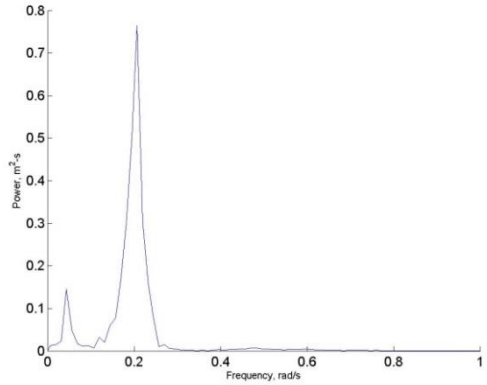

f) Heave PSD

Figure A 2-12 The FOWT Results for Case 15

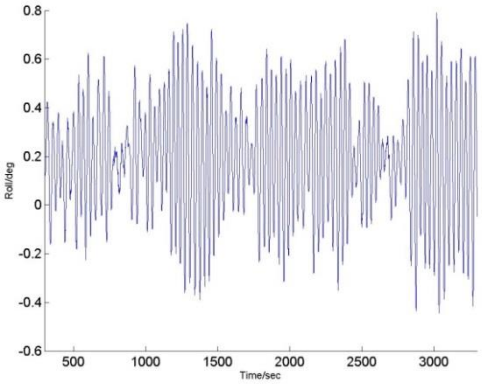

g) Roll

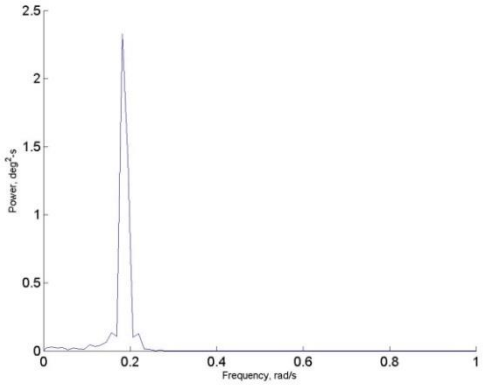

h) Roll PSD

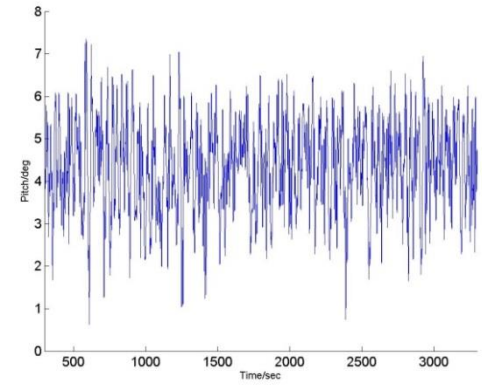

i) Pitch

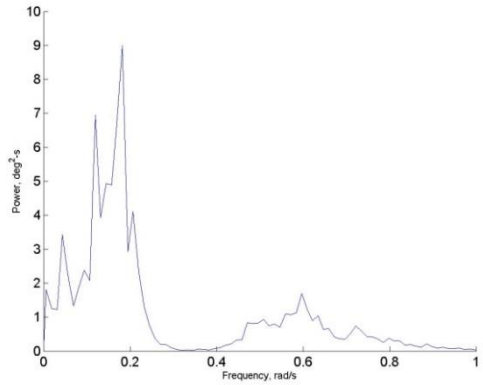

j) Pitch PSD

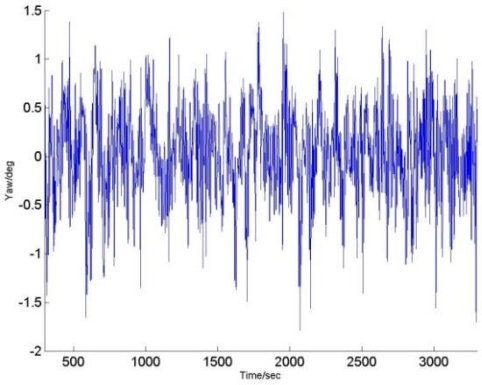

k) Yaw

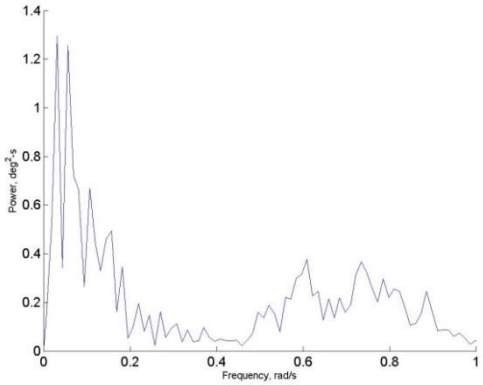

l) Yaw PSD

Figure A 2-12 Continued

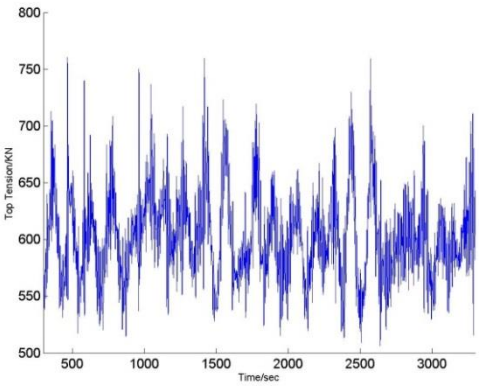

m) Top Tension of ML1

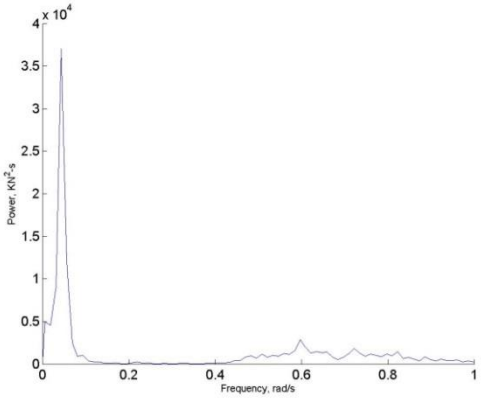

n) Top Tension PSD of ML1

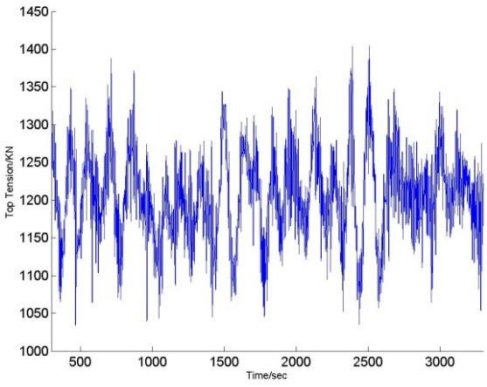

o) Top Tension of ML2

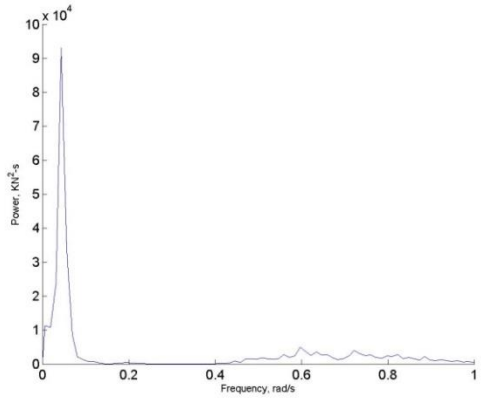

p) Top Tension PSD of ML2

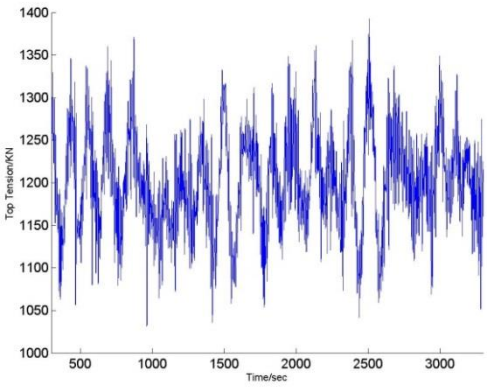

q) Top Tension of ML3

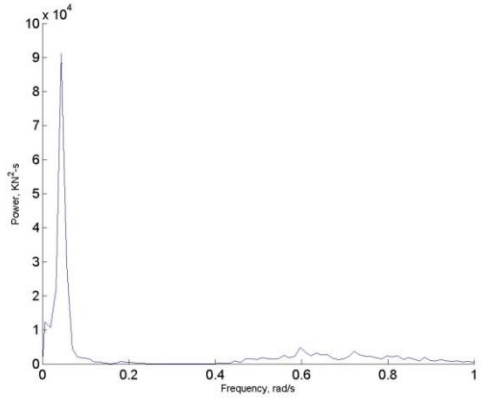

r) Top Tension PSD of ML3

Figure A 2-12 Continued

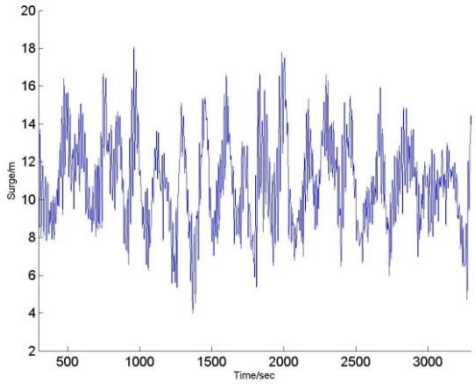

a) Surge

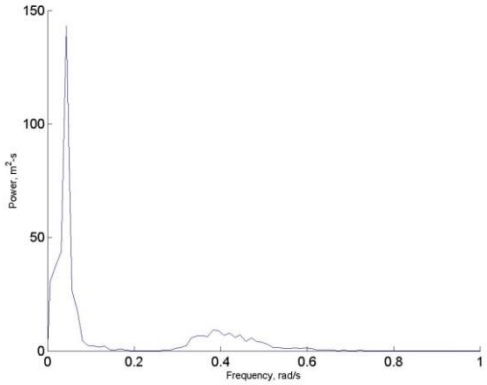

b) Surge PSD

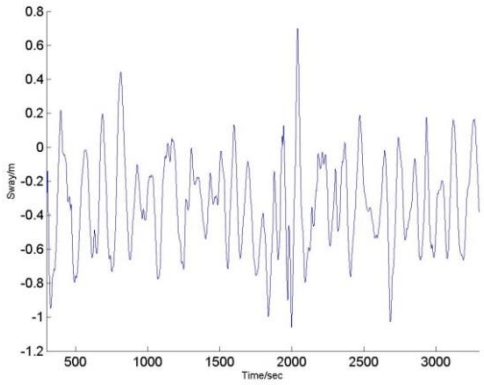

c) Sway

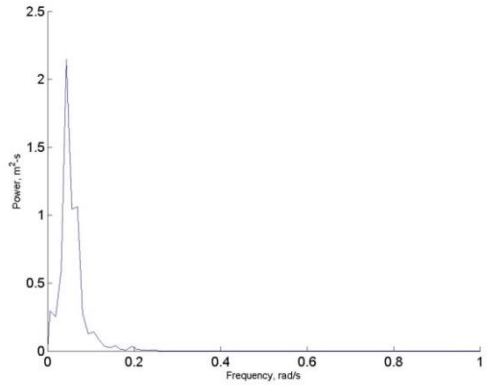

d) Sway PSD

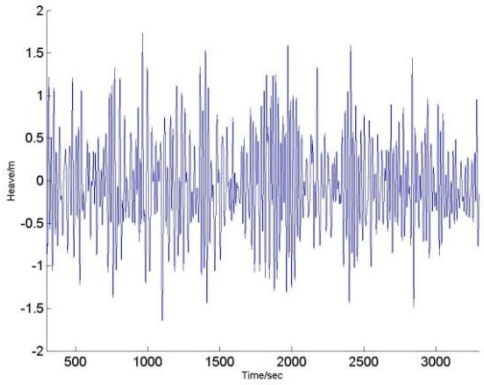

e) Heave

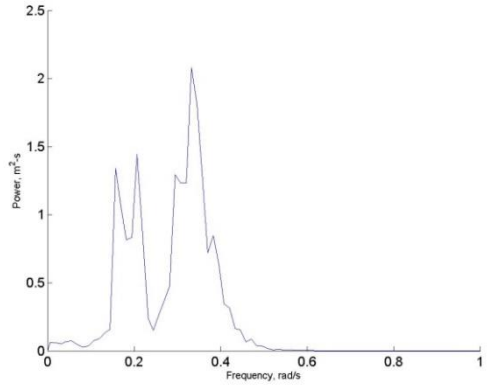

f) Heave PSD

Figure A 2-13 The FOWT Results for Case 16

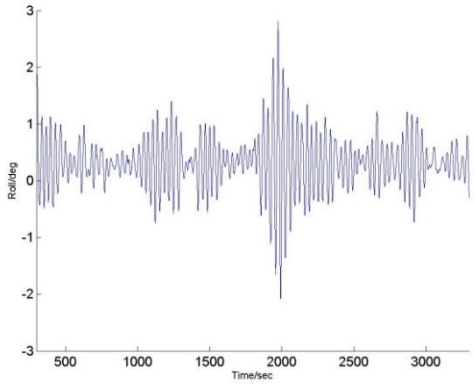

g) Roll

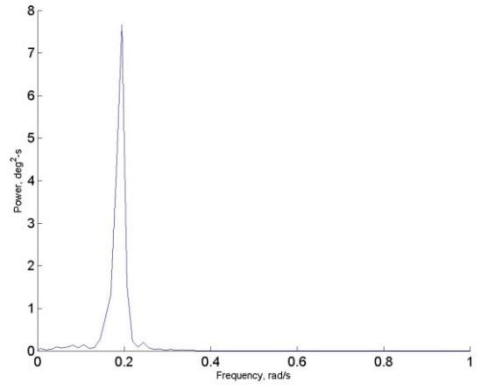

h) Roll PSD

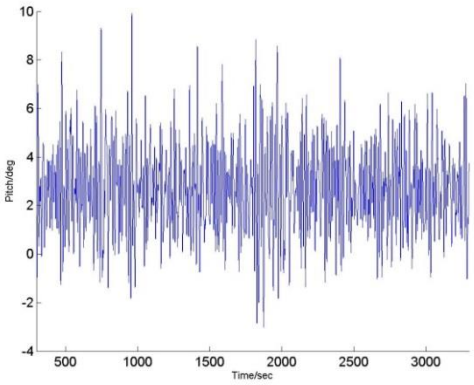

i) Pitch

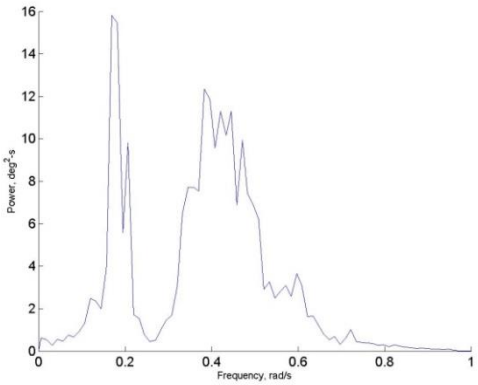

j) Pitch PSD

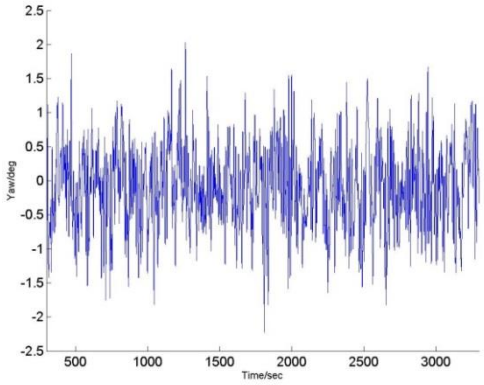

k) Yaw

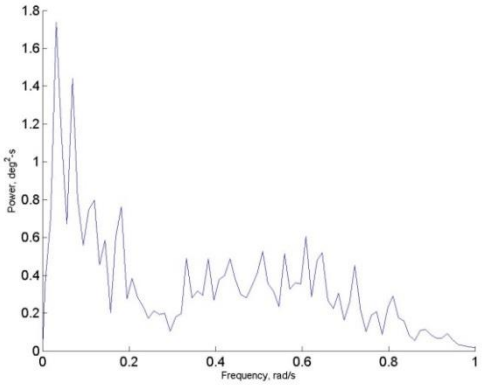

l) Yaw PSD

Figure A 2-13 Continued

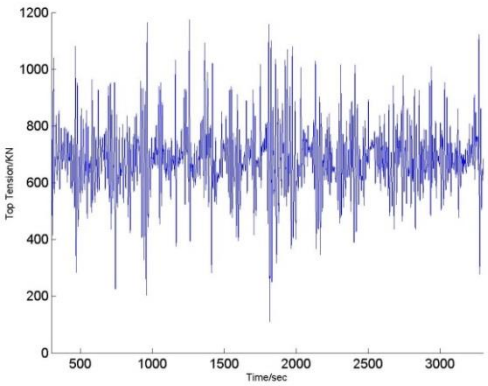

m) Top Tension of ML1

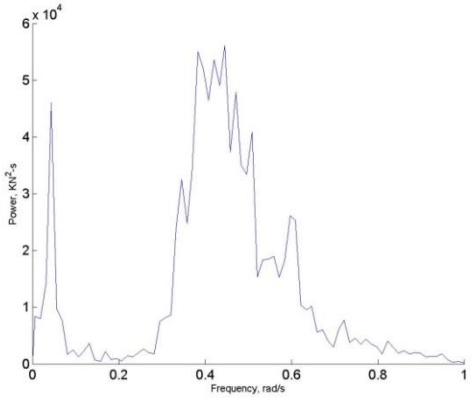

n) Top Tension PSD of ML1

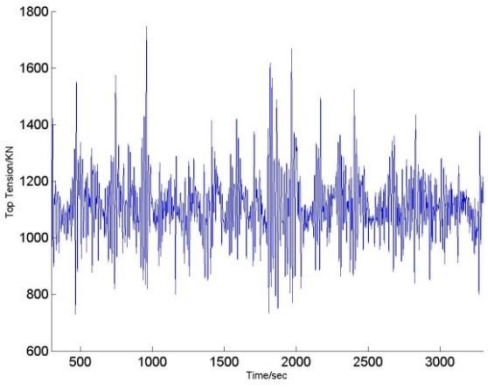

o) Top Tension of ML2

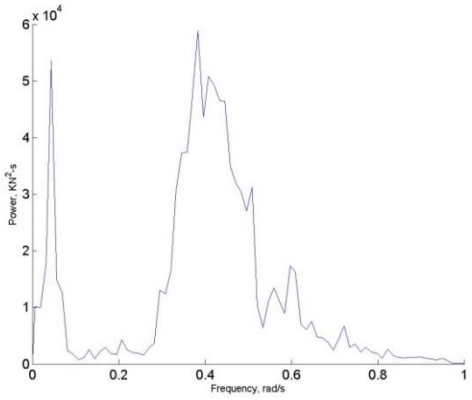

p) Top Tension PSD of ML2

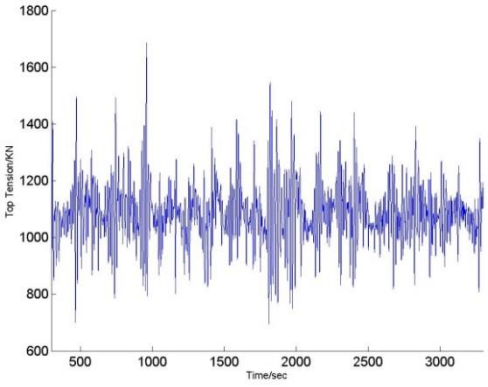

q) Top Tension of ML3

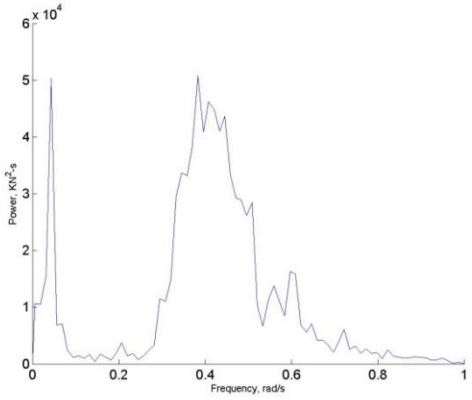

r) Top Tension PSD of ML3

Figure A 2-13 Continued

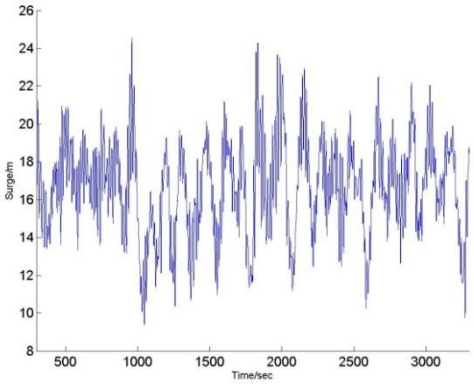

a) Surge

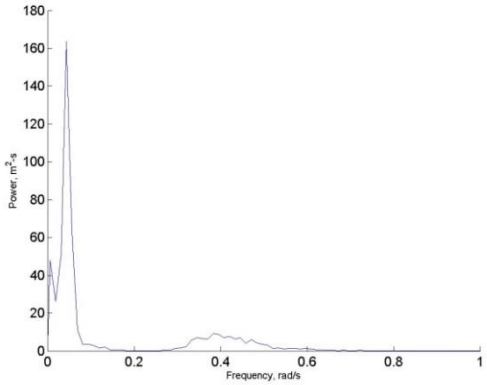

b) Surge PSD

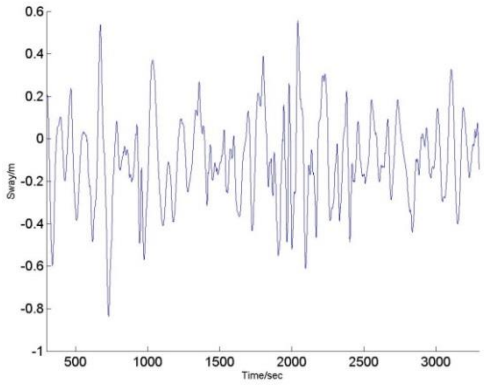

c) Sway

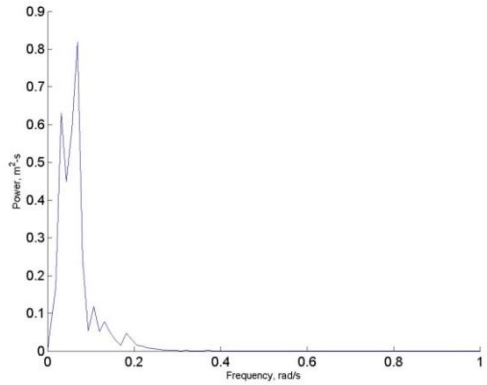

d) Sway PSD

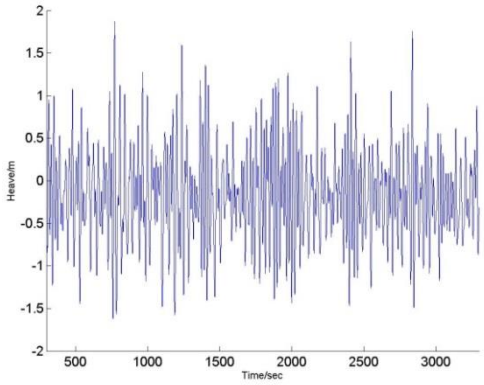

e) Heave

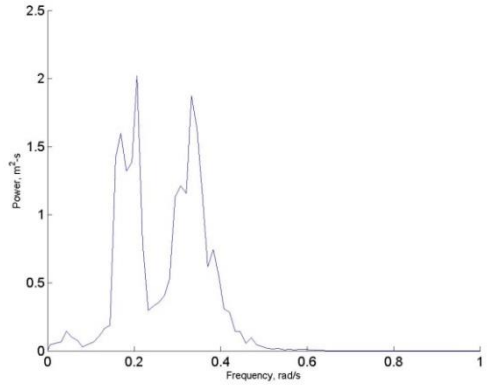

f) Heave PSD

Figure A 2-14 The FOWT Results for Case 17

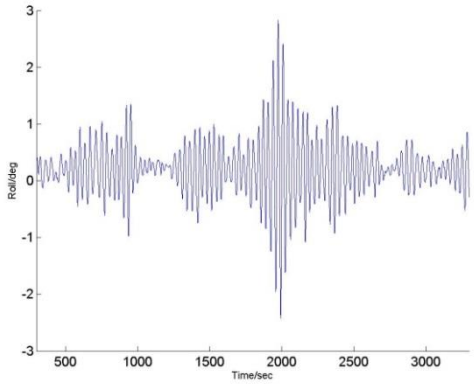

g) Roll

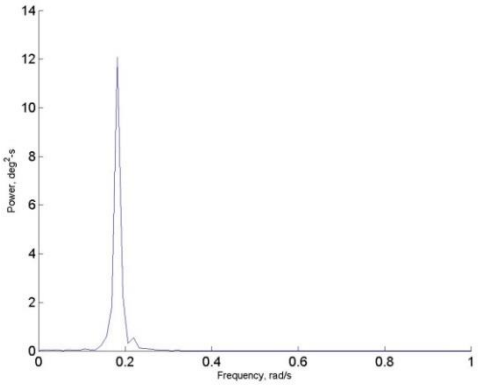

h) Roll PSD

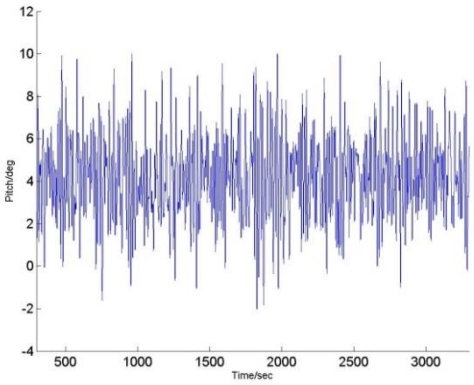

i) Pitch

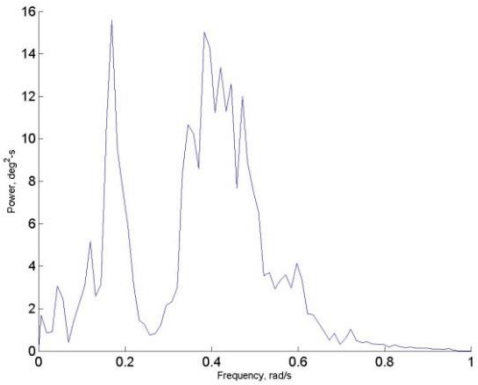

j) Pitch PSD

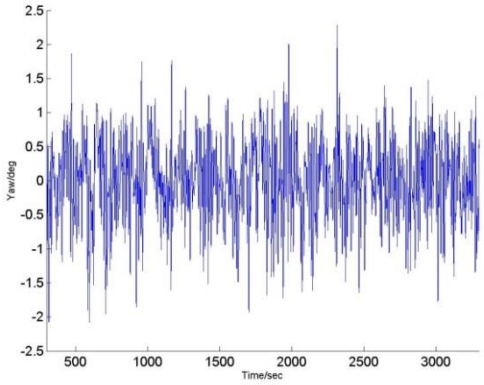

k) Yaw

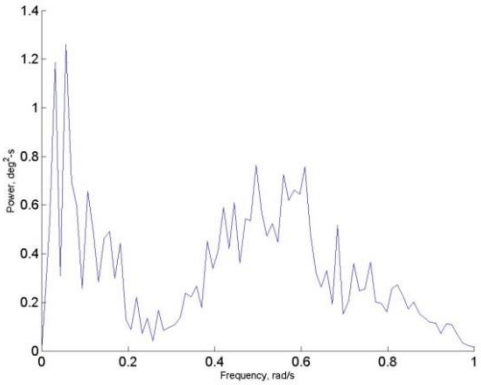

l) Yaw PSD

Figure A 2-14 Continued

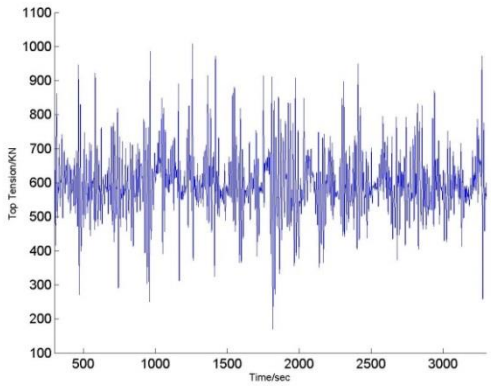

m) Top Tension of ML1

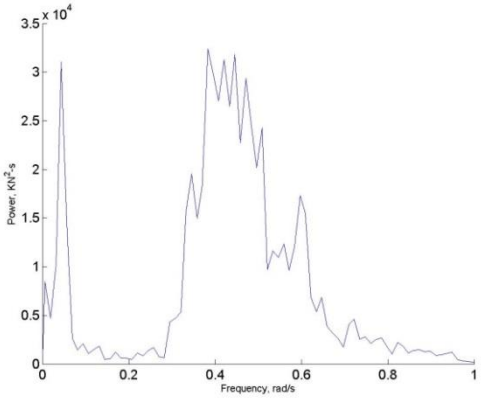

n) Top Tension PSD of ML1

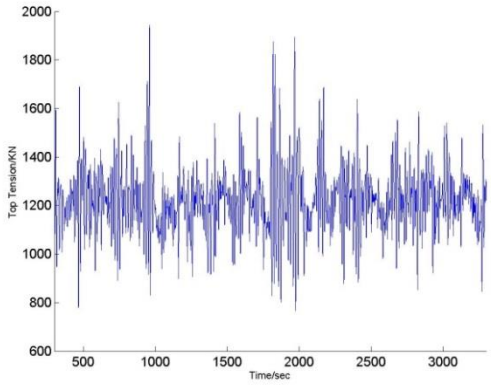

o) Top Tension of ML2

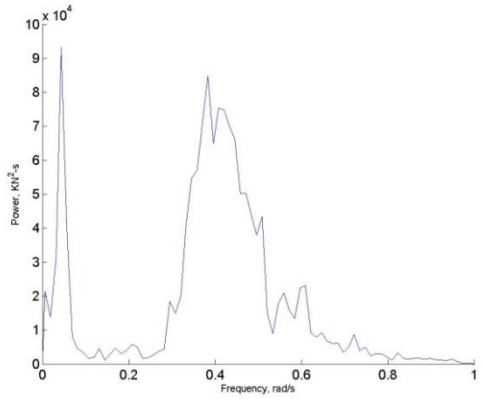

p) Top Tension PSD of ML2

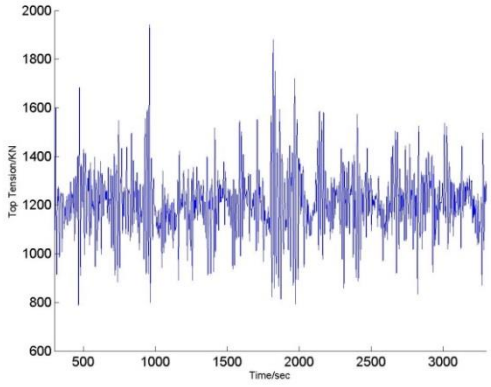

q) Top Tension of ML3

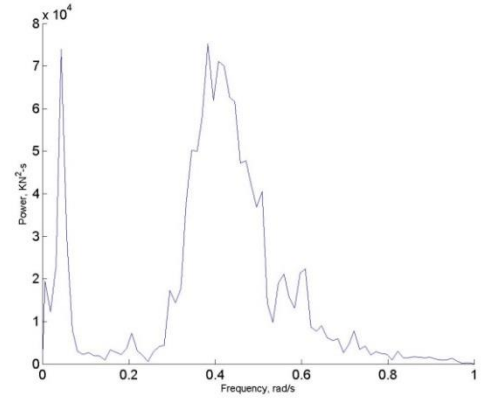

r) Top Tension PSD of ML3

Figure A 2-14 Continued

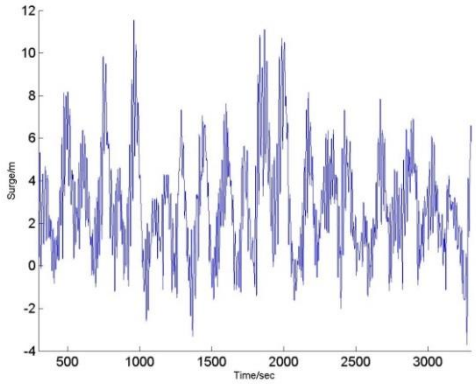

a) Surge

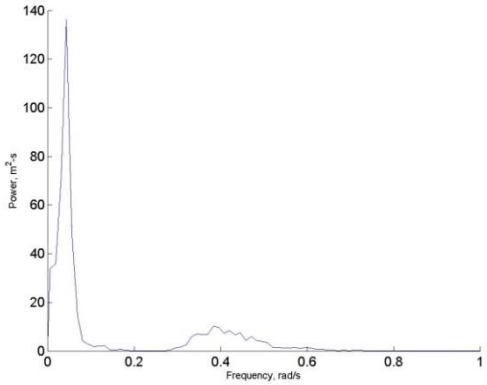

b) Surge PSD

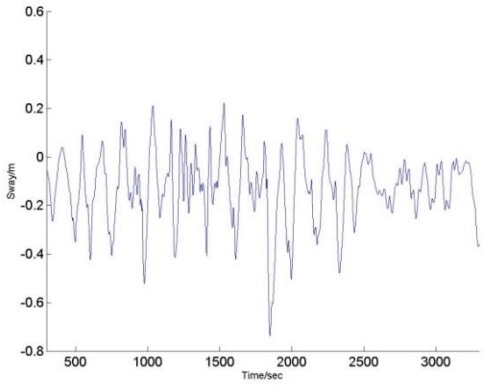

c) Sway

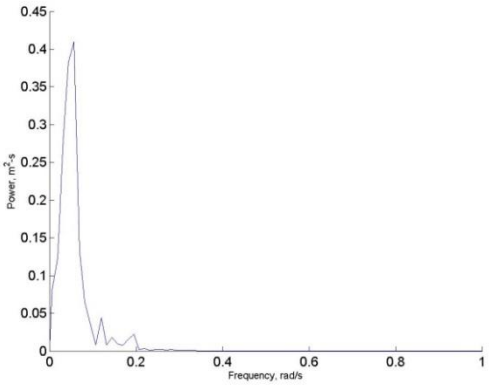

d) Sway PSD

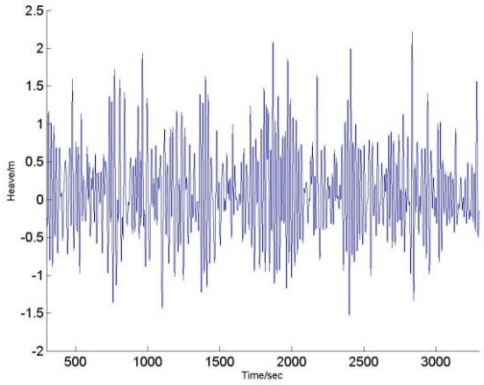

e) Heave

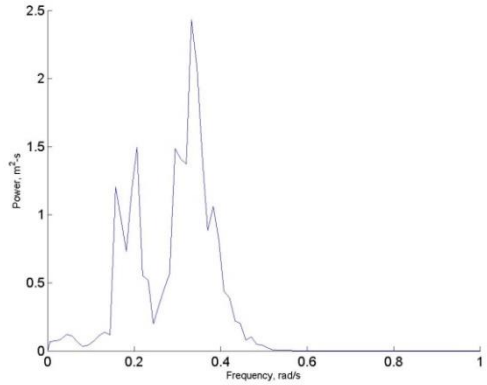

f) Heave PSD

Figure A 2-15 The FOWT Results for Case 18

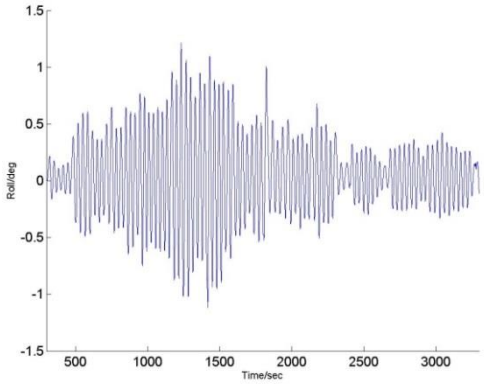

g) Roll

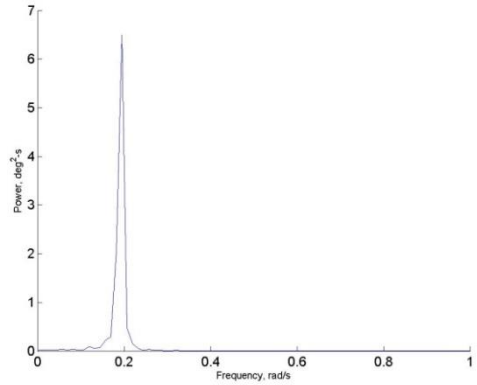

h) Roll PSD

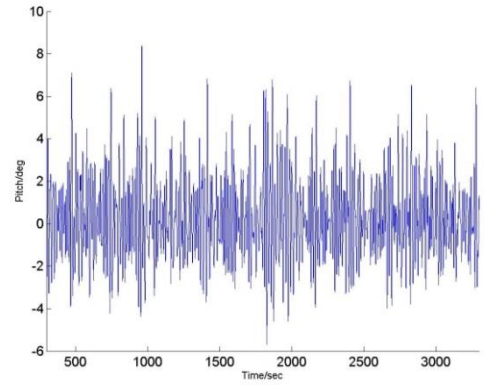

i) Pitch

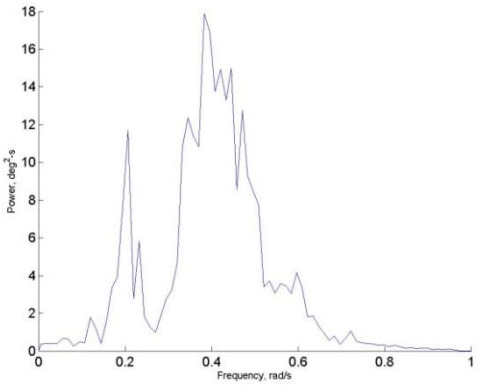

j) Pitch PSD

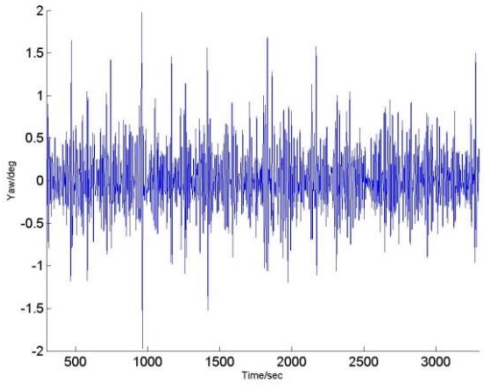

k) Yaw

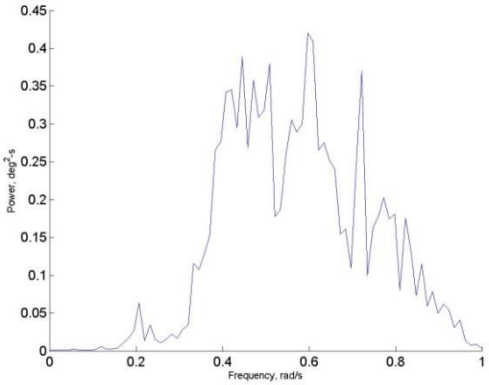

l) Yaw PSD

Figure A 2-15 Continued

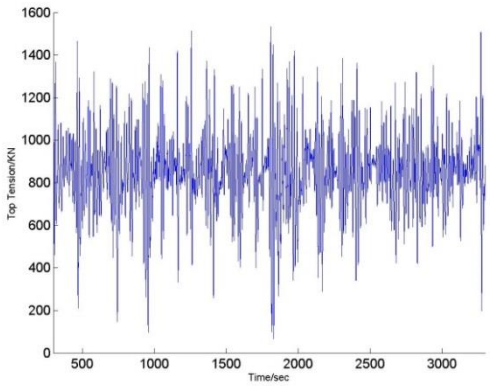

m) Top Tension of ML1

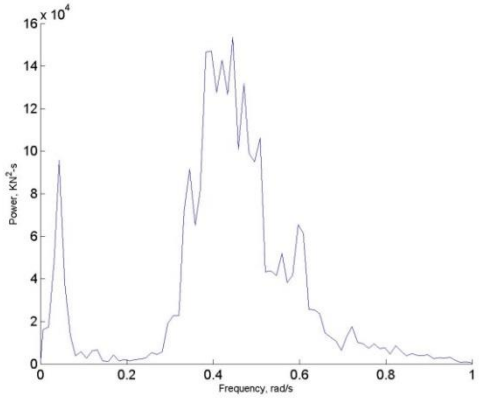

n) Top Tension PSD of ML1

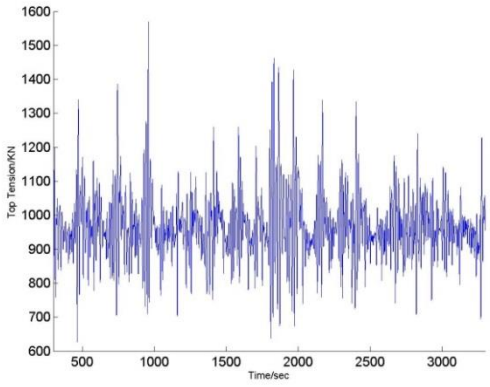

o) Top Tension of ML2

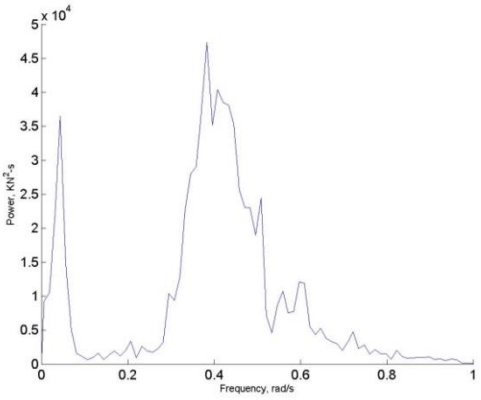

p) Top Tension PSD of ML2

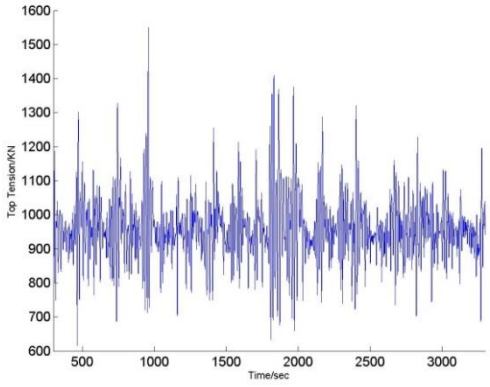

q) Top Tension of ML3

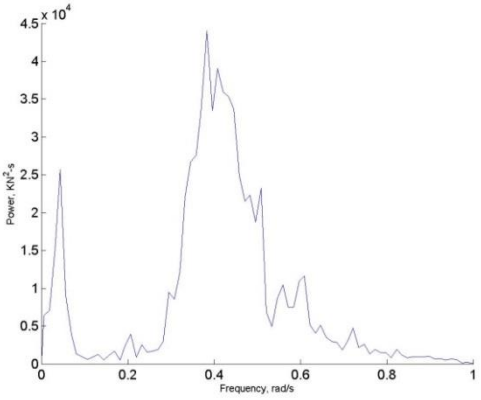

r) Top Tension PSD of ML3

Figure A 2-15 Continued

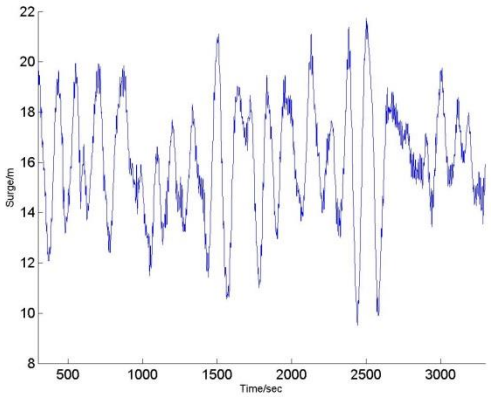

a) Surge

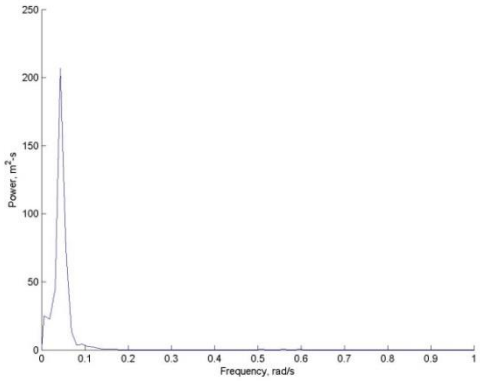

b) Surge PSD

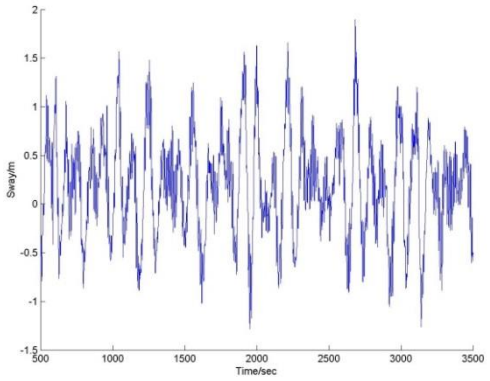

c) Sway

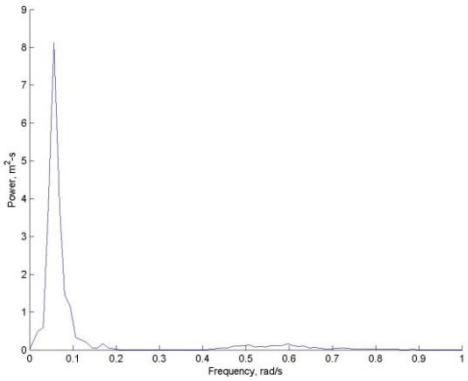

d) Sway PSD

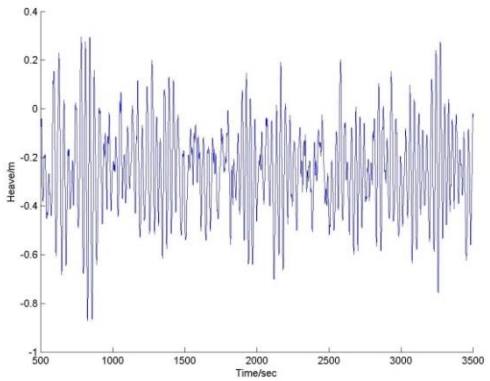

e) Heave

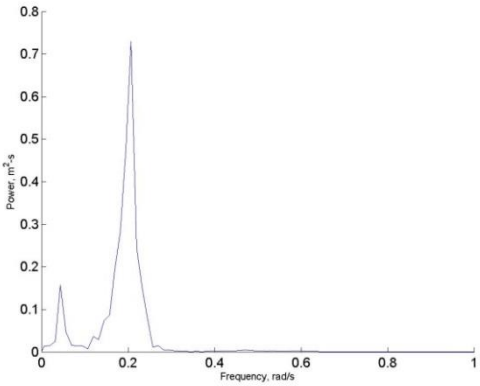

f) Heave PSD

Figure A 2-16 The FOWT Results for Case 19

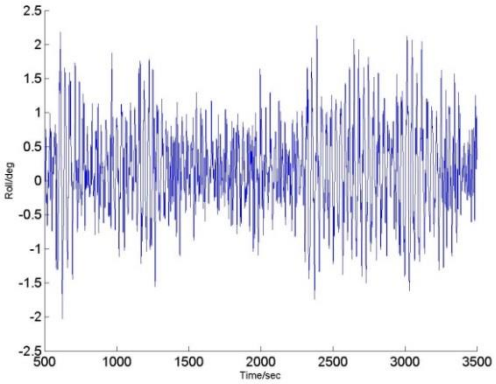

g) Roll

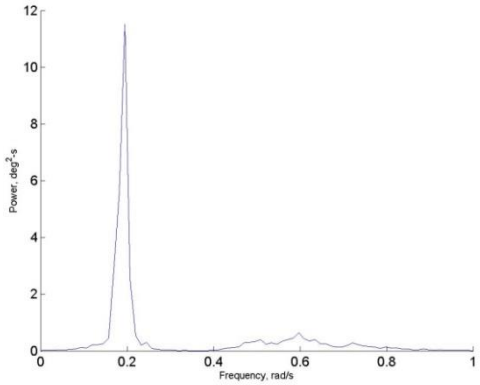

h) Roll PSD

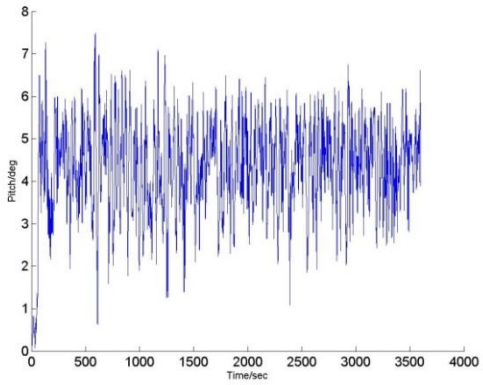

i) Pitch

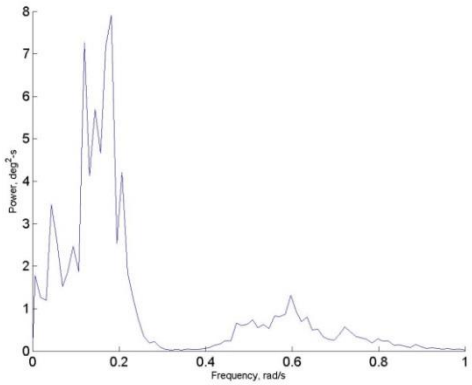

j) Pitch PSD

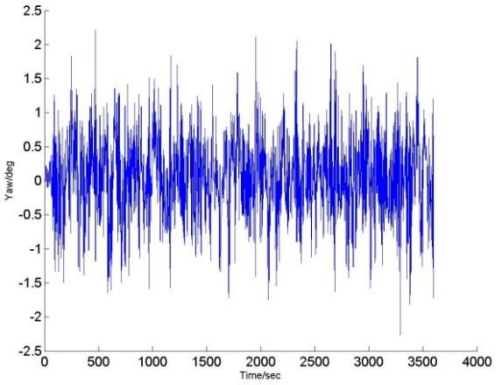

k) Yaw

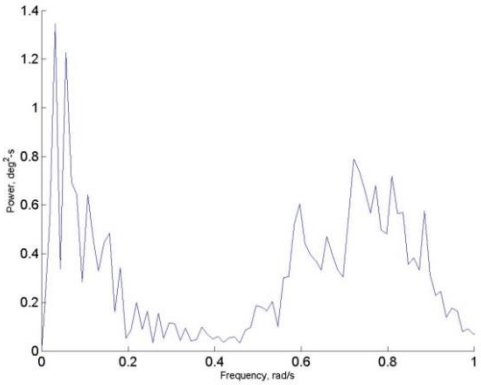

l) Yaw PSD

Figure A 2-16 Continued

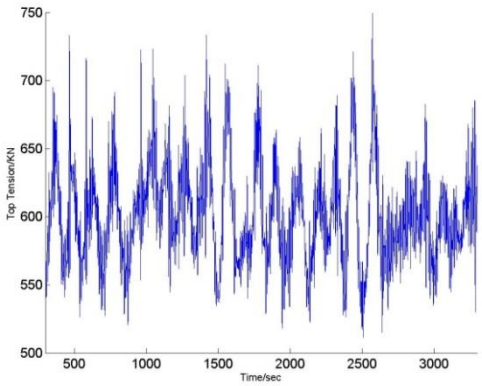

m) Top Tension of ML1

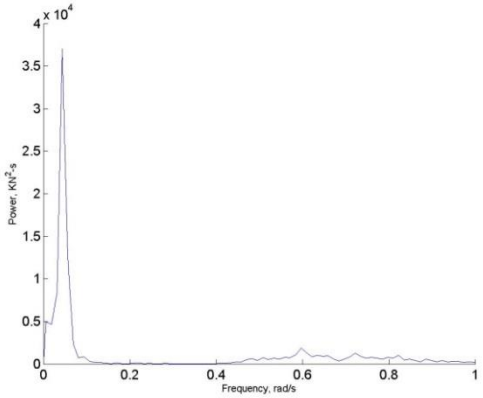

n) Top Tension PSD of ML1

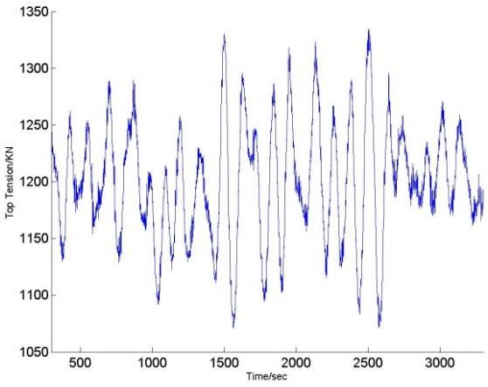

o) Top Tension of ML2

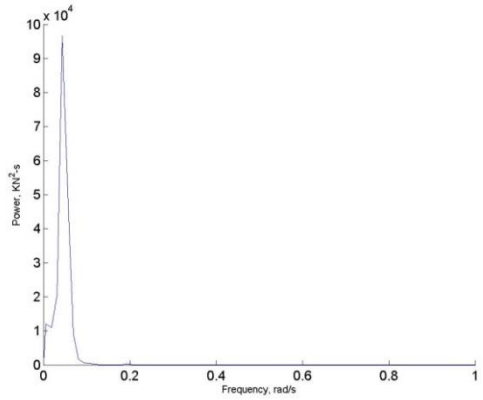

p) Top Tension PSD of ML2

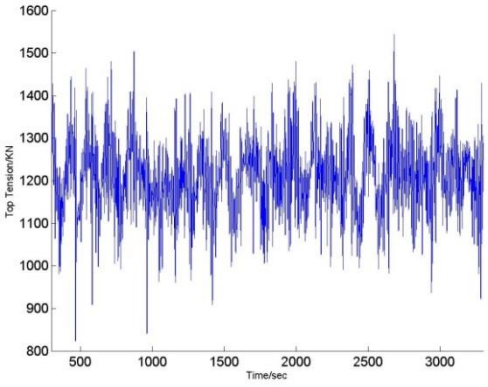

q) Top Tension of ML3

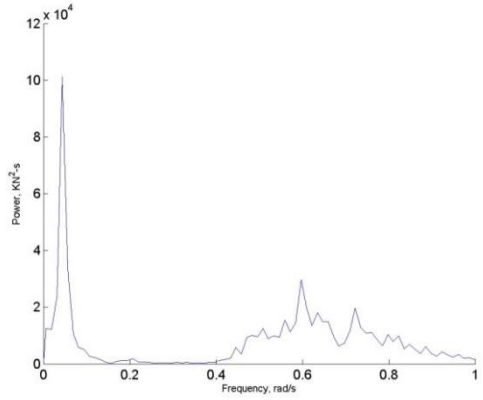

r) Top Tension PSD of ML3

Figure A 2-16 Continued

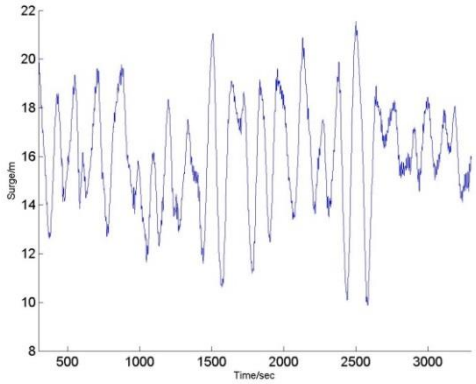

a) Surge

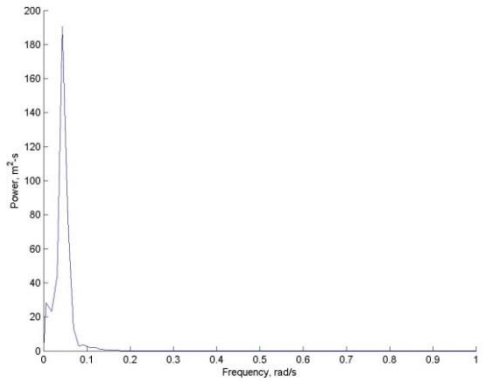

b) Surge PSD

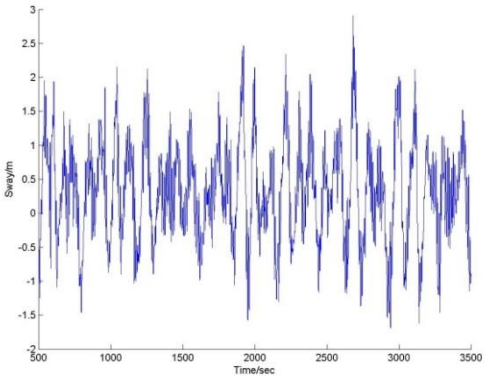

c) Sway

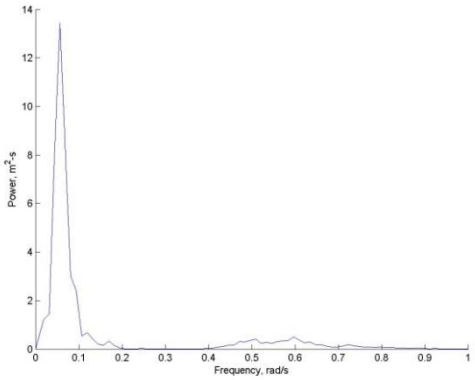

d) Sway PSD

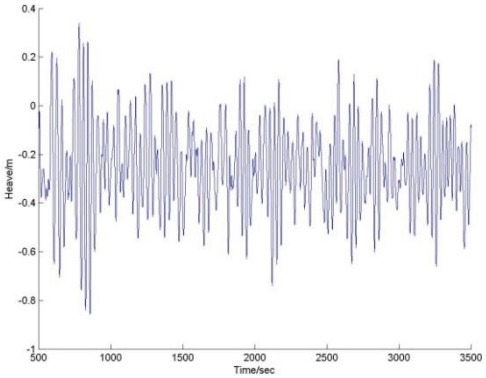

e) Heave

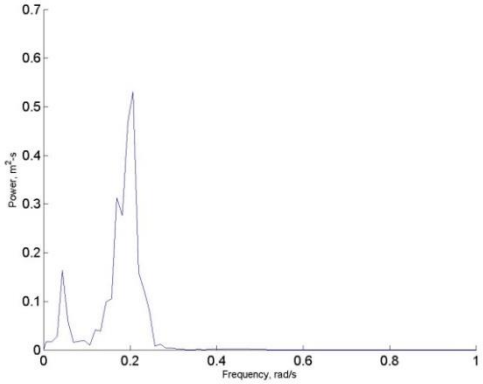

f) Heave PSD

Figure A 2-17 The FOWT Results for Case 20

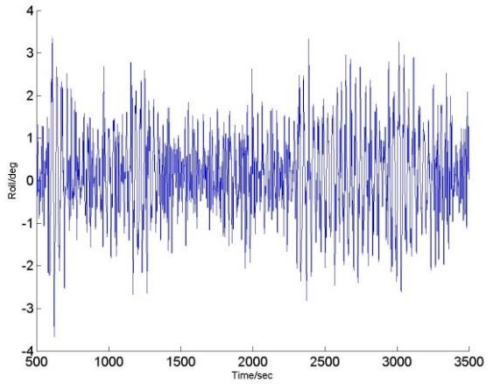

g) Roll

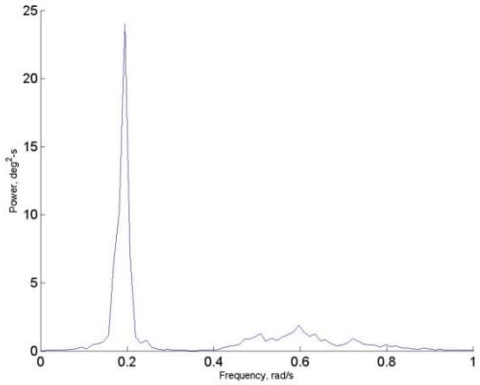

h) Roll PSD

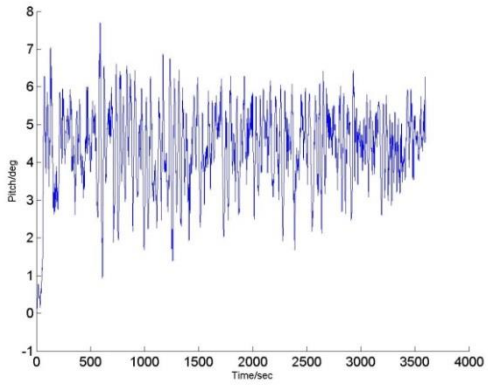

i) Pitch

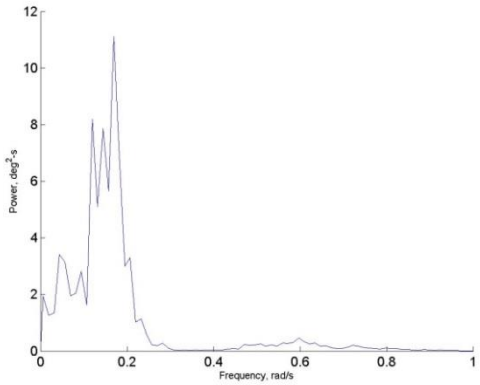

j) Pitch PSD

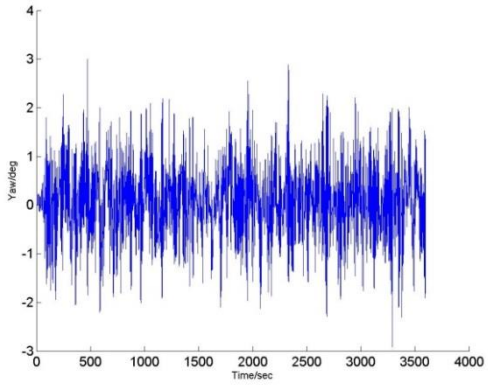

k) Yaw

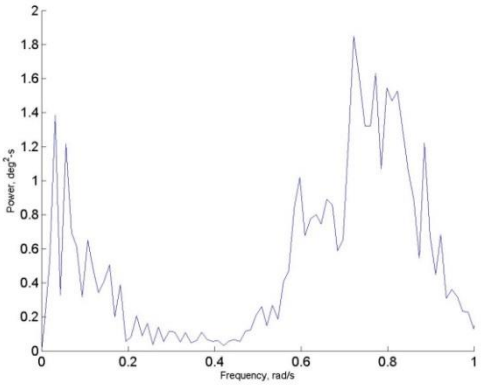

l) Yaw PSD

Figure A 2-17 Continued

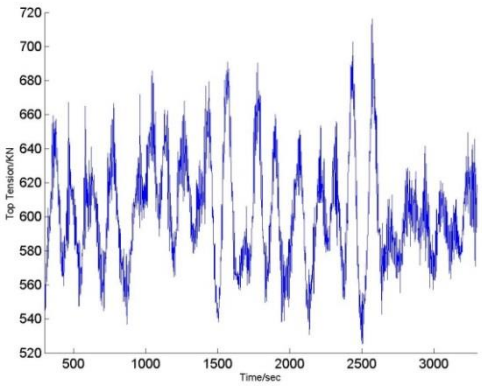

m) Top Tension of ML1

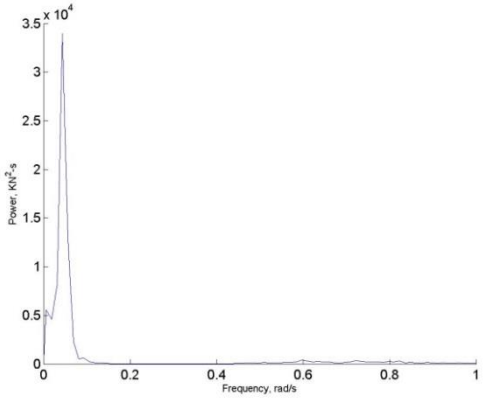

n) Top Tension PSD of ML1

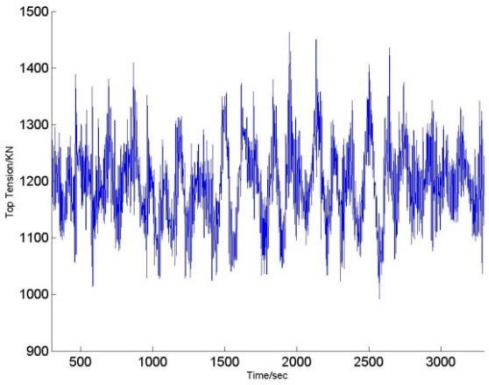

o) Top Tension of ML2

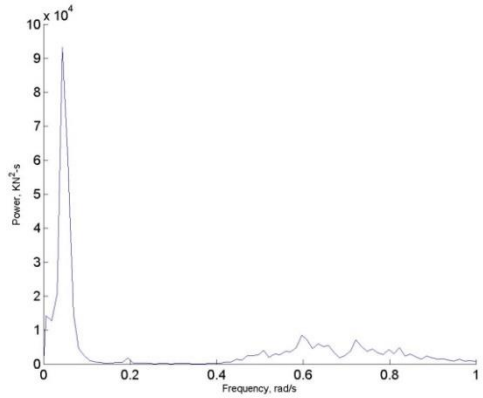

p) Top Tension PSD of ML2

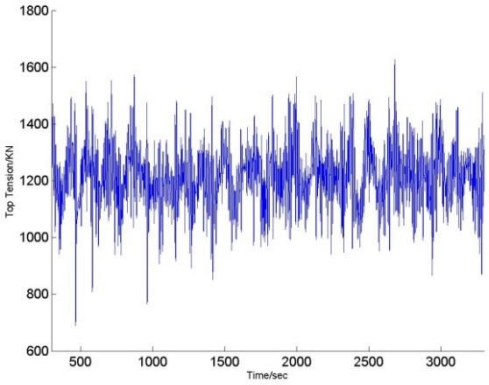

q) Top Tension of ML3

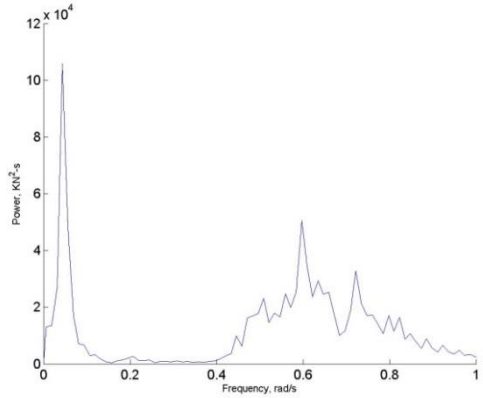

r) Top Tension PSD of ML3

Figure A 2-17 Continued

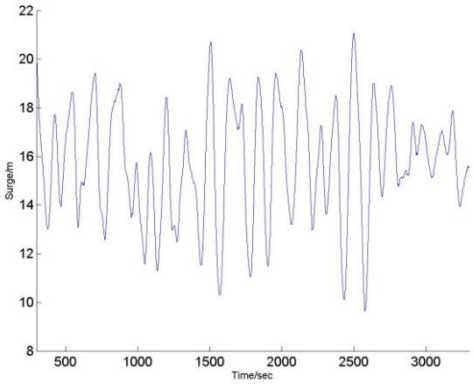

a) Surge

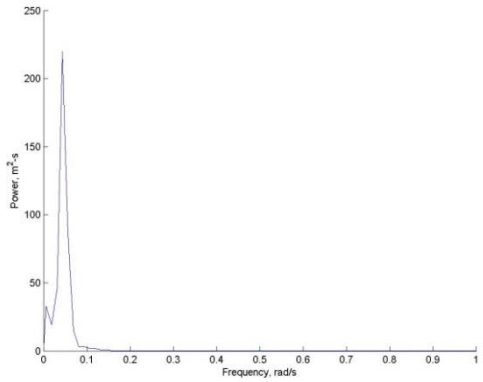

b) Surge PSD

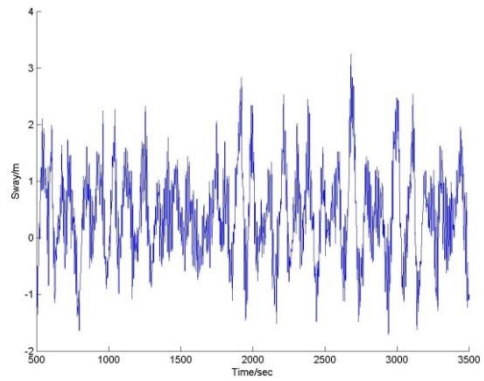

c) Sway

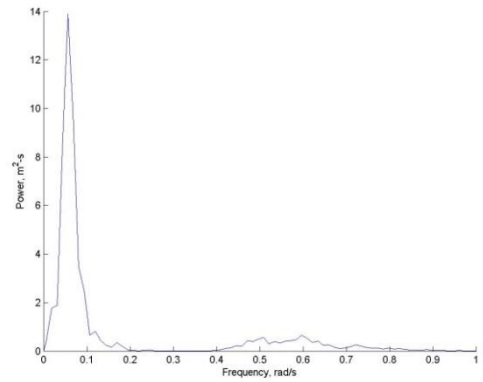

d) Sway PSD

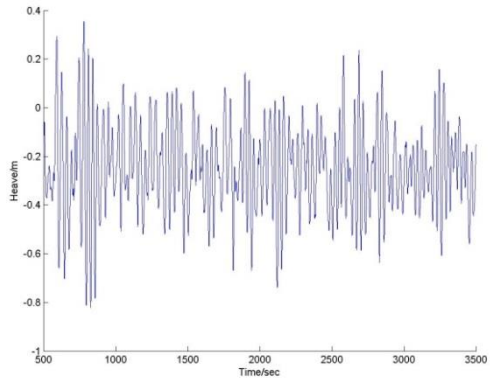

e) Heave

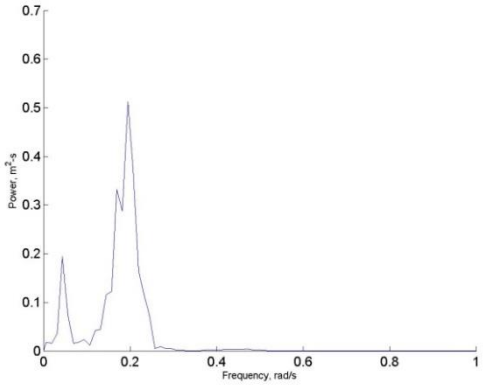

f) Heave PSD

Figure A 2-18 The FOWT Results for Case 21

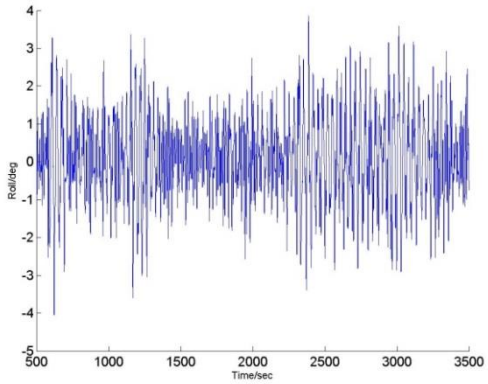

g) Roll

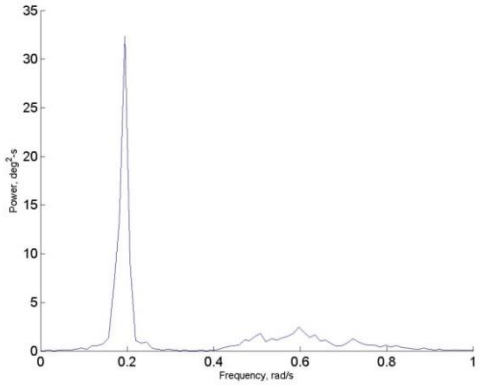

h) Roll PSD

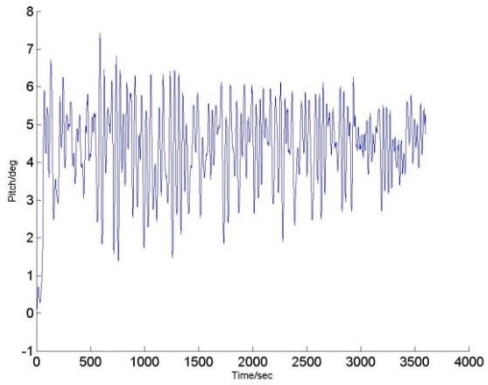

i) Pitch

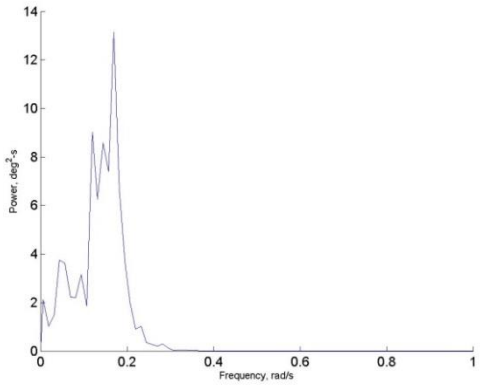

j) Pitch PSD

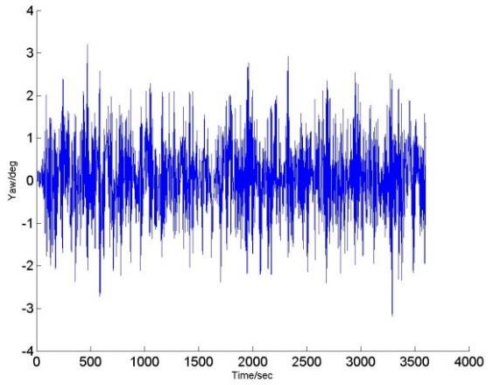

k) Yaw

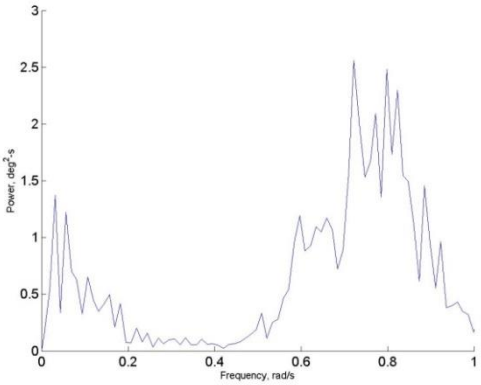

l) Yaw PSD

Figure A 2-18 Continued

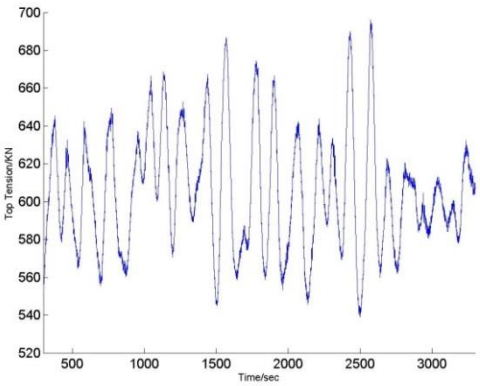

m) Top Tension of ML1

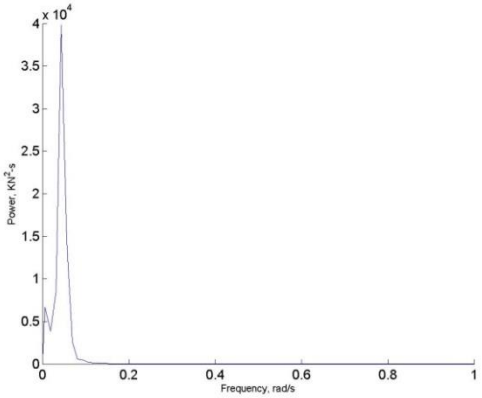

n) Top Tension PSD of ML1

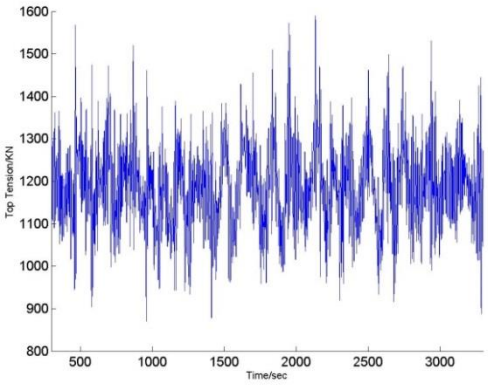

o) Top Tension of ML2

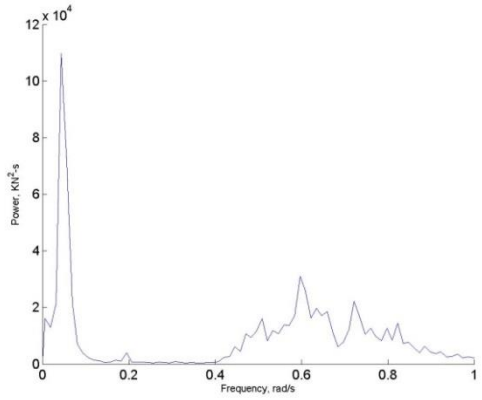

p) Top Tension PSD of ML2

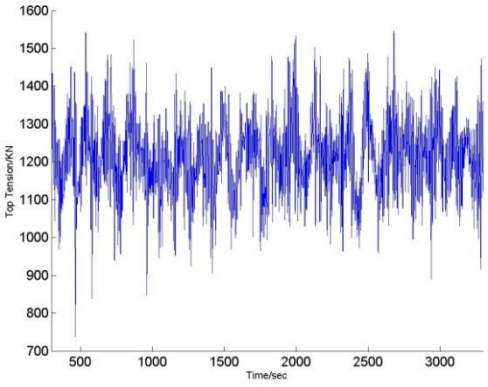

q) Top Tension of ML3

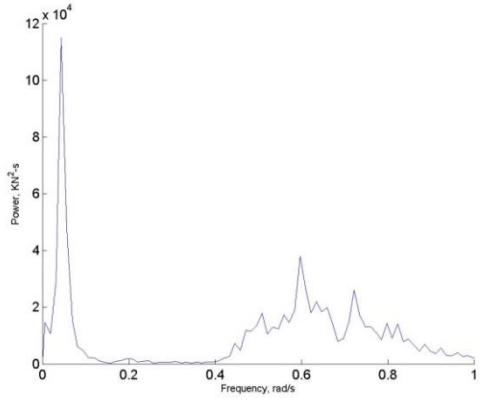

r) Top Tension PSD of ML3

Figure A 2-18 Continued

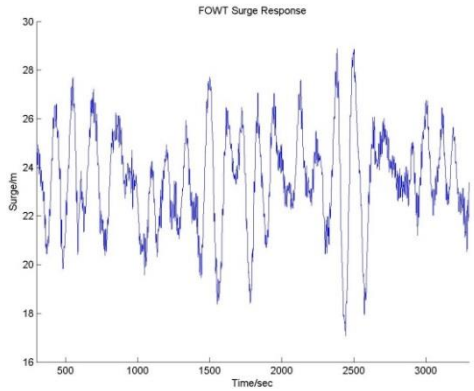

a) Surge

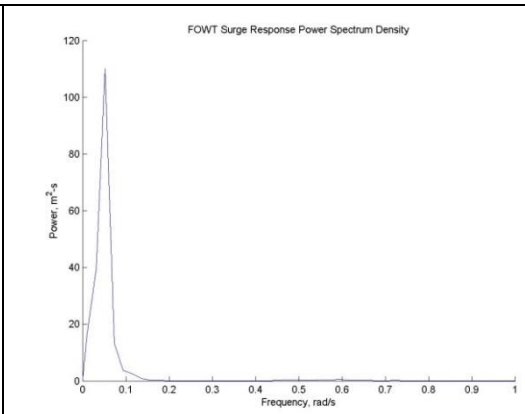

b) Surge PSD

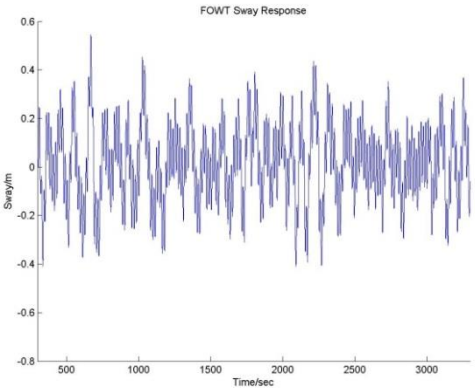

c) Sway

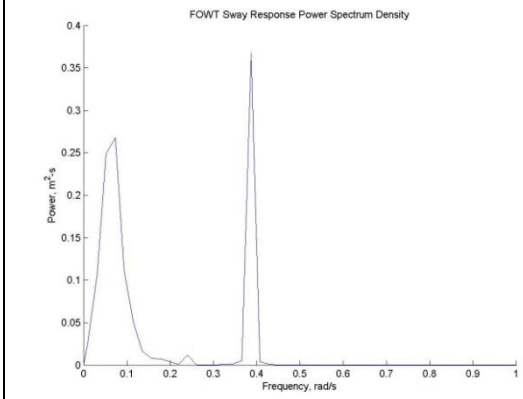

d) Sway PSD

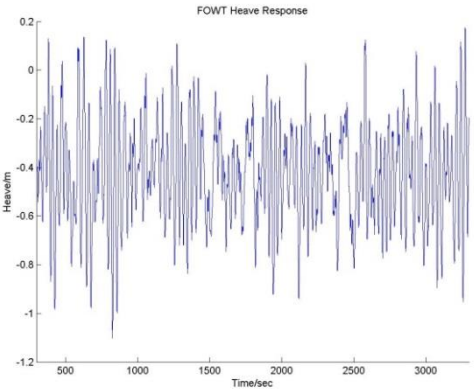

e) Heave

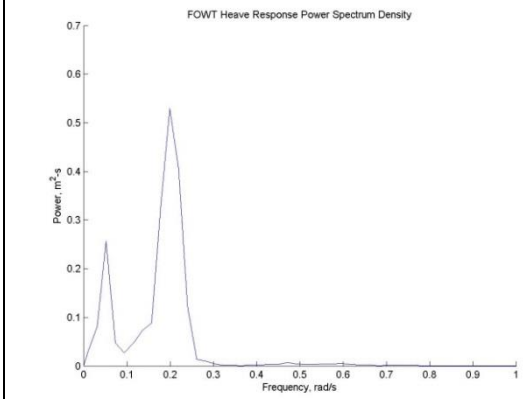

f) Heave PSD

Figure A 2-19 The FOWT Results for Case 22

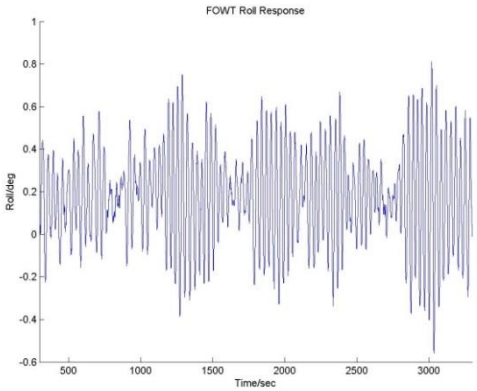

g) Roll

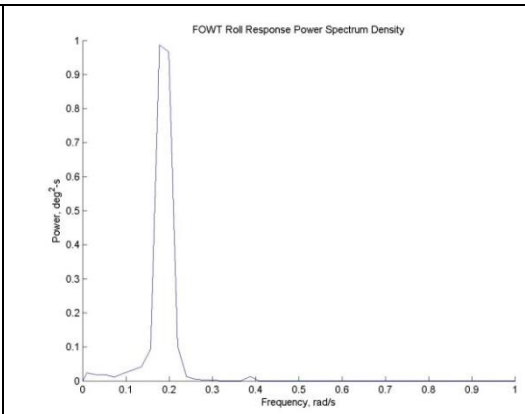

h) Roll PSD

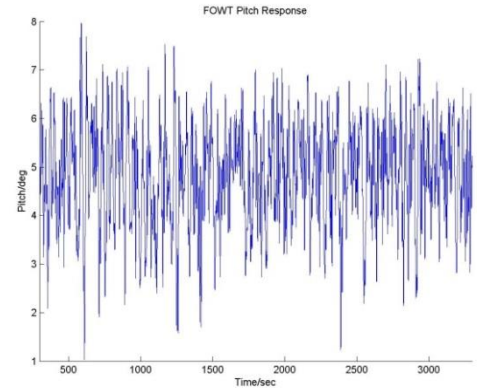

i) Pitch

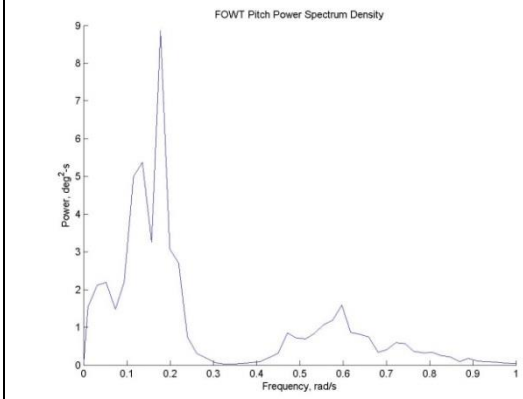

j) Pitch PSD

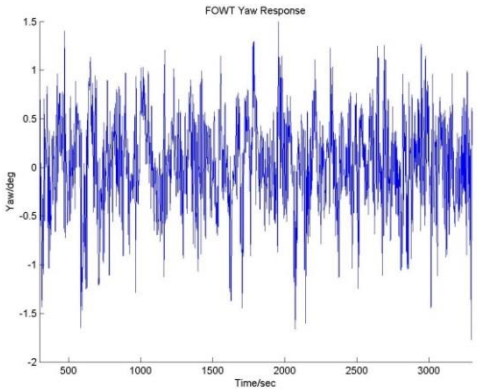

k) Yaw

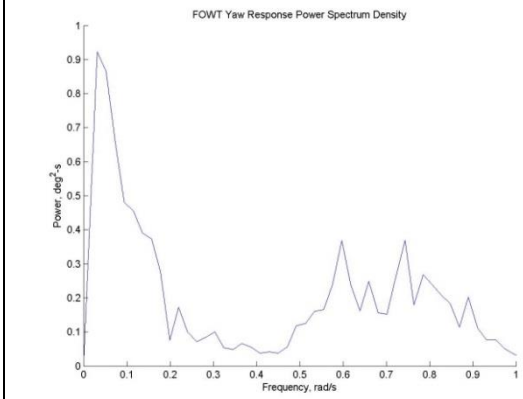

l) Yaw PSD

Figure A 2-19 Continued

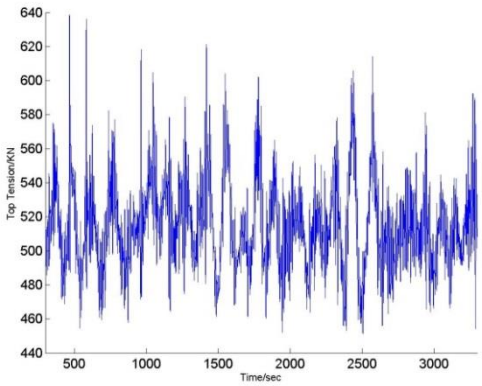

m) Top Tension of ML1

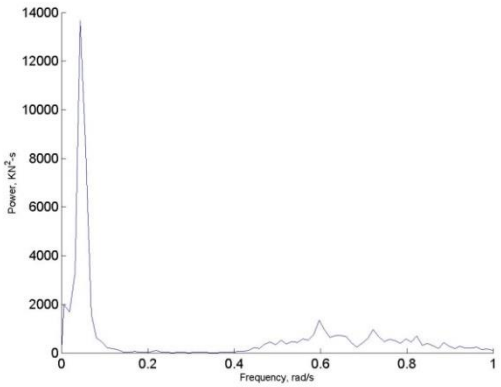

n) Top Tension PSD of ML1

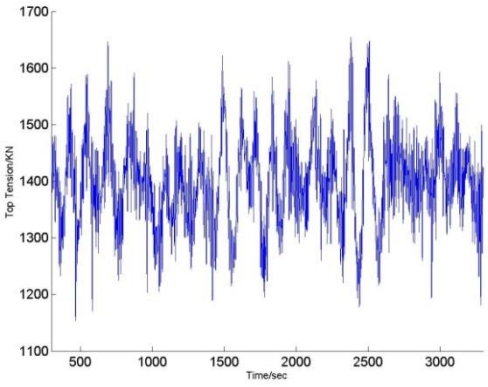

o) Top Tension of ML2

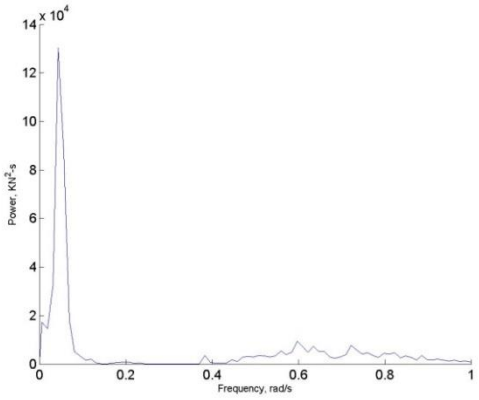

p) Top Tension PSD of ML2

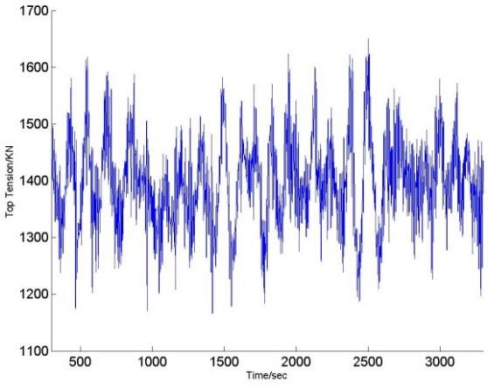

q) Top Tension of ML3

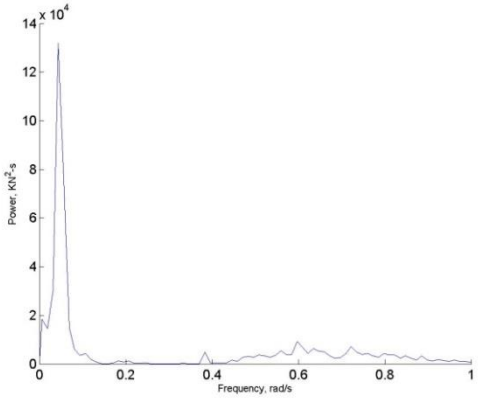

r) Top Tension PSD of ML3

Figure A 2-19 Continued

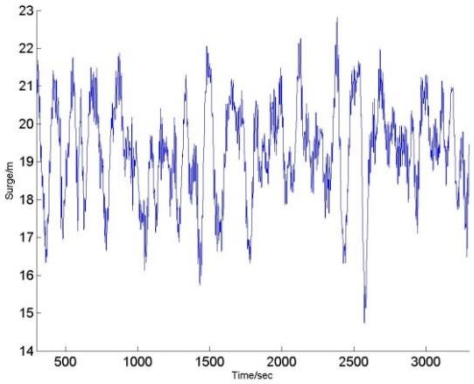

a) Surge

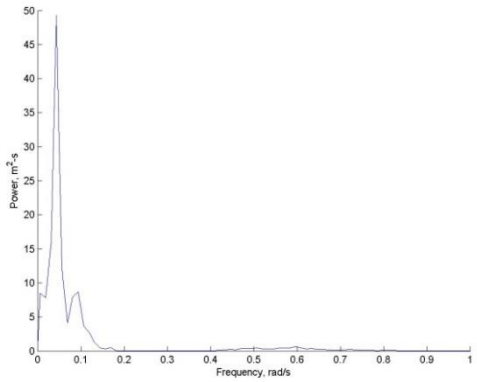

b) Surge PSD

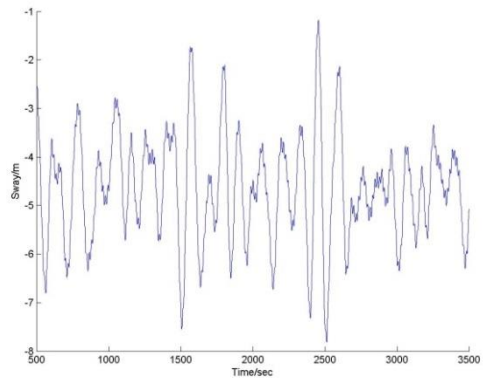

c) Sway

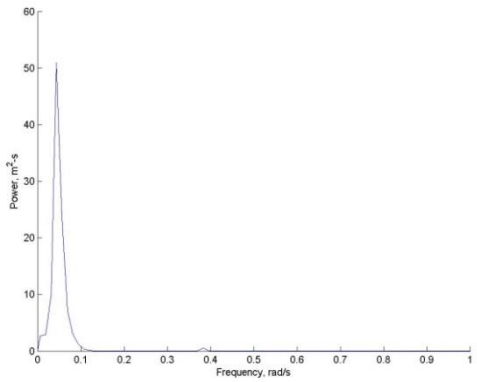

d) Sway PSD

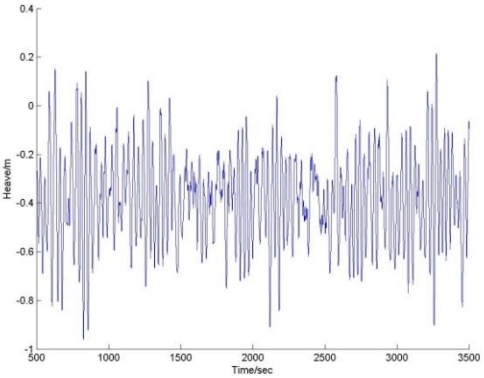

e) Heave

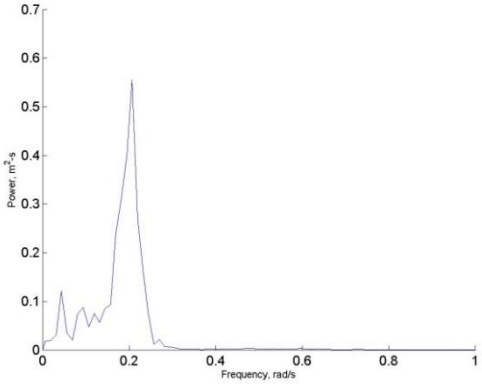

f) Heave PSD

Figure A 2-20 The FOWT Results for Case 23

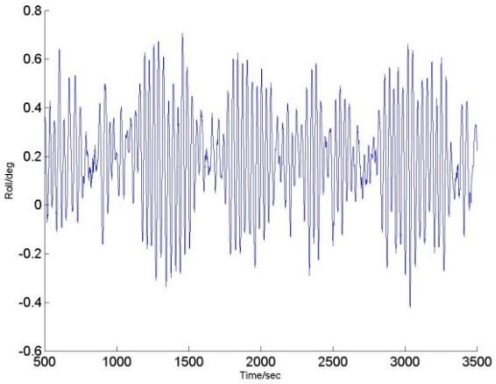

g) Roll

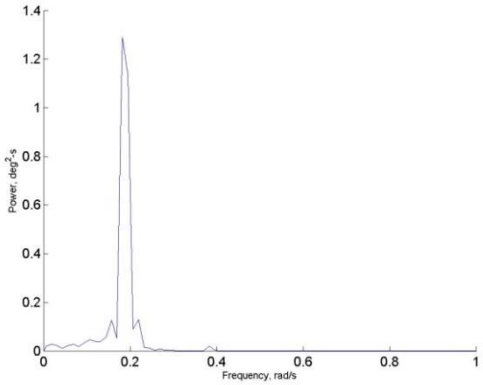

h) Roll PSD

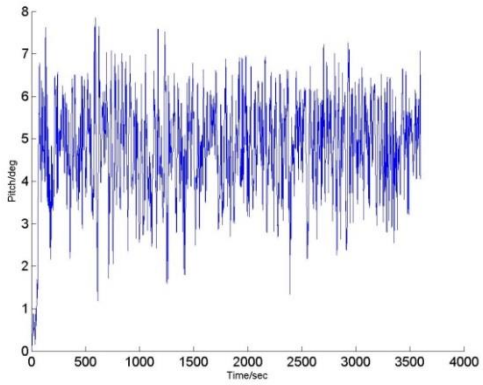

i) Pitch

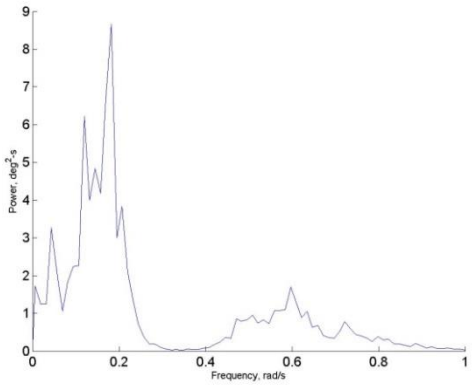

j) Pitch PSD

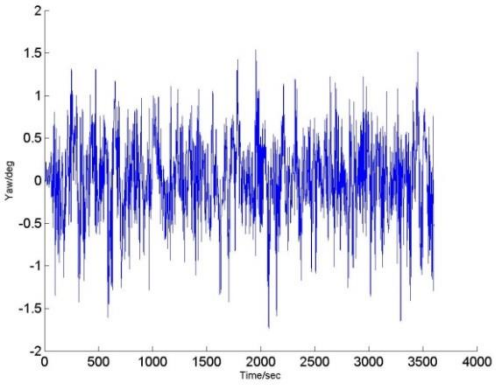

k) Yaw

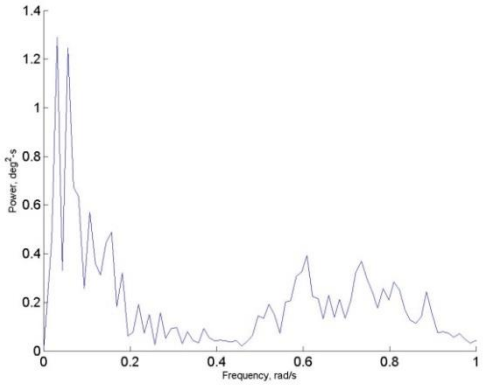

l) Yaw PSD

Figure A 2-20 Continued

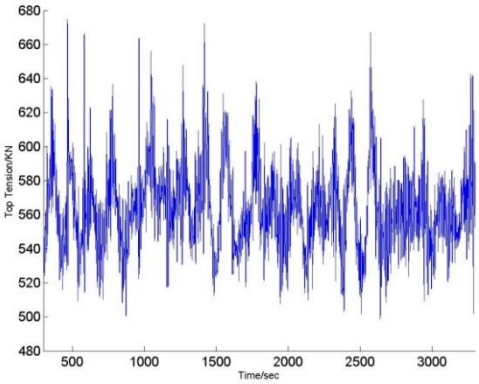

m) Top Tension of ML1

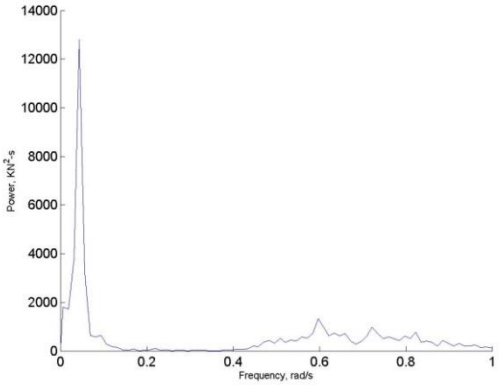

n) Top Tension PSD of ML1

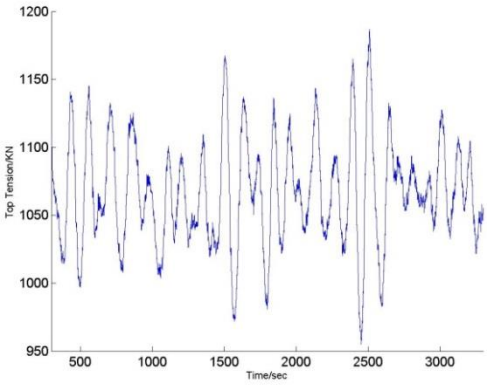

o) Top Tension of ML2

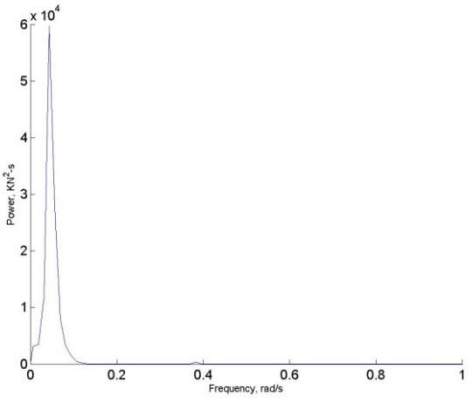

p) Top Tension PSD of ML2

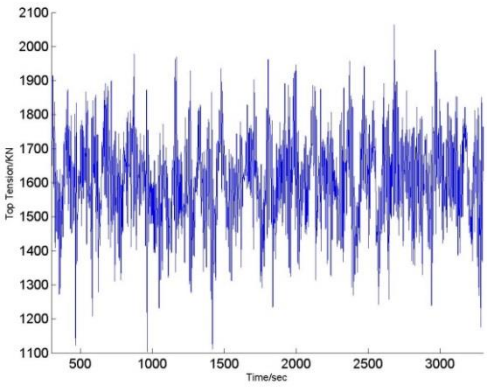

q) Top Tension of ML3

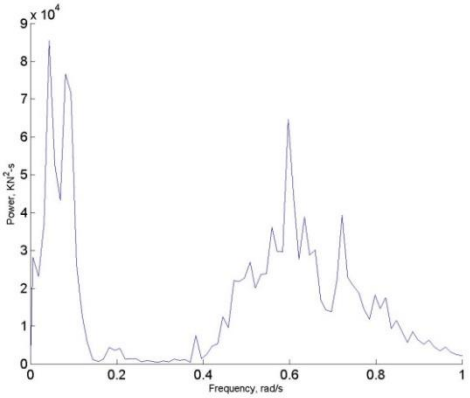

r) Top Tension PSD of ML3

Figure A 2-20 Continued

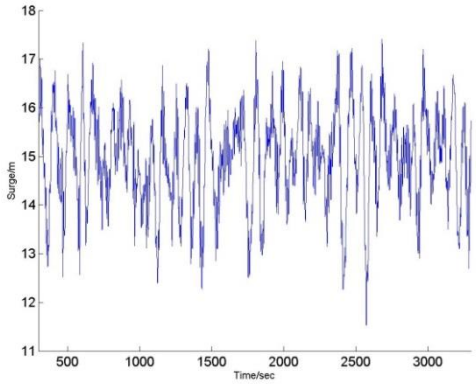

a) Surge

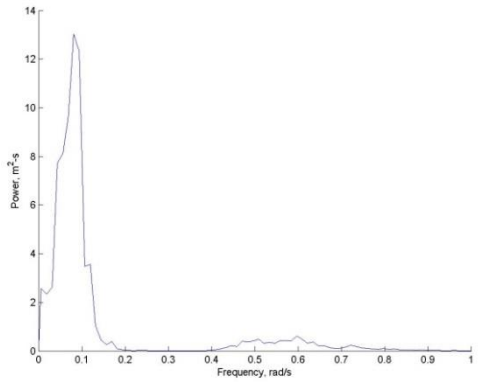

b) Surge PSD

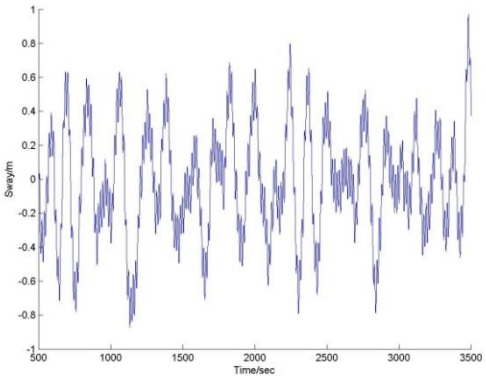

c) Sway

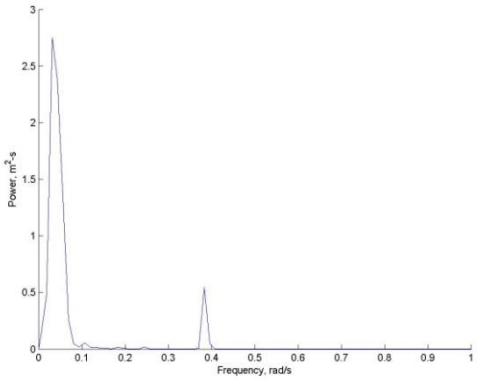

d) Sway PSD

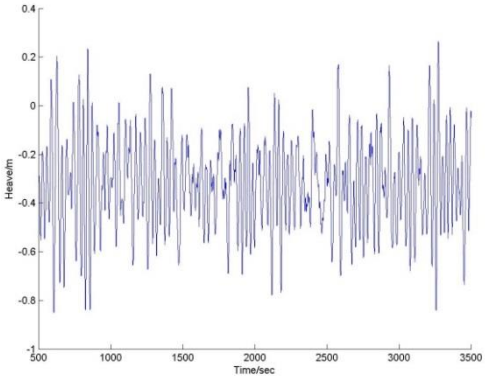

e) Heave

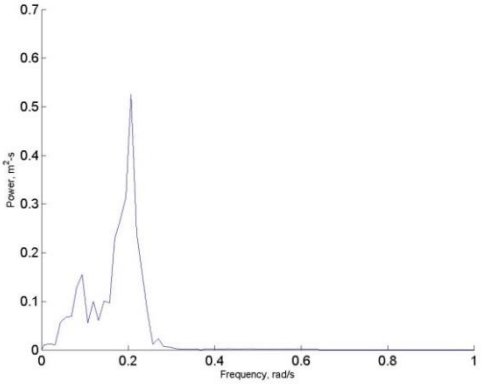

f) Heave PSD

Figure A 2-21 The FOWT Results for Case 24

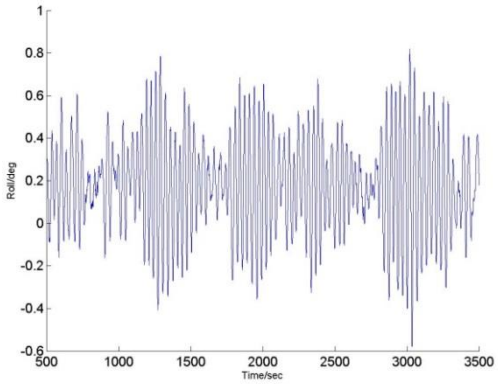

g) Roll

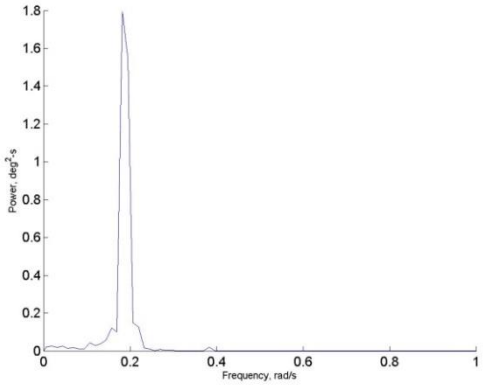

h) Roll PSD

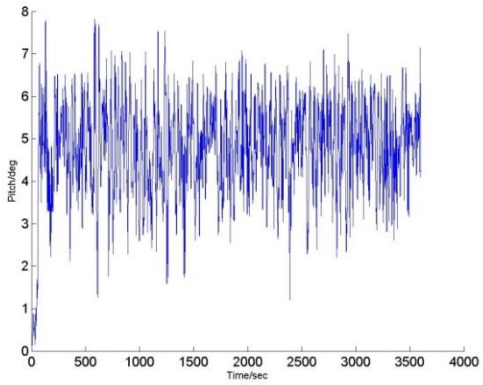

i) Pitch

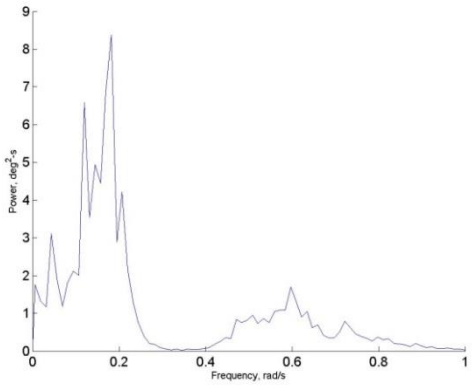

j) Pitch PSD

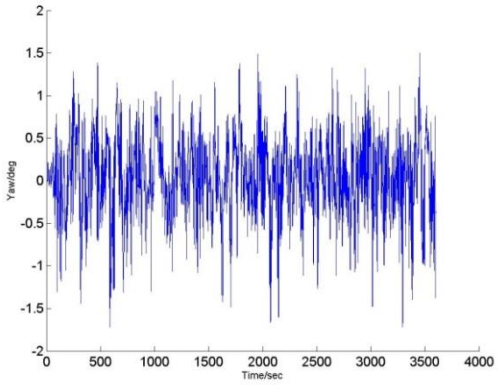

k) Yaw

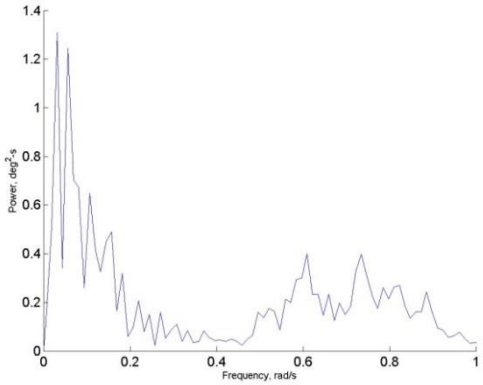

l) Yaw PSD

Figure A 2-21 Continued

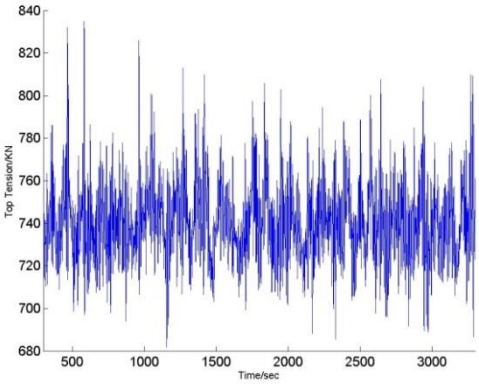

m) Top Tension of ML1

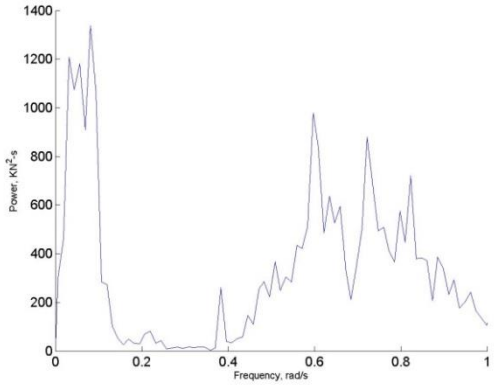

n) Top Tension PSD of ML1

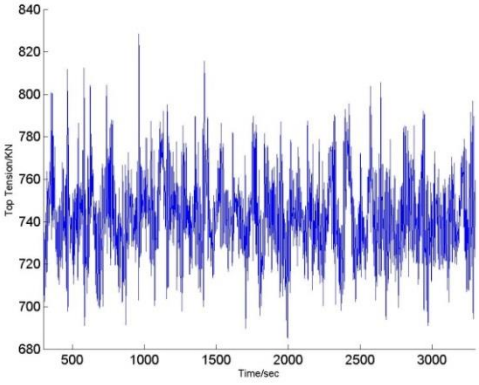

o) Top Tension of ML2

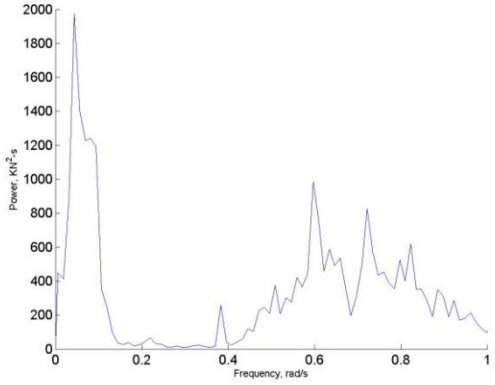

p) Top Tension PSD of ML2

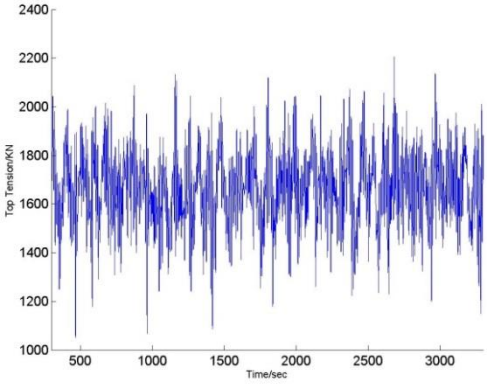

q) Top Tension of ML3

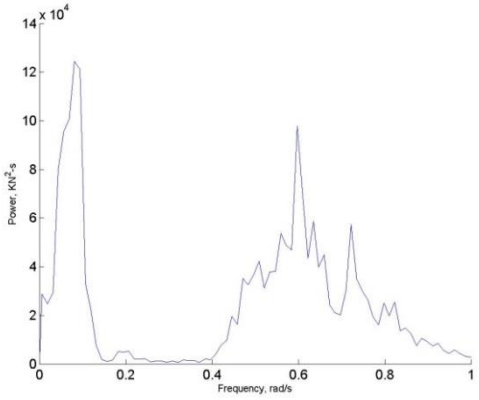

r) Top Tension PSD of ML3

Figure A 2-21 Continued

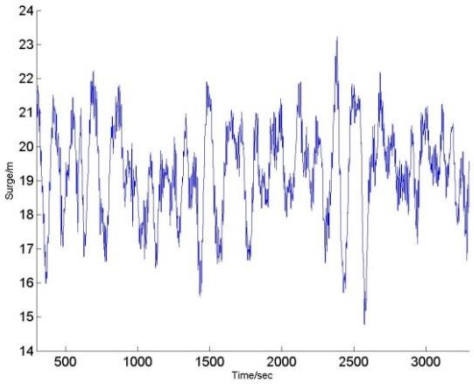

a) Surge

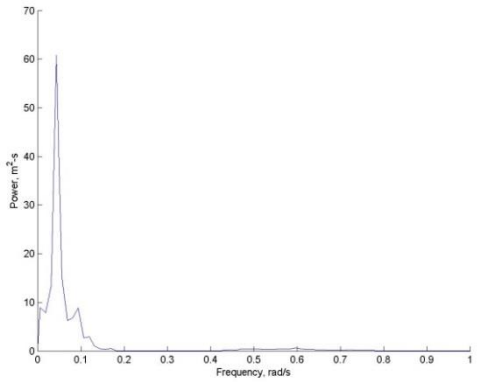

b) Surge PSD

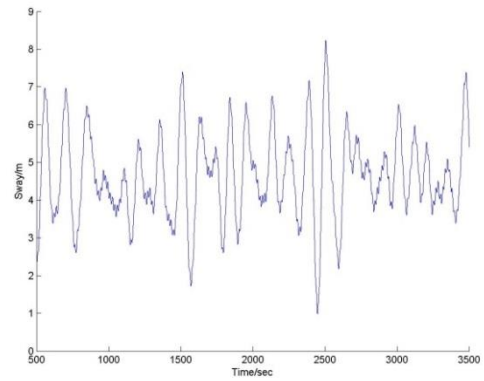

c) Sway

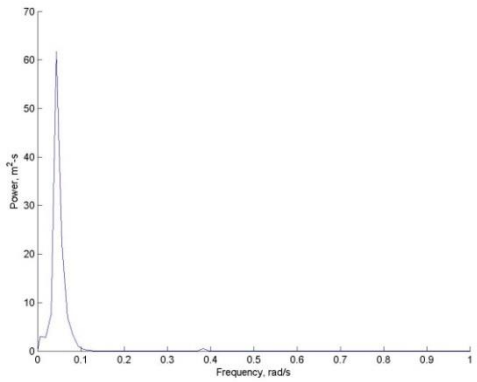

d) Sway PSD

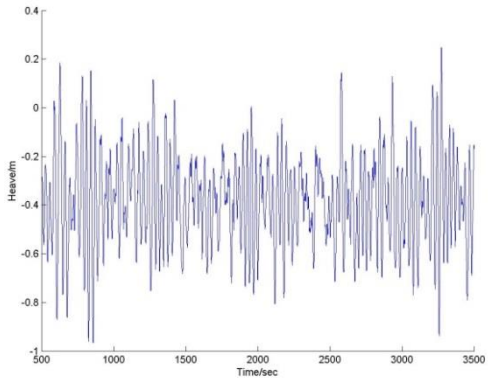

e) Heave

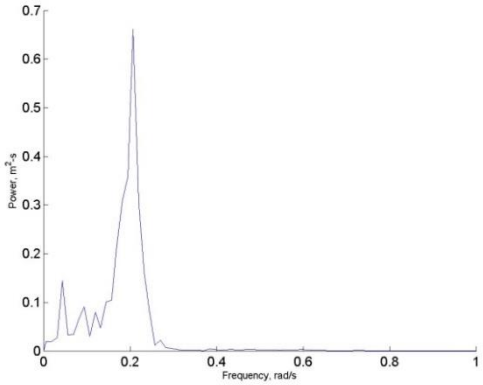

f) Heave PSD

Figure A 2-22 The FOWT Results for Case 25

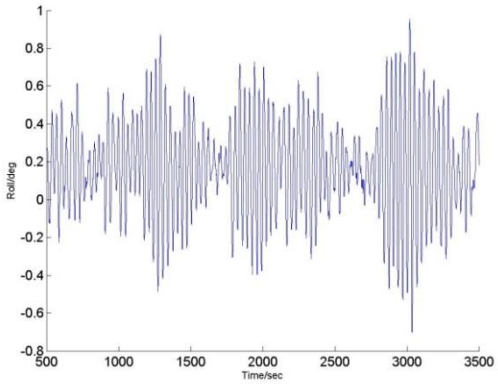

g) Roll

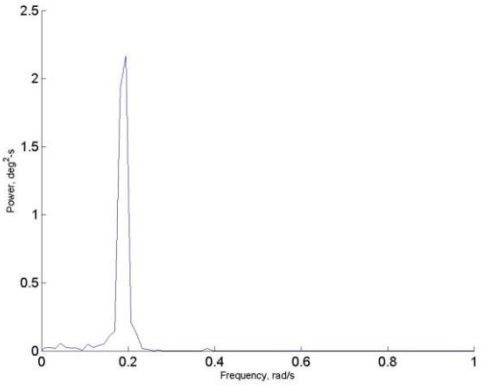

h) Roll PSD

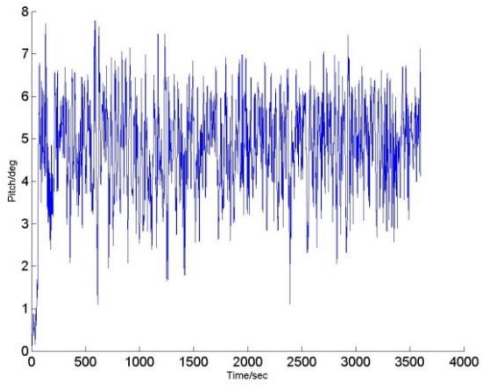

i) Pitch

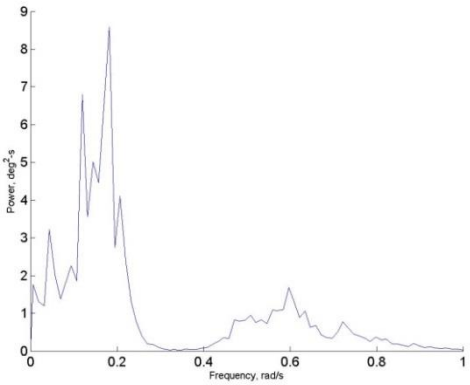

j) Pitch PSD

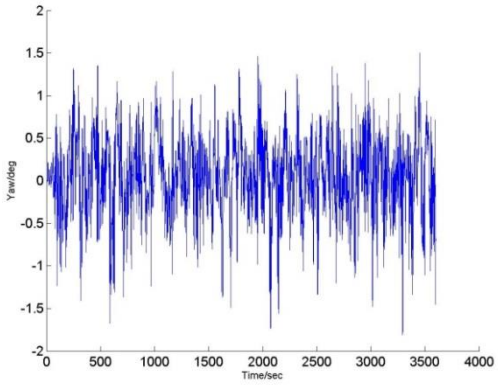

k) Yaw

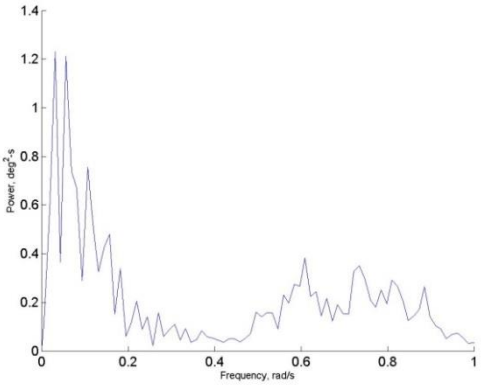

l) Yaw PSD

Figure A 2-22 Continued

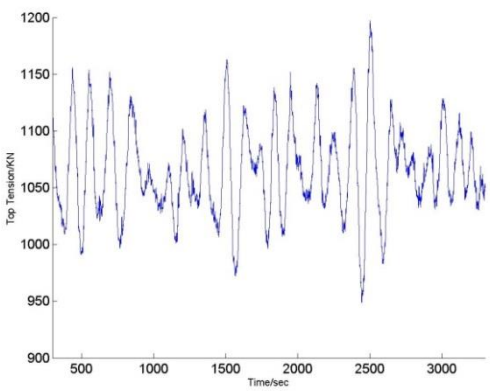

m) Top Tension of ML1

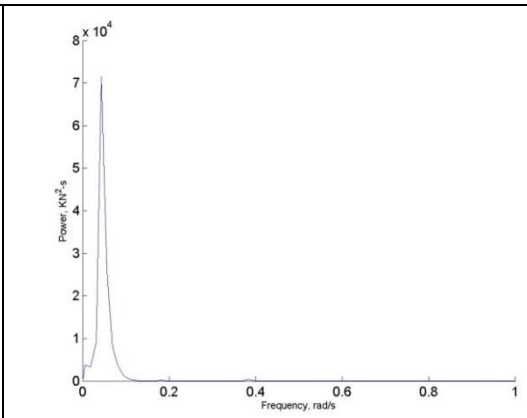

n) Top Tension PSD of ML1

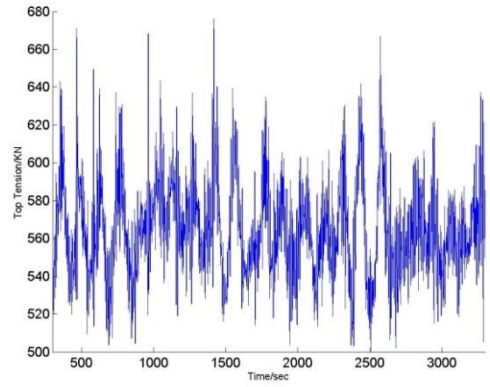

o) Top Tension of ML2

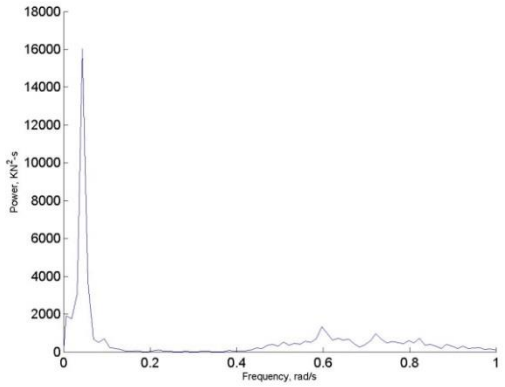

p) Top Tension PSD of ML2

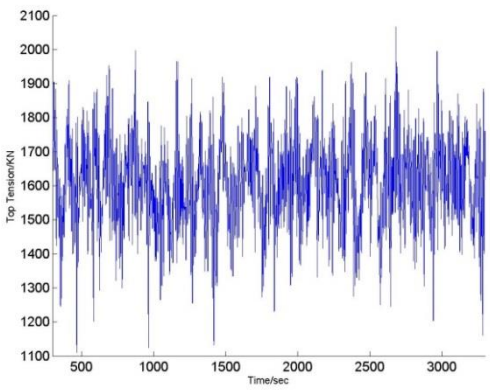

q) Top Tension of ML3

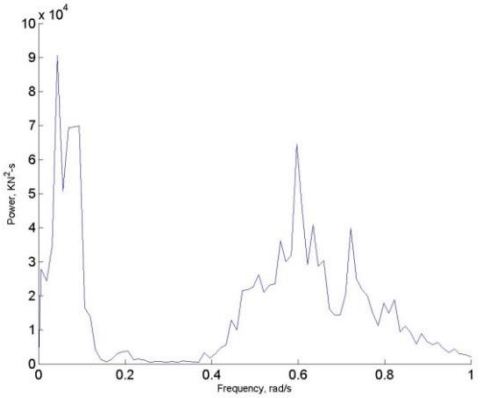

r) Top Tension PSD of ML3

Figure A 2-22 Continued